UNIVERSITY OF SÃO PAULO
SAO CARLOS SCHOOL OF ENGINEERING

Gustavo de Souza

Modified Nanofibrillated Cellulose (NFC) Films: Different Strategies to Enhance Hydrophobicity and Barrier to Water Vapor and Oxygen.

São Carlos

2021

Gustavo de Souza

Modified Nanofibrillated Cellulose (NFC) Films: Different Strategies to Enhance Hydrophobicity and Barrier to Water Vapor and Oxygen.

Thesis presented to the postgraduate Program in Science and Materials Engineering at the University of Sao Paulo, to obtain the title of Doctor of Science.

Research area: Development, Characterization and Application of Materials.

Supervisor: Prof. Dr. Antonio José Felix de Carvalho.

Revised Version

São Carlos

2021

Ficha catalográfica elaborada pela Biblioteca Prof. Dr. Sérgio Rodrigues Fontes da EESC/USP com os dados inseridos pelo(a) autor(a).

D982m

de Souza, Gustavo
Modified Nanofibrillated Cellulose (NFC) Films: Different Strategies to Enhance Hydrophobicity and Barrier to Water Vapor and Oxygen / Gustavo de Souza; orientador Antonio José Felix de Carvalho. São Carlos, 2021.

Tese (Doutorado) - Programa de Pós-Graduação em Ciência e Engenharia de Materiais e Área de Concentração em Desenvolvimento, Caracterização e Aplicação de Materiais -- Escola de Engenharia de São Carlos da Universidade de São Paulo, 2021.

1. nanofibrillated cellulose. 2. Blocked isocyanates. 3. Beeswax. 4. Films. 5. Hydrophobization. 6. Barrier to water vapor and oxygen. 7. Packaging. I. Título.

Eduardo Graziosi Silva - CRB - 8/8907

FOLHA DE JULGAMENTO

Candidato: Engenheiro**GUSTAVO DE SOUZA.**

Título da tese:"Filmes de Celulose Nanofibrilada (NFC) modificadas: diferentesestratégias para aumentar a hidrofobicidade e a barreira a vapor de água e oxigênio".

Data da defesa: 17/08/2021.

Comissão Julgadora **Resultado**

Prof. **Antonio José Felix de Carvalho** Aprovado
(Orientador)
(Escola de Engenharia de São Carlos/EESC-USP)

Profa. **Denise Freitas Siqueira Petri** Aprovado
(Instituto de Química/IQ-USP)

Prof. **Mohamed NaceurBelgacem** Aprovado
(INP/Pagora)

Dr. **Rafael Grande** Aprovado
(AALTO UNIVERSITY)

Profa. Dra. **Sílvia Helena Prado Bettini** Aprovado
(Universidade Federal de São Carlos/UFSCar)

Coordenador do Programa de Pós-Graduação em Engenharia de Materiais:
Prof. Associado **Rafael Salomão**

Presidente da Comissão de Pós-Graduação:
Prof. Titular**Murilo Araujo Romero**

I dedicate this work to my mother, Maria Inês.

ACKNOWLEDGEMENTS

To Prof. Dr. Antonio José Felix de Carvalho (Toni), for the opportunity, guidance and motivation, essential to carry out this work.

To Professors Mohammed Naceur Balgacem and Alessandro Gandini for receiving and guiding me during my sandwich doctorate, in Grenoble-France.

To the colleagues from the research group, especially Ricardo Kramer, Emanoelle, Fábio and the technician Ricardo Gomes, for their assistance in the laboratory and for the coffees.

To Ricardo Kramer, also for the partnership in the development of ideas and writing of papers.

To all colleagues in the PGrCEM postgraduate program.

To the secretariat of the postgraduate program PGRCEM, in particular to Victor Barioto.

To my friends from Grenoble, Matheus, Igor, João, Vinicius and Gabriel for the hours of talking about science.

To my friends Carla, Jéssica, Paula and Larissa, incredible and inspiring women.

To the longtime friends Daniel, Rafael and Jorge, partners for all hours.

To Mirella, for the support and companionship, crucial at the beginning of this work.

To Suzano Papel e Celulose S.A for the supply of nanofibrilated cellulose.

To CNPq for the doctoral fellowship granted (CNPq proc. 140249/2017-6) and CAPES for the sandwich doctoral fellowship granted (proc. 88887.371652/2019-00).

Learning is the only thing the mind never exhausts, never fears and never regrets.

Leonardo Da Vinci

Harder, Better, Faster, Stronger.

Daft Punk

ABSTRACT

SOUZA, G. **Modified Nanofibrillated Cellulose (NFC) Films: Different Strategies to Enhance Hydrophobicity and Barrier to Water Vapor and Oxygen**. 2021. 245p. Thesis (Doctorate) - Sao Carlos School of Engineering, University of Sao Paulo, Sao Carlos, 2021.

Unmodified or modified nanofibrilated cellulose (NFC) can be employed to produce films by means of controlled drying processes to form compact three-dimensional networks, giving rise to low permeable and high strength films, with the potential to compete with synthetic polymers in packaging applications. However, due to the high hydrophilicity these films have applications limited to conditions of relative humidity below 60%. Above this value, water acts as a plasticizer, drastically reducing mechanical and barrier properties. The present work describes four strategies for obtaining hydrophobic and low permeable films to water vapor and oxygen. Three strategies involve chemical modification through the use of blocked isocyanates, being **1)** superficial modification of the NFC film by dipping in solution; **2)** obtaining films from a composition containing an aqueous suspension of NFC and an aqueous emulsion of a blocked (poly) isocyanate; **3)** synthesis of a blocked polyethylene glycol diisocyanate and its use for the production of a composite where the matrix is formed by the PEG chains covalently bonded to the NFC reinforcement. For the three chemical modification strategies, the films were produced by casting and subjected to a thermal treatment to de-block the isocyanate. In strategy **4)** a physical modification was proposed in which the films were formed by casting of a mixture containing an emulsion of beeswax and a suspension of NFC. Each strategy gave rise to a scientific paper that is presented individually. The set of published and not yet published papers makes up the present thesis. The physical properties (density and porosity), mechanical, morphological, thermal, water absorption, contact angle with water and water vapor and oxygen permeation were evaluated. In addition to the papers, a comparative discussion between the strategies is presented. In general, the proposed chemical and physical modifications were responsible for hydrophobization, increased water resistance and gas barrier properties, demonstrating the potential of the proposed strategies for the manufacture of high performance films in packaging whose raw material is from renewable source.

Key-words: Nanofibrilated Cellulose. Blocked Isocyanates. Beeswax. Films. Hydrophobization. Barrier to water vapor and oxygen. Packaging.

RESUMO

SOUZA, G. **Filmes de Celulose Nanofibrilada (NFC) modificadas: Diferentes estratégias para aumentar a hidrofobicidade e a barreira a vapor de água e oxigênio**. 2021. 245p. Tese (Doutorado) - Escola de Engenharia de São Carlos, Universidade de São Paulo São Carlos, 2021.

A celulose nanofibrilada (NFC) não modificada ou modificada pode ser empregada para a fabricação de filmes por meio de processos de secagem controlados para formar redes tridimensionais compactas, dando origem a filmes de elevada resistência mecânica e pouco permeáveis, com potencial para a substituição de polímeros sintéticos em aplicações em embalagens. Contudo, devido a elevada hidrofilicidade esses filmes têm aplicações limitadas à condições de umidade relativa abaixo de 60%. Acima desse valor a água atua como plastificante, reduzindo drasticamente as propriedades mecânicas e de barreira. O presente trabalho descreve quatro estratégias para obtenção de filmes de NFC hidrofóbicos e de baixa permeação a vapor de água e oxigênio. Três estratégias envolvem a modificação química por meio do uso de isocianatos bloqueados sendo **1)** modificação superficial do filme de NFC por mergulho em solução; **2)** obtenção de filmes a partir de uma composição contendo uma suspensão aquosa de NFC e uma emulsão aquosa de um (poli)isocianato bloqueado; **3)** síntese de um di-isocianato bloqueado de polietileno glicol e sua utilização para a produção um compósitos onde a matriz é formada pelas cadeias de PEG ligadas covalentemente ao reforço de NFC. Para as três estratégias de modificação química os filmes foram produzidos por secagem (*casting*) e submetidos a um tratamento térmico de desbloqueio do isocianato. Na estratégia **4)** foi proposta uma modificação física na qual os filmes foram formados a partir da secagem de uma mistura contendo uma emulsão de cera de abelha e uma suspensão de NFC. Cada estratégia deu origem a um artigo científico que é apresentado individualmente. O conjunto dos artigos publicados compõe a presente tese. Foram avaliadas as propriedades físicas (densidade e porosidade), mecânicas, morfológicas, térmicas, de absorção de água, de ângulo de contato e de permeação a vapor de água e ao oxigênio. Além dos artigos, uma discussão comparativa entre as estratégias é apresentada. De modo geral, as modificações químicas e física propostas foram responsáveis pela hidrofobização, aumento da resistência à agua e das propriedades de barreira a gases, demonstrando o potencial das estratégias propostas para a fabricação de filmes de alto desempenho em embalagens cuja matéria prima seja de fonte renovável.

Keywords: Celulose nanofibrilada. Isocianatos bloqueados. Cera de abelha. Filmes. Hidrofobização. Barreira à vapor de água e oxigênio. Embalagens.

LIST OF FIGURES

LIST OF TABLES

LIST OF ABBREVIATIONS AND ACRONYMS

N_{kn}	Knudsen Number
γ_{LV}	Liquid-Vapor Energy
γ_{SL}	Solid-Liquid Energy
γ_{SV}	Solid-Vapor Energy
AGU	Anhydroglucose Units
AKD	Alkyl Ketene Dimer
APMS	Amino Propryl Trimethoxysilane
BOPP	Bioriented Polypropylene
BW	Beeswax
CNC	Cellulose Nanocrystals
D_{eff}	Fick Diffusion Coefficient
DIM	Diiodomethane
DSC	Differential Dcanning Calorimetry
EVOH	Ethylene Vinyl Alcohol
FT-IR	Fourier Transformed Infrared
HDPE	High Density Polyethylene
LDPE	Low Density Polyethylene
MAP	Modified Atmosphere Packaging
MDI	Methylene Diphenyl Isocyanate
NFC	Nanofibrillated Cellulose
NMR	Nuclear Magnetic Ressonance
OP	Oxygen Permeabity
OTR	Oxygen Transmission Rate
PBAT	Polybutyrate
PE	Polyethylene

PEG	Polyethylene Glycol
PET	Polyethylene Terephthalate
PHB	Polyhydroxybutyrate
PLA	Polylactic Acid
PP	Polypropylene
PS	Polystyrene
PVC	Polyvinyl Chloride
PVdC	Poly (Vinylidene Chloride)
TDI	Toluene Diisocyanate
TG	Thermogravimetric Analysis
TPS	Thermoplastic Starch
WCA	Water Contact Angle
WVP	Water Vapor Permeability
WVTR	Water Vapor Transamission Rate
Λ	Free Path
σ_1	Surface Tension of Liquid
$\sigma_{1,2}$	Interfacial Tension
σ_2	Surface Tension of Solid
τ	Tortuosity
θ	Contact Angle

CONTENTS

1 INTRODUCTION

Polymeric packaging has been considered one of the major causes of current environmental problems due to the combination of high production and incorrect disposal of the various items produced, especially those of short duration. However, despite the caused problems packaging is difficult to replace, as they are part of the daily life of modern society, providing convenience and practicality in the protection, transport and storage of consumer goods and food. Therefore, there is a huge challenge for packaging sector as, for example, there is an effort to ban short duration synthetic plastic in the European Economic Community from 2022 onwards (AHMADZADEH; KHANEGHAH, 2020; ANAGNOSTI et al., 2021; BARLOW; MORGAN, 2013; BHARATHI; MOSES; ANANDHARAMAKRISHNAN, 2018).

The search for biodegradable materials, from renewable sources, as an alternative to petroleum based materials has been motivated mainly by the demand of society and governments, as is the case of the European Economic Community. Nonetheless, one of the biggest challenges for applying materials from renewable sources in packaging is to develop materials based on natural resources that have mechanical properties and barrier properties to gases such as O_2, CO_2 and water vapor at the similar levels of synthetic polymers, mainly when applied in wet environments (VILARINHO et al., 2017; WANG et al., 2017).

When the relative humidity of the environment is below 60% the films obtained from hydroxylated natural polymers such as starch and cellulose have good O_2 barrier and possess mechanical properties comparable to some synthetic polymers used for packaging (DUFRESNE; DUPEYRE; VIGNON, 2000). However, above this moisture threshold, these biopolymers lose their mechanical and barrier properties due to the strong interaction with water molecules, which causes plasticization of their structures. In addition, regarding to the water vapor permeation, natural polymers present considerable lower properties in relation to the main synthetic polymers used in packaging such as LDPE (low-density polyethylene), PVdC (poly (vinylidene chloride)) and especially the BOPP (bioriented polypropylene). Another challenge is the difficulty of large-scale production, which makes manufacturing more expensive and often prevents the widespread use of polymers from renewable sources (AHMADZADEH; KHANEGHAH, 2020; BARLOW; MORGAN, 2013; BRIASSOULIS; GIANNOULIS, 2018; BHARATHI; MOSES; ANANDHARAMAKRISHNAN, 2018).

Cellulose is the most abundant biopolymer on the planet, representing 50% of the available biomass. Its traditional use in packaging is as raw material for secondary and tertiary packaging of cardboard and kraft paper together with food cellophane films.

However, with the advancement of the technology of fibrillation processes, nanofibrillated cellulose (NFC) can now be obtained at a competitive cost of 20 dollars per dry kilogram of material (LI et al., 2021). The great advantage of this nanostructured material is the formation of compact three-dimensional networks with the possibility for use in films with high mechanical and gas barrier properties, which opens up new possibilities of applications, especially in primary packaging (KLEMM et al., 2018; LI et al., 2021). Composites reinforced with NFC or cellulose nanocrystals (CNC) are a widely explored aspect in the literature and have characteristics that make the properties of renewable polymers more competitive compared to synthetic ones. Films made solely of NFC appear as a promising material since, the high aspect ratio and presence of hydroxyl groups allow strong inter- and intramolecular interactions, enabling the formation of compact and mechanically resistant films, with good gas barrier properties in the dry state. However, water acting as a plasticizer ends up requiring some type of structural modification (chemical or physical) so that these materials can be applied in wet or high humidity environments (FARUK et al., 2012; SIQUEIRA; BRAS; DUFRESNE, 2010).

In general, chemical modification of cellulose involves laborious procedures, since the reactions can hardly be conducted in an aqueous medium, requiring one or a few steps of solvent exchange. However, even after several exchange steps, the residual water is not completely eliminated because of the high activation energy of bonded water (KRAMER, 2014). Chemical modifications that can be made in aqueous media by less laborious processes, are simple potential solutions to overcome the high hydrophilicity of NFC films and can be of great industrial interest (DUFRESNE, 2017; GIRONÈS et al., 2007).

Thus, the present work proposes strategies for obtaining modified NFC films and composites directly in aqueous medium or in medium with residual water, using chemical modification agents (blocked isocyanates) and physical modification agent (beeswax). Strategies were not only considered to simplify the stages of the process, but also to develop a methodology that can be scaled, with potential for application from both an economic and an environmental point of view. Therefore, the contribution of the work is focused on the development of NFC-based films with hydrophobic characteristics, and with potential application in packaging, in which the mechanical, optical and morphological characteristics, of gas permeation and absorption susceptibility to water and moisture are important (LAVOINE et al., 2012; SETHI et al., 2019).

1.1 Polymeric packaging and the problem with solid waste

Polymers are the most used materials in the manufacture of packaging due to their low cost, ease of processing, high availability of raw material and flexibility of properties, adjusting to a wide variety of applications. In 2011, the packaging sector was responsible for about 40% of the world consumption of polymers, with five main ones being

responsible for more than 90% of the total volume of plastics used for this purpose. They are polyethylene (PE), polypropylene (PP), polyethylene terephthalate (PET), polyvinyl chloride (PVC) and polystyrene (PS), which are mainly used in the form of thin films (BARLOW; MORGAN, 2013; BHARATHI; MOSES; ANANDHARAMAKRISHNAN, 2018).

The polymers used in packaging come from a non-renewable source (petroleum) and most of them are not biodegradable according to the current standards. These materials are the result of great environmental concerns, since the correct destination of post-consumer packaging is still difficult to be achieved in its entirety, generating waste accumulation and harming innumerous ecosystems. For example, in Europe, where environmental legislation is more severe and government policies strictly regulate the correct destination of post-consumer materials, only 40% of the polymers produced annually are recycled or incinerated (AHMADZADEH; KHANEGHAH, 2020; BARLOW; MORGAN, 2013; BHARATHI; MOSES; ANANDHARAMAKRISHNAN, 2018). In 2014, 25.8 million tons of the plastic produced were discarded and it is estimated that 63 % of that number is due to short-lived packaging. In addition, the additives used in the processing of thermoplastic materials, such as flame retardants, stabilizers and plasticizers, can migrate from the material during disposal and subsequent recycling, posing challenges for circular economy practices (GEUEKE; GROH; MUNCKE, 2018; GUTIÉRREZ; MENDIETA; ORTEGA-TORO, 2021; PAYNE; MCKEOWN; JONES, 2019; WAGNER; SCHLUMMER, 2020).

Globally, 48% of the plastic produced is disposed of in landfills and 32% of the waste produced worldwide is discarded in nature. This number is expected to double in 2030 due to the growing incorrect disposal of plastic (WAGNER; SCHLUMMER, 2020). Furthermore, the global pandemic situation caused by the COVID-19 virus is an aggravating factor that can accelerate this number, since the virus can survive longer on plastic surfaces than in other materials and, as a health precautionary measure, disposable plastic materials are preferable over other more durable options. Therefore, even that plastic materials are valuable material to combat the contamination and propagation of the virus, its disposal volume are of environmental concern. (SILVA et al., 2021).

Because of these limitations and pressure from society, research on the topic of biodegradable packaging, whose raw material comes from renewable sources, has grown significantly in recent years (BARLOW; MORGAN, 2013). In the literature, the number of publications around materials from renewable sources for food packaging has remained approximately constant over the period 1946-2016. However, since 2016, the growth in the volume of published works has been exponential. Brazil appears in third in the list of countries that are most popular on the topic, in front of the United States and China (RODRÍGUEZ-ROJAS et al., 2019).

In the industrial scenario, materials such as the packaging lines Mater-bi® (Novamonte), thermoplastic starch and regenerated cellulose, and Ecovio® blend of PBAT

and PLA), are already available on the market. NatureFlex 913 is even certified for home composting. However, despite the green route of obtaining, most biodegradable polymers such as polylactic acid (PLA), polyhydroxybutyrate (PHB) and thermoplastic starch have low stiffness and water vapor barrier properties when compared to polymers derived from petroleum as LDPE and mainly BOPP. Another limiting factor is the non-competitive cost of these materials (BARLOW; MORGAN, 2013; BRIASSOULIS; GIANNOULIS, 2018). (BARLOW; MORGAN, 2013; BRIASSOULIS; GIANNOULIS, 2018). Therefore, new biodegradable alternatives, with high mechanical and barrier properties, combined with a competitive cost of production should be sought (LAVOINE et al., 2012; WANG et al., 2017).

1.2 Requirements for food packaging

The quality of the food consumed is directly related to the conditions of its storage. The permeation of water vapor and / or oxygen are the main causes for the modification of organoleptic characteristics and the deterioration of food. For the conservation of its physical chemical characteristics and sensory attributes, the product must be stored in packaging that presents low permeation to O_2 and H_2O vapor, since the passage of these gases causes oxidation and plasticization of the food, altering the taste and affecting crunchiness. Thus, packages with good H_2O vapor and O_2 barrier properties are primarily responsible for extending the shelf life of food (BORÉM et al., 2019; EUROMONITOR INTERNATIONAL, 2017).

The gas barrier property is one of the main requirements for right selection of packaging. However, generally a single polymer is not able to meet the requirements of OTR (Oxygen Transmission Rate) and WVTR (Water Vapor Transmission Rate), and it is common to manufacture multilayer films such as, for example, with the polymers shown in Table 1. It is interesting to note that not necessarily a polymer that has low O_2 permeation will present the same barrier for water vapor, as is the case of PP and HDPE, which are considered “poor” materials for O_2, but have a high barrier for water vapor. Hence, multilayer films are produced to achieve barrier requirements. For example, a possible combination is the production of a film with layers of PP or HDPE and another layer of EVOH or PVdC (EBNESAJJAD, 2013; WANG et al., 2017).

In addition to the individual properties of each layer, the cost, thickness and appearance of the film must also be taken into account, which makes the design process of packaging quite complex. Films intended to be applied as MAP (modified atmosphere packaging) can have up to seven layers (EBNESAJJAD, 2013; WANG et al., 2017). In general, a layer of aluminum film is also added both to reinforce the gas barrier and to protect food from ultraviolet radiation, while also avoiding oxidation by photocatalysis (BORÉM et al., 2019)).

Table 1 – Classification of OP and WVP and examples of the main polymers in each class.

Grade	Oxygen Permeability ($cm^3.\mu m.m^{-2}.day^{-1}.atm^{-1}$)	Exemple
Poor	>40000	HDPE, PP, PS, PHB, LDPE
Low	4000-40000	PVC, BOPP, PHA, PLA
Average	400-4000	EVOH (wet), OPET, PA6 (wet), PET
High	40-400	PVdC, PA6 (dry)
Very High	<40	EVOH (dry)
Grade	Water Wapor Permeability ($g.\mu m.m^{-2}.day^{-1}.kPa$)	Exemple
Poor	>3000	Silicone Elastomer
Low	1000-3000	PA6, PLA
Average	400-1000	OS, PHA, PLA
High	40-400	PAN, PVC, PET, LDPE
Very High	<40	HDPE, PP, PVdC, OPET, BOPP

Source: Adapted from Wang et al. (2017).

Thermoplastic polymers are the most suitable materials for the manufacture of low-permeable packaging, in addition to barrier properties, other technical requirements, such as mechanical and thermal resistance, the ability to be stored frozen and resistance to microwave degradation are crucial for its application. In addition, their raw material is cheap and they present ability to form films in industrial processes (WANG et al., 2017). The graph in Figure 1 shows the required OTR and WVTR values for storing various foods.

Figure 1 – OTR values as a function of WVTR required for the preservation of the main types of food.

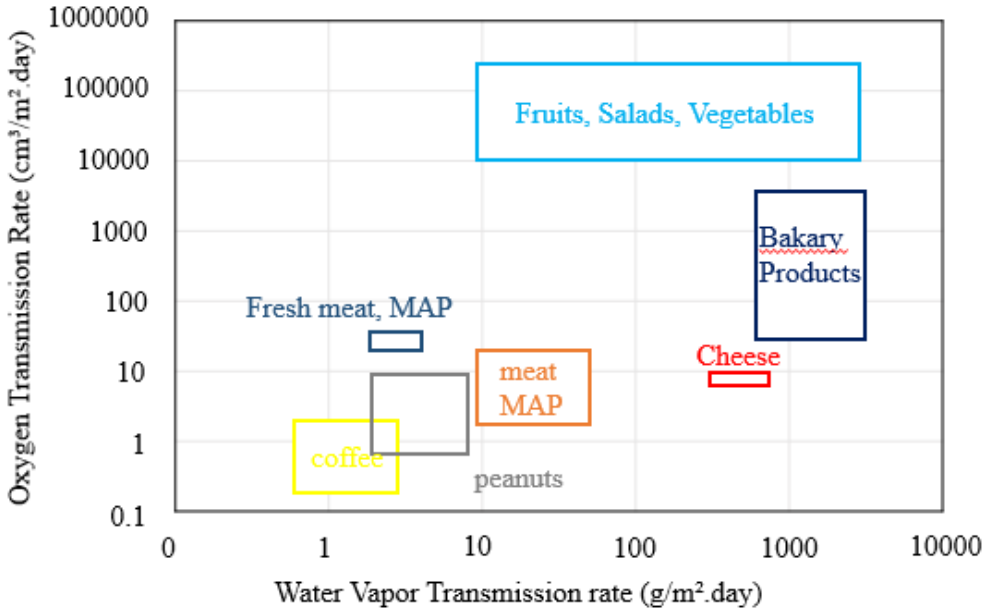

Source: Adapted from Wang et al. (2017).

1.3 The potential of biomass: Nanofibrillated Cellulose (NFC)

Cellulose is a natural polymer abundant in almost all regions of the planet, with an estimated biosynthetic production between 100-200 million tons per year (DUFRESNE, 2017; GANDINI, 2011). It can be extracted from a variety of plant species such as trees, hemp, coconut, cotton, among others. It is also possible to obtain it via animal route, with the tunicates and through bacteria such as *Acetobacter xylinum*. Cellulose is a semi-crystalline carbohydrate composed of anhydroglucose units (AGUs) covalently linked by the -1,4 glycosidic bond. The repeteated unit of cellulose is cellobiose and is represented on 2. The presence of hydroxyl functional groups, allows the formation of intramolecular hydrogen bonds, inhibiting the rotation of the rings and, therefore, contributing to the stiffness of the material (DUFRESNE, 2017; GANDINI, 2011; KLEMM et al., 2005).

Figure 2 – Single cellulose chain repetition unit, showing the directionality of the 1-4 bond and internal hydrogen bond (dotted line) also naming the carbons of the rings.

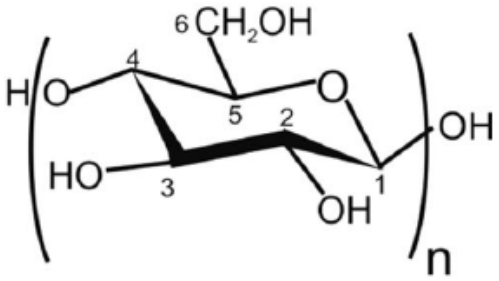

Source: French (2017).

In nature, cellulosic fibers form the plant cell wall providing mechanical support to the matrix formed by lignin and hemicellulose. The hierarchical architecture of the vegetables (Figure 3 3) allows the obtaining of fibers of different lengths and diameters through mechanical and chemical methods or a combination of both (DUFRESNE, 2017; KLEMM et al., 2005). Cell walls are divided between primary (P) and secondary (S1-S3), the more internal the wall, the smaller the length and diameter of the fibers (DUFRESNE, 2017).

Isolated single NFCs have a length of the order of micrometers and a nanometric diameter. They are flexible materials, composed of crystalline domains alternated with amorphous formations. Its advantageous characteristics such as wide availability of raw material, being from renewable sources, low density, high aspect ratio due to the nanometric dimensions, high rigidity and unique morphology, allow for unique chemical and physical properties, which makes this material the object of study in several technological applications (CHIROMITO; TROVATTI; CARVALHO, 2019; DUFRESNE, 2013; KLEMM et al., 2018).

Figure 3 – Cellulose fiber cell wall model: S1, S2 and S3 are secondary wall layers; arrangement of fibril, microfibrils and cellulose in the plant cell wall; schematic organization of crystalline and amorphous domains in cellulose fiber.

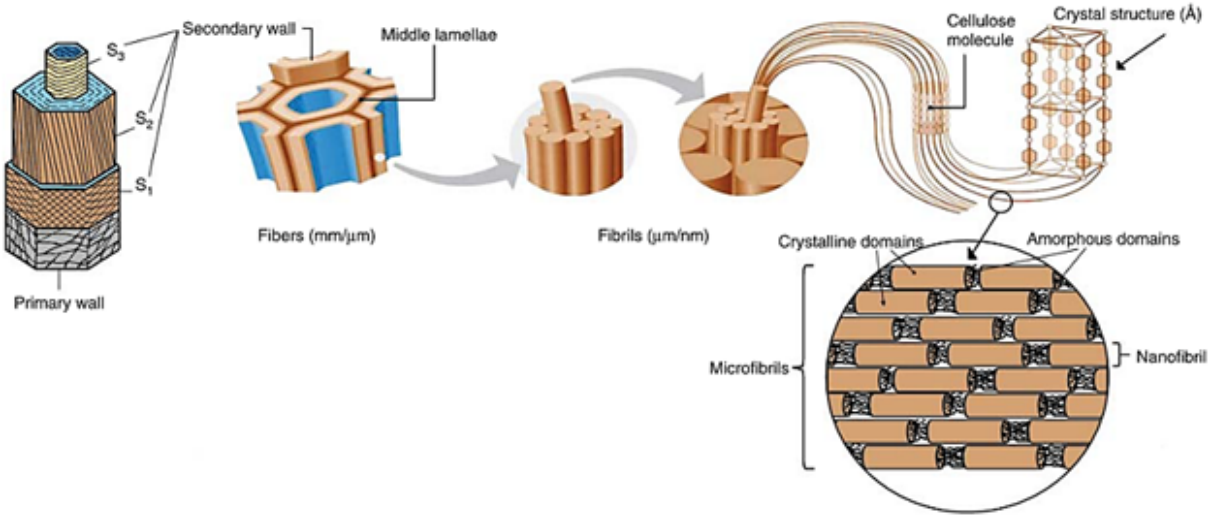

Source: Dufresne (2017).

Another fact that encourages that favors the application of nanocelluloses is the search of the paper industry for the development of innovative products as a means of biomass. It is estimated that the nanocelluloses market will reach the mark of US $ 700 million in 2023 (VARTIAINEN; MALM, 2016).

One of the main NFC applications is as a reinforcing agent in natural or synthetic polymers (DUFRESNE, 2017). The incorporation of NFC or even fibers to obtain nanocomposites is challenging, since they have a high amount of hydroxyl groups and, therefore, are highly polar, hydrophilic and hygroscopic materials, nom compatible with non-polar synthetic polymers (CARVALHO; TROVATTI; CASALE, 2018). In addition, they tend to aggregate easily in the absence of water due to intermolecular hydrogen bonds, in a process called hornification. Once agglomerated, NFCs are no longer able to return to their fibrillated state, which makes their adequate dispersion difficult. Another point is that the conventional injection and extrusion processes for obtaining these composites also have serious limitations, as the maximum processing temperature allowed for cellulosic materials is around 200 ° C. Thus, obtaining NFC-based films, also called nanopapers, are generally produced by casting (DUFRESNE, 2017; KLEMM et al., 2005; KLEMM et al., 2018; LAVOINE et al., 2012; SIQUEIRA; BRAS; DUFRESNE, 2010).

Paper packaging has always been highlighted as secondary packaging for the protection of consumer goods. The application of paper or cardboard as primary packaging is less common since this material has a high permeation to water vapor, requiring the addition of some protective polymeric layer. However, with the evolution of cellulose

fibrillation processes, NFCs are produced at a viable energy cost and have a greater application potential due to the greater compaction of the fibers (DUFRESNE, 2013; KLEMM et al., 2018).

Among the outstanding properties of NFC films, high rigidity and mechanical resistance together with barrier properties such as low permeability to water vapor and other gases in the dry state are the most reported in the literature. In the so-called dry state (relative unit below 60 %), NFC films and its composites usually have an excellent oxygen barrier and moderate water vapor barrier. However, with the increase in the relative unity these films become quite permeable and plasticized (DUFRESNE, 2017; FERRER; PAL; HUBBE, 2017; KLEMM et al., 2005; KLEMM et al., 2018; LAVOINE et al., 2012; SIQUEIRA; BRAS; DUFRESNE, 2010). Among the studies that addressed permeation, water vapor transmission (WVTR) of 200 g / m^2.day was observed for 100% NFC films and between 300 and 500 g / m^2.day for NFC samples with considerable lignin levels (FERRER; PAL; HUBBE, 2017; KLEMM et al., 2018; LAVOINE et al., 2012). Studies also show that the level of fiber entanglement, the degree of compaction and porosity on a nanoscale are more determinant factors in barrier properties than the crystalline percentage of precursor NFCs (FERRER; PAL; HUBBE, 2017).

In some applications, NFCs are also used as coatings on polymeric films or even on paper, helping to raise the barrier properties of the base film without compromising other properties, such as, for example, greater elongation. Figure 4 presents the possible strategies for using NFC to obtain films with barrier properties described by Lavoine et al Lavoine et al. (2012), where the strategies for inserting nanofibers (ie, composites, coatings or 100% NFC films), the barrier properties sought and the variables that most influence these properties are presented. In addition to the described variables, for 100% NFC films, it is usually necessary to perform surface chemical modification (post-treatment) in order to decrease its high hydrophilicity (LAVOINE et al., 2012; ROL et al., 2019).

There is a wide variety of chemical modifications that can be applied directly to NFC films, most of them involving chemical reactions with the hydroxyl groups present on the surface of the fibers (GANDINI; BELGACEM, 2015). Among surface chemical treatments applied to NFC films, there are the treatment with alkyl ketene dimer (AKD) (ARBATAN et al., 2012; REVERDY et al., 2018; YANG et al., 2016), amino propryl trimethoxysilane (APMS) (REVERDY et al., 2018), titanium dioxide (DU et al., 2017), esterification with anhydrous moieties (SEHAQUI; ZIMMERMANN; TINGAUT, 2013), eand some more sophisticated such as plasma treatment followed by deposition of a compound fluorinated (CAO et al., 2017).Some applications with isocyanates are also found (NADA, a; TAN; ZHANG; WENG, 2011),however studies are limited due to the toxicity and the need to work with such reagents in anhydrous medium (ROL et al., 2019).

Figure 4 – Strategies for the production of films described by (LAVOINE et al., 2012) and obtained barrier properties and characteristics that affect their use considering low permeability films.

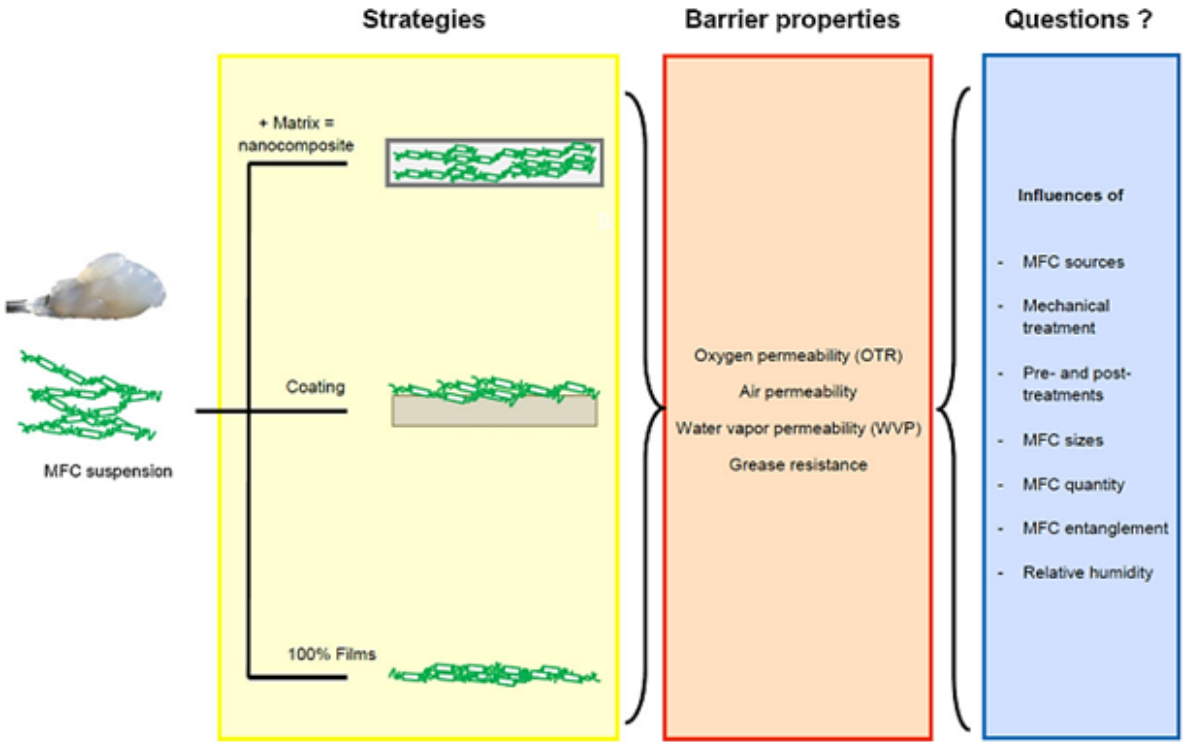

Source: Lavoine et al. (2012).

1.4 Isocyanates and blocked isocyanates

1.4.1 Isocyanates: structures and related compounds

Isocyanates are molecules that have a linear structure composed of two consecutive double bonds. They show high reactivity due to the fact that a carbon atom is linked to two electronegative atoms, oxygen and nitrogen, as shown in the Figure 5 (DELEBECQ et al., 2012).

Figure 5 – Resonance structures of the isocyanate group.

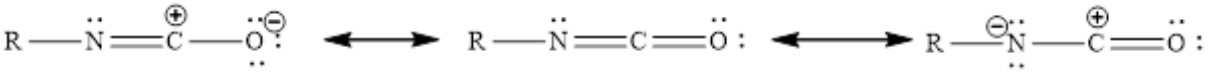

Source: Adapted from Delebecq et al. (2012).

The study of isocyanates and their reactions started around 1900. However, its practical use was discovered around 1940 by the work of Bayer and collaborators, who synthesized the first polyurethane by reacting a polyester diol with a diisocyanate, opening doors to make diisocyanate one of the most produced chemicals in the world. The most common processes for obtaining isocyanates involve reactions of amines (or their salts) and

phosgene, whose besides the main product, also forms disubstituted urea by the reaction between the formed isocyanates and free amines (DELEBECQ et al., 2012; SAUNDERS; SLOCOMBE, 1948).

Isocyanates react with molecules of type XH, in which the nucleophilic center X attacks the electrophilic carbon of the isocyanate. Compounds containing active hydrogen atoms, that is, hydrogen bonded to a nitrogen atom or hydrogen bonded to an oxygen atom, reacts easily with isocyanates. Amines react with isocyanates to form substituted urea and, in turn, urea reacts with isocyanates to form biurets. The reactions of primary, secondary and tertiary alcohols with isocyanates give rise to carbamates (or urethanes). Reactions of isocyanates with thiols are also possible, giving rise to urethanethiols (DELEBECQ et al., 2012). The Figure 6 summarizes the main reactions involving isocyanates. The reaction with alcohol, generating a urethane (Figure 6a), the reaction with a thiol, forming a urethane (Figure 6b), the reaction with an amine, forming a disubstituted urea (Figure 6c) and finally, the reaction with water, which gives rise to an unstable intermediate compound called carbamic acid, which decomposes to an amine, releasing CO_2 (Figure 6d). The amine, in turn, can react again with a free isocyanate molecule, according to the scheme (Figure 6c)

Figure 6 – Common reactions used on the chemistry of polyurethanes.

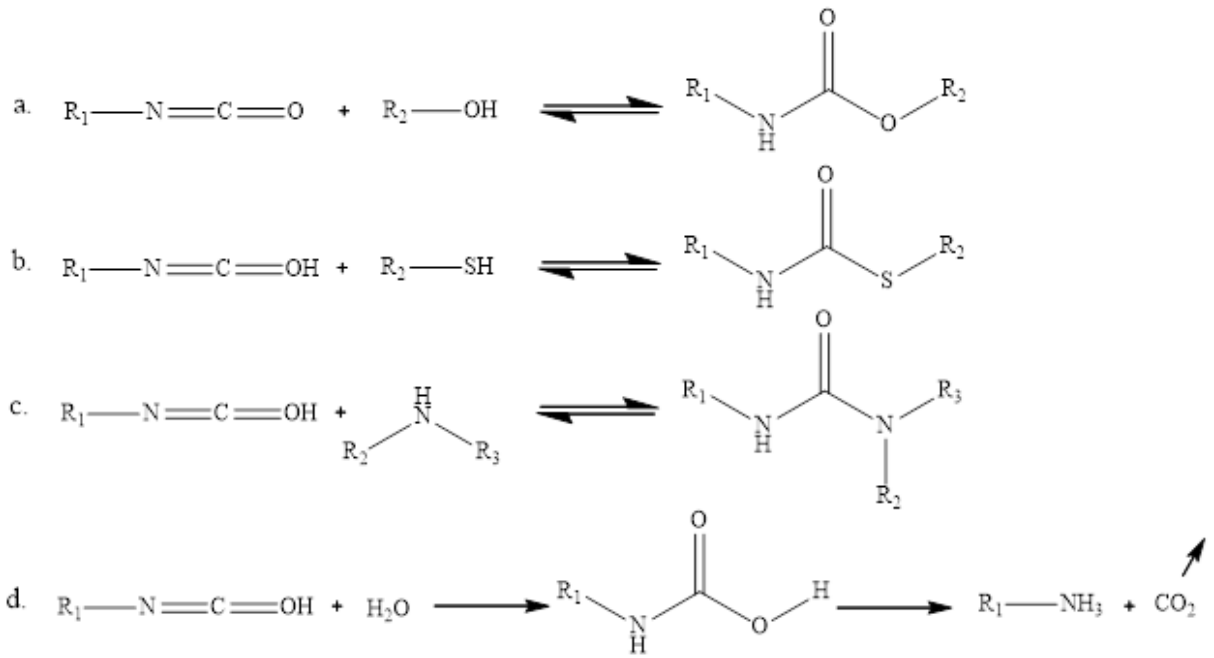

Source: Delebecq et al. (2012).

In addition to reactions with other molecules, isocyanates go through self-addition and transcondensation reactions, which can give rise to dimers (uretodione) and trimers (isocyanurates), as shown in Figure 7. Reactions between isocyanates are favored at high

temperatures. For example, the formation of isocyanurates occurs above 250 °C and can be catalyzed by the presence of urethanes in the reaction medium. When heated for a long time at a temperature of 180-200 ° C, isocyanates can be converted to carbodiimides, also with CO_2 release Figure 8) (DELEBECQ et al., 2012; SAUNDERS; SLOCOMBE, 1948).

Allophanates and biurets can be formed by the reaction of isocyanates with urethanes and ureas, respectively, as shown in Figure 9. Biurets are more stable and their formation rate is an order of magnitude above the constant of allophanate formation, which are mainly formed when the NCO / OH ratio is greater than 1. In general, the thermal stability of the products of the isocyanate reactions follows the order: allophanates <biurets <urethanes <urea <isocyanurates (DELEBECQ et al., 2012).

Figure 7 – Self-reaction of isocyanates.

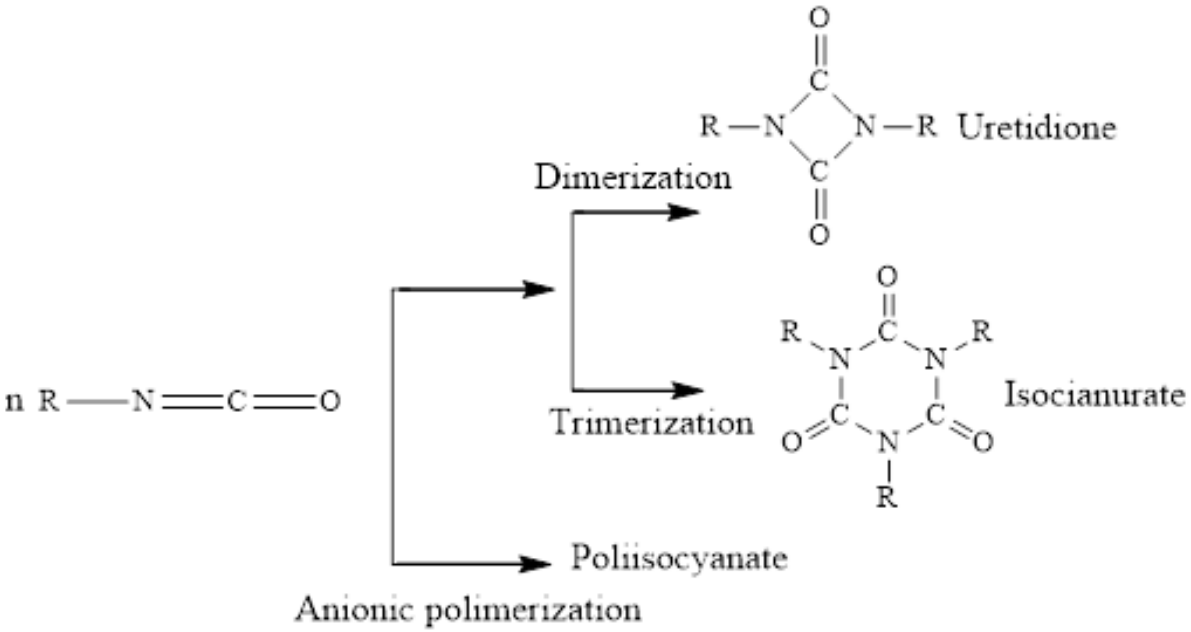

Source: Delebecq et al. (2012).

Figure 8 – Carbodiimide formation from isocyanates.

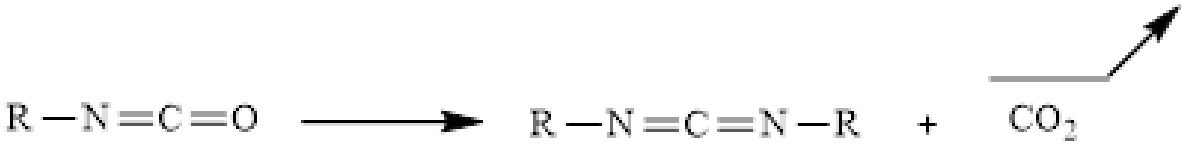

Source: Delebecq et al. (2012).

Figure 9 – Two pathways of allophanates and biurets formation.

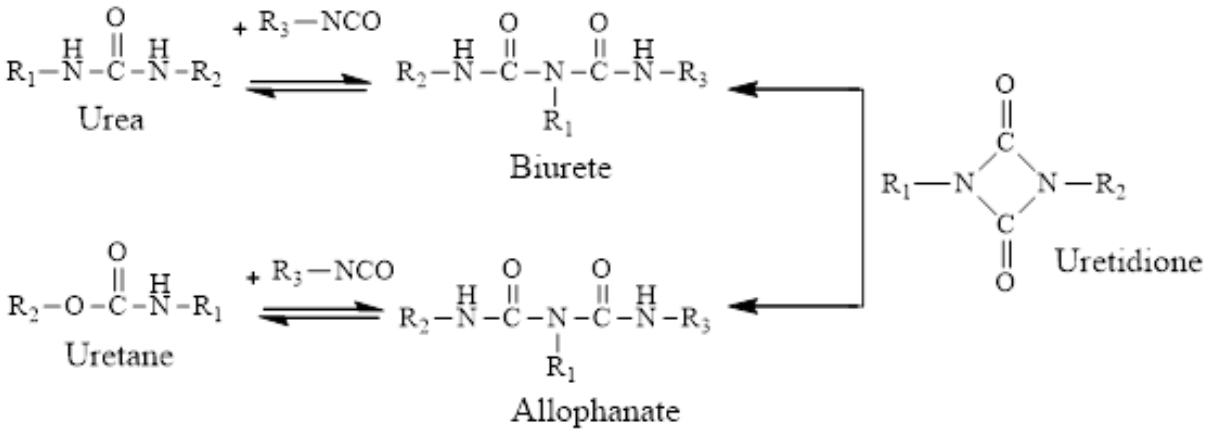

Source: Delebecq et al. (2012).

The wide range of possible reactions makes isocyanate chemistry quite complex. With regard to reactivity, amines react much faster with isocyanates than alcohols, which in turn react faster than water. The basicity of the atom bound to the active hydrogen, as well as steric factors, solvents, catalysts and the reaction temperature influence the reaction rate. Most reactions involving isocyanates can be reversed with heating. However, reactions with water consume the NCO group irreversibly, forming disubstituted urea and releasing carbon dioxide, making the handling and storage of isocyanates laborious (DELEBECQ et al., 2012). Table 2 2 shows the relative reactivities of some compounds towards isocyanates.

Table 2 – Relative reactivities of active hydrogen compounds towards isocyanate group.

Compound baring active hydrogen	Group	Relative rate of reactivity (without catalyst, 25 °C)
Aliphatic primary amine	R-NH_2	1000
Aliphatic secondary amine	R_2NH	200-500
Aromatic primary amine	Ar-NH_2	2-3
Primary alcohol	$RCH_2 - OH$	1
Water	HOH	1
Secondary alcohol	$R_2CH - OH$	0,3
Urea	R-NH-CO-NH-R	0,15
Tertiary alcohol	$R_3CH - OH$	0,005
Phenolic alcohol	AR-OH	0,001-0,005
Uretane	R-NH-COOR	0,001

Source: Delebecq et al. (2012).

In a symmetric diisocyanate, initially the two NCO groups present the same

reactivity ($k1 = k2 = k$). However, when the first group reacts, the reactivity of the second group is decreased (k') by the electronic and steric effect of the formed urethane or urea (Figure 10). In general, the fast the formed urethanes are less stable and have lower decomposition temperatures. The urethane formed by the addition of an isocyanate and an alcohol has a weak C-NH bond, with dissociation energy in the order of 100130 kJ/mol. Above 150 °C, four urethane decomposition paths are possible, as shown in Scheme 7. Electronic effects influence both kinetics and thermal decomposition products. Aromatic groups favor the reverse reaction (Figura 11a) while aliphatic groups promote dissociation into primary amine (Figura 11b) (DELEBECQ et al., 2012).

Figure 10 – Reactivity difference of one diisocyanate after the reaction of the first group.

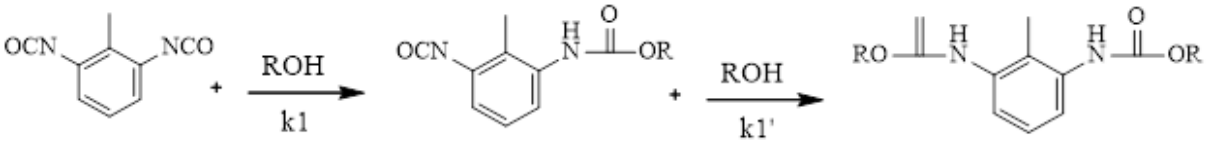

Source: Delebecq et al. (2012).

Figure 11 – Possible pathways for the degradation of the urethane bond.

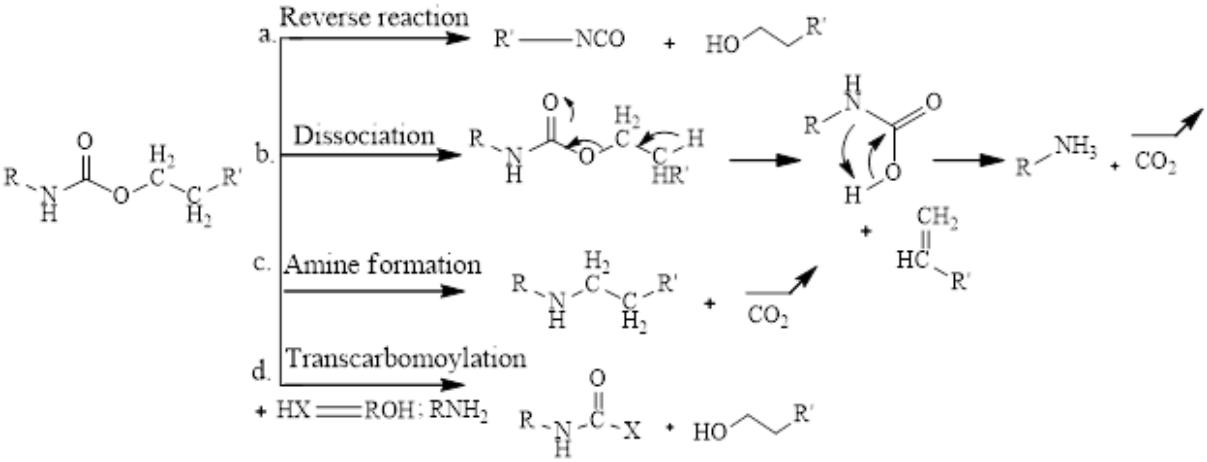

Source: Delebecq et al. (2012).

1.4.2 Application of isocyanates on the synthesis of polyurethanes

The reaction of a diisocyanate with a polyol gives rise to a polyurethane. Due to the great variability of polyols (polyether, polyester, polycarbonate, polyolefin), polyurethanes are very versatile, presenting a wide range of properties, e.g. elastomers, thermoplastics, foams (rigid and flexible), coatings, adhesives, sealants and fibers. The great advantage that makes polyurethanes competitive in the polymer market is the fact that this wide variety of materials can be prepared basically with two precursor diisocyanates, toluene

diisocyanate (TDI) and methylene diphenyl isocyanate (MDI) (DELEBECQ et al., 2012; WICKS; WICKS, 2001).

One or two types of diols can be used in the synthesis of polyurethanes, being a macrodiol, with a molar mass in the order of 5.10^3 g/mol and a short chain diol, usually 1,4-butanediol. The synthesis can be done by mixing the three components in solution, or by the initial preparation of a prepolymer, reacting the macrodiol with the isocyanate and, in a later step, the prepolymer with the short chain diol, which has the role of chain extender. In the synthesis of polyurethanes, the reaction of the isocyanate with water forming carbamic acid and, decomposing into primary amine and carbon dioxide, is used for the production of foams with different densities (DELEBECQ et al., 2012).

As shown in Figure 12, in the synthesis of the polyurethane there is a phase separation. The chains are grouped into rigid segments (rich in short chain diol) and flexible segments (rich in macrodiol). Generally, the rigid segments are semi-crystalline, with Tg in the range of 50-100 °C, while the flexible segments are amorphous, with Tg below room temperature. Melting temperatures range from 120-180 °C. The separation between rigid and flexible segments, together with the formation of hydrogen bonds between the urethanes also contributes to the versatility obtained in terms of mechanical properties. If the functionality of the polyol present in the rigid segment is greater than 2, the same process can be used for the production of a cross-linked polyurethane (DELEBECQ et al., 2012).

Figure 12 – Polyurethane synthesis.

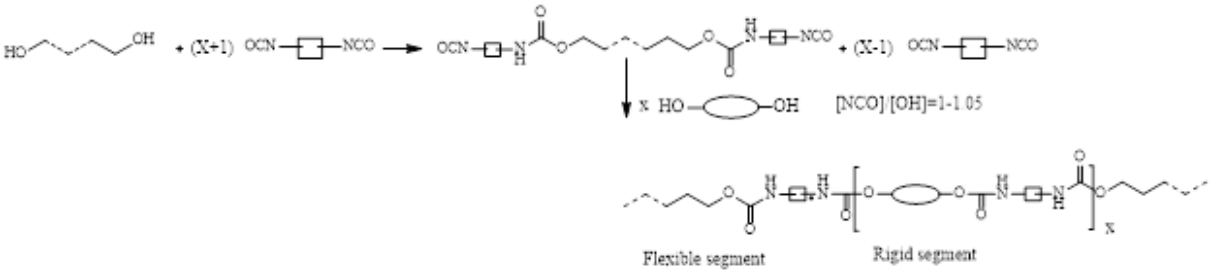

Source: Delebecq et al. (2012).

1.4.3 Blocked isocyanates and blocking agents

One strategy to deal with the high reactivity of isocyanates and susceptibility to hydrolysis is the production of blocked isocyanates. Blocked isocyanates are products that use the advantage of isocyanates to form compounds dissociable with increasing temperature. Below the so-called deblocking temperature, the blocked isocyanate has its reactivity and toxicity significantly reduced (WICKS; WICKS, 1999).

The blocking of the isocyanate occurs by the reaction of the NCO group with a molecule containing an active hydrogen that forms a weak and thermally reversible bond.

During heating, in the presence of a second nucleophilic molecule, the isocyanate reacts again to form more stable bonds, as shown in Figure 13. This reaction can occur through two mechanisms, namely elimination-addition or addition-elimination.

Figure 13 – Isocyanate reaction to form stable bonds: (a) Blocking and deblocking of an isocyanate molecule; and (b) Curing reaction of na isocyanate.

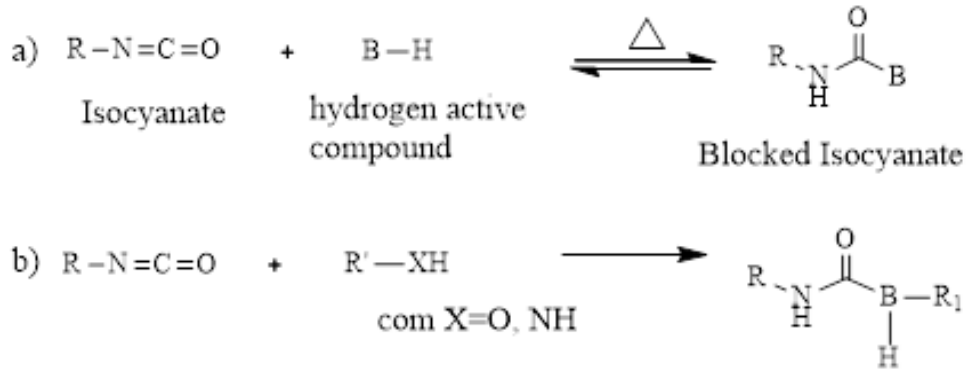

Source: Author.

In the elimination-addition mechanism, when the blocked isocyanate is heated at the deblocking temperature, the equilibrium tends to regenerate the isocyanate group, releasing the blocking agent (elimination). The free isocyanate then reacts with a nucleophilic molecule (NuH), forming more stable bonds (addition). Figure 14 illustrates the steps. The reaction rate can be estimated by Equation 1.1.

Figure 14 – Deblocking of a blocked isocyanate by the elimination-Addition mechanism.

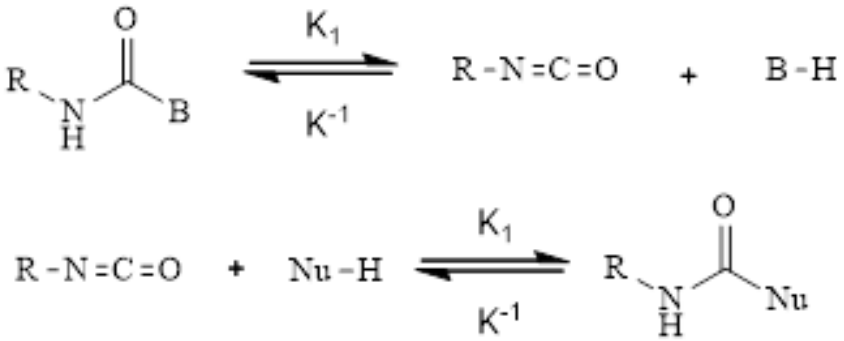

Source: Delebecq et al. (2012)

$$rate = \frac{K_1 K_2 [NuH][BI]}{K_{-1}[NH] + K_2[NuH]} \tag{1.1}$$

On the other hand, in the addition-elimination mechanism there is a pairing of the nucleophilic molecule (NuH) with the blocked isocyanate (addition), forming an intermediate tetrahedral compound. In a second step, the blocking agent (elimination) is released, as shown in Figure 15. The reaction kinetics can be studied by Equation 1.2. In general, at low temperatures the addition-elimination mechanism is favored, while at elevated temperatures, the elimination-addition mechanism is more likely. In general, aromatic blocked isocyanates unblock at a lower temperature than blocked aliphatic chain isocyanates, due to the greater potential for electron removal from the aromatic ring, compared to the aliphatic group (DELEBECQ et al., 2012; WICKS; WICKS, 1999).

Figure 15 – Deblocking of a blocked isocyanate by the Addition-Elimination mechanism.

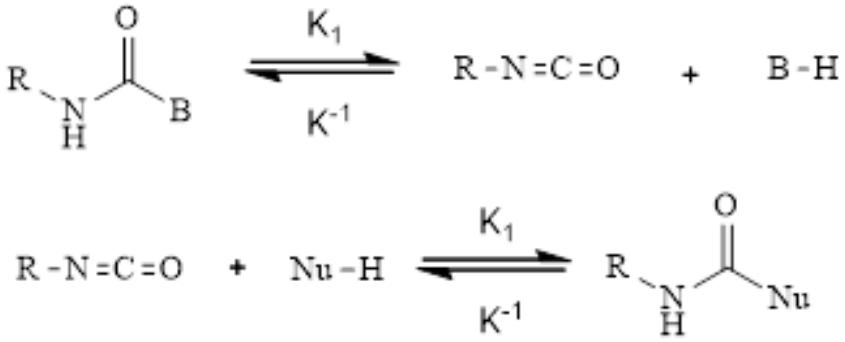

Source: Author.

$$rate = \frac{K_3[NuH][BI]}{K_{-3}[TI]} \tag{1.2}$$

The temperature at which the isocyanate is deblocked is governed mainly by the blocking agent. The, isocyanate deblocking is not on a specific temperature, but in a temperature range, which is commonly determined by a thermogravimetric analysis (TG). The characterization by TG allows to follow the loss of mass as a function of temperature due to the elimination of the blocking agent, as illustrated in Figure 16. Other techniques such as cone and plate rheometry, which measures viscosity as a function of temperature and differential scanning calorimetry (DSC), which provides alteration of the baseline as a function of the dissociation heat of the molecule can also be used to identify the release temperatures. However, these tests need to be carried out with care, since, unlike TG, which is done with the sample holder open, rheometry and DSC confine the sample. In the case of an equilibrium, the non-elimination of the blocking agent through its volatilization can alter the reaction kinetics, influencing the measurements. FT-IR and ^{1}H e ^{13} C NMR spectroscopy analyzes allow monitoring the change in vibrations relative to the NCO

group, measuring its appearance and disappearance as the blocking reaction proceeds (WICKS; WICKS, 1999; WICKS; WICKS, 2001). During a blocked isocyanate synthesis, the content of free NCO in the reaction medium can also be determined by titration with N-butylamine, as described in ASTM D-1638–74.

Figure 16 – Curve of Weight loss as a function of temperature, signing the elimination of the isocyanate blocking agent.

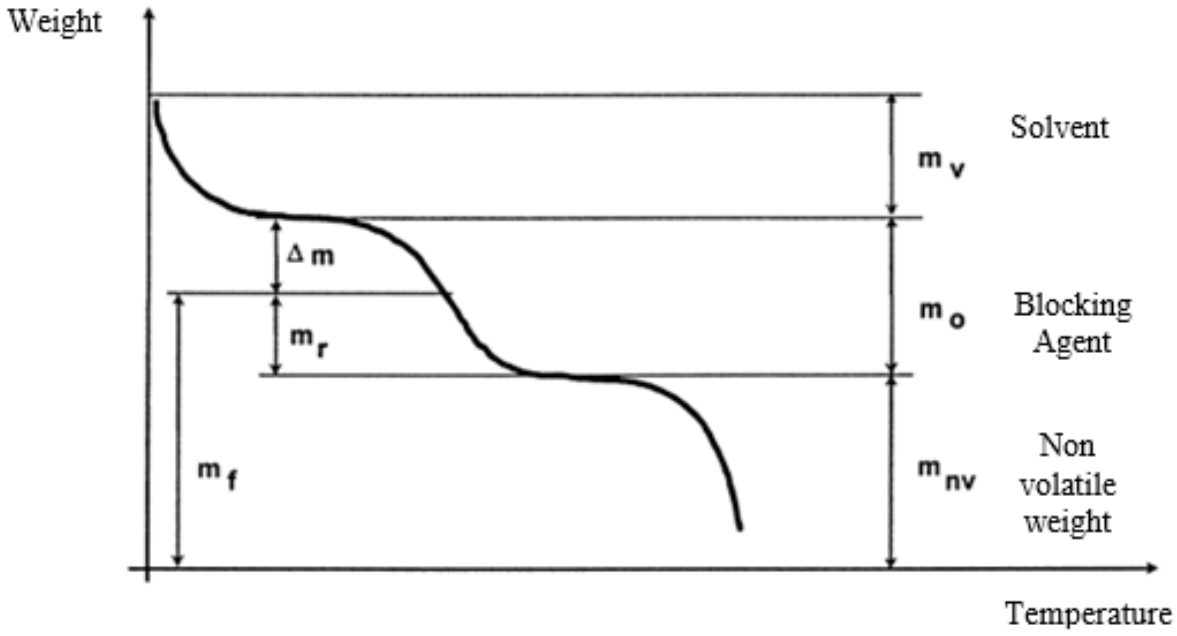

Source: Adapted from Wicks e Wicks (1999).

The most used blocking agents for obtaining blocked isocyanates are alcohols, phenols, caprolactams, cetoximes, acetoacetic esters and hydroxyamines. Phenols react more slowly with isocyanates than linear alcohols, deblocking at lower temperatures than aliphatic urethanes, in a slower reaction (WICKS; WICKS, 1999).

In general, it can be said that the carbonyl group of the blocked isocyanate is positively charged. Thus, the carbonyl carbon bond with the blocking agent is unstable and the smaller the difference between the charges in the group, that is, the lower the nucleophilicity of the blocking agent, the lower the bond strength. Due to the electronic withdraw effect of the aromatic ring, phenol has a lower blocking temperature than alcohols but higher than cyclic aliphatic compounds (Table 3). The applications of adducts vary according to the blocking agent, with frequent use of isocyanates blocked with aliphatic alcohols in aqueous systems for powder coatings and adhesives, also of latex for coating fabrics, while isocyanates blocked with caprolactams are more common in the paint industry (DELEBECQ et al., 2012; WICKS; WICKS, 1999).

Table 3 – A few blocking agents and its respective deblocking temperatures.

Blocking agent	Deblocking temperature (°C)
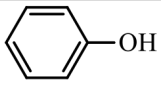 Phenol	>180
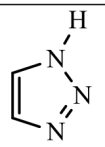 Triazol	180
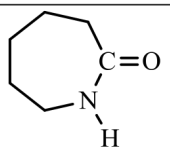 Caprolactam	150
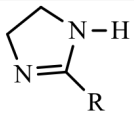 Imidazoline	160
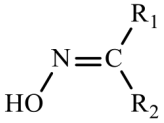 Oxime	130
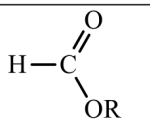 Formiate	110
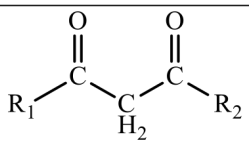 Diacetone	130

Source: Author.

The production of dimers or trimers is also an efficient strategy for producing blocked isocyanates. The advantage of this mechanism is that there is no need for a blocking agent, which needs to be volatilized and released later. Blocking occurs using only

the isocyanate molecules, as shown in Figure 17 (MEYER-STORK; HöCKER; BERNDT, 1992; WICKS; WICKS, 1999).

Figure 17 – Dimer formation from two isocyanate moieties.

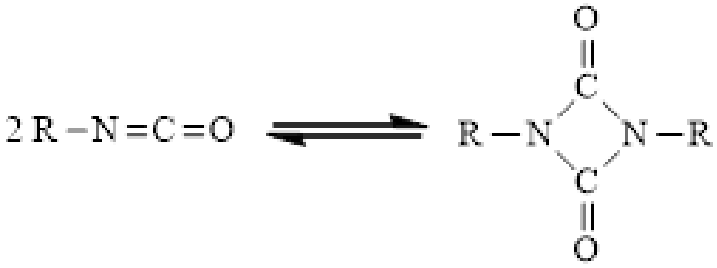

Source: Meyer-Stork, Höcker e Berndt (1992).

1.4.4 Application of blocked isocyanates on the modification of cellulose fibers

Since cellobiose has three hydroxyls in its structure, its functional groups are liable to be modified by the reaction with isocyanates, forming urethanes. Few studies have explored this possibility in the literature, mainly due to the difficulty of working with isocyanates in an aqueous medium, which easily promotes its hydrolysis. Studies are also limited by the toxicity of the compound (ROL et al., 2019). Blocked isocyanates have the advantage of reducing both limitations since they possses lower reactivity than free isocyanates until they are heated above their deblocking temperature and therefore are much less toxic.

Meyer-Stork, Höcker e Berndt (1992) used the possibility of formation of uretodione to introduce covalent bonds between regenerated cellulose molecules. The study was initially conducted on a model compound (cellobiose) and later applied to the polysaccharide. The reactions were monitored by FT-IR and ^{13}C-RMN. Figure 18 illustrates the process.

Figure 18 – Crosslinking reaction of cellobiose with dimers.

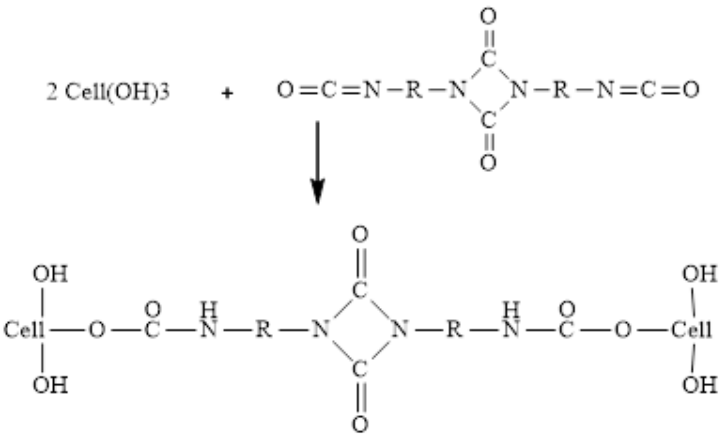

Source: Meyer-Stork, Höcker e Berndt (1992).

Carvalho, Curvelo e Gandini (2005) proposed a surface chemical modification treatment of thermoplastic starch (TPS) using a phenol-blocked isocyanate consisting of 1 mol of trimethylol propane, 3 mol of toluene and 3 mol of phenol (TMP-TDI-3Ph), whose trade name is Desmudur AP stabil®. The most efficient modification process reported by the authors consisted of immersing the TPS films in the blocked isocyanate solution, drying in N2 flow, delocking treatment at 170 °C for 10 minutes and washing. The surface modification was confirmed by an increase in the contact angle with water.

Gironès et al. (2007) proposed the use of blocked isocyanates and isocyanates containing linear alcohols and phenol as a compatibilizing agent in the preparation of apolar matrix composites (PS) reinforced with cellulose fibers. Coupling agents were incorporated via reactive extrusion and despite a moderate increase in mechanical properties, scanning electron microscopy images showed an increase in interfacial adhesion between fiber and matrix due to the presence of MDI and MDI-2F. As the main advantage of the treatment, the authors emphasized that there was no need for an organic solvent to incorporate the compatibilizing agent at the interface. In another study Gironès et al. (2008) applied the same methodology to make PP and pin fiber composites compatible, using phenol and linear alcohols of longer chain length as blocking agents. The results showed the difference in final properties due to the blocking agent used. In treatments with phenol-blocked MDI there was an increase in interfacial adhesion and mechanical properties, while in treatments with MDI blocked with long-chain alcohol, there was no significant increase in properties, since the adduct deblocking temperature was not reached.

Recently, Zhou et al. (2020), modified paper filter with MDI and confirmed that the treatment with isocyanate increases the hydrophobicity of the paper, in addition to increasing the wet resistance and bactericidal properties against *Escherichia coli*. Lu et al. (2020) applied blocked isocyanates to crosslink a hydroxyethylcellulose composite reinforced with (CNC), with a significant increase in the mechanical strength and thermal stability of the modified materials.

1.4.5 Possibilities not yet explored in the use of blocked isocyanates and cellulosic materials

In the literature, few studies are found using blocked isocyanates as agents of modification and/or compatibility of materials containing cellulose fibers. No nanocelluloses have been found to date.

As presented in section 1.3 nanocellulose films present greater compaction than paper due to the entanglement of fibers on a nanometric scale. This low permeable structure has the potential to be used in packaging films, membranes with selective permeability, flexible printed circuits, among others. Once the limitation of hydrophilicity is properly adddressed, in processes that allow production on a commercial scale at a competitive cost

and through a route that results in a low environmental impact, these films will possibly be viable alternatives to the use of petroleum-derived polymers. The chemical modification of nanocellulose films through blocked isocyanate treatments has the potential to increase hydrophobicity, resistance to contact with water and decrease the permeability to water vapor and oxygen.

1.5 Beeswax

Beeswax is a natural material with a complex structure, composed mainly of monoesters (35%), diesters (14%), mono- and polyester hydroxides (12%), hydrocarbons (14%) and free acids (12%) (TULLOCH, 1980). Its use as a coating of cellulosic materials for hydrophobization is known in the literature and industry, mainly to increase the moisture resistance of cardboard (MORRISSETTE et al., 2018; TEDESCHI et al., 2018; BHARATHI et al., 2021). Recently, its use with nanocelluloses has shown promise for obtaining films resistant to water and with barrier properties (FORSMAN et al., 2017; LU et al., 2014; PAN et al., 2015; SETHI et al., 2019; YANG; PAULSON, 2000; ZHANG; XIAO, 2013; ZHANG; XIAO; QIAN, 2014). In addition, as the wax can be ingested, its applications extend to edible films and coatings for capsules of controlled release of drugs and essential oils, with the objective of slowing down the digestion speed of the compounds in the digestive system (CEREMPEI et al., 2015; CHITPRASERT; SUTAPHANIT, 2014; NGAMEKAUE; CHITPRASERT, 2019).Another point is that the presence of wax in the composition of cellulose-derived films can accelerate its degradation (CHOI; KANG; CHO, 2016; JEONG et al., 2014), a desirable feature for short term use packaging.

Nonetheless, the literature shows that covering NFC food films with beeswax has some limitations, because during storage under refrigeration, the outer layer of wax becomes brittle and tends to become cracked, damaging the barrier membrane and impairing the use of film (SPENCE et al., 2011). AIn addition, some studies show that in compositions where the wax is dispersed in the bulk, there is a decrease in the interaction between the cellulose fibers, considerably decreasing the mechanical properties (INDRIYATI; INDRARTI, 2018). The challenge of using the wax is to incorporate it into the NFC film without significantly changing the mechanical properties, while providing greater water resistance and low gas permeability.

2 OBJECTIVES

The purpose of this thesis is to manufacture nanofibrillated cellulose (NFC) films with good mechanical properties, hydrophobic character and low permeation to H_2O vapor and O_2. To achieve this objective, four different routes have been proposed, which are related to each other depending on the use of chemical modification agents or the use of hydrophobic agents through aqueous emulsions. Therefore, three of the methods involve chemical modification by the use of blocked isocyanates and one of the proposed methods involves physical modification by the use of beeswax. The chemical modification strategies are divided into: : i) surface modification of the film by diping in solution), ii) emulsion modification by mixing NFC suspension and blocked isocyanate solution; iii) synthesis of blocked isocyanate macrodiol and its use in the preparation of crosslinked NFC composites. The specific objectives were:

1. Establish a drying protocol for aqueous suspensions of nanofibrilated cellulose (NFC) to obtain homogeneous, smooth and compact films, which are free of edge defects.
2. Characterize the changes made in the structure of the obtained films along with the thermal, mechanical, morphological and barrier of water vapor and oxygen properties.
3. Compare the different modification routes used depending on the properties presented by the films and the ease of the manufacturing process.

The thesis is that combining an adequate drying process with a hydrophobization step, NFC films acquire greater resistance to the presence of water and have an increased gas barrier, expanding the range of applications (mainly in packaging). Each paper presented in Chapter 4 corresponds to the results obtained (and in some cases already published) for each strategy.

3 THEORETICAL BACKGROUND

3.1 Surface phenomena

3.1.1 Surface tension

In a liquid phase surrounded by air in all directions, each molecule is attracted by the adjacent molecules. However, at the interface of the liquid with the external environment (air), the molecules are not surrounded by the largest possible number of close neighbors, experiencing void in one direction. This situation forces the liquid molecules to reorganize themselves in order to seek an equilibrium configuration (i.e., less energy state). In this way, the molecules in the last layer become more stressed than those inside the liquid, creating what is called surface tension. Therefore, the tension at the interface is necessary to balance the preference of the molecules to diffuse into the liquid phase. In a solid, the cohesive force between the molecules in the form of mechanical resistance is greater than the surface tension, thus it is impossible to measure the surface tension independently and it is measured indirectly, through the use of liquids (contact angle) or gases (gas chromatography) (HUBBE; GARDNER; SHEN, 2015).

The interaction forces responsible for surface phenomena can be Van der Waals forces, whose interactions are subdivided into Keesom forces (two permanent dipoles), Debye forces (one permanent and one induced dipole) and London or Lifshitz dispersive forces (between two instantly induced dipoles). Dispersive forces are the main components of Van der Waals' forces since Keesom's forces are at least an order of magnitude less than the dispersive component (HUBBE; GARDNER; SHEN, 2015).

The interactions can also be of the hydrogen bonding type, Lewis acid or base, ionic forces or metal bonds. London forces are the main cohesive forces in solids and liquids commonly encountered. This is because they generally present greater contributions to the surface tension values than the other forces since they do not necessarily depend on the presence of specific chemical groups on the surface, as is the case, for example, with hydrogen bonds. The Hamaker constant is indicative of the intensity of the dispersive forces. The higher the value of a material's Hamaker constant, the greater the influence of dispersive forces on its surface tension. For example, lignin, due to the presence of aromatic rings, has a greater Hamaker constant than cellulose (HUBBE; GARDNER; SHEN, 2015).

All materials have an attractive force between them due to the action of dispersive forces. Thus, the London forces are responsible for a portion of the surface tension of liquids and the contribution of that portion can be measured by measuring the angle of contact with nonpolar liquids, such as, for example, diiodomethane (DIM). While the polar components of the surface energy are relatively easy to be changed depending on the

treatments applied, it is extremely difficult to change the dispersive component. In general using only two liquids, such as DIM and water, it is possible to classify different surfaces with respect to their dispersive forces and polar nature (HUBBE et al., 2008; HUBBE; GARDNER; SHEN, 2015; RAS; TIAN; BAYER, 2017).

3.1.2 Wettability

Wettability is a fundamental property of solid surfaces and can be defined as the tendency of a given liquid to wet, i.e., to spread on the surface when both come into contact. The angle formed between the liquid and the surface is defined by the interaction of the three phases involved (solid, liquid and gaseous) and is called the contact angle. Its value will depend on the nature of the liquid (polar or non-polar) as well as the nature of the surface. When the test fluid is water, the measured contact angle is called WCA (Water Contact Angle). The scattering coefficient S measures the tendency of the liquid to spread over the surface and is measured by the difference between the surface tension of the liquid (σ_1), the surface tension of the solid (σ_2) and the interfacial tension ($\sigma_{1,2}$). If S is positive the phase under consideration spreads over the surface, if S is negative the wetting is not complete (HUBBE; GARDNER; SHEN, 2015; SONG; ROJAS, 2013).

In general, materials with high affinity for water, or hydrophilic, have WCA below 90° while materials with low affinity for water, or hydrophobic, have WCA greater than 90°. The energy balance in the line of intersection of the phases can be obtained by the equation of Young (Equation 3.1), where γ_{SV}, γ_{SL} e γ_{LV} are the energies attributed to the forces acting between solid-vapor, solid-liquid and liquid-vapor, respectively and θ is the contact angle. Young's relationship considers an ideal case, that is, a case where the surface is perfectly smooth at an atomic level (without roughness), chemically homogeneous and not changeable by interaction with the liquid. In addition, the relation (1) assumes that the contribution portion of the different existing forces, which result in the global energy of the surface under study, are independent and do not overlap (HUBBE; GARDNER; SHEN, 2015; SONG; ROJAS, 2013).

$$\cos(\theta) = \frac{\gamma_{SV} - \gamma_{SL}}{\gamma_{LV}} \tag{3.1}$$

Young's equation is a limited approximation, but it is valid when applied in a macroscopic perspective, i.e, far from the contact line between the three phases. According to the equation (3) the largest contact angle is achieved by the lowest value of γ_{SV}, that is, a material with the lowest possible surface energy. The lowest surface energy ever measured is 6,7 mJ/m^2, for densely packed trifluoromethyl groups (-CF_3), and provides a WCA of approximately 120° (HUBBE; GARDNER; SHEN, 2015).

In nature, it is extremely difficult to find perfectly flat and smooth materials as assumed by Young's model and, therefore, in most cases, roughness must be considered. Another point is that, working with cellulose fibers, there is a naturally roughness of the material and, therefore, the effect of the morphology must be accounted for in the contact angle. In addition, so-called superhydrophobic materials have WCA values much greater than 120°, which cannot be explained by Young's equation (HUBBE; GARDNER; SHEN, 2015).

Adding a roughness factor r to Young's relationship, Equation 3.2 is obtained, which defines the Wenzel model, where r is the ratio between the real area of a rough surface and the ideal area of its geometric projected shape (HUBBE; GARDNER; SHEN, 2015).

$$\cos(\theta') = \frac{r(\gamma_{SV} - \gamma_{SL})}{\gamma_{LV}} = r\cos(\theta) \tag{3.2}$$

Since r will always be greater than the unit, 90° is a critical contact angle value. When θ is less than 90 ° the roughness factor will decrease the contact angle θ' and when θ is greater than 90°, the same factor will increase θt. That is, according to this relationship, the roughness will increase the wettability of a hydrophilic surface and decrease the wettability of a hydrophobic surface. Therefore, the roughness amplifies both hydrophilicity and hydrophobicity (HUBBE; GARDNER; SHEN, 2015; SONG; ROJAS, 2013).

The Wenzel model is accurate in calculating the contact angle when the tested liquid is capable of wetting the entire surface under study. That is, when the liquid "fills in" the roughness. However, depending on the geometry of the roughness, the surface depressions can act as pores, trapping air and not allowing the liquid to wet the entire surface. In this case, the Wenzel relation is adapted for the Cassie-Baxter model. In this model, in addition to the morphological factors, the chemical factors that affect wettability are also taken into account. In the Cassie-Baxter (Equation 3.3), f represents the fraction of the surface actually in contact with the liquid, since the liquid touches the solid material only at the peak points of the roughness. In this equation it is assumed that the contact angle between the liquid (usually water) and the air is 180°. The transition from the Wenzel model to Cassie-Baxter occurs when θt $= \theta_c$, that is, when there is a change between a fully wetted surface to a case where the liquid interacts with the solid only in some points of contact θ_c is a function of f e r according to the Equation 3.4 (HUBBE; GARDNER; SHEN, 2015; SONG; ROJAS, 2013).

$$\cos(\theta') = f\cos(\theta) + (1-f)cos(180^\circ) = fcos(\theta) + f - 1 \tag{3.3}$$

$$\cos(\theta_c) = \frac{f-1}{r-f} \tag{3.4}$$

The essential features of the models discussed above are summarized in 19. Although evolving in complexity and considerations, Young's (Figure 19a), Wenzel (Figure 19b) e Cassie-Baxter (Figure 19c) models do not take into account possible partial penetration of the liquid into the surface when liquid and surface exhibit high affinity. This occurs, for example, in the case of water and cellulose, where the high interaction through the hydrogen bonds causes the water molecules to permeate the solid structure between the inter- and intra-molecular bonds of the anhydroglucose units in the amorphous region, causing the material to swell. For this type of system, the equations are more complex and difficult to be faithfully modeled, especially when the so-called static contact angle is desired (HUBBE; GARDNER; SHEN, 2015).

Figure 19 – Surface wettability depending on the model studied, being (a) Young, representing the ideal case of a totally smooth surface, without roughness (b) Wenzel, where the liquid totally wets the rough surface of the material and (c) Cassie-Baxter, where the liquid only touches the roughness peaks, with air being trapped in the cavities.

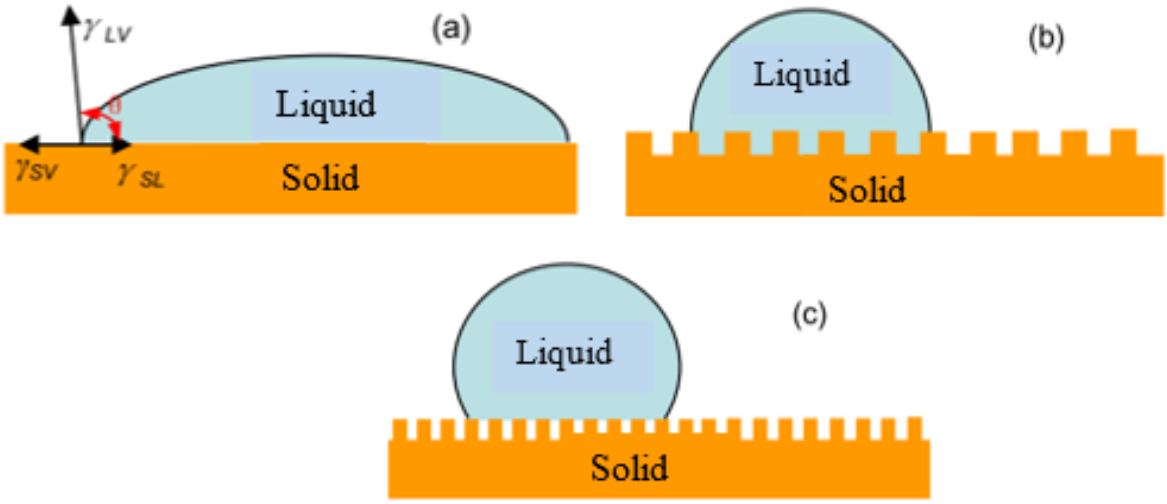

Source: Adapted from Song e Rojas (2013).

A common way of measuring whether the test liquid is in close contact with the surface (Wenzel regime) or if it has only points of tangency between the liquid and the solid (Cassie-Baxter regime) is by measuring the advance angle and of the retraction angle. This test consists of depositing a drop of liquid on the surface, which after reaching equilibrium is tilted continuously and, at the limit of the drop's movement (sliding), the advancing and retracting angles are measured. Surfaces with a low sliding angle are found in the Cassie-Baxter regime. On the other hand, surfaces with a high sliding angle are

in the Wenzel regime, because the intimate contact between the surface and the liquid restricts the movement of the drop (HUBBE et al., 2008; RAS; TIAN; BAYER, 2017).

When the static contact angle is measured, it is considered that the system has been given enough time so that the drop and the surface have reached a balance of forces and that this angle will no longer change over time. However, equilibrium may not be achieved or even achieved and passed, since the absorption effects by the capillarity and diffusion mechanisms can occur quickly after the contact of the liquid with the surface, as is the case of the water/cellulose system. In addition, since the structure of paper and also of nanocellulose films is complex, formed by a network of packaging fibers and nanofibers, the morphology, composed of roughness and possible surface porosity, makes it more difficult to accurately quantify the contact angle, mainly because the water can cause swelling and plasticization of the structure (HUBBE; GARDNER; SHEN, 2015).

From an experimental point of view, it is usually possible to take accurate measurements at intermediate time intervals, that is, between the moment of drop contact and total equilibrium. In this case, the angle is called the apparent contact angle. In the present work, the equipment used allowed to monitor the evolution of the WCA value as a function of time for relatively small time intervals (14 milliseconds), where the drop of water showed a tendency to reach a plateau of contact angle as a function of time within a short period of time (640 milliseconds).

Another point regarding the interaction between liquids and surfaces is that wettability is extremely sensitive to imperfections in the composition due to contamination on the surface. In the case of cellulose, the contamination may be from the biomass itself (lignin, hemicellulose and fatty acid residues). Superficial chemical modifications can also increase the hydrophobic character of cellulosic materials. This phenomenon is interesting from an industrial point of view because, a cellulosic material more resistant to wetting with water for example will be less susceptible to its plasticizing effect and will be able to maintain its mechanical, thermal properties and dimensional stability in humid environments. In addition, this fact calls attention to the need to take several measurements and in different regions of the surface under study in order to acquire WCA values with greater reliability (RAS; TIAN; BAYER, 2017).

In the paper industry, the practical use of the wettability measurements is to check the adhesion of cellulose with various adhesives and resins, always looking for higher values of wettability for greater adhesion. Since wettability is directly related to an excess of surface energy, the greater the surface energy of the substrate (paper, cardboard, etc.) given by a contact angle below 90°, the greater the potential for bond (HUBBE; GARDNER; SHEN, 2015).

3.1.3 Superhydrophobic materials

A material that has a contact angle with water higher than 150 ° and a sliding angle lower than 10 ° is called superhydrophobic. Such material also has morphological characteristics that make it difficult to wet the surface, which allows its application in products that require non-stick and self-cleaning surfaces (HUBBE; GARDNER; SHEN, 2015; RAS; TIAN; BAYER, 2017; SONG; ROJAS, 2013). Producing a superhydrophobic surface is not in the scope of the present work, since no efforts will be made to increase the roughness beyond that already naturally presented by the studied cellulosic materials. However, efforts were made to precisely measure the roughness of the films obtained since compositions with non-homogeneous surfaces can lead to differences in contact angle measurements, which can superimpose on the effect of the proposed chemical and physical modifications and consequently, be misinterpreted.

3.2 Water Absorption

After wetting, water is absorbed by the surface. The measure of water absorption can be performed by direct immersion of the material in water or, when it has the potential to be dismantled or dissolved by direct contact with water, by exposing the material to an environment with a relative humidity controlled at 95%. The absorption of water (or water vapor) can then be calculated by Equation 3.5, where M_t is the mass at the measurement time t and M_0 is the dry mass, at time equal to zero (DUFRESNE; DUPEYRE; VIGNON, 2000).

$$\frac{M_t - M_o}{M_o} \times 100 \tag{3.5}$$

The mass of water absorbed as a function of time t can be expressed by Equation 3.6, where M_∞ is the mass of water absorbed at equilibrium, $2L$ is the thickness of the film and D is the diffusion coefficient (DUFRESNE; DUPEYRE; VIGNON, 2000).

$$\frac{M_t - M_0}{M_\infty} = 1 - \sum_{n=0}^{\infty} \frac{8}{(2n+1)^2 \pi^2} xexp\left[\frac{-D(2n+1)^2 \pi^2 t}{4L^2}\right] \tag{3.6}$$

In short time intervals, Equation 6 can be reduced to Equation 3.7. When $\frac{M_t - M_0}{M_\infty} < 0,5$ the error of Equation 3.7 in the determination of the diffusion coefficient is less than 0,1% (DUFRESNE; DUPEYRE; VIGNON, 2000).

$$\frac{M_t - M_0}{M_\infty} = \frac{2}{L}\left(\frac{D}{\pi}\right)^{1/2} t^{1/2} \tag{3.7}$$

Generally, two distinct absorption zones are observed for cellulosic materials. In zone I, which occurs for $t \leq 100$ h, the absorption kinetics is fast whereas in zone II the absorption is slow and reaches a plateau, where the saturation point is measured. The diffusion coefficient D can be obtained through the trend line of the graph of $\frac{M_t - M_0}{M_\infty}$ as a function of $(\frac{t}{L^2})^{1/2}$ (DUFRESNE; DUPEYRE; VIGNON, 2000; LAVOINE et al., 2012).

3.3 Oxygen and water vapor permeation

The permeation of a gas through a non-porous solid material takes place in three stages. First, gas adsorption occurs on the surface followed by diffusion in the material structure, ending with desorption on the opposite surface. In this process, three parameters can be calculated: the transmission rate, the permeation and the permeability. The transmission rate is the volume or mass of the permeating gas passing through the film per unit of surface area and time, within the equilibrium of the test conditions. Permeation is the rate of transmission divided by the partial pressure difference across the film section. The permeability in turn is the permeation multiplied by the thickness of the film. Table 4 summarizes the equations and units of the main parameters related to the oxygen and water vapor permeation (WANG et al., 2017).

Table 4 – Barrier properties, equations, and units.

Barrier Property	Equation	Unit
Water Vapor Transmission Rate (WVTR)	$WVTR = \frac{weight}{area.time}$	$g.m^{-2}.day^{-1}$
Water Vapor Permeability (WVP)	$WVTR = \frac{WVTR.thickness}{\Delta pressure\%RH}$	$g.\mu m.m^{-2}.day^{-1}.kPa^{-1}$
Oxygen Transmission Rate (OTR)	$OTR = \frac{volume}{area.time}$	$cm^{-3}.m^{-2}.day^{-1}$
Oxygen Permeability (OP)	$OP = \frac{OTR.thickness}{\Delta pressure}$	$cm^3.\mu m.m^{-2}.day^{-1}.atm^{-1}$

Source: Wang et al. (2017).

In general, the permeability is independent of the thickness of the material if it is thick enough (thickness $>$ 10 μm). The units of the international system of $mol/m.s$ and barrers are reported in the literature. Nonetheless, $cm^3.\mu mm^{-2}.day^{-1}.atm^{-1}$ e $g.\mu m.m^{-2}.day^{-1}.kPa^{-1}$ are the most used for OP and WVP for being more intuitive of the occurring physical phenomenon (WANG et al., 2017).

In food packaging, the water vapor barrier mainly prevents the plasticization of food while the oxygen barrier prevents oxidation and bacterial activity. For application in MAP (modified Atmosphere Packaging), the recommended OTR is 10-20 $cm^3.m^{-2}.day^{-1}$. NFC films generally have low OTR values in low relative humidity, with properties superior to that presented by cellophane. When the humidity is above 65% the water limits the

hydrogen bonds between the fibers, leaving the films less compact and more permeable to oxygen (LAVOINE et al., 2012).

The water vapor transmission test is performed according to the standard ASTM E96 (ASTM, 2002). The dissecting method of the standard consists of coupling the film under study to an open circular container with a minimum area of 3000 mm^2, previously filled with 15 g (6 cm high from the bottom) of calcium chloride desiccant salt. The device is then sealed at the edges with a sealing ring, closed with a hollow cover and placed in an environment with controlled humidity of 50%. The moisture gradient is the driving force for the permeation of water vapor from the environment into the container, diffusing through the film. The standard recommends between 6-10 spaced measurements over the period of the test, to draw the curve of change of mass as a function of time. Figure 20 shows the schematic drawing and photos of the device that was machined in aluminum for this test.

Figure 20 – Schematic drawing of the permeation testing cup, designed for the water vapor transmission rate test according to ASTM E96; and Photo of the system during the test.

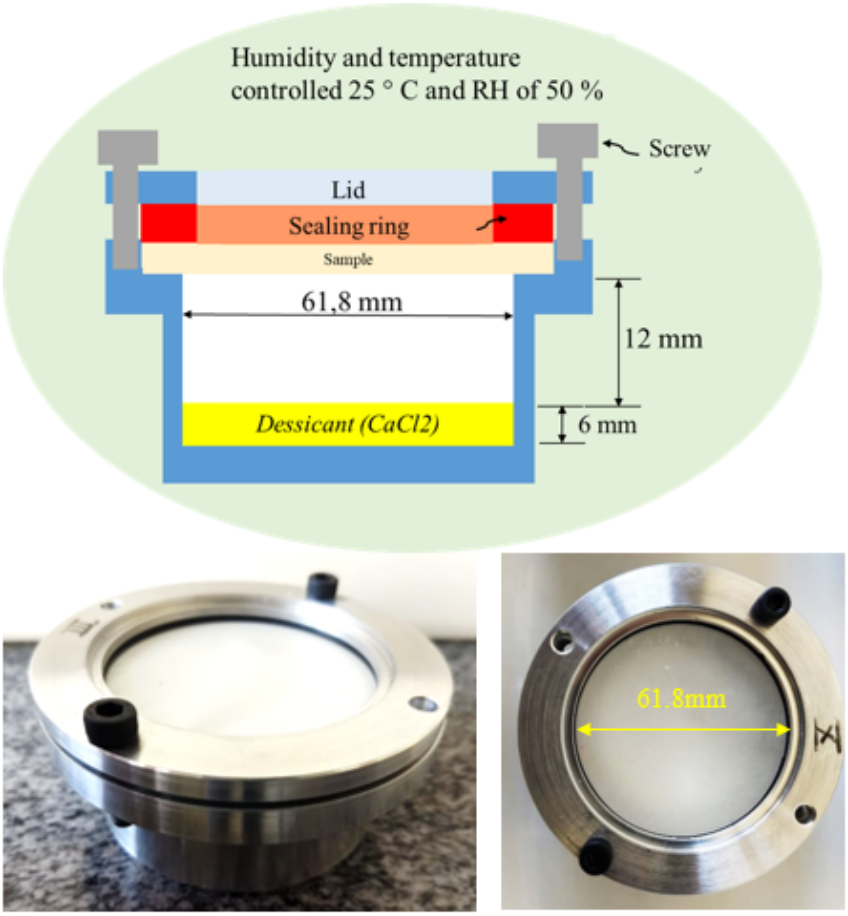

Source: Author

From the graph of change in mass as a function of time with the minimum of necessary measures, the linear trend line is estimated and its slope is the rate of vapor transmission. The WVTR can be calculated from Equation 3.8 below, where G/t) is the slope calculated in g/h and A is the mouth area in m^2 (ASTM, 2002; LAVOINE et al., 2012; SPENCE et al., 2011).

$$WVTR = \left(\frac{G}{t}\right)/A \tag{3.8}$$

The permeation can then be calculated by the Equation 3.9, where ΔP is the pressure vapor difference in mmHg (1,333 x10^2 Pa); S is the saturation of the vapor pressure at the test temperature, R1 and R2 = relative humidity (%) of the environment, and inside the glass, respectively.

$$Permeation = \frac{WVT}{\Delta P} = \frac{WVT}{S(R1 - R2)} \tag{3.9}$$

S can be obtained by Equation 3.10, where T is the room temperature in Kelvin.

$$S = e^{(77{,}3450+0{,}0057*T-\frac{7235}{T})}/T^{8,2} \tag{3.10}$$

The transport of H_2O vapor vapor in paper can occur through the mechanisms of diffusion between fibers, by Fick diffusion, by Knudsen diffusion, by surface diffusion, bulk diffusion and capillarity. Inter-fiber diffusion is the dominant mechanism on paper, since it occurs at a higher rate. In the case of NFC films, where the volume and size of the voids are smaller, Fick and Knudsen diffusion are the main mechanisms. Knudsen diffusion occurs when the pore diameter is less than 10 nm (SPENCE et al., 2011).

For Knudsen's mechanism to be dominant over Fick's, the Knudsen number N_{kn} (Equation 3.11) must be greater than 10. When N_{kn} is close to unity, the regime is transient between Fick and Knudsen diffusion. In Equation 3.11, λ is the free path and is worth 66.38 nm, while r is the mean radius of the material pore (SPENCE et al., 2011).

$$N_{kn} = \frac{\lambda}{2r} \tag{3.11}$$

The equation for the molar flow of the Knudsen N_A diffusion in the z direction is defined by Equation 3.12, where D_{KA} is the diffusivity in $m^2.s^{-1}$ and dca/dz is the concentration gradient component in the z direction. The concentrations C_i (interior) and C_e (exterior) in $mol.m^{-3}$ are calculated by Equation 3.13, where local RH is the difference of relative humidity between inside and outside respectively. $Psat$ is the vapor pressure at temperature T and R is the universal gas constant (8,314 m^3.Pa. $mol^{-1}.K^{-1}$). D_{KA}

diffusivity is defined by Equation 3.14, with $2r$ being the pore diameter and MA the molar mass of the permeate gas in g.mol^{-1} (SPENCE et al., 2011).

$$N_A = -D_{KA}\frac{dc_A}{dz} \tag{3.12}$$

$$C_i - C_e = \frac{(RH_i - RH_e)\,.Psat}{100RT} \tag{3.13}$$

$$D_{KA} = 97.\,(2r)\,.\left(\frac{T}{M_A}\right)^{1/2} \tag{3.14}$$

The main difference between the Fick and Knudsen diffusions is that the Knudsen coefficient takes into account the molecular movement based only on pore size, while the Fick coefficient is calculated from a more complete measure that takes into account the movement of all molecules subjected to the concentration gradient. That is, unlike Knudsen's diffusion, Fick's diffusion is also affected by the composition and/or chemical modification of the material. Flow J (mol.cm^{-2}.s^{-1}) can be obtained by the Equation 3.15 with D_{eff} being the effective diffusion coefficient (cm^2.s^{-1}) and H is the thickness of the film (cm).

$$J = \frac{\left(\frac{G}{t}\right)}{A} = \frac{D_{eff}}{H}\,(c_i - c_e) \tag{3.15}$$

With the data from the permeation test, Equation 3.16 can provide the value of the Fick diffusion coefficient Fick D_{eff}, which is composed of two parts, namely the diffusivity related to the transport between the pores and the diffusivity related to the transport through the surface, represented in Equation 3.16. D_a is the interporus diffusivity and D_f is the intrinsic diffusion of the fibers; τ is the tortuosity, and ε is the porosity fraction.. It is estimated that the relationship between D_f e D_a is 0.02. Therefore, the second portion of the sum can be discarded and interpore diffusion determined only based on the porosity and tortuosity values (SPENCE et al., 2011).

$$D_{eff} = D_a\frac{\varepsilon}{\tau_p} + D_f\frac{(1-\varepsilon)}{\tau_f} \tag{3.16}$$

4 HYPOTHESIS OF PAPERS AND PAPERS PRESENTATION

Below are listed the main hypotheses of the experimental procedure that resulted in five papers. The published or submitted version of the manuscripts are presented below, which can be changed due to the submission process of each journal. Chapter 5 presents a comparative discussion between the papers. Chapter 6 presents the conclusions and Chapter 7 the suggestions for future work.

4.1 (Paper 1) – Surface hydrophobization of pulp paper and nanofibrilated cellulose film using blocked diisocyanates

The objective of the first work was the synthesis of MDI adducts with a functionality blocked with phenol and the other with a linear alcohol of varying chain length. The isopropanol, butanol, octanol, dodecanol and octadecanol alcohols with 3, 4, 8, 12 and 18 carbon atoms in the chain, respectively, were used. The hydrophobization process was performed by a dipping followed by thermal treatment and the effect of this process was measured by the variation of the contact angle with water, as already done by Carvalho et al (2005), for TPS films. The initial hypothesis was that, treating the surface of NFC films (and also cellulose pulp) with adducts of varying chain length, there would be a progressive increase in the contact angle, due to the increase chain length of the pending group attached to the film surface by the formation of new urethanes bonds, after deblocking the phenol. Both effects of chemical modification and the difference in roughness (NFC film or pulp) on increasing the angle of contact with water were studied. *This paper was submitted to the Industrial crops and Products.*

4.2 (Paper 2) - Low permeable hydrophobic nanofibrilated cellulose films modified by dipping and heating processing technique

In the second work, the blocked adduct that had the greatest hydrophobization effect in the first work, that is, the one whose treatment resulted in the greatest contact angle with water, was used to hydrophobize NFC films of larger dimensions, in order to study the effect of surface hydrophobization in properties like water absorption, vapor permeation to water and oxygen in films. The initial hypothesis was that in addition to the increase in the contact angle, the surface treatment would also assist in increasing the water vapor and oxygen barrier properties of the base film. The experimental procedure in article 1 was repeated. *This paper was published on Cellulose (http://link.springer.com/10.1007/s10570-020-03619-3)*

4.3 (Paper 3)- Nanofibrillated cellulose films modified by blocked isocyanates emulsions: Barrier properties to water vapor and oxygen

The objective of the third work was to change the hydrophobization strategy. Instead of concentrating the adducts on the surface of the material, creating a hydrophobic layer, an emulsion was made of two isocyanates blocked with phenol, one bi and one tri-functional, which were mixed with aqueous suspensions of NFC and dried to obtain films. After drying, the thermal treatment to release the isocyanates was carried out, releasing the phenol and creating new urethane bonds, chemically modifying the internal structure of the films. The hypothesis of this work was that the performance of a superficial hydrophobization treatment, (as performed in other works) may not be enough to inhibit the plasticizing effect of water when the film is wet or is in a high humidity environment, since in this case, water diffuses into the structure. If the modifying agents were dispersed among the fibers during the drying of the film, in a subsequent heat treatment, connection points between the fibers would be created, being more efficient for maintaining the mechanical and barrier properties of the films in a humid environment. *This paper was submitted the carbohydrate polymer technologies and application.*

4.4 (Paper 4) - Nanofibrilated cellulose (NFC)/Polyethylene Glycol (PEG) composite films crosslinked with blocked isocyanates: enhanced mechanical properties, thermal stability and barrier to oxygen

In the third work, since the internal connection points were created between the nanofibers through the formation of urethane bonds, the resulting films showed brittle behavior, that is, the maximum deformation significantly decreased compared to the non-modified NFC films. In the fourth work, a solution was proposed for this limitation, in which a macrodiol was used to produce isocyanate adducts blocked with a longer chain. The hypothesis of this work was that the larger chain of the blocked macrodiol would allow greater mobility between the fibers, though maintaining the water resistance and barrier properties presented in the third work. As a result, the strain at break would be greater, increasing the range of applications of packaging films. *This paper was submitted to the journal of applied polymer science.* .

4.5 (Paper 5) - Nanofibrilated Cellulose/Beeswax Films: Barrier Properties and Perspective Application in Packaging

Differently from other works in which the strategies used for hydrophobization were based on chemical modification, the fifth work sought a solution based on physical modification, by preparing NFC and beeswax composites through the drying of stable emulsions. A green production route was used, that is, without the use of organic solvents and only with biodegradable raw materials and from renewable sources. The hypothesis

of the work was that on drying, the hydrophobic beeswax would coat the nanofibers, decreasing the wettability with water, filling in the inter-fiber voids and consequently reducing the permeation. In this case, the films obtained would be hydrophobic, with low gas permeation and with potential for application in food films. *This paper was submitted to ACS sustainable Chemistry and Engineering*

PAPER 1

Surface hydrophobization of pulp and nanofibrilated cellulose using blocked diisocyanates

Gustavo de Souza, Ricardo Klaus Kramer, Antonio Jose Felix Carvalho*

*toni@sc.usp.br

São Carlos School of Engineering, University of São Paulo, CEP 13566-590, São Carlos, São Paulo, Brazil

Highlights

- Blocked diisocyanates with pendant chain length with 3 to 18 carbons were synthetized;
- Pulp and nanofibrilated cellulose films were modified by a dipping and heating process;
- Hydrophobization led to Water Contact Angle of 144° for pulp and 113° for NFC film;
- WCA increased with the increase of adduct chain length and with surface roughness;

Table of Content (TOC)

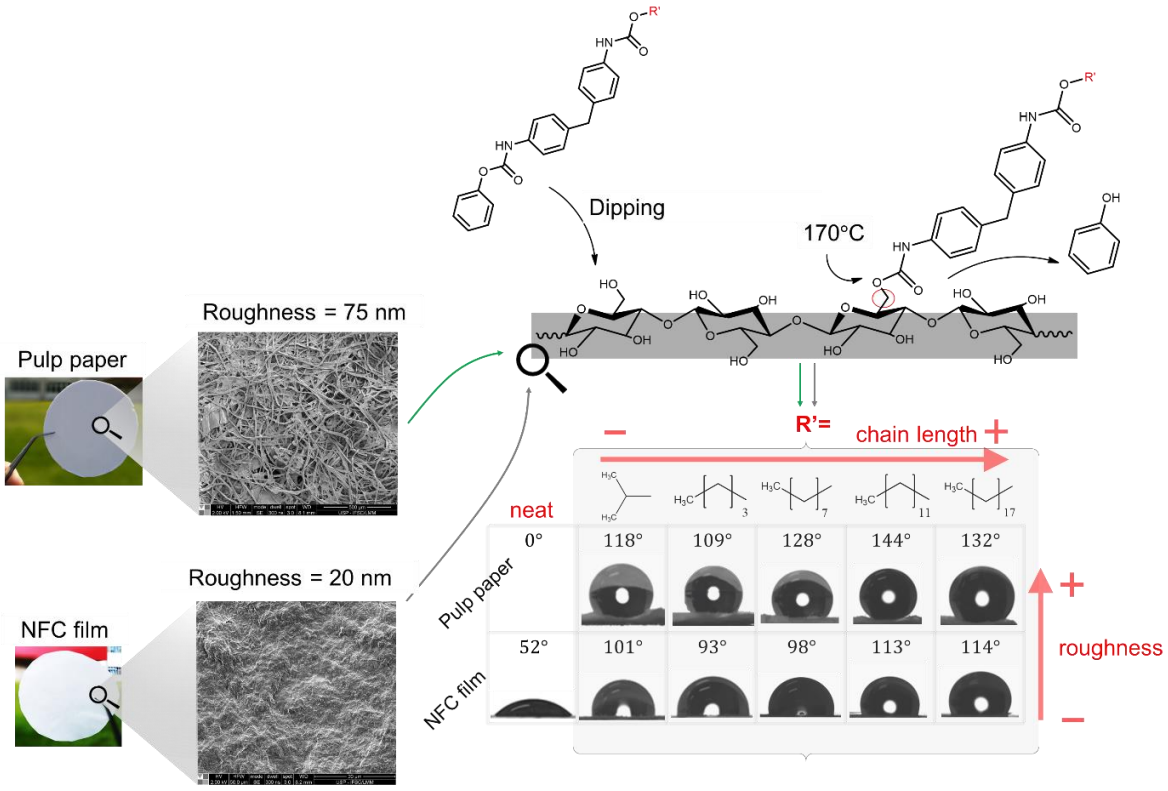

Abstract

The unique structure of cellulose fibers and nanofibrilated cellulose (NFC) allows the formation of interesting all cellulose products. Some limitations as high hydrophilicity and poor resistance in the presence of water can be overcome by hydrophobization treatments. Here, films of pulp fibers and NFC from eucalyptus were produced and submitted to a surface hydrophobization process in two steps (dipping and heating) with blocked diisocyanates. The adducts were synthetized with phenol and linear chain alcohols with length varying from 3 to 18 carbons. Hydrophobized papers and films were characterized by SEM, AFM, FT-IR and water contact angle (WCA). The degree of hydrophobization showed dependence on the length of adduct moiety and the roughness of the surface. Hydrophobized pulp paper had WCA varied from 109 to 144° whereas NFC film presented WCA between 93° and 114°.

Key-Words: cellulose fiber; nanofibrilated cellulose (NFC); cellulose films; blocked isocyanates; hydrophobization

1. INTRODUÇÃO

The polymers from renewable resources became an area of intense research due to the need for environmental friendly materials to replace non-biodegradable materials. Today, approximately 40 % of the polymer production is destined to packaging, which are mainly short term use materials and are key element for oceans and ecosystems pollution. One very attractive solution is the replacement of part of these materials by biodegradable materials (Ahmadzadeh and Khaneghah, 2019; Vilarinho et al., 2018). However, despite of considerable effort, until now, the most relevant biodegradable polymers on the market as PLA and PCL have low competitiveness against PE, PP, PVdC, EVOH (Wang et al., 2018) and the search for new materials directly derived from renewable resources, which keep its biodegradable character continues to be of great importance(Li et al., 2021).

Cellulose, the most abundant biopolymer on earth have the potential to replace synthetic polymers in packaging applications (Klemm et al., 2005; Nathalie Lavoine, Isabelle Desloges, Alain Dufresne, 2012) Cellulose fibers, extracted mainly from wood plants by chemical/mechanical process present low cost, low density and good mechanical properties. Some of its byproducts as cardboard paper are already widely applied on tertiary packaging, being responsible for carrying and protection of manufactured products(Ahmadzadeh and Khaneghah, 2019). More recently, nanofibrilated cellulose (NFC) started its first steps towards industrial scale production.(Klemm et al., 2018; Shatkin et al., 2014; Shatkin and Kim, 2017) The obtaining process, firstly developed by Turbak et al, 1980 and improved over the last 40 years based on mechanical shearing in combination with an enzymatic and/or chemical pre-treatment produces thin nanoscale elements with high aspect ratio (Gandini and Belgacem, 2016; Rol et al., 2019a).

The drying process of NFC suspensions from water or other solvent leads to high stiff and compact NFC films, with less porosity than paper, which has opened some opportunities for high valuable application on films for modified atmosphere packaging(Ferrer et al., 2017; Martin A. Hubbe, Ana Ferrer, Preeti Tyagi, Yuanyuan Yin, Carlos Salas, 2017; Pawar and Purwar, 2013; Zhu et al., 2016), flexible films for printed circuits(Agate et al., 2018; Sundararajan et al., 2017), controlled drug releasing media(Chen et al., 2017) and so on(Ferrer et al., 2017; Martin A. Hubbe, Ana Ferrer, Preeti Tyagi, Yuanyuan Yin, Carlos Salas, 2017).Nonetheless, in the

presence of water, paper and NFC films present a swelling effect, causing loss of dimension stability and stiffness, limiting their application on packaging.

Surface modification can turn NFC more hydrophobic while maintain unaltered the bulk material and its properties such as low permeability(de Souza et al., 2021).Several reports on the literature present success on surface chemical modification of cellulose using a variety of reagents and protocols such as amino propyl trimethoxysilane (APMS)(Reverdy et al., 2018a; Zhang et al., 2014), titanium dioxide(Zhang et al., 2014), esterification with anhydrous moieties(Sehaqui et al., 2014) and plasma etching with fluorinate deposition(Balu et al., 2008a). However, most of these procedures are expensive and hardly applied to large scale. Therefore, cost effective alternatives for surface hydrophobization of cellulose films are desired and the use of blocked isocyanates which could be used in non-anhydrous conditions seems to be an alternative(Carvalho et al., 2005; Gironès et al., 2007).

Unlike isocyanate that require water-free conditions (Botaro and Gandini, 1998; Carvalho et al., 2005; Rol et al., 2019b; Stenstad et al., 2008), blocked isocyanates are good candidates to modify materials such as cellulose fibers and nanofibers which are difficult to be dried. Blocked isocyanates are adducts containing urethane bonds characterized by its relative low dissociation temperature that ranges from 110 °C to 240 °C depending on the blocking agent (Delebecq et al., 2013; Wicks and Wicks, 2001) In addition to its stability, the blocked isocyanate shows a low toxicity (Paquet et al., 2010). The efficiency of blocked isocyanates along with natural materials have been demonstrate for thermoplastic starch (Carvalho et al., 2005) (TPS) with phenyl blocked isocyanates in a dipping and heating process and obtained good response on reducing the sensitive to moisture. Besides, Blocked isocyanates was successfully applied recently with filter paper, hydroxyethyl cellulose and cellulose nanocrystals giving good results of wet resistance on the modified materials (Lu et al., 2020; Zhou et al., 2020).

Here, phenyl/alkyl blocked isocyanates were synthetized by attaining one function of 4,4’-methylenebis (phenyl isocyanate) -MDI to react with phenol (to be deblocked late) and the other to react with a linear chain alcohol, to form stronger and stable urethane bonds. The chain length of the alkylic moiety was varied in numbers of carbons as 3, 4, 8, 12 and 18, respectively with isopropanol, butanol, octanol, dodecanol, and octadecanol as precursor alcohols. Wood pulp fibers and NFC films were obtained by casting and were further submitted to a two steps hydrophobization process involving a dipping in the adduct solution and then to a thermal

treatment for ten minutes at 170 °C to deblock and promote new urethane bonds. Materials were characterized by SEM, AFM and water contact angle (WCA) from which the role of roughness and the length of the alkylic chain on the hydrophobization process is discussed.

2. MATERIALS AND METHODS

2.1 Materials

Never dried bleached eucalyptus pulp fibers with 33 % solid content (15µm length and 4µm diameter, on average) and nanofibrilated cellulose (NFC) (3.2%$_{wt}$ water suspension), with diameter distribution of d_{50}=23nm and d_{90}=75nm were kindly supplied by Suzano Papel e Celulose S/A., Brazil. 4,4-Methylenebis (phenyl isocyanate) (MDI), phenol, isopropanol, butanol, octanol, dodecanol, octadecanol and dibutyltin dilaurate (DBTL) were supplied by Sigma–Aldrich and used as received. Zinc octanoate was supplied by Iracema and used as received. Reagent grade butyl acetate, xylene and methylene chloride were also supplied by Sigma–Aldrich and dried with 4Å molecular sieves at least 72 h before use. Commercial blocked isocyanate (TMP-TDI-3Ph) also used in the hydrophobization process was supplied by Bayer under name of Desmodur AP Stabil®. TMP-TDI-3Ph is condensation product of one mole of trimethylol propane, three moles of toluene diisocyanate blocked and three moles of phenol as blocking agent.

2.2 Pulp and NFC films preparation

Never-dried Kraft wood pulp was suspended in water and homogenized using an Ultra-Turrax IKA model T25 operating at 20,000 rpm for 5 min to give a 0.1%$_{wt}$ suspension. The suspension was vacuum filtrated in a 90 mm diameter Buchner funnel with filter paper. The wet fiber cake was carefully removed from the filter paper, sandwiched between two fresh filter papers to remove the excess of water and placed between two metal plates with a 1 mm metal mask. The assembly was placed in a hydraulic press and heated at 120 °C for 30 min under a weight of 100 kg to form a compact paper sheet with grammage of 190 g/m².

To produce NFC film, the NFC aqueous suspension was diluted to 1 %$_{wt}$ and homogenized with an Ultra-Turrax IKA model T25 operating at 10,000 rpm for 3 minutes. 90 g

of the suspension was dropped into a glass dish plate and dried in a circular oven for 24 hours at 60 °C to give rise to a film with a grammage of 60g/m².

2.3 Blocked diisocyanate synthesis

5 g (20 mmol) of MDI was solubilized with 100 ml of anhydrous butyl acetate into a 3 neck round bottom flask at 45 °C with a constant flow of N_2. 1.88 g (20 mmol) of phenol and 0.1 ml of DBTL were solubilized with 30 ml of anhydrous butyl acetate at 50 °C and added dropwise during 15 min into MDI flask under vigorous magnetic stirring. After two hours, the initial amount of NCO was reduced to half as confirmed by titration with di-n-butylamine (ASTM D-1638-74) and the 20 mmol of the linear alcohol was added. The reaction was reated for each one of the alcohols given in Table 1.Agitation was maintained for more two hours to ensure full conversion of NCO, as checked again by titration with di-n-butylamine. The products were recovered by solvent evaporation at room temperature using a rotary evaporator working with reduced pressure, washed with 2-propanol and dried in an oven at 60 °C. Scheme 1 presents the aimed structure of adducts in which R' is one of the pending groups present in Table 1, obtained with its respective precursor alcohols.

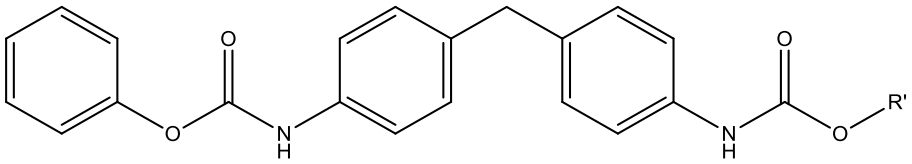

Scheme 1. Structure of the main component formed during isocyanate blocking reactions.

Table 1 Precursor alcohol, structure and label of the synthetized adducts based on the different alkylic chain.

Precursor alcohol	Alcohol structure	R'-	Adduct label
Isopropanol	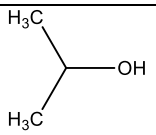	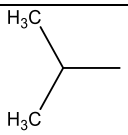	Ph-MDI-I
Butanol	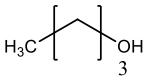	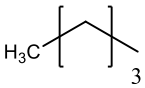	Ph-MDI-B
Octanol	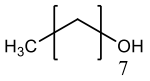	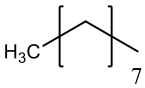	Ph-MDI-O
Dodecanol	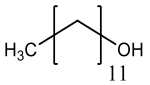	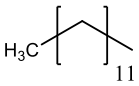	Ph-MDI-D
Octadecanol	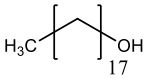	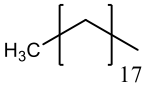	Ph-MDI-Oc
Phenol	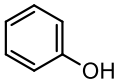		Ph-MDI-Ph

2.4 Hydrophobization process

For each blocked isocyanate synthetized (Table 1) and for the commercial TMP-TDI-3 Ph, 6 g of the adduct with 0.25 g of zinc octanoate were solubilized in a mixture of 75 ml of xylene and 25 ml of butyl acetate with a magnetic stirrer at 60 °C into a 150 ml glass becker. Three samples of pulp paper and three samples of NFC film, in dimensions of 2.5 cm x 2.5 cm were dipped for 60 s into the solution, dried under a nitrogen flow and then placed in an oven for 10 min at 170 °C. They were subsequently washed twice with 100 ml of hot xylene and butyl acetate (75/25v) and rinsed several times with methylene chloride to remove the excess of adduct that did not react. Finally, samples were dried at 60 °C for 1h.

2.5 Characterization

2.5.1 Fourier Transformed Infrared Spectroscopy- FT-IR

FT-IR spectra were collected with a PerkinElmer Spectrum 100 with an attenuated total reflection (ATR) accessory in the range of 4000 cm^{-1} to 650 cm^{-1}. Each spectrum was an average

of 32 measurements and at least two spectra in different regions were collected per analysis. Surface modified paper and film spectra were normalized with respect to the vibration at 896 cm^{-1} related to the cellulose C-O-C stretching bond.

2.5.2 Scanning Electron Microscopy- SEM

Scanning electron images were obtained in an Inspect F-50 (FEI) microscope with beam tension of 2.0 -4.0kV and working distances of around 8.0 mm. Images were acquired in the mode of secondary electrons (SE). Papers and films were prepared by bonding squares of the material to a double sided carbon tape, further metalized for 90 s with a platinum target.

2.5.3 Atomic Force Microscopy - AFM

AFM images were obtained using an AFM model Flex-Axiom (Nanosurf) working in tapping air mode with a silicon scanning probe (Tap190Al-G) having a maximum radius of curvature of 10 nm and 150 kHz as the cantilever resonance frequency. Film squares of 1 x 1 cm, previously dried at 60 °C for 2 hours, were bonded by a double sided tape and pressed in the sample holder. Images processing and roughness calculation (ASME B46.1-1995) were performed using the freeware software Gwyddion®.

2.5.4 Water contact angle - WCA

Water contact angles were measured using a KSV - CAM 101 instrument with specimens in dimensions of 25 x 5 mm. The values were collected from five measurements with distilled water (droplet of ~5 µl). and the static contact angles were obtained by plotting the contact angle *vs* time, where the equilibrium value (static) was determined. Measurements were performed at 23 °C and 30 % RH.

2.5.6 Statistical analysis

Variance analysis (ANOVA) and Tukey's multiple comparison test were performed using the software Minitab®. The statistical analyses for the WCA values were conducted using a significance level of 5% (α=0.05).

3. RESULTS AND DISCUSSION

3.1 Adduct synthesis characterization

Figure 1 shows the FTIR spectra of the adducts prepared with MDI phenol and the linear chain alcohols. Adducts synthesis are confirmed by the disappearance of -NCO vibration at 2260 cm^{-1} and the replacement of –OH stretching vibration at 3323 cm^{-1} from the alcohols for narrow vibrations related to N-H bond from urethane. The presence of the C=O vibrations at 1720 cm^{-1} and 1700 cm^{-1} confirms the formation of phenyl and alkyl carbamates, respectively(Gironès et al., 2008, 2007). Vibrations comprised between 2920 cm^{-1} and 2850 cm^{-1} are related to the -CH_2 group and exhibit increasing intensity as the length of the linear alcohols increase.

3.2 Pulp paper and NFC film characterization

The higher aspect ratio of NFC enhances the compaction and also the surface smoothness of the dried films. With the AFM data presented on three parameters of roughness were calculated using Gwydion®, being those Ra, Rq and Rt. The obtained values are presented in **Erro! Fonte de referência não encontrada.**, where for all parameters pulp papers presented higher values, as expected.

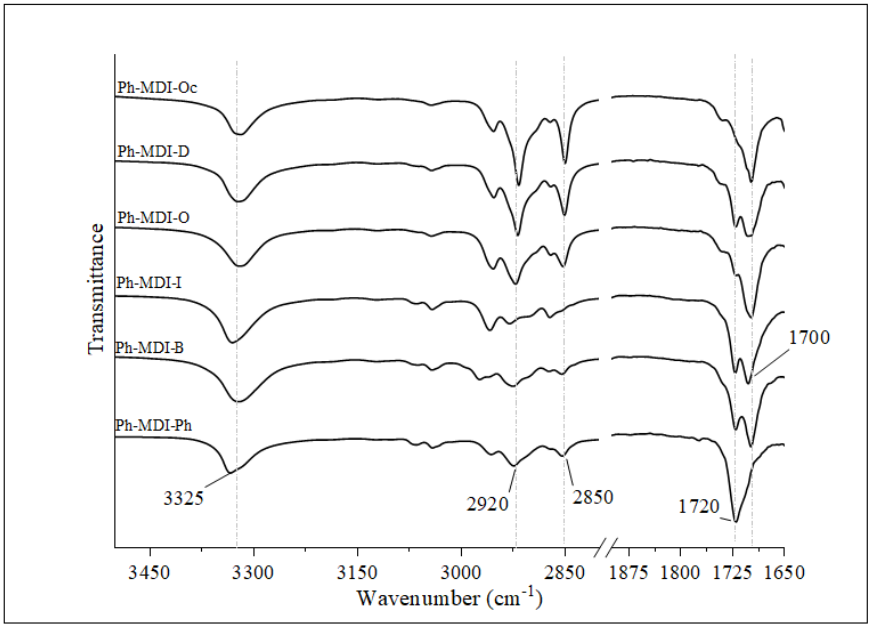

Figure 1. FT-IR spectra of the adducts formed with different alkyl chain length whith indications for hydroxyl, metyl and carbonyl bands of urethane.

Table 2. Roughness values measured with AFM data for casted pulp paper and NFC film.

	Ra (nm)	Rq (nm)	Rt (nm)
Pulp paper	75 ± 21	106 ± 30	980 ± 300
NFC film	20 ± 1	25 ± 1	165 ± 13

3.3 Surface modification characterization

Figure 2 presents the FT-IR spectra of the pulp papers after surface modification by the dipping and heating process. Pulp -TMP-TDI (the one treated with the commercial blocked isocyanate) presents spectra almost identical of the pristine pulp paper, with very small absorptions at the aforementioned regions. The main differences after modification are the absorptions in the region of 1790-1230 cm^{-1} due to amides and amines groups of urethane bonds and the bands at 1592 cm^{-1}, 1415 cm^{-1} and 1310 cm^{-1}. It is observed that when the alkylic group is short as is isopropanol and butanol (Pulp-MDI-I and Pulp-MDI-B), the urethane bands in the region 1750-1230 cm^{-1} are more prominent than that of long chain alkylic groups as octanol, (Pulp-MDI-O), dodecanol, (Pulp-MDI-D) and octadecanol, (Pulp-MDI-Oc). This could indicate a higher degree of chemical grafting for short chain adducts.

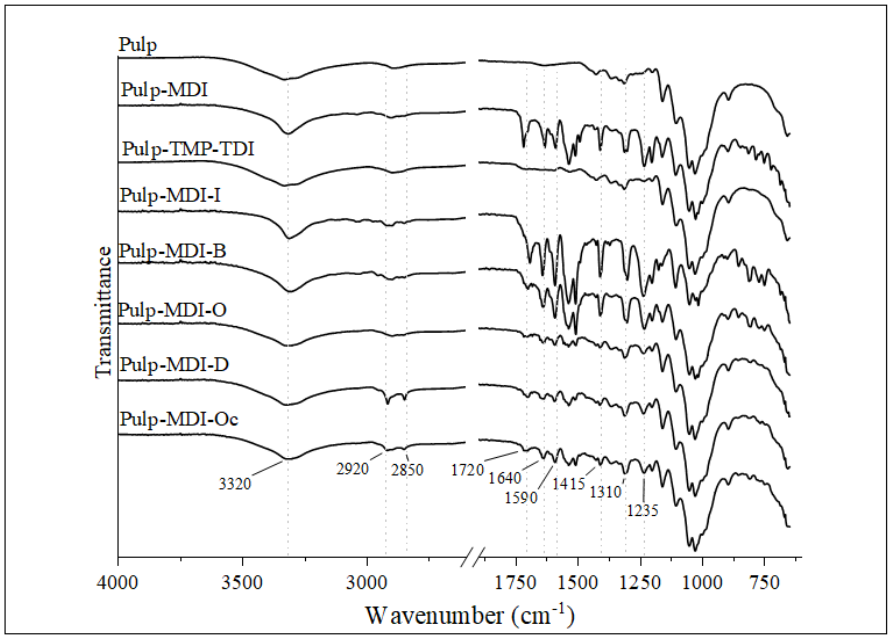

Figure 2. FT-IR spectra of surface modified pulp with blocked isocyanates by the dipping and heating process.

Figure 3 shows the FT-IR spectra of the NFC films after surface modification by the dipping and heating process. Surface hydrophobized NFC-films presents similar trends on the FT-IR spectra of those observed for pulp, with the presence of the amine and amide bands. The intensity of the bands is also associated with the length of the alkylic moieties, i.e, shorter the molecule, more intense the peaks related to urethane bonds. NFC-MDI presents remarkable sharpened vibrations in the region of 1750-1230 cm^{-1} and, as discussed elsewhere (de Souza et al., 2021) the synthesis of this compound let to the formation of other adducts than only Ph-MDI-Ph, as disubstituted ureas and alophanates, which could extend the degree and complexity of functionalization.

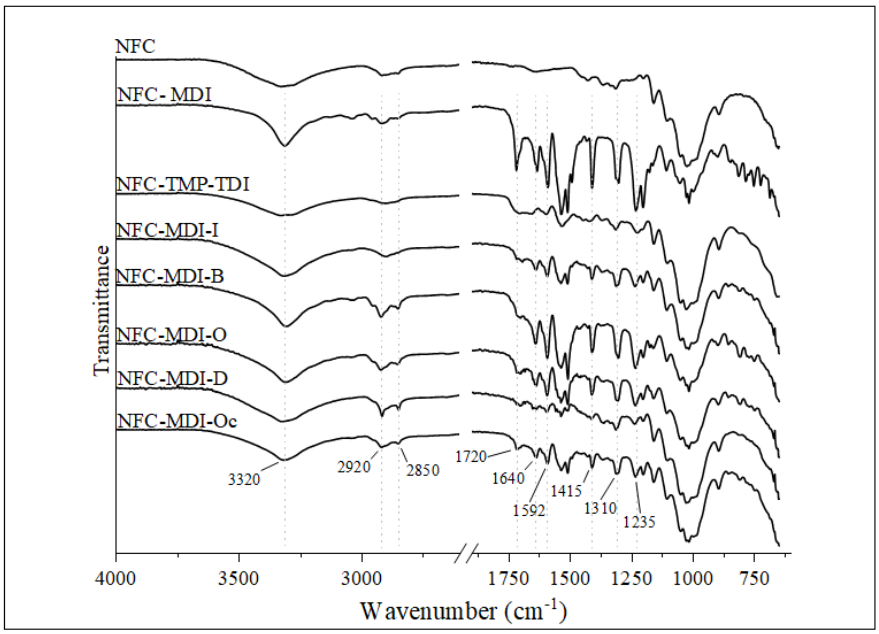

Figure 3. FT-IR spectra of surface modified NFC films with blocked isocyanates by the dipping and heating process.

3.4 Hydrophobization characterization

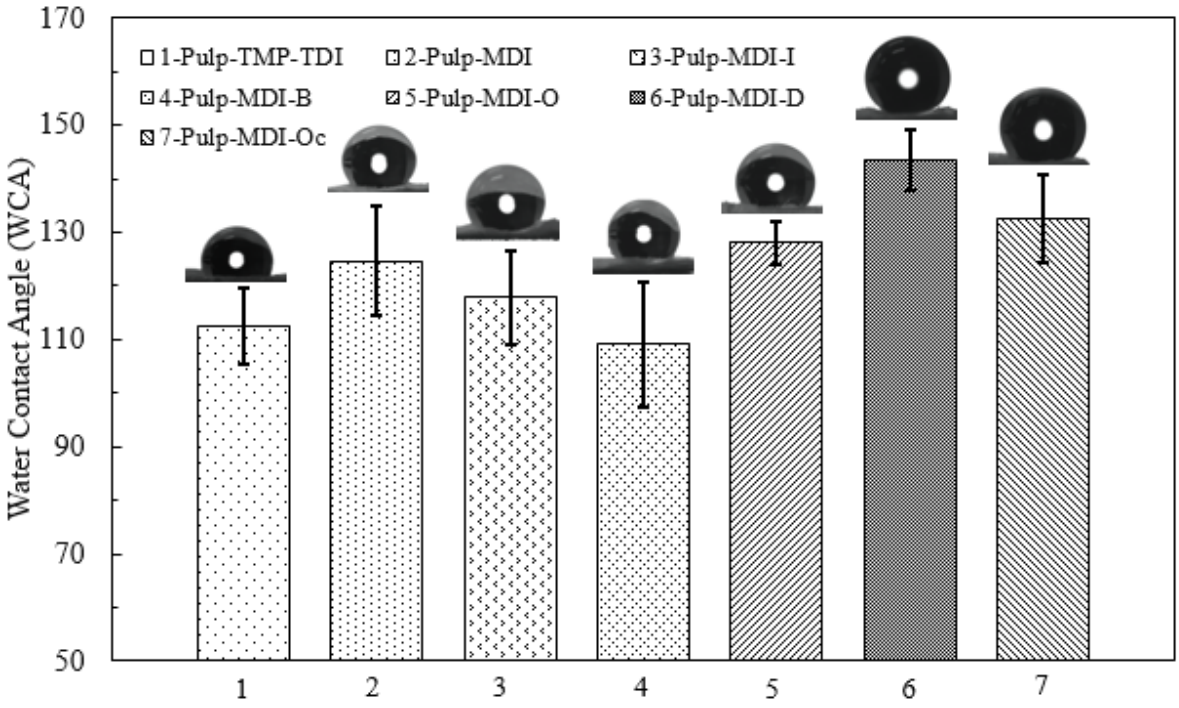

Figure 4 shows water contact angle (WCA) for the pulp sheet after modification with the blocked diisocyanates. Pulp passed from a state of readily absorbing water (WCA = 0°) to a

value of at least 110°, measured for the pulp treated with the commercial blocked isocyanate (Pulp-TMP-TDI). Table 3 presents statistical analysis in which four overlapping groups (a-d) can be detached within WCA data. One can observe that Pulp-MDI-O, Pulp-MDI-D and Pulp-MDI-OC (compositions 5,6 and 7), which were hydrophobized using adducts with longer alkyl chain length (octanol, dodecanol and octadecanol as precursors alcohols, respectively) present the average WCA slightly higher than the other compositions. Therefore, as general trend, statistical analysis confirms that WCA is increasing as the alkyl length of the precursor adduct is enhanced and the group D presents the more hydrophobic surface, reaching almost 145°.

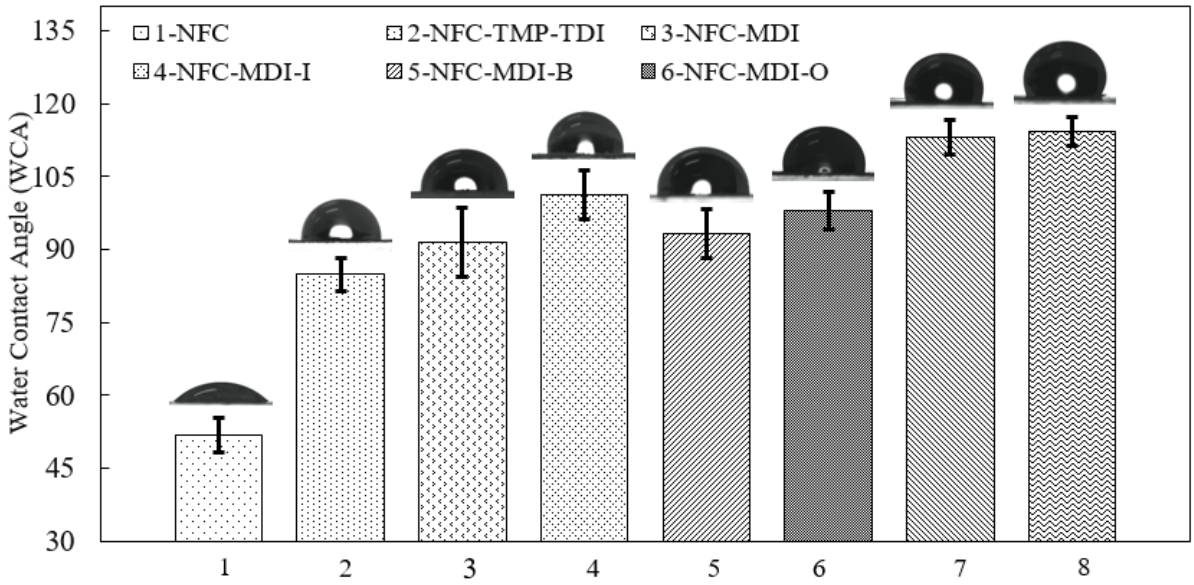

Figure 5 presents the WCA of the NFC films. A WCA of 52° was measured for the pristine NFC film. As observed for pulp paper, all hydrophobizing treatments were effective on enhancing the WCA significantly in relation to the pristine composition as values at least 33° higher than the non-modified NFC film were measured. The statistical analysis for NFC films is also presented in Table 3. The trend is the similar as the observed above for pulp paper i.e, four average groups and the longer the alkyl chain length of the precursor adducts, higher is the contact angle. Group D' that comprises dodecanol and octadecanol as precursor, reached the higher values of nearly 115°, among the highest presented in literature.

When comparing group D and D' on Table 3, one can observe that, although passing by the same hydrophobization process, pulp papers reached more expressive values of WCA than the NFC films. As measured with AFM data, pulp paper presents a Ra value of almost 4 times the value of the smooth NFC film (**Erro! Fonte de referência não encontrada.**). Therefore, the

results follow the Wenzel model in which the effect of a hydrophobic surface is amplified by a major contact area, i.e, higher roughness.

Comparing the results with the literature, Balu et al, 2008(Balu et al., 2008b) performed plasma etching of amorphous regions at the cellulose paper surface and coated the etched regions with fluorinate by chemical vapor deposition. Values of WCA comprised in between 144.8-166.7° were achieved. However, the feasibility of the process in a cost effect manner would be limited on large scale products. In another study, Reverdy *et al*, (Reverdy et al., 2018b) promoted a protocol for paper surface modification by applying a combination of NFC, AKD and calcium carbonate to form a superhydrophobic coating layer, reaching WCA values of 150°. Calcium carbonate was used as an element to increase the surface area, giving the surperhydrophobic characteristic to the paper surface. The main problem of coating layers is that on long term it can be compromised and expose the bulk paper. Here, the natural roughness of the constituent fibers and the length of the alkylic moiety grafted on the surface of the paper were responsible for WCA as high as 144°.

Regarding to the production of NFC films, on the literature Sethi et al, 2018(Sethi et al., 2018) manufactured a Polyurethane/NFC composited and WCA as high as 81° were measured on the PU rich surface. In other study, Sethi et al 2019(Sethi et al., 2019) produced hybrid NFC/lignin films with WCA reaching 107°(Sethi et al., 2019). Sehaqui et al,2014(Sehaqui et al., 2014) performed solvent exchange of NFC suspension and soaked the wet cake with anhydride moieties to promote surface esterification with different chain lengths, from which WCA as high as 118° was measured. The long time and the multi steps involved on the preparation and further hydrophobization of the films are among the limitation of the cited works. The two step chemical modification with blocked diisocyanate presented here is a good alternative to lead surface hydrophobization in a simple manner, towards an industrial scale process.

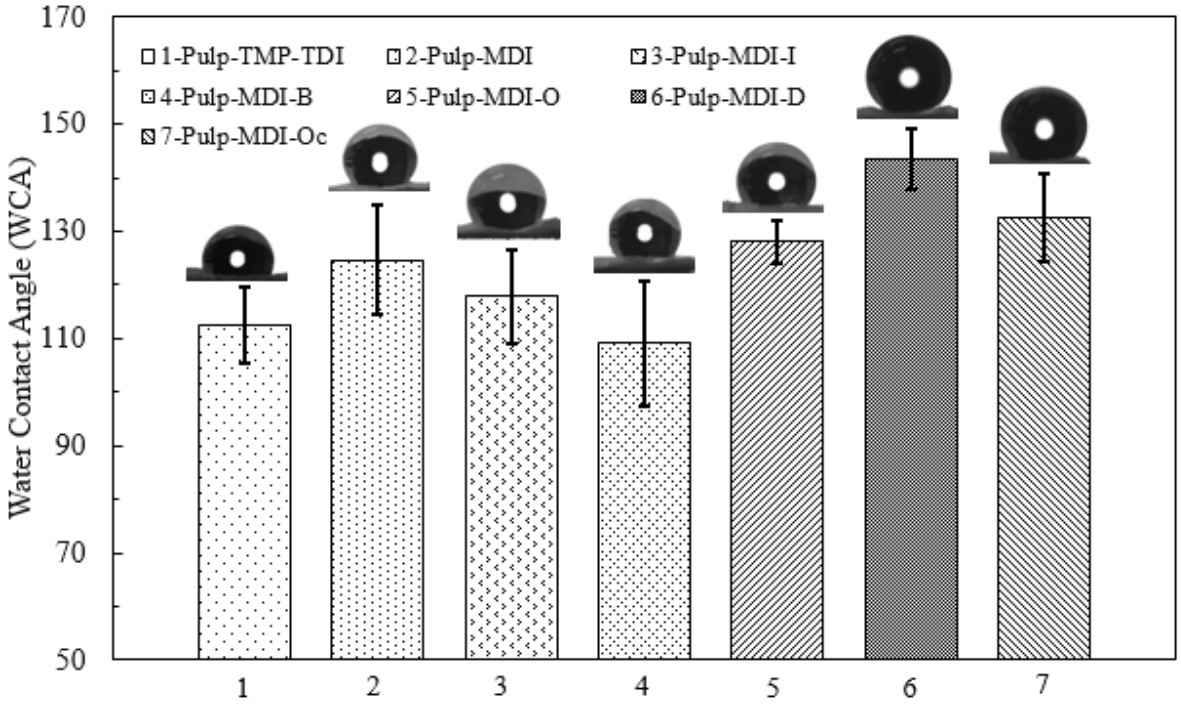

Figure 4. Water Contact Angle (WCA) of the surface modified pulp papers using different blocked isocyanates hydrophobizing adducts

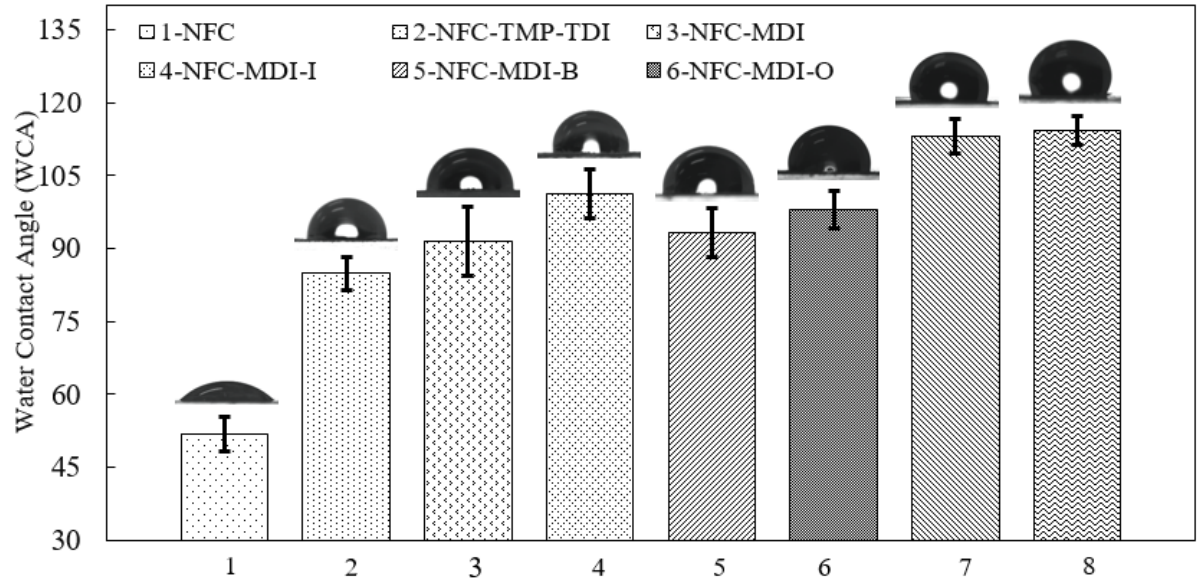

Figure 5 Water Contact Angle (WCA) of the surface modified NFC films using different blocked isocyanates hydrophobizing adducts.

Table 3. Statistical analysis of the Water Contact Angles (WCA) values for pulp papers and NFC films, by Tukey comparisson test at 95% of condidence.

Sample		Pulp Paper	Statistical Group	NFC film	Statistical Group
C1	neat	0°	A	52°	A’
C2	-MDI	109°	B	85°	B’
C3	-TMP-TDI	112°	B	91°	B’,C’
C4	-B	118°	B,C	93°	B’,C’
C5	-I	125°	B,C	98°	C’
C6	-O	128°	B,C,D	101°	C’
C7	-D	133°	C,D	113°	D’
C8	-Oc	144°	D	114°	D’

4. CONCLUSION

Pulp and nanofibrilated cellulose (NFC) films were successfully surface modified with a commercial blocked triisocyanate and a series of blocked diisocyanates of 4,4-Methylenebis (phenyl isocyanate) with linear chain alcohols having 3, 4, 8, 12 or 18 carbons (isopropanol, butanol, octanol, dodecanol and octadecanol, respectively). The blocking agent for all materials was phenol and the modification was performed by a dipping and heating process. FT-IR analysis confirmed formation of both phenyl and alkyl carbamates and evidenced that the thermal treatment at 170° C for 10 minutes was able to promote reactions at the paper and films surface

The hydrophobization treatments led to an increase in water contact angle (WCA) of pulp paper from water readily absorption to values comprised between 113° and 144°. Hydrophobized NFC films presented WCA varying from 85° to 114°, at least 32 ° above the non-treated film. The rougher surface of pulp papers, measured by AFM enabled reaching near superhydrophobic state. As general trend, as the alkyl chain of the adduct increased, higher was the WCA of its respective hydrophobized film. Moreover,

One of the major limitation of cellulose films is its inherent ability of water absorption, which lead to swelling and consequent loss of stiffness and dimension stability, restricting its use. The cost effective hydrophobization protocol presented here showed positive results on increasing water repellency of pulp paper and NFC films enhancing its application possibilities.

AUTHOR INFORMATION

Corresponding author

Antonio José Felix Carvalho- Department of Materials Engineering, Sao Carlos School of Engineering (EESC), University of São Paulo (USP), São Paulo, SP, Brazil. https://orcid.org/0000-0001-8403-1135 E-mail: (toni@sc.usp.br)

Authors

Gustavo de Souza- Department of Materials Engineering, Sao Carlos School of Engineering (EESC), University of São Paulo (USP), São Paulo, SP; https://orcid.org/0000-0002-9056-8550

Ricardo Klaus Kramer- Department of Materials Engineering, Sao Carlos School of Engineering (EESC), University of São Paulo (USP), São Paulo, SP https://orcid.org/0000-0001-7860-6895

AUTHOR CONTRIBUTIONS

The manuscript was written through contributions of all authors. All authors have given approval to the final version of the manuscript.

ACKNOWLEDGEMENTS

This study was financed in part by the Coordenação de Aperfeiçoamento de Pessoal de Nível Superior - Brasil (CAPES) - Finance Code 001. Also, authors acknowledge CNPq for the doctoral fellowship granted to G.S (CNPq proc. 140249/2017-6). AJFC acknowledge CNPq for research funding project # 303847/2019-0.

NOTES

The authors declare no competing financial interest.

5. REFERENCES

Agate, S., Joyce, M., Lucia, L., Pal, L., 2018. Cellulose and nanocellulose-based flexible-hybrid printed electronics and conductive composites – A review. Carbohydr. Polym. 198, 249–260. https://doi.org/10.1016/j.carbpol.2018.06.045

Ahmadzadeh, S., Khaneghah, A.M., 2019. Role of Green Polymers in Food Packaging, in: Reference Module in Materials Science and Materials Engineering. Elsevier, pp. 1–15. https://doi.org/10.1016/B978-0-12-803581-8.10576-4

Balu, B., Breedveld, V., Hess, D.W., 2008a. Fabrication of "Roll-off" and "Sticky" Superhydrophobic Cellulose Surfaces via Plasma Processing. Langmuir 24, 4785–4790. https://doi.org/10.1021/la703766c

Balu, B., Breedveld, V., Hess, D.W., 2008b. Fabrication of "roll-off" and "sticky" superhydrophobic cellulose surfaces-via plasma processing. Langmuir 24, 4785–4790. https://doi.org/10.1021/la703766c

Botaro, V.R., Gandini, A., 1998. Chemical modification of the surface of cellulosic fibres. 2. Introduction of alkenyl moieties via condensation reactions involving isocyanate functions. Cellulose 5, 65–78. https://doi.org/10.1023/A:1009216729686

Carvalho, A.J.F., Curvelo, A.A.S., Gandini, A., 2005. Surface chemical modification of thermoplastic starch: Reactions with isocyanates, epoxy functions and stearoyl chloride. Ind. Crops Prod. 21, 331–336. https://doi.org/10.1016/j.indcrop.2004.04.027

Chen, X., Chen, C., Zhang, H., Huang, Y., Yang, J., Sun, D., 2017. Facile approach to the fabrication of 3D cellulose nanofibrils (CNFs) reinforced poly(vinyl alcohol) hydrogel with ideal biocompatibility. Carbohydr. Polym. 173, 547–555. https://doi.org/10.1016/j.carbpol.2017.06.036

de Souza, G., Belgacem, M.N., Gandini, A., Carvalho, A.J.F., 2021. Low permeable hydrophobic nanofibrilated cellulose films modified by dipping and heating processing technique. Cellulose 3. https://doi.org/10.1007/s10570-020-03619-3

Delebecq, E., Pascault, J.P., Boutevin, B., Ganachaud, F., 2013. On the versatility of urethane/urea bonds: Reversibility, blocked isocyanate, and non-isocyanate polyurethane. Chem. Rev. 113, 80–118. https://doi.org/10.1021/cr300195n

Ferrer, A., Pal, L., Hubbe, M., 2017. Nanocellulose in packaging: Advances in barrier layer technologies. Ind. Crops Prod. 95, 574–582. https://doi.org/10.1016/j.indcrop.2016.11.012

Gandini, A., Belgacem, M.N., 2016. The Surface and In-Depth Modification of Cellulose Fibers, in: Rojas, O.J. (Ed.), Cellulose Chemistry and Properties: Fibers, Nanocelluloses and Advanced Materials. Springer International Publishing, Cham, pp. 169–206. https://doi.org/10.1007/12_2015_305

Gironès, J., Pimenta, M.T.B., Vilaseca, F., Carvalho, A.J.F., Mutjé, P., Curvelo, A.A.S., 2008. Blocked diisocyanates as reactive coupling agents: Application to pine fiber-polypropylene composites. Carbohydr. Polym. 74, 106–113. https://doi.org/10.1016/j.carbpol.2008.01.026

Gironès, J., Pimenta, M.T.B., Vilaseca, F., de Carvalho, A.J.F., Mutjé, P., Curvelo, A.A.S., 2007. Blocked isocyanates as coupling agents for cellulose-based composites. Carbohydr. Polym. 68, 537–543. https://doi.org/10.1016/j.carbpol.2006.10.020

Klemm, D., Cranston, E.D., Fischer, D., Gama, M., Kedzior, S.A., Kralisch, D., Kramer, F., Kondo, T., Lindström, T., Nietzsche, S., Petzold-Welcke, K., Rauchfuß, F., 2018. Nanocellulose as a natural source for groundbreaking applications in materials science: Today's state. Mater. Today 21, 720–748. https://doi.org/10.1016/j.mattod.2018.02.001

Klemm, D., Heublein, B., Fink, H.P., Bohn, A., 2005. Cellulose: Fascinating biopolymer and sustainable raw material. Angew. Chemie - Int. Ed. 44, 3358–3393. https://doi.org/10.1002/anie.200460587

Li, T., Chen, C., Brozena, A.H., Zhu, J.Y., Xu, L., Driemeier, C., Dai, J., Rojas, O.J., Isogai, A., Wågberg, L., Hu, L., 2021. Developing fibrillated cellulose as a sustainable technological material. Nature 590, 47–56. https://doi.org/10.1038/s41586-020-03167-7

Lu, Z., Huang, J., E, S., Li, J., Si, L., Yao, C., Jia, F., Zhang, M., 2020. All cellulose composites prepared by hydroxyethyl cellulose and cellulose nanocrystals through the crosslink of polyisocyanate. Carbohydr. Polym. 250, 116919. https://doi.org/10.1016/j.carbpol.2020.116919

Martin A. Hubbe, Ana Ferrer, Preeti Tyagi, Yuanyuan Yin, Carlos Salas, L.P. and O.J.R., 2017. Nanocellulose in Thin Films, Coatings, and Plies for Packaging Applications: A Review. BioResources 12, 2143–2233.

Nathalie Lavoine, Isabelle Desloges, Alain Dufresne, J.B., 2012. Microfibrillated cellulose – Its barrier properties and applications in cellulosic materials: A review. Carbohydr. Polym. 90, 735–764. https://doi.org/http://dx.doi.org/10.1016/j.carbpol.2012.05.026

Paquet, O., Krouit, M., Bras, J., Thielemans, W., Belgacem, M.N., 2010. Surface modification of

cellulose by PCL grafts. Acta Mater. 58, 792–801. https://doi.org/10.1016/j.actamat.2009.09.057

Pawar, P.A., Purwar, A.H., 2013. Bioderadable Polymers in Food Packaging. Am. J. Eng. Res. 02, 151–164.

Reverdy, C., Belgacem, N., Moghaddam, M.S., Sundin, M., Swerin, A., Bras, J., 2018a. One-step superhydrophobic coating using hydrophobized cellulose nanofibrils. Colloids Surfaces A Physicochem. Eng. Asp. 544, 152–158. https://doi.org/10.1016/j.colsurfa.2017.12.059

Reverdy, C., Belgacem, N., Moghaddam, M.S., Sundin, M., Swerin, A., Bras, J., 2018b. One-step superhydrophobic coating using hydrophobized cellulose nanofibrils. Colloids Surfaces A Physicochem. Eng. Asp. 544, 152–158. https://doi.org/10.1016/j.colsurfa.2017.12.059

Rol, F., Belgacem, M.N., Gandini, A., Bras, J., 2019a. Recent advances in surface-modified cellulose nanofibrils. Prog. Polym. Sci. 88, 241–264. https://doi.org/10.1016/j.progpolymsci.2018.09.002

Rol, F., Belgacem, M.N., Gandini, A., Bras, J., 2019b. Recent advances in surface-modified cellulose nanofibrils. Prog. Polym. Sci. 88, 241–264. https://doi.org/10.1016/j.progpolymsci.2018.09.002

Sehaqui, H., Zimmermann, T., Tingaut, P., 2014. Hydrophobic cellulose nanopaper through a mild esterification procedure. Cellulose 21, 367–382. https://doi.org/10.1007/s10570-013-0110-5

Sethi, J., Farooq, M., Österberg, M., Illikainen, M., Sirviö, J.A., 2018. Stereoselectively water resistant hybrid nanopapers prepared by cellulose nanofibers and water-based polyurethane. Carbohydr. Polym. 199, 286–293. https://doi.org/10.1016/j.carbpol.2018.07.028

Sethi, J., Visanko, M., Österberg, M., Sirviö, J.A., 2019. A fast method to prepare mechanically strong and water resistant lignocellulosic nanopapers. Carbohydr. Polym. 203, 148–156. https://doi.org/10.1016/j.carbpol.2018.09.037

Shatkin, J.A., Kim, B., 2017. Environmental Health and Safety of Cellulose Nanomaterials and Composites for Nanomaterials.

Shatkin, J.A., Wegner, T.H., Bilek, E.M., Cowie, J., 2014. Market projections of cellulose nanomaterial-enabled products -Part 1: Applications. Tappi J. 13, 9–16. https://doi.org/10.32964/tj13.5.9

Stenstad, P., Andresen, M., Tanem, B.S., Stenius, P., 2008. Chemical surface modifications of

microfibrillated cellulose. Cellulose 15, 35–45. https://doi.org/10.1007/s10570-007-9143-y

Sundararajan, S., Samui, A.B., Kulkarni, P.S., 2017. Shape-stabilized poly(ethylene glycol) (PEG)-cellulose acetate blend preparation with superior PEG loading via microwave-assisted blending. Sol. Energy 144, 32–39. https://doi.org/10.1016/j.solener.2016.12.056

Vilarinho, F., Sanches Silva, A., Vaz, M.F., Farinha, J.P., 2018. Nanocellulose in green food packaging. Crit. Rev. Food Sci. Nutr. 58, 1526–1537. https://doi.org/10.1080/10408398.2016.1270254

Wang, J., Gardner, D.J., Stark, N.M., Bousfield, D.W., Tajvidi, M., Cai, Z., 2018. Moisture and Oxygen Barrier Properties of Cellulose Nanomaterial-Based Films. ACS Sustain. Chem. Eng. 6, 49–70. https://doi.org/10.1021/acssuschemeng.7b03523

Wicks, D.A., Wicks, Z.W., 2001. Blocked isocyanates III - Part B: Uses and applications of blocked isocyanates. Prog. Org. Coatings 41, 1–83. https://doi.org/10.1016/S0300-9440(00)00164-8

Zhang, Z., Sèbe, G., Rentsch, D., Zimmermann, T., Tingaut, P., 2014. Ultralightweight and flexible silylated nanocellulose sponges for the selective removal of oil from water. Chem. Mater. 26, 2659–2668. https://doi.org/10.1021/cm5004164

Zhou, X., Fu, Y., Chen, L., Wang, R., Wang, X., Miao, Y., Ji, X., Bian, H., Dai, H., 2020. Diisocyanate modifiable commercial filter paper with tunable hydrophobicity, enhanced wet tensile strength and antibacterial activity. Carbohydr. Polym. 248, 116791. https://doi.org/10.1016/j.carbpol.2020.116791

Zhu, Y., Romain, C., Williams, C.K., 2016. Sustainable polymers from renewable resources. Nature 540, 354–362. https://doi.org/10.1038/nature21001

PAPER 2

Low permeable hydrophobic nanofibrilated cellulose films modified by dipping and heating processing technique

Gustavo de Souza[a,b], Mohamed Naceur Belgacem[b], Alessandro Gandini[b], Antonio José Felix Carvalho[a*]

[a]*Department of Materials Engineering, Sao Carlos School of Engineering (EESC), University of São Paulo (USP), São Paulo, SP, Brazil*

[b]*Univ. Grenoble Alpes, CNRS, Grenoble INP, LGP2, F-38000, Grenoble, France*

ABSTRACT

Nanofibrilated cellulose (NFC) films have potential to replace synthetic polymers as flexible films for packaging. However, NFC is hydrophilic and water acts as plasticizer decreasing the stiffness of the films and reducing its barrier effectiveness against water vapor and oxygen. Here we describe the surface modification of cellulose films with blocked diisocyanates through a dipping and heating process not requiring the previous drying of the materials. The reactions were conducted at 170 °C for a few minutes during which deblocking led to a new urethane bond formation with NFC surface hydroxyl groups, thus hydrophobizing the films. A remarkable enhancement in water repellent properties was confirmed by water contact angles higher than 110 ° and water vapor transmission rate (WVTR) of 40 g/m² day, which is very low when compared to similar materials, representing a reduction of 74 % with respect to the non- modified films.

KEY-WORDS: Nanofibrilated Cellulose (NFC), Films, Chemical Modification, Blocked Isocyanates, Barrier Properties.

AUTHOR INFORMATION

Corresponding author

Antonio José Felix Carvalho- Department of Materials Engineering, Sao Carlos School of Engineering (EESC), University of São Paulo (USP), São Paulo, SP, Brazil. https://orcid.org/0000-0001-8403-1135 E-mail: (toni@sc.usp.br)

Authors

Gustavo de Souza- Department of Materials Engineering, Sao Carlos School of Engineering (EESC), University of São Paulo (USP), São Paulo, SP; Univ. Grenoble Alpes, CNRS, Grenoble INP, LGP2, F-38000, Grenoble, France. https://orcid.org/0000-0002-9056-8550

Mohamed Naceur Belgacem- Univ. Grenoble Alpes, CNRS, Grenoble INP, LGP2, F-38000, Grenoble, France https://orcid.org/0000-0002-3317-7369

Alessandro Gandini- Univ. Grenoble Alpes, CNRS, Grenoble INP, LGP2, F-38000, Grenoble, France. https://orcid.org/0000-0003-0538-8764

Graphical Abstract

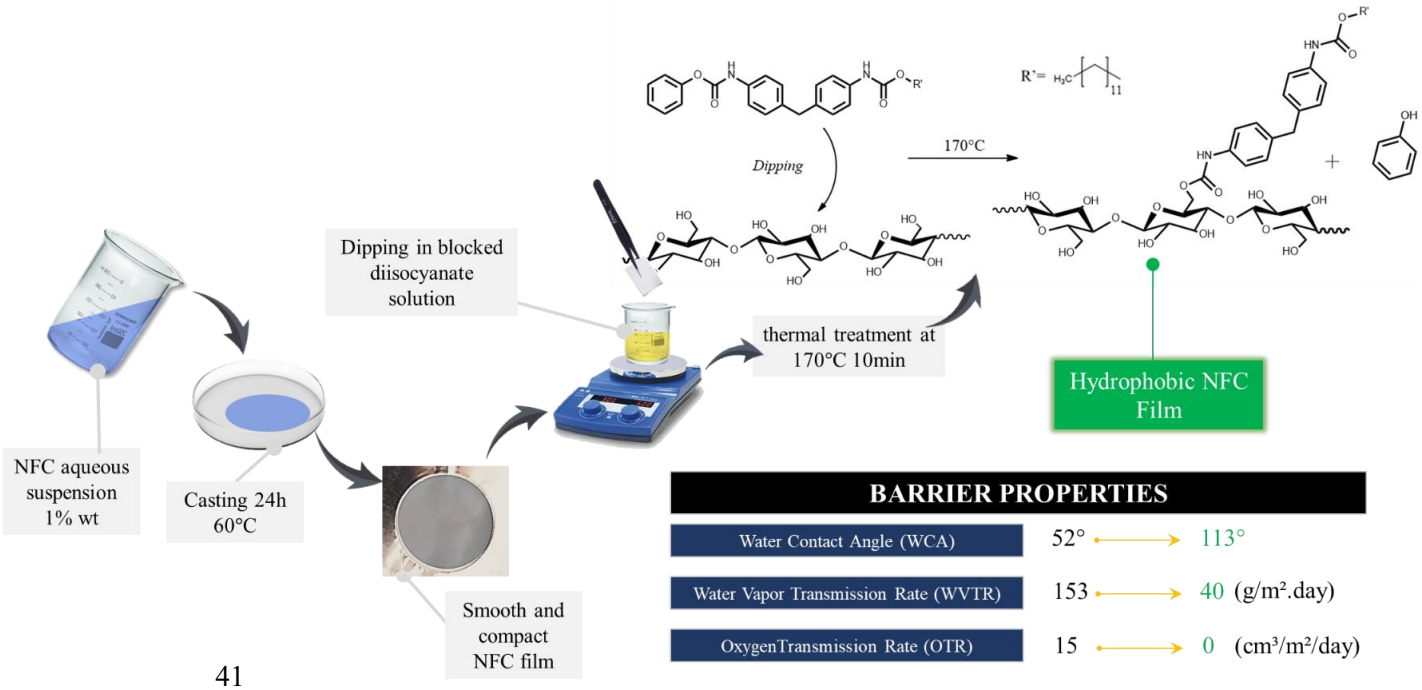

Introduction

The carbon footprint and pollution caused by polymers derived from fossil resources, notably in the context of short-term food packaging, are a serious source of concern, resulting in government pressure by society and sparking an intense search for renewable and biodegradable materials possessing sustainable competitive properties (Heinze 2016; Wang et al. 2018). Cellulose and its derivatives are good candidates for this task as the main source is worldwide abundant biomass. Besides, they display advantageous properties such as low density and high specific stiffness, putting them on the spotlight of the new generation of bioproducts with applications in high technological fields such as flexible substrates for printed electronics, media for controlled drug releasing delivery systems and in modified atmosphere films for food packaging (Klemm et al. 2005, 2018a).

Indeed, paper has been a common food packaging material for a very long time, it was progressively substituted by synthetic polymers thanks to their low cost, easy processing and sealing and better barrier properties. The recent development of nanocelluloses, among then the nanofibrilated cellulose (NFC) at a competitive energetic cost(Dufresne 2017; Klemm et al. 2018a) opened the possibility of producing films with barrier properties similar to those of several thermoplastic polymers used for packaging such as polystyrenes, polyamides and polylactic acid(Wang et al. 2018). Due to the low size and high cohesiveness of the cellulose nanofibrils these films are substantially less porous then conventional paper resulting in high stiffness (6- 10 GPa), high compaction (density near 1.5 g/cm^3) and low oxygen permeability (below 10 cm3·µm/m2·day·atm)(Arbatan et al. 2012; Yousefi et al. 2013; Sehaqui et al. 2014; Solala et al. 2018; Operamolla 2019; Sethi et al. 2019). Nonetheless, the inherent hydrophilicity of NFC leads to

69 water plasticization, decreasing its stiffness and reducing its barrier effectiveness
70 against water vapor and oxygen (Sehaqui et al. 2014; Hubbe et al. 2015).
71 Two major strategies reported to produce NFC films with enhanced barrier
72 properties include surface modification and production of composites with
73 crystalline and ceramic particles such as bentonite, talc, graphene oxide and
74 montmorillonite (Liu et al. 2011; Liimatainen et al. 2013; Garusinghe et al. 2018;
75 Zheng et al. 2019). The filler used in composites not only decrease permeability
76 but also the flexibility and in some cases, as with graphene and graphene oxide,
77 increasing remarkably the costs (Ouyang et al. 2015). The surface chemical
78 modification have been used to enhance the barrier properties and water
79 repellency keeping the mechanical properties of NFC films unaltered (Sehaqui et
80 al. 2014; Solala et al. 2018; Operamolla 2019; Zhang et al. 2019).
81 The development of simple and efficient process to produce more efficient films
82 of NFC is subject of research. One interesting process is the use of blocked
83 isocyanates which can be used in non dried films. The reaction of poliisocyanates
84 with cellulose forming urethane(Rueda et al. 2011) is well known (Quinney et al.
85 1995; Gironès et al. 2007, 2008; Paquet et al. 2010). Blocked isocyanates allows
86 the possibility of produce modified cellulose without the need for drying (Wicks
87 and Wicks 1999; Delebecq et al. 2013) and was used for carbohydrates such as
88 starch and cellulose as described by Carvalho et al. Regarding the safety of the
89 material for use in food packaging and the concern with the blocking agent,
90 phenol, we must consider that as the mass gain is less than 0.01% the amount of
91 hay in the final material must be less than 0.001 %. In addition, phenol is a
92 volatile compound that must be removed by evaporation during the dipping and
93 heating process. (Carvalho et al. 2005)

Here, we propose the hydrophobization of NFC films by a dipping and heating treatment using blocked diisocyanates synthetized with 4,4-methylenebis-(phenyl isocyanate) (MDI) and having both phenol and dodecanol as blocked agents. The materials were characterization by infrared spectroscopy, thermogravimetric analysis, 1H-nuclear magnetic resonance, water contact angle, and oxygen and water transmission and water vapor absorption.

Experimental

Materials

Nanofibrilated cellulose (NFC) from eucalyptus was kindly supplied by Suzano S/A., Brazil and received as a 3.2 weight % water suspension. 4,4-Methylenebis (phenyl isocyanate) (MDI), phenol, dodecanol and dibutyltin dilaurate (DBTL) were supplied by Sigma–Aldrich and used as received. Zinc octanoate was supplied by Iracema and was used as received. Reagent grade butyl acetate, xylene and methylene chloride were supplied by Sigma–Aldrich and were dried by storing them with 4Å molecular sieves for at least 72 h before use.

Films preparation

The NFC suspension was diluted to 1% and homogenized with an Ultra-Turrax IKA model T25 operating at 10,000 rpm for 3 minutes. 90 g of the homogenized suspension were dropped into a glass dish plate mold (15x10 cm) to produce a films with gramage of 60 g/m². A sticky tape was used to cover the mold edges in order to avoid wrinkling during the films drying process and a teflon® film was used as demolding agent. The dishes were dried in a circular oven for 24h at 60°C and the smooth NFC films were obtained by trimming the tapes after the drying process.

Blocked diisocyanate synthesis

5 g (20mmol) of 4,4-methylenebis (phenyl isocyanate) and 100ml of anhydrous butyl acetate were introduced into a three neck round bottom flask immersed in a water bath at 45°C with a constant flow of nitrogen.

In another flask, 1.88 g (20 mmol) of phenol (blocking agent) and 0.1 ml of DBTL were diluted in 30 ml of anhydrous butyl acetate at 45°C and this mixture was slowly added (15 min) dropwise into the flask with MDI under vigorous magnetic stirring. After two hours, the initial amount of NCO was reduced to half as confirmed by titration with di-n-butylamine (ASTM D-1638-74), when 20 mmol of dodecanol were added and the agitation was kept for two more hours to ensure full conversion as checked again by titration with di-n-butylamine (Gironès et al. 2007). The product, hereafter termed Ph-MDI-D, was recovered by solvent evaporation at room temperature using a rotary evaporator working at reduced pressure, washed twice with 2-propanol and dried at 60 °C for 1 hour.

Hydrophobization process

A solution of 6 g of Ph-MDI-D, 0.25 g of zinc octanoate in 100ml of xylene/butyl acetate (75/25) mixture was prepared at 60 °C (Gironès et al. 2007). Specimens of NFC films were dipped for 60s into this solution at 60 °C, dried under a nitrogen flow and then placed in an oven for 10 min at 170 °C. The treated films were then washed twice with 100ml of hot xylene and butyl acetate (75/25 v/v), rinsed several times with methylene chloride to remove the excess of Ph-MDI-D, and dried at 60 °C for 1 h.

Characterization

Fourier Transformed Infrared (FT-IR)

FT-IR spectra were collected with a Spectrum 100 (PerkinElmer, USA) with an attenuated total reflection (ATR) accessory in the range of 4000 cm^{-1} to 650 cm^{-1}. Each spectrum was an average of 32 measurements. Spectra were taken reproduced at least twice in different regions. For the purpose of use the FTIR of a semi-quantitative analysis based on the relative absorptions, films spectra were normalized with respect to the absorptions at peak at 1025 cm^{-1} related to the cellulose C-O stretching bond, which should be almost invariable as the chemical modification of cellulose is performed.

Thermogravimetric analysis (TG)

TG measurements were conducted with a Pyris 1 Thermogravimetric Analyzer (Perkin Elmer, USA) analyzer operating under a constant N_2 flow of 20 $mL \cdot min^{-1}$, between 25 and 700 °C and a heating rate of 10 $°C \cdot min^{-1}$.

Liquid ^{1}H-Nuclear Magnetic Resonance (NMR)

^{1}H nuclear magnetic resonance (NMR) analyses were carried out using a AVANCE 600 NMR (Bruker, USA). Samples (200 mg) were added to 4 mL of deuterated dimethyl sulfoxide (DMSO-d6) and stirred for 5 min to get a homogeneous solution which was introduced into a 10 mL NMR tube. NMR data was used to confirm the structure of the hydrophobizing moieties.

Tensile test

Tensile tests were recorded in an universal testing machine model 3365 (Instron, USA) equipped with a load cell of 5 kN and with extension rate of 0.5 mm min^{-1} and 25 mm distance between the grips. For each sample, five rectangular specimens of 35x5 mm were tested in an environment at 23°C with a relative humidity of 48%. The samples were preconditioned in the same environment for at least 24h before testing. The specimen thickness was measured using a digital micrometer (Adamel Lhomargy-120mm, France).

Grammage

The grammage, measured as mass per unit area (g/m^2), were obtained by weighing ten samples of 50 x 50 mm (0.1 mg accuracy).

Tear Testing

The tear resistance was measured using a Noviprofibre tear tester (Elmendorf, France) equipped with a 4000 mN pendulum. Tear resistance is a measured of the out of plane resistance displayed by the films in response to the tear movement automatically initiated by the testing device after a notch of 20 mm is made in the midplane of the film. Three specimens of each composition were cut in squares of 50x50 mm and the tear index was calculated using the gramage values of the dry specimens.

Scanning Electron Microscopy (SEM)

An Inspect F-50 (FEI, USA) microscope working at 2.0 kV and working distances from around 8.0 mm was employed for SEM analysis. Images were acquired in

193 the mode of secondary electrons (SE). Films were prepared by bonding squares of
194 the material to a double sided carbon tape, which were further metalized for 90s
195 with a platinum target.
196

197 *Atomic Force Microscopy (AFM)*

198 AFM images were obtained using an AFM model Flex-Axiom (Nanosurf,
199 Switzerland) working in tapping air mode. Films squares of 1x1 cm, previously
200 dried at 60 °C for 2 hours, were bonded by a double sided tape and pressed in the
201 sample holder The silicon scanning probe used was a Tap190Al-G with a
202 maximum radius of curvature of 10 nm and 150 kHz as the resonance frequency
203 of the cantilever. Images processing and roughness calculation were performed
204 using the freeware software Gwyddion®. The average roughness (Ra), the mean
205 square root roughness (Rq), and the maximum profile height (Rt) were calculated
206 from the average values of five parallel horizontal lines of 30 μm, spaced by 5
207 μm. The parameters were obtained in accordance with ASME B46.1-1995
208

209 *Water contact angle*

210 Contact angles were measured using a tensiometer model CAM 101 (KSV
211 Instruments Ltd., Finland). Specimens were cut into rectangular shapes with a
212 width of 5 mm and length of 30 mm from different regions of the films for each
213 composition. The values were collected from five measurements with distilled
214 water (droplet of ~5 μl). and the static contact angles were obtained by plotting
215 the contact angle *vs* time, where the equilibrium value (static) was determined.
216 Measurements were performed at 23 °C and 30% RH.
217

Water vapor absorption test

The test was conduct in accordance with ASTM E-104 (1985 using a desiccator with potassium sulphate (K_2SO_4) saturated with distilled water (RH=97.5%). 3 specimens of each sample in dimensions of 2.5x2.5 cm were weighted at regular intervals until complete saturation. The vapor water uptake, and the diffusion coefficient were calculated as reported by Dufresne *et al*. (Dufresne et al. 2000), using equation 1, where M_∞ is the mass at saturation point, M_0 the dry mass and M_t the mass at the given time t. 2L is the thickness of the films and D the diffusion coefficient. Fickian diffusion coefficient is obtained by the plot of $(M_t - M_0)/M_\infty$ as a function of $\sqrt{(t/L^2)}$.

$$\frac{M_t - M_0}{M_\infty} = \frac{2}{L}\sqrt{\left(\frac{D}{\pi}\right) * t} \qquad (1)$$

Water vapor transmission rate (WVTR)

WVTR measurements were performed in accordance with ASTME96, using the desiccant method. Samples were attached to aluminum cups filled with 15g of calcium chloride and open area of 3000 mm². Sealed assemblies were placed in a 50% humidity chamber and the increase in mass due the water absorption was measured over time. The linear coefficient of the trend line (G/t) was determined in g/h. WVTR values were calculated dividing (G/t) by the open area and is reported in g/m²*day. Permeability is calculated dividing WVTR by the product of vapor pressure difference and the vapor pressure saturation at the test temperature. The desiccant method was chosen over the wet cup method for experimental easiness, as the movement of the cup could wet the bottom surface of the films

and harm the experiment. As will be discussed in the text, the desiccant method provide WVTR values in the same range as wet cup test.

The diffusion coefficient D_{eff} can be described as a function of D_a and D_f (equation 2), where τ_p and τ_f are the tortuosities, respectively and Ɛ the porosity. As $D_a >>>> D_f$, D_{eff} can be written as a function of $D_a \frac{\varepsilon}{\tau_p}$ without major losses. Also, an approximation can be made for the tortuosity τ_p, relating it to the porosity using equation 3, where α = 0.65, m =0.19 and ε_p is the percolation threshold and its value is 0.33 (Hu et al. 2019).

$$D_{eff} = D_a \frac{\varepsilon}{\tau_p} + D_f \frac{(1-\varepsilon)}{\tau_f} \quad (2)$$

$$\tau_p = 1 + \alpha \frac{(1-\varepsilon)}{(\varepsilon-\varepsilon_p)^m} \quad (3)$$

Also, the Knudsen number N_{Kn} and Knudsen diffusivity D_{KA} were calculated as reported elsewhere (Spence et al. 2011).

Oxygen Transmission rate (OTR)

OTR of the films which is given in cm³/m²/day (ASTMF1927-07) was determined using an 8001 Oxygen Permeation Analyser (Systech Illinois, USA) equipped with a coulometric oxygen sensor. Double bonded adhesive aluminum foils, with an open area of 2.54 cm², were used to place films samples in the measurement device. Test were initiated when purge level was below 10 OTR. Three specimens of each sample were analyzed and the transmission rate was followed until the steady-state flow rate was achieved and OTR values were obtained.

Results and discussion

Adduct characterization

Figure 1 shows the FT-IR spectra of the reactants (MDI, phenol, and dodecanol) and the adduct Ph-MDI-D. The spectrum of Ph-MDI-D presents the bands of C-O stretching vibrations of phenol at 1180-1260 cm^{-1} and the -CH_2- vibration of dodecanol in the range of 2920-2855 cm^{-1}. Also, the changes on -NCO absorption at 2262 cm^{-1} and hydroxyl absorption at 3323 cm^{-1}, indicating the reaction of the diisocyanate with phenol and dodecanol. At 3323 cm^{-1} the new steep absorption is due to the N-H vibration of urethanes (Gironès et al. 2007) .C=O bands at 1720 cm^{-1} and 1705 cm^{-1} arise respectively from the phenyl carbamate and alky carbamate moieties (Gironès et al. 2007) and C=O band related to the formation of urea at 1638cm^{-1} The absence of bands at 1770 cm^{-1} from uretdiones (Meyer-Stork et al. 1992) indicates that no self-polymerization of MDI had occurred. Moreover, in an additional test in which the thermal treatment was not applied, i.e a sample was dipped and washed afterwards one observed that the described peaks were not observed in the spectra indicating that there is no significant physisorption of the moieties during the treatment.

Figure 2 and **Table 1** shows the ^{1}H-NMR spectrum and the area under the peaks of Ph-MDI-D, respectively. N-H peaks regarding to phenyl and alkyl carbamates are observed at 9.4 ppm (B) and 9.2 ppm (C) with areas of 1.2 and 1, respectively, indicating that blocked diphenyl MDI (Ph-MDI-Ph) was also formed. Peaks (I), (K), (L) and (M) are related to the C-H from -CH, -CH_2 and -CH_3 of dodecane moieties and C-H peaks of aromatic rings are observed at 7.4-7.3 ppm (E) for MDI and 7.1 (F) ppm for phenol. CH_2 peak from MDI is observed

at 4.1-3.9 ppm (H). The remaining peaks are product of the reaction of MDI with residual moisture, as is the case of alophanates (A- 10 ppm) and disubstituted ureas (D-8.5 ppm). Nonetheless, as showed in. **Scheme 1** and **Scheme 2**, blocked isocyanates could still be formed regardless the presence of alophanates or ureas. Therefore, the presence of alophanates and disubstituted ureas, even if not desired, can also contribute to decrease the cellulose hydrophilic character.

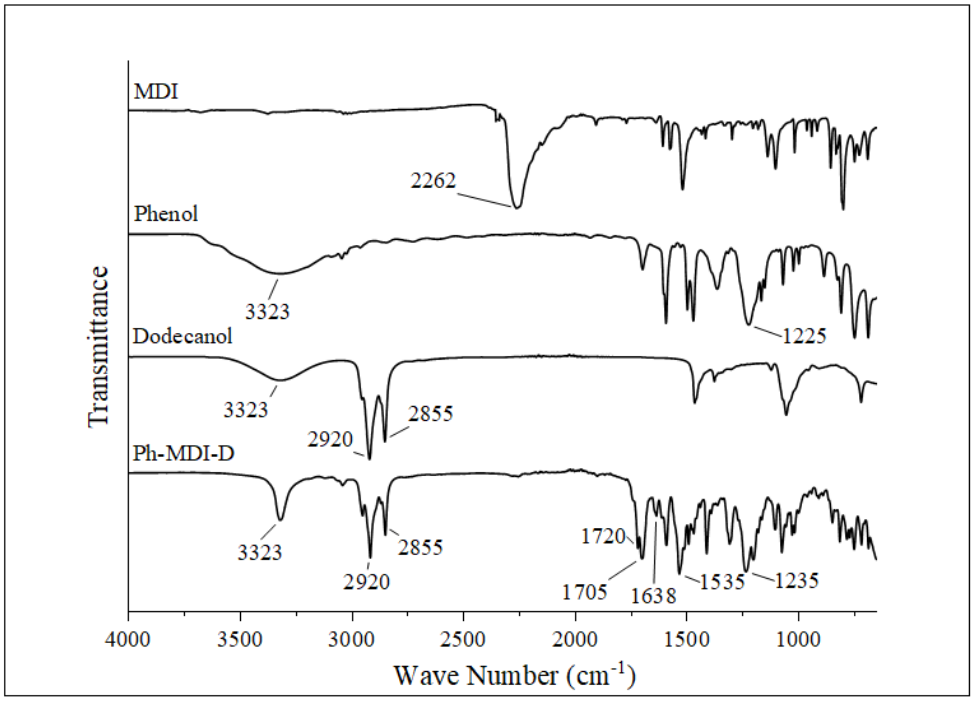

Figure 1. ATR-FTIR spectra of the reactants and the synthetized blocked Ph-MDI-D diisocyanate.

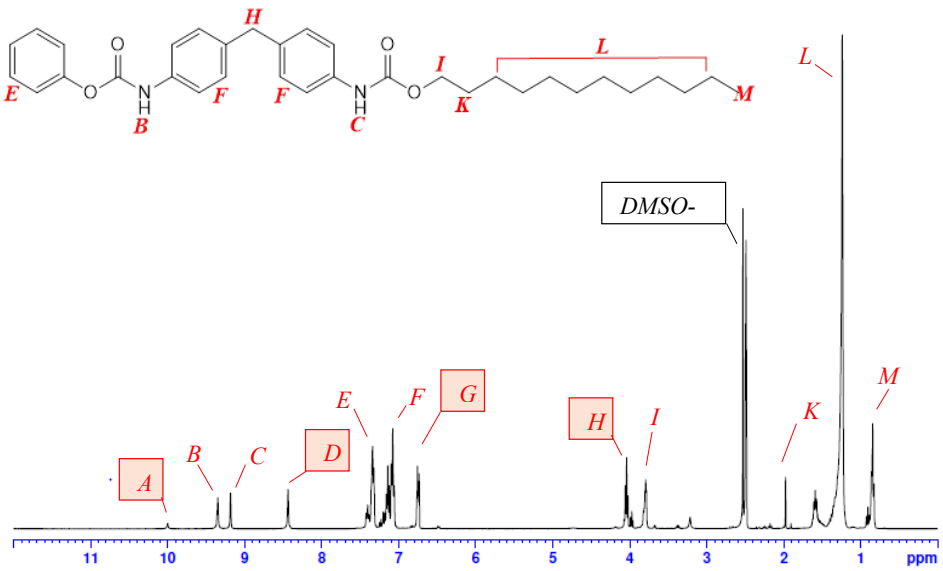

Figure 2. ^{1}H-NMR spectra of the synthetized Ph-MDI-D blocked diisocyanate.

Table 1. ^{1}H-NMR peaks identification and their corresponding areas.

Peak	ppm	Identification	Area
A	10.0	Alophanates	0.2
B	9.4	Phenyl carbamate	1.2
C	9.2	Alkyl carbamate	1.0
D	8.5	Disubstituted urea	1.3
E	7.4-7.3	Aromatic rings (phenol)	6.8
F	7.1	Aromatic rings (MDI)	9.2
G	6.9-6.7	Primary amine	3.1
H	4.1-3.9	-CH_2- MDI	3.4
I	3.8-3.7	C1-CH_2- dodecanol	3.0
K	1.6-1.5	C2-CH_2- dodecanol	3.8
L	1.3-1.1	-CH_2- dodecanol	29.8
M	0.9-0.8	-CH_3 dodecanol	5.6

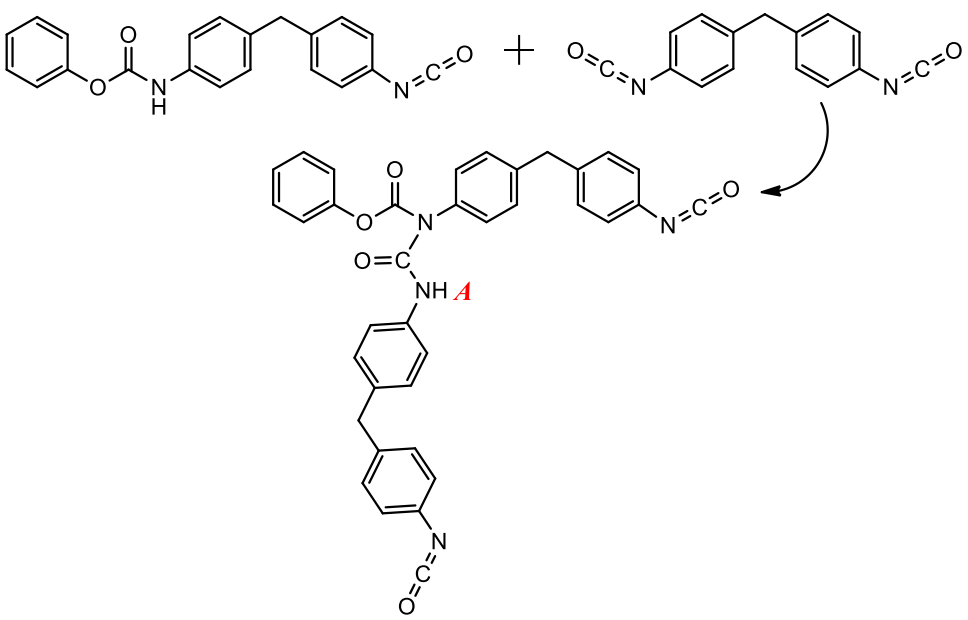

305

306 **Scheme 1**. A possible path for alophanates formation due the reaction of a partially blocked
307 phenol-MDI with a second MDI molecule.

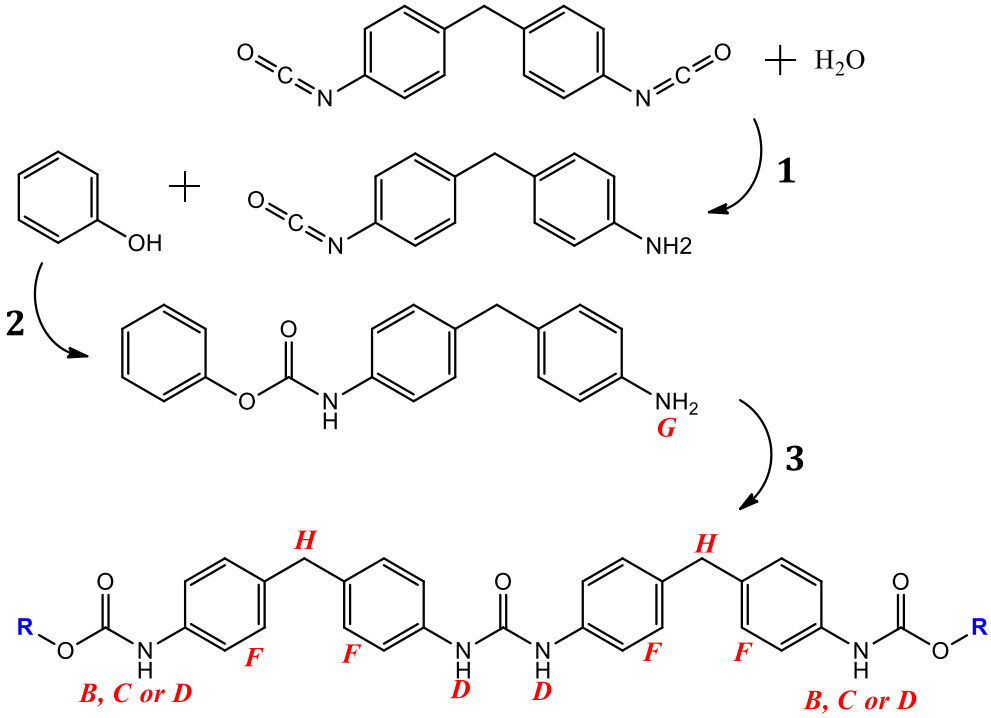

308
309

310 **Scheme 2**. A possible path for the reaction of MDI with residual moisture and formation of
311 disubstituted ureas due the reaction of two partially blocked phenol-MDI having primary amines
312 as second groups.

313

Figure 3 shows the thermogravimetric analysis (TG) plot, evidencing the phenyl carbamate dissociation (de-blocking) between 150 and 230 °C. The loss of mass of 21 $\%_{wt}$ is close to the theoretical value estimated of about 18 $\%_{wt}$ if we consider expected Ph-MDI-D structure with a phenol residue at one side and an dodecanol one at the other. The difference is ascribed to the formation of other products as discussed above.

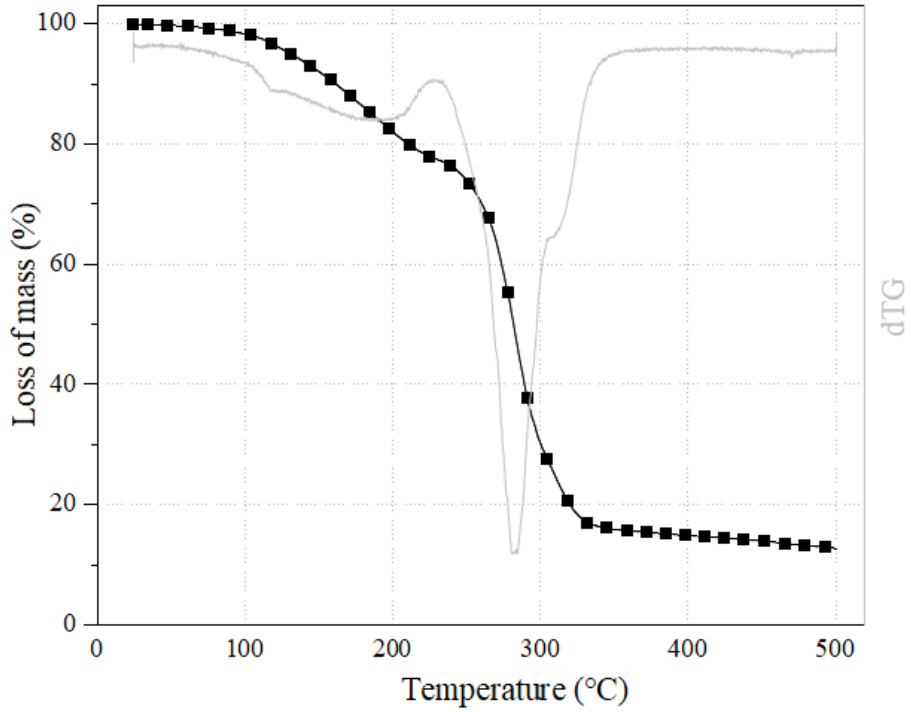

Figure 3. Loss of mass as a function of temperature for the adduct Ph-MDI-D sinthetized

Physical properties of NFC films

NFC films presented a Young's modulus of 6.5 ± 0.7 GPa, tensile strength of 108 ± 10 MPa, elongation at break of 9.0 ± 1.0% and work to fracture of 8.0 ± 1.0 MJ/m^3. Tensile properties remained unaltered by the hydrophobization process (results not shown). Besides no evidence of thermal degradation was observed due

to the thermal treatment as the color of the films was remained unaltered (Figure S 1).

Table 2 present the gramage, thickness, density, porosity and tear resistance. As observed there is no significant change among the non-treated and treated compositions, which points that the physical properties remained unchanged due to the hydrophobization process and the thermal treatment at 170 °C. This evidences that the net NFC film already presented an excellent compaction and further treatment apparently did not cause an additional hornification, which was reported after thermal treatments for 100% NFC films(Sharma et al. 2014a; Xia et al. 2018) In fact, porosity is below the average values reported in literature (Sehaqui et al. 2014; Ferrer et al. 2015; Solala et al. 2018), revealing the good quality of the drying protocol.

Table 2. Phisical properties of the NFC films obtained by casting

	Gramage (g/m^2)	Thickness (μm)	Density (g/cm^3)	Porosity (%)	Tear testing index ($mN*m^2/g$)
NFC	50 ± 10	46 ± 2	1.1 ± 0.2	29 ± 2	0.70 ± 0.09
NFC-MDI-D	49 ± 4	43 ± 3	1.1 ± 0.1	27 ± 1	0.75 ± 0.08

Surface modification characterization

The idealized process of films modification by dipping and heating is showed in Scheme 3. The idealized situation is one in which one MDI molecule react with one phenol and one dodecanol molecules and during the treatment, after phenol releasing, the adduct attach to cellulose surface by forming new urethane bonds with hydroxyl groups mainly from C6, as the primary alcohols are more reactive than the secondary alcohols.

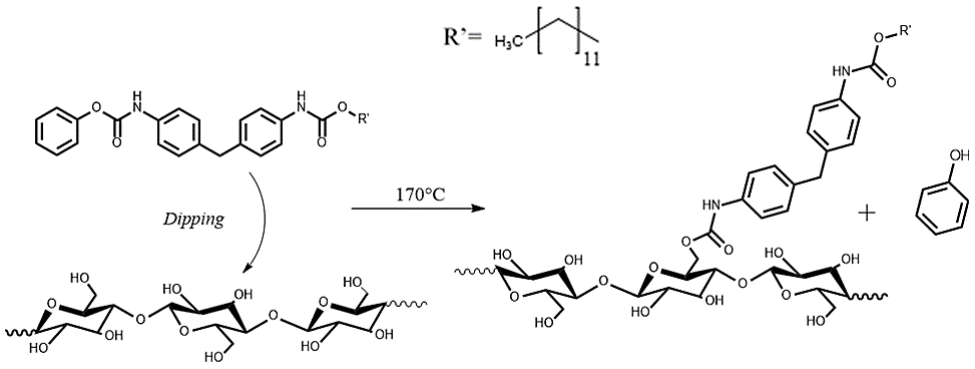

Scheme 3. Reaction involved in the films treatment with the Ph-MDI-D blocked diisocyanate.

Figure 4 displays the FTIR spectra of NFC and NFC-MDI-D films. Absorptions in the range of 1720-1510 cm^{-1} observed in the modified films spectra confirmed the chemical modification since they are related to the presence of carbonyl groups from urethane, as discussed for **Figure 1**. The absorption at 1705 cm^{-1} is related to the alkyl carbamate bond. The presence of the alkyl group is further evidenced by the sharp bands at 2920-2850 cm^{-1} related to methylene groups of the dodecanol moiety. The absorption at 1638 cm^{-1} is related to the presence of disubstituted urea at the films surface, as identified by ^{1}H-NMR spectroscopy.

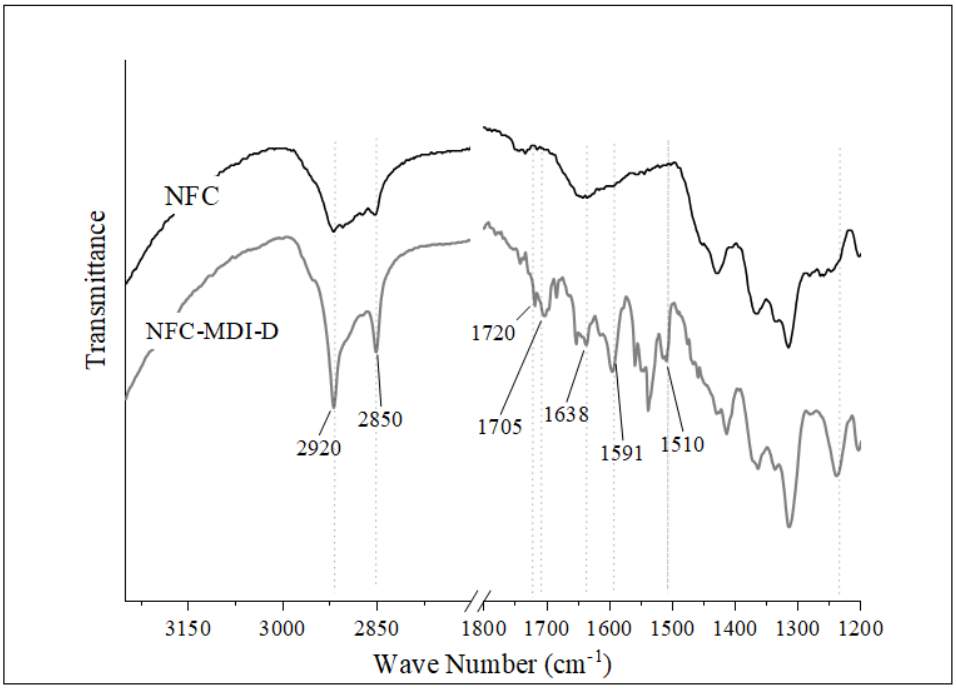

Figure 4. ATR-FTIR spectra of the prestine NFC films and the chemical modified NFC-MDI-D films, hydrophobized by the dipping and heating treatment with the Ph-MDI-D blocked diisocyanate.

Figure 5 shows the image of scanning electron microscopy of the NFC films (5.a-b) and NFC-MDI-D films surfaces (5.c-d). These images show compact and homogeneous surfaces for both samples without apparent voids, with no clear differences between the two materials. It is interesting to observe that the surface morphologies of the films were more compact than those described in the literature. For example, Sehaqui *et al*. (Sehaqui et al. 2014) employed a solvent exchange from water to acetone to obtain NFC films and obtained SEM surface images with visible spaces between the individual fibers. Yufei *et al*. (Chen et al. 2017) observed more compaction at the surface of their films, but distinguishable small size nanofibers were still noticed, which are also observed when films from BC-NFC are obtained (Klemm et al. 2018b; Urbina et al. 2019). We attribute the present features to a combination of the conditions of drying, being the most

relevant conditions the drying time and temperature and initial nanofiber suspension concentration, which led to high compaction between the closely attached filaments during the casting drying process.

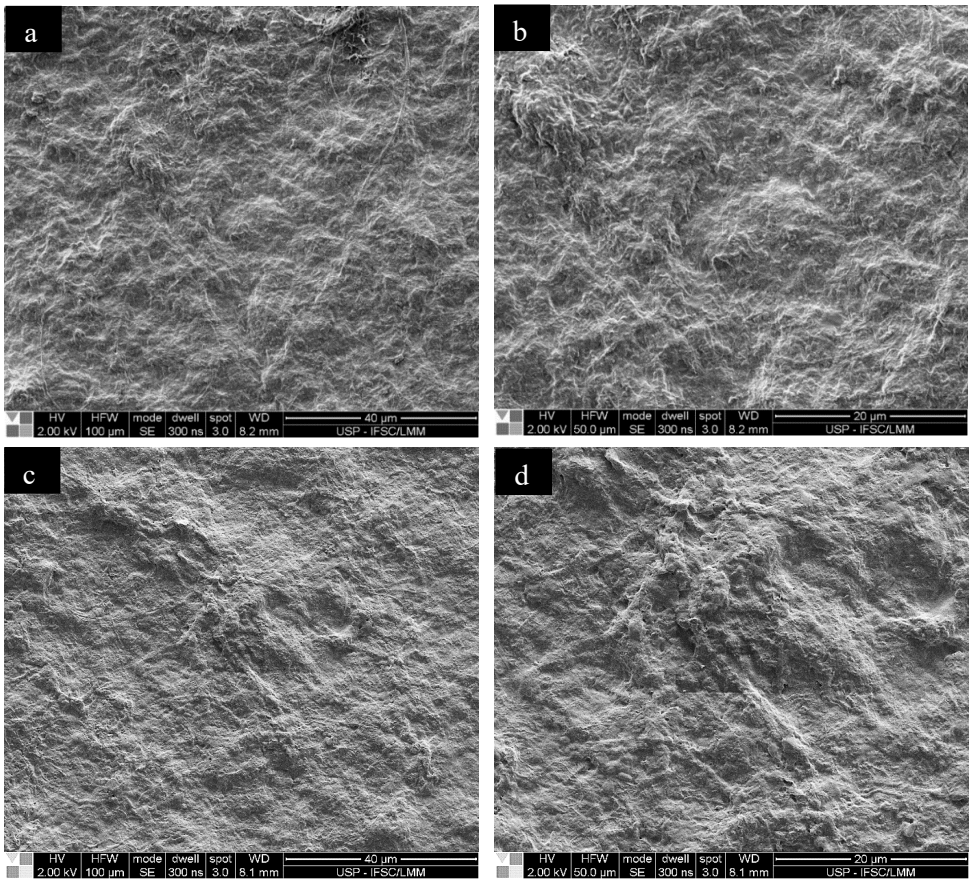

Figure 5. Surface SEM images of NFC films (a-b) and chemical modified NFC-MDI-D films (c-d) showing no morphological difference between the hydrophilic and hydrophobic films.

Figure 6 shows the AFM images of NFC films (6.a-b) and NFC-MDI-D films (6.c-d). 6.a,c illustrate the surface topography of the samples within a 30 µm x 30 µm area and 6.b,d show the isometric views, which reveal some features about the roughness at each surface. The NFC-MDI-D films displays a higher height in comparison to that of the untreated one (1.6 over 1.1 µm), although a more compact structure is seen in the perspective view. NFC films, on the other hand, presents morphology more resembling “cloud” shapes. It is possible that during

the thermal treatment, the NFC films under modification shrank due water losses and then its surface became more compact, even if the bulk structure remained unaltered (Li et al. 2019a). As the NFC-MDI-D films was already hydrophobized, it did not reabsorb moisture from the environment until the tests were performed, thus keeping its shrank surface. **Figure 7** shows three parameters of roughness calculated using Gwydion® from where one observes the undoubtedly increase in roughness due the surface treatment onto NFC films.

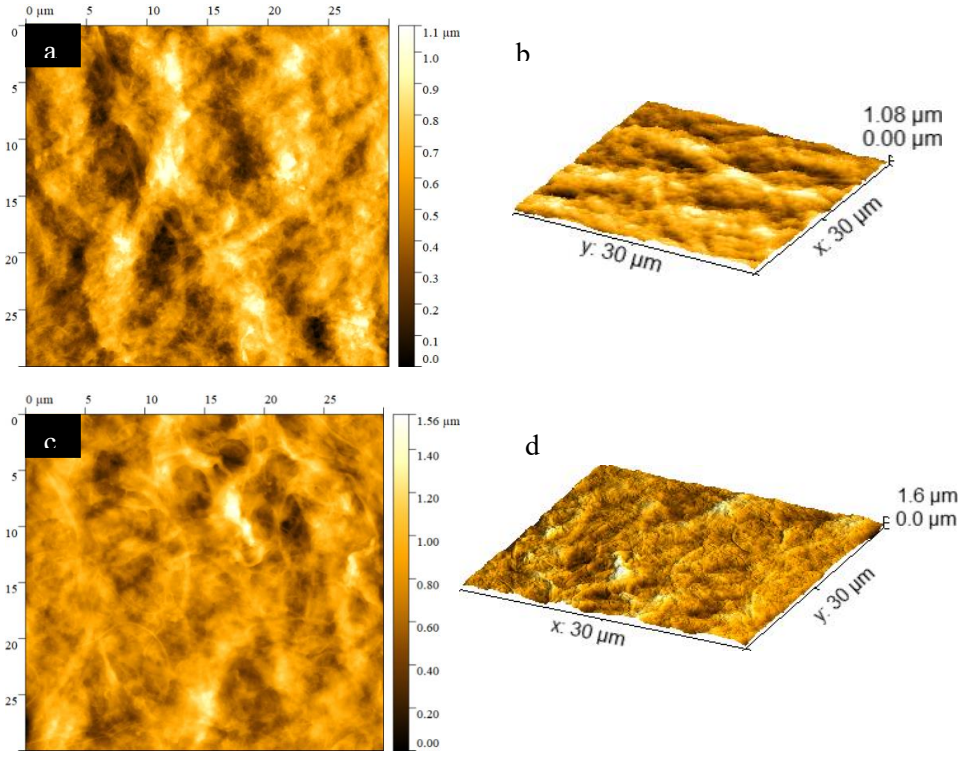

Figure 6. Surface AFM images of the NFC films (a-b) and of the chemical modified NFC-MDI-D films (c-d).

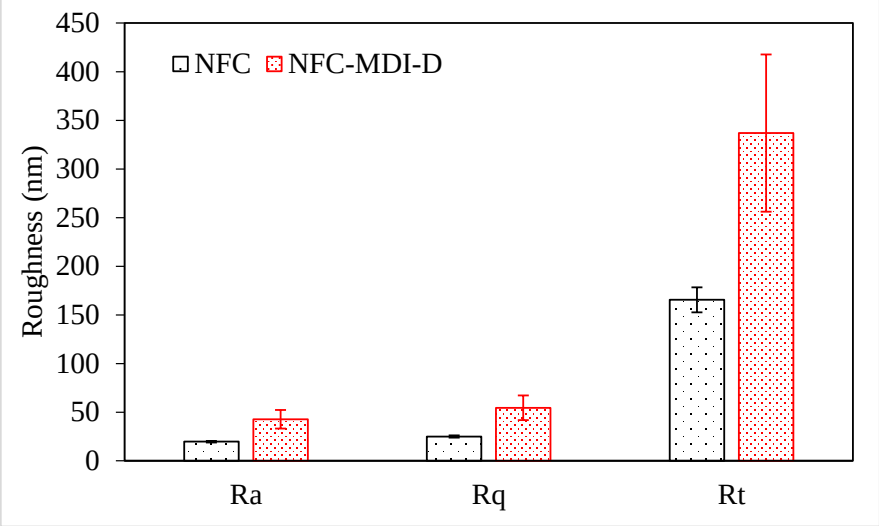

Figure 7. Three parameters of roughness measured for NFC and NFC-MDI-D films.

Hydrophobicity

Figure 8 highlights that the apparent static contact angles value of NFC-MDI-D films more than doubled in relation to that of the pristine NFC films. The increase in roughness due the chemical treatment also contributed to a higher WCA for the chemical modified films (Hubbe et al. 2015; Ferrer et al. 2017). The WCA value of the hydrophobized surface is similar to that obtained by Sehaqui *et al*. (Sehaqui et al. 2014), where a 118° was achieved by grafting the NFC films surface with a C-16 alkyl chain. Sharma et *al* and Xia et *al* performed thermal treatments at 170 °C for 3 hours to enhance hydrophobicity of NFC films (Sharma et al. 2014b; Xia et al. 2018). The treatments gave rise to NFC films with WCA around 90 °C, which are values lower than the obtained here for the dipping and heating treatment. This indicates that the hydrophobizing agent was responsible for enhancing the hydrophobicity of the films more than the thermal treatment alone

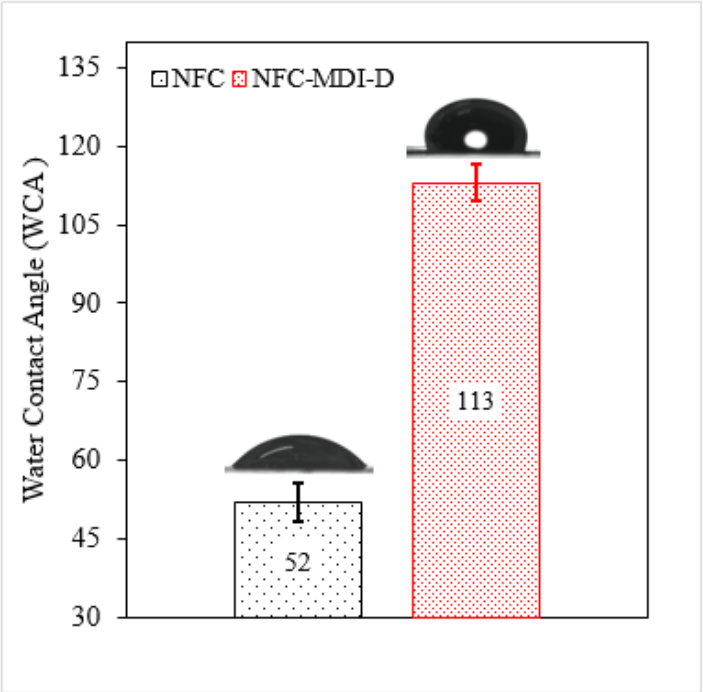

Figure 8. Water contact angle for the pristine NFC films and the surface modified NFC-MDI-D films, chemical modified by the dipping plus heating treatment with the blocked diisocyanate.

Water absorption

The water repellency was not accompanied by a reduction in water vapor absorption, as can be observed in **Figure 9**. The NFC films absorbed a very low amount of moisture (~5%) during the entire period of test (nearly 400 h). The hydrophobized NFC films (NFC-MDI-D) showed the same trend until around 53 h after which the uptake increased sharply to 20%, a value which then was maintained until the end of the experiment. Beyond the surface modification the only difference among the produced films is the roughness. NFC-MDI-D presented twice the roughness value, as measured by AFM, and as the hydrophobization was performed by a dipping process, only 0.1-1% of the cellulose C6-hydroxyls were accessible for functionalization (Gironès et al. 2008). One can assume that the higher surface area of NFC-MDI-D played a more important role on the water absorption than the hydrophobization barrier, leading

to superior water uptake. In spite of the difference, the value of water vapor uptake is still small when compared to the literature data where composite NFC/PU films gave a reduction from 93% to 33% in water absorption due the presence of 60% of PU (Sethi et al. 2018; Li et al. 2019b).

The Fickian diffusion coefficient, *D*, calculated using equation 1 show values of 9.0E-07 cm/s for NFC films and 2.0E-06 cm/s for NFC-MDI-D films. The values should be regarded with care as the films did not show a well-defined plateau of moisture absorption, and hence the trend line did not display a good linear regression, with R^2=0.26 for NFC films and R^2=0.77 for NFC-MDI-D films.

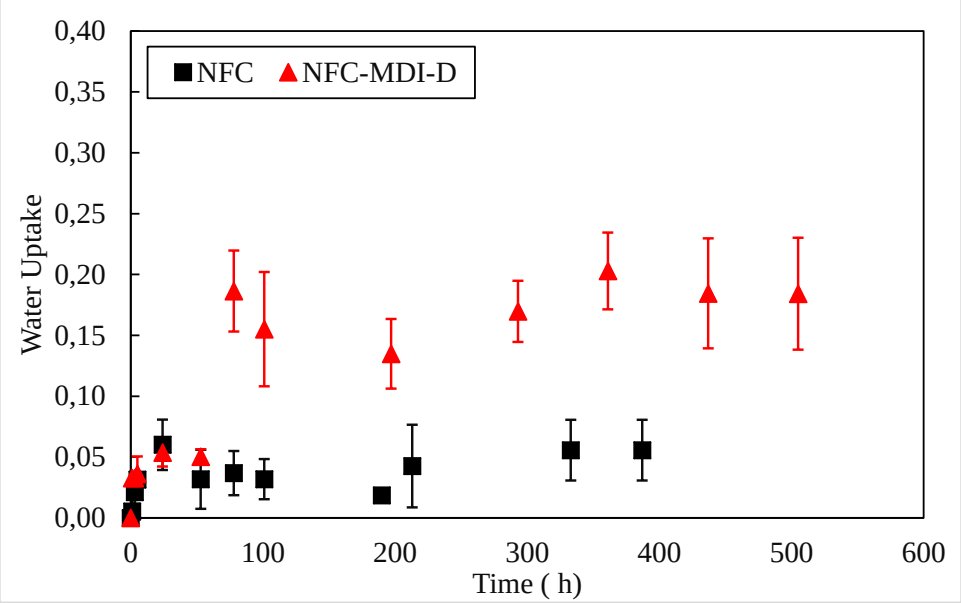

Figure 9. Water vapor uptake as a function of time (h) for NFC and NFC-MDI-D films.

Barrier properties to water vapor and oxygen

Figure 10 shows the increase in mass (g) as a function of time (h) for the permeation tests. The Water Vapor Transmission Rate (WVTR) was obtained from the tangent of the trend line (*W* -**Table 3**). For the NFC films, *W* was calculated from the linear fitting of the first four points as the overall mass absorption followed a second order trend instead of a linear one. The second order

behavior of untreated films can be ascribed as the plasticizing effect that water had on the fiber-fiber interactions. After adsorption, water started accumulating within the pores, instead of desorbing from the lower humidity interface of the films and then continually changed the humidity gradient over time, which culminated to a different path for mass transport (Li et al. 2019a). The WVTR of the neat NFC film is similar to the ones presented by other authors using wood NFC and the same test conditions (50% RH). Therefore the calculation was not significantly affected by the linear extrapolation (Rodionova et al. 2011; Djafari Petroudy et al. 2019). Moreover, the above mentioned authors employed a dynamic analyzer equipped with a wet cup tester in their test, indicating that there is no plausible variation between results obtained from the wet and desiccant method while measuring WVTR of wood NFC films with the same level of porosity.

The NFC-MDI-D films, on the other hand, fitted with good approximation within a linear plot (R^2=0.97) and thus all points were used to calculate *W*. The hydrophobic nature of the modified surface hindered the water molecules adsorption (one of the key steps of mass transportation) and thus contributed to a lower WVTR (Li et al. 2019a).

Comparing the measured WVTR values with those in the literature, one can observe that even the pristine NFC films produced shows a very good water vapor barrier property when compared to other drying protocols. Solala *et al*. (Solala et al. 2018) obtained values of 800-900 g/m²*day for surface esterified NFC films. Willberg-keyriläinen *et al*. (Willberg-keyriläinen et al. 2017) measured a WVTR of 650 g/m²*day for neat NFC films and 400 g/m²*day for ester coated ones. Ferrer *et al*. (Ferrer et al. 2017) reached a value of 234 g/m²*day for pristine NFC films and Spence *et al*. (Spence et al. 2011) measured values of 100-150 g/m²*day

for NFC films coated with 5%$_{wt}$ with kaolin, calcium carbonate and starch. More recently, Seyed *et al*. (Djafari Petroudy et al. 2019) reported a WVTR of 206 g/m²*day for pristine NFC films which was reduced to values as low as 108 g/m²*day for lignin rich films. Lignin content was further increased in lignocellulosic films prepared by Rojo *et al*. (Rojo et al. 2015) with unbleached pulps. It was argued that lignin was responsible for filling the voids between the films, enhancing tortuosity and thus reducing WVTR. Films that presented higher WVTR values were in general more porous than the NFC film obtained in the present study, an indicative that our casting protocol conditions led to more compact and less water permeable films.

The WVTR found here for the NFC-MDI-D films is among the lowest values reported, showing the benefits of the surface modification with a blocked diisocyanate. This treatment brought about a reduction of approximately 75% in relation the pristine precursor, i.e. one of the best achievement attained to the best of our knowledge (Sehaqui et al. 2014; Willberg-keyriläinen et al. 2017; Solala et al. 2018).

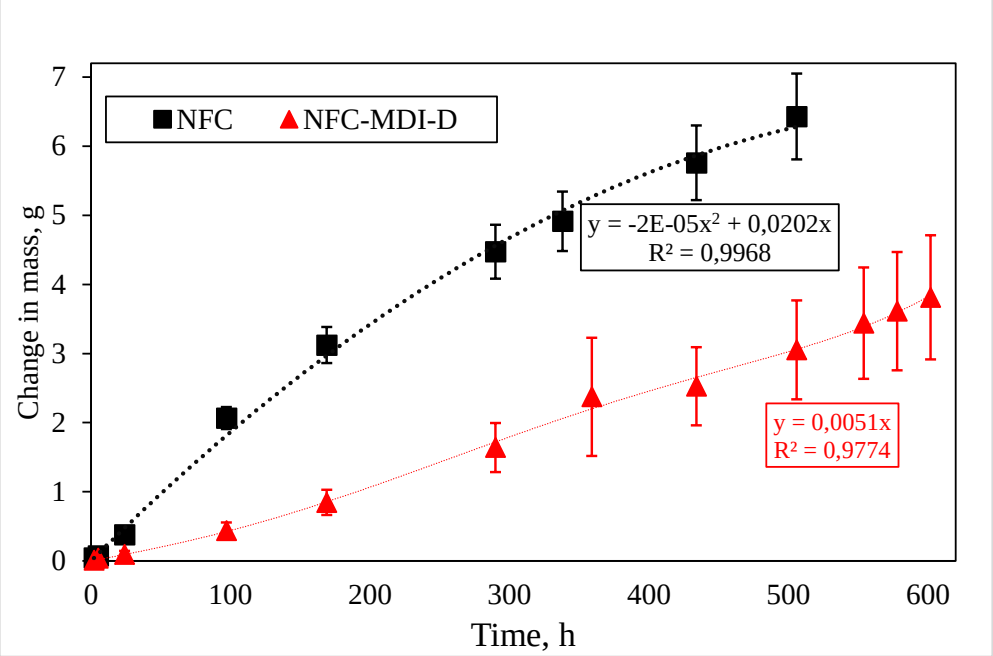

Figure 10. Mass variation as a function of time for NFC and NFC-MDI-D films obtained by the wet cup permeance test.

Water Vapor Permeability, which takes the humidity amplitude and the film thickness into account, are also present in **Table 3**. Based on WVP values, pristine NFC film is framed as a poor water barrier material(Wang et al. 2018), as it had a WVP higher than 3000. The modified NFC-MDI-D jumped to the "low" category, having a WVP comparable to some specific PVC, BOPP, PHA and PLA compositions(Wang et al. 2018).

Table 3. Physical parameters calculated using the data from wet cup permeance test applied to equation 2.

	W (g/h)	WVTR (g/(m²*day))	WVP (g*µm/(m²*day*kPa))
NFC	0.0191	152.82	5065
NFC-MDI-D	0.0051	40.81	1264

The Fickian flux (J), the Diffusion coefficient (D_{eff}), the tortuosity (τ) and the pore space diffusion coefficient (Da) were calculated from the *W* values using equations 2 and 3 and are given in **Table 4**. The diffusion coefficient Da, show

521 the same order of magnitude (10^{-8}cm/s) as values reported for other NFC films
522 (Rahmani Seraji et al. 2017) and it was reduced by 3.5 times following the surface
523 hydrophobization.

524

525 **Table 4.** Fickian diffusion parameters calculated using the data from wet cup permeance test.

	W (g/h)	w (mol/s)	J (mol/cm²*s)	H (cm)	Deff (cm²/s)	τ	Da (cm²/s)
NFC	0.0191	2.95E-07	9.83E-09	0.0046	8.01E-09	1.85	5.11E-08
NFC-MDI-D	0.0051	7.87E-08	2.62E-09	0.0043	2.00E-09	1.81	1.34E-08

526

527 As NFC film did not follow a linear trend of mass variation over time during the
528 permeation test, it is worth examining mechanisms of mass transport other than
529 the Fickian model. Knudsen diffusion is a candidate for water vapor diffusion
530 since the nano size of NFC filaments could produce very small pore sizes (Spence
531 et al. 2011; Solala et al. 2018). Knudsen numbers were calculated and are reported
532 in **Table 5** and a value below 10 indicates the flux is not following predominant
533 Knudsen diffusion (Spence et al. 2011). This is confirmed by the huge difference
534 of 10^4 between D_a and Na. In fact, a porous radius smaller than 0.02 nanometer
535 would be needed to reflect a Knudsen as main diffusion mechanism. This is a
536 different conclusion from that reached by Solala *et al*. (Solala et al. 2018) who
537 opted for a Knudsen diffusion mechanism, even with films with porosity as high
538 as 50% and Knudsen number below 10.

539

540 **Table 5.** Knudsen diffusion parameters calculated using the data from wet cup permeance test.

	Fiber diameter (nm)	Pore radius (nm)	Knudsen number	Na NFC (cm²/s)	Na NFC-MDI-D (cm²/s)
Min	23	6	1.7	2.89E-04	3.10E-04
Max	75	20	5.5	9.65E-04	1.03E-03

541

The oxygen transmission rate (OTR) performed at dry state (0%RH) resulted in 15 ± 3 $cm^3/m^2/day$ for the pristine NFC film, the same as obtained by Zheng *et al*. (Zheng et al. 2019). This value is already suitable for applications of modified atmosphere packaging in food storage(Wang et al. 2018) and the hydrophobization process to produce NFC-MDI-D resulted in a remarkable reduction to below 0.1 $cm^3/m^2/day$, below the bottom limit of the testing equipment. As far as we know only the hybrid composite films of NFC and talc particles prepared of Liimatainen *et al*. (Liimatainen et al. 2013) displayed such high barrier efficiency. In that case, the well dispersed ceramic particles were responsible for increasing the tortuosity of the films.

The paramount criteria for a material to be applied as a food packaging film is that it has to contribute significantly for conservation and shelf life of the food. This is accomplished mostly by gas barrier features. Reduced oxygen transmission rate combined with reduced water vapor transmission rate and water vapor permeability are the most relevant properties that enables the packaging to preserves the food quality, taste and texture over the time.

The dipping and heating surface chemical modification using blocked diisocyanates was performed in few minutes and exhibited encouraging results, as deeply discussed in the present text. The low quantity of reagent requirement (less than 0.1% in mass of NFC) allied to the low toxicity and chemical inertia at room temperature of blocked isocyanates when compared to non-blocked isocyanates make the protocol controllable and scalable at a minimum environmental cost, making it a promising candidate for future applications in sustainable packaging.

CONCLUSION

The major drawbacks to nanofibrilated cellulose (NFC) films applications are the high hydrophilicity which leads to poor barrier properties in high humidity environments. Here, a hydrophobizing agent based on blocked diisocyanates was synthetized and applied to the surface of NFC based films by a dipping and heating process, which insured its chemical attachment to the cellulosic surface, avoiding water adsorption. Besides, the tight entanglement of nanofibers imposed a tortuous pathway, leading the diffusing molecules to migrate around the solid and homogeneous nanofibers.

The ensuing material displayed remarkable barrier properties as its water contact angle (WCA) increased from 52° to 113°, its water vapor transmission rate (WVTR) reduced from 153 to 40 g/m²*day (a decrease of 74%) and its oxygen transmission rate (OTR) shows a value below 0.1 cm³/m²/day. As the modification was only performed at the surface NFC films had high mechanical strength and its biodegradability maintained after the treatment. The barrier properties obtained are among the lowest reported and the simple and straightforward application of the hydrophobization protocol is suitable for upscaling to an industrial process, since blocked diisocyanates are non-toxic and inert at room temperature.

SUPPLEMENTARRY INFORMATION

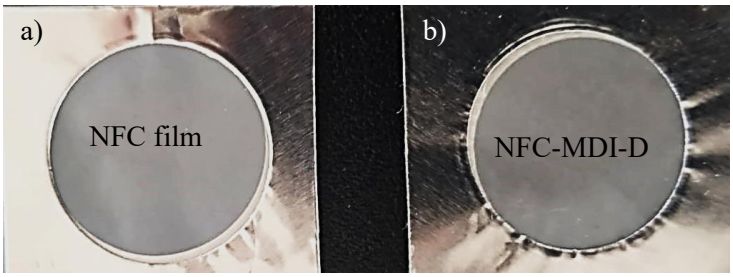

Figure S 1. Pictures of neat NFC film and NFC film treated with blocked diisocyanate at 170 ° C for 10 minutes.

REFERENCES

Arbatan T, Zhang L, Fang X-Y, Shen W (2012) Cellulose nanofibers as binder for fabrication of superhydrophobic paper. Chem Eng J 210:74–79. https://doi.org/10.1016/j.cej.2012.08.074

Carvalho AJF, Curvelo AAS, Gandini A (2005) Surface chemical modification of thermoplastic starch: Reactions with isocyanates, epoxy functions and stearoyl chloride. Ind Crops Prod 21:331–336. https://doi.org/10.1016/j.indcrop.2004.04.027

Chen Y, Geng B, Ru J, et al (2017) Comparative characteristics of TEMPO-oxidized cellulose nanofibers and resulting nanopapers from bamboo, softwood, and hardwood pulps. Cellulose 24:4831–4844. https://doi.org/10.1007/s10570-017-1478-4

Delebecq E, Pascault JP, Boutevin B, Ganachaud F (2013) On the versatility of urethane/urea bonds: Reversibility, blocked isocyanate, and non-isocyanate polyurethane. Chem Rev 113:80–118. https://doi.org/10.1021/cr300195n

Djafari Petroudy SR, Rahmani N, Rasooly Garmaroody E, et al (2019) Comparative study of cellulose and lignocellulose nanopapers prepared from hard wood pulps: Morphological, structural and barrier properties. Int J Biol Macromol 135:512–520. https://doi.org/10.1016/j.ijbiomac.2019.05.212

Dufresne A (2017) Handbook of Nanocellulose and Cellulose Nanocomposites. Wiley-VCH Verlag GmbH & Co. KGaA, Weinheim, Germany

Dufresne A, Dupeyre D, Vignon MR (2000) Cellulose microfibrils from potato tuber cells: Processing and characterization of starch-cellulose microfibril composites. J Appl Polym Sci 76:2080–2092. https://doi.org/10.1002/(SICI)1097-4628(20000628)76:14<2080::AID-APP12>3.0.CO;2-U

Ferrer A, Pal L, Hubbe M (2017) Nanocellulose in packaging: Advances in barrier layer technologies. Ind Crops Prod 95:574–582. https://doi.org/10.1016/j.indcrop.2016.11.012

Ferrer A, Salas C, Rojas OJ (2015) Dewatering of MNFC containing microfibrils and microparticles from soybean hulls: mechanical and transport properties of hybrid films. Cellulose 22:3919–3928. https://doi.org/10.1007/s10570-015-0768-y

Garusinghe UM, Varanasi S, Raghuwanshi VS, et al (2018) Nanocellulose-montmorillonite composites of low water vapour permeability. Colloids Surfaces A Physicochem Eng Asp 540:233–241. https://doi.org/10.1016/j.colsurfa.2018.01.010

Gironès J, Pimenta MTB, Vilaseca F, et al (2007) Blocked isocyanates as coupling agents for cellulose-based composites. Carbohydr Polym 68:537–543. https://doi.org/10.1016/j.carbpol.2006.10.020

Gironès J, Pimenta MTB, Vilaseca F, et al (2008) Blocked diisocyanates as reactive coupling agents: Application to pine fiber-polypropylene composites. Carbohydr Polym 74:106–113. https://doi.org/10.1016/j.carbpol.2008.01.026

Heinze T (2016) Cellulose Chemistry and Properties: Fibers, Nanocelluloses and Advanced Materials. In: Rojas OJ (ed) Advances in Polymer Science 271. Springer International Publishing, Cham, p 341

Hu Y, Acharya S, Abidi N (2019) Cellulose porosity improves its dissolution by facilitating solvent diffusion. Int J Biol Macromol 123:1289–1296. https://doi.org/10.1016/j.ijbiomac.2018.10.062

Hubbe MA, Gardner DJ, Shen W (2015) Wettability of cellulosics. BioResources 10:8657–8749

Klemm D, Cranston ED, Fischer D, et al (2018a) Nanocellulose as a natural source for groundbreaking applications in materials science: Today's state. Mater Today 21:720–748. https://doi.org/10.1016/j.mattod.2018.02.001

638 Klemm D, Cranston ED, Fischer D, et al (2018b) Nanocellulose as a natural source for
639 groundbreaking applications in materials science: Today's state. Mater Today 21:720–748.
640 https://doi.org/10.1016/j.mattod.2018.02.001

641 Klemm D, Heublein B, Fink HP, Bohn A (2005) Cellulose: Fascinating biopolymer and
642 sustainable raw material. Angew Chemie - Int Ed 44:3358–3393.
643 https://doi.org/10.1002/anie.200460587

644 Li L, Zhou ZH, Yang B, et al (2019a) Robust cellulose nanocomposite films based on covalently
645 cross-linked network with effective resistance to water permeability. Carbohydr Polym
646 211:237–248. https://doi.org/10.1016/j.carbpol.2019.01.084

647 Li W, Wang S, Wang W, et al (2019b) Facile preparation of reactive hydrophobic cellulose
648 nanofibril film for reducing water vapor permeability (WVP) in packaging applications.
649 Cellulose 26:3271–3284. https://doi.org/10.1007/s10570-019-02270-x

650 Liimatainen H, Ezekiel N, Sliz R, et al (2013) High-strength nanocellulose-talc hybrid barrier
651 films. ACS Appl Mater Interfaces 5:13412–13418. https://doi.org/10.1021/am4043273

652 Liu A, Walther A, Ikkala O, et al (2011) Clay nanopaper with tough cellulose nanofiber matrix for
653 fire retardancy and gas barrier functions. Biomacromolecules 12:633–641.
654 https://doi.org/10.1021/bm101296z

655 Meyer-Stork LS, Höcker H, Berndt H (1992) Syntheses and reactions of urethanes of cellobiose
656 and cellulose-containing uretdione groups. J Appl Polym Sci 44:1043–1049.
657 https://doi.org/10.1002/app.1992.070440613

658 Operamolla A (2019) Recent advances on renewable and biodegradable cellulose nanopaper
659 substrates for transparent light-harvesting devices: Interaction with humid environment. Int J
660 Photoenergy 2019:. https://doi.org/10.1155/2019/3057929

661 Ouyang X, Huang W, Cabrera E, et al (2015) Graphene-graphene oxide-graphene hybrid
662 nanopapers with superior mechanical, gas barrier and electrical properties. AIP Adv 5:.
663 https://doi.org/10.1063/1.4906795

664 Paquet O, Krouit M, Bras J, et al (2010) Surface modification of cellulose by PCL grafts. Acta
665 Mater 58:792–801. https://doi.org/10.1016/j.actamat.2009.09.057

666 Quinney RF, Banks WB, Lawther JM (1995) The activation of wood fibre for thermoplastic
667 coupling, the reaction of wood with a potential coupling agent. J Wood Chem Technol
668 15:529–544. https://doi.org/10.1080/02773819508009524

669 Rahmani Seraji H, Karimi M, Mahmoudi L (2017) In situ monitoring the change of mechanical
670 response induced by the diffusion of saline water in glassy cellulose acetate. Desalination
671 420:191–207. https://doi.org/10.1016/j.desal.2017.07.013

672 Rodionova G, Lenes M, Eriksen ??yvind, Gregersen ??yvind (2011) Surface chemical
673 modification of microfibrillated cellulose: Improvement of barrier properties for packaging
674 applications. Cellulose 18:127–134. https://doi.org/10.1007/s10570-010-9474-y

675 Rojo E, Peresin MS, Sampson WW, et al (2015) Comprehensive elucidation of the effect of
676 residual lignin on the physical, barrier, mechanical and surface properties of nanocellulose
677 films. Green Chem 17:1853–1866. https://doi.org/10.1039/c4gc02398f

678 Rueda L, Fernández d'Arlas B, Zhou Q, et al (2011) Isocyanate-rich cellulose nanocrystals and
679 their selective insertion in elastomeric polyurethane. Compos Sci Technol 71:1953–1960.
680 https://doi.org/10.1016/j.compscitech.2011.09.014

681 Sehaqui H, Zimmermann T, Tingaut P (2014) Hydrophobic cellulose nanopaper through a mild
682 esterification procedure. Cellulose 21:367–382. https://doi.org/10.1007/s10570-013-0110-5

683 Sethi J, Farooq M, Österberg M, et al (2018) Stereoselectively water resistant hybrid nanopapers
684 prepared by cellulose nanofibers and water-based polyurethane. Carbohydr Polym 199:286–

293. https://doi.org/10.1016/j.carbpol.2018.07.028

Sethi J, Visanko M, Österberg M, Sirviö JA (2019) A fast method to prepare mechanically strong and water resistant lignocellulosic nanopapers. Carbohydr Polym 203:148–156. https://doi.org/10.1016/j.carbpol.2018.09.037

Sharma S, Zhang X, Nair SS, et al (2014a) Thermally enhanced high performance cellulose nano fibril barrier membranes. RSC Adv 4:45136–45142. https://doi.org/10.1039/c4ra07469f

Sharma S, Zhang X, Nair SS, et al (2014b) Thermally enhanced high performance cellulose nano fibril barrier membranes. RSC Adv 4:45136–45142. https://doi.org/10.1039/c4ra07469f

Solala I, Bordes R, Larsson A (2018) Water vapor mass transport across nanofibrillated cellulose films: effect of surface hydrophobization. Cellulose 25:347–356. https://doi.org/10.1007/s10570-017-1608-z

Spence KL, Venditti RA, Rojas OJ, et al (2011) Water vapor barrier properties of coated and filled microfibrillated cellulose composite films. BioResources 6:4370–4388

Urbina L, Corcuera MÁ, Eceiza A, Retegi A (2019) Stiff all-bacterial cellulose nanopaper with enhanced mechanical and barrier properties. Mater Lett 246:67–70. https://doi.org/10.1016/j.matlet.2019.03.005

Wang J, Gardner DJ, Stark NM, et al (2018) Moisture and Oxygen Barrier Properties of Cellulose Nanomaterial-Based Films. ACS Sustain Chem Eng 6:49–70. https://doi.org/10.1021/acssuschemeng.7b03523

Wicks D a., Wicks ZW (1999) Blocked isocyanates III: Part A. Mechanisms and chemistry. Prog Org Coatings 36:148–172. https://doi.org/10.1016/S0300-9440(99)00042-9

Willberg-keyriläinen P, Vartiainen J, Pelto J, Ropponen J (2017) Hydrophobization and smoothing of cellulose nanofibril films by cellulose ester coatings. Carbohydr Polym 170:160–165. https://doi.org/10.1016/j.carbpol.2017.04.082

Xia J, Zhang Z, Liu W, et al (2018) Highly transparent 100% cellulose nanofibril films with extremely high oxygen barriers in high relative humidity. Cellulose 25:4057–4066. https://doi.org/10.1007/s10570-018-1843-y

Yousefi H, Faezipour M, Hedjazi S, et al (2013) Comparative study of paper and nanopaper properties prepared from bacterial cellulose nanofibers and fibers/ground cellulose nanofibers of canola straw. Ind Crops Prod 43:732–737. https://doi.org/10.1016/j.indcrop.2012.08.030

Zhang C, Zhang Y, Cha R, et al (2019) Manufacture of Hydrophobic Nanocomposite Films with High Printability. ACS Sustain Chem Eng 7:15404–15412. https://doi.org/10.1021/acssuschemeng.9b02856

Zheng M, Tajvidi M, Tayeb AH, Stark NM (2019) Effects of bentonite on physical, mechanical and barrier properties of cellulose nanofibril hybrid films for packaging applications. Cellulose 26:5363–5379. https://doi.org/10.1007/s10570-019-02473-2

BRIEFS

- A MDI blocked diisocyanate was synthetized with phenol and dodecanol as blocking agents;
- NFC films were obtained by casting and surface modified by dipping and heating;

- Hydrophobic NFC films displayed remarkable barrier properties;
- Water repellency was proved by measuring water contact angle higher than 110°;
- Films with water-vapor transmission reduced to 40 g/m² day by blocked diisocyanates;
- Cellulose hydrophobization by blocked diisocyanates in non-dried conditions;

PAPER 3

Nanofibrillated cellulose films modified by blocked isocyanates emulsions: Barrier properties to water vapor and oxygen

Gustavo de Souza[a,b], Mohamed Naceur Belgacem[b], Alessandro Gandini[b], Antonio José Felix Carvalho[a*]

toni@sc.usp.br

[a]Department of Materials Engineering, Sao Carlos School of Engineering (EESC), University of São Paulo - USP, 13563-120 São Carlos/SP, Brazil

[b]Université Grenoble Alpes, CNRS, Grenoble INP, LGP2, F-38000, Grenoble, France

Highlights

- Modification of nanofibrillated cellulose with blocked isocyanates in aqueous emulsion;
- Films prepared by emulsion casting followed by drying and thermal treatment;
- Chemical modification avoided water plasticizing effect and enhanced barrier properties to water vapor and oxygen;
- Young's modulus up to 5 GPa for urethane modified nanofibrillated cellulose films in wet state;
- Reduced water-vapor transmission rate of 40 $g.m^{-2}.day^{-1}$was obtained for NFC films;

Graphic Abstract

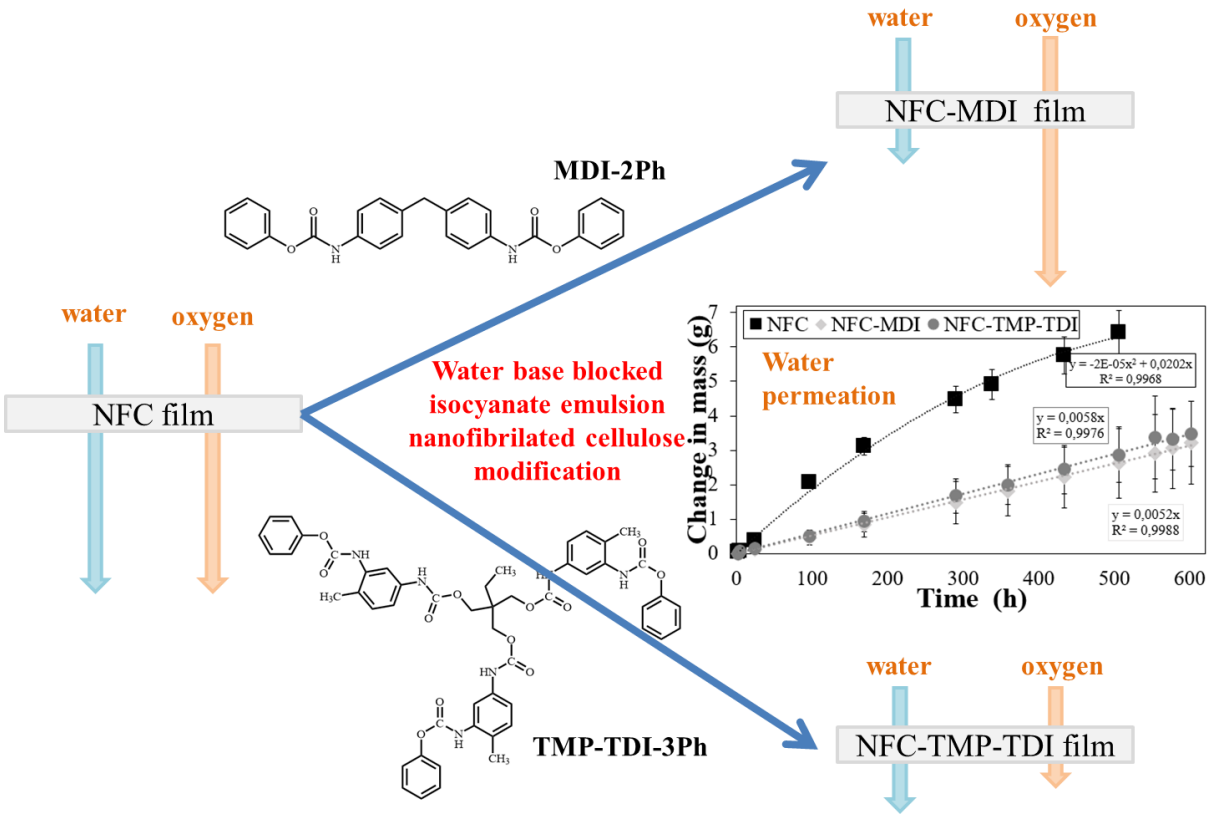

Abstract

The preparation of hydrophobic films of Nanofibrillated Cellulose (NFC) by chemical modification in water media using an emulsion of blocked isocyanates was investigated. After casting at 60°C, the films were heated at 170 °C, allowing water removal followed by isocyanate deblocking and the formation of new urethane bonds with cellulose. Two blocked isocyanates were used, one prepared in our laboratory with 4,4-methylenebis(phenyl isocyanate) and phenol (MDI-2Ph) and the other a commercial product of trimethylol propane and toluene diisocyanate designated as Desmodur AP Stabil® (TMP-TDI-3Ph). The chemical modification of cellulose was confirmed by FT-IR and ^{13}C-NMR**.** The NFC modified films exhibited water vapor transmission rate of around 40 g.m^{-2}.day^{-1}which is 75 % lower than the non-modified NFC film (153 g.m^{-2}.day^{-1}). The film modified with TMP-TDI-3Ph also presented oxygen transmission rate near zero cm³/m²/day. Besides, when exposed to wet environment modified films maintained their stiffness (Young's modulus around 5 GPa) while non- modified films presented a decrease from values around 6.5 GPa to values below 0.1 GPa.

Keywords: Nanofibrillated cellulose films; blocked isocyanate emulsion; nanopaper; isocyanate deblocking; urethane bonds; urethane modified Nanofibrillated cellulose films

1. INTRODUCTION

Short-term materials such as polymeric packaging have become one of the main technical issues of our time due to the incorrect discard, generating environmental pollution and damage to a variety of ecosystems. Naturally occurring polymers, headed by cellulose and its derivatives, have the potential of gradually replacing synthetic polymers in the field of packaging (Klemm et al., 2018; Mahmud et al., 2021).

Cellulose is a worldwide available polysaccharide derived mainly from wood and plants with an annual production of about 7.5×10^{10} tons (Habibi, 2014) and produced as a commodity by the cellulose and paper industry at very competitive price.

The emergence of nanocelluloses headed by nanofibrillated celluloses (NFC) opens new opportunities for conventional plastics replacement (Nechyporchuk, Belgacem, & Bras, 2016; Rol, Belgacem, Gandini, & Bras, 2019). NFC is a valuable derivate of biomass not only due to its renewable character and biodegradability but also due to its outstanding strength/weight ratio, the high reinforcing effect when used in composites and the possibility of being easily functionalized (Gandini & Belgacem, 2016; Habibi, 2014).

NFC can be used for the production of several advanced materials, such as high performance nanocomposites (Siqueira, Bras, & Dufresne, 2010) and high performance all-cellulose films or nanopapers (González et al., 2014; Operamolla, 2019; Sethi, Farooq, Österberg, Illikainen, & Sirviö, 2018; Sethi, Visanko, Österberg, & Sirviö, 2019). These films are produced by drying NFC suspension, leading to an intimately entanglement of the nanofilaments, producing compact, smooth and resistant films with excellent oxygen barrier, making them good candidates for packaging (J. Wang et al., 2018).

Nonetheless, cellulose inherent hydrophilicity make NFC films susceptible to moisture, affecting its mechanical properties, dimension stability, barrier properties to oxygen and water and other characteristics (Lindström & Aulin, 2014; Sehaqui, Zimmermann, & Tingaut, 2014). Thus, it is of fundamental importance the control of its sensitivity to humidity.

In general, the methods most often used to reduce the hydrophilicity of NFC films, involve chemical modifications that require special conditions, such as performing operations in an anhydrous medium and using expensive or toxic reagents. (Balu, Breedveld, & Hess, 2008; Forsman et al., 2017; Operamolla, 2019; Sehaqui et al., 2014; Solala, Bordes, & Larsson, 2018).

One interesting approach to overcome these limitations is the use of blocked isocyanates as chemical modifying agents, which are of low toxicity and can be used in wet environment (Carvalho, Curvelo, & Gandini, 2005; Delebecq, Pascault, Boutevin, & Ganachaud, 2013; Gironès et al., 2008, 2007; Lu et al., 2020; Rol et al., 2019; Wicks & Wicks, 1999; Zhou et al., 2020).

The blocked isocyanates are in fact urethane compounds that are thermo-reversible and depending on the blocked agent used, deblocking or activation temperature take place at temperatures above moisture removal and well below cellulose degradation temperature. It is relevant to observe that below the deblocking temperature the adduct is an inert and non-toxic product (Paquet, Krouit, Bras, Thielemans, & Belgacem, 2010). Phenol is a good candidate as blocking agent because it has a deblocking temperature in the range of 170 - 180° C, i.e. above the temperature of complete water evaporation and below the onset of cellulose degradation (Gironès et al., 2007).The toxicity of the phenol can be dealt by releasing it in controlled environment. Besides, the amount of this compound released is very small, since the modification occurs only on the surface of the fibers.

In our previously research (de Souza, Belgacem, Gandini, & Carvalho, 2021), a phenyl/alkyl blocked diisocyanate was prepared by reacting 4,4-methylenebis(phenyl isocyanate) (MDI) with phenol and dodecanol in equal molar ratios. A film of NFC was surface treated with a solution of the blocked isocyanate in an organic solvent and deblocking conducted at 170 °C.

Here, we propose a new strategy for the production of modified nanocellulose films that consists in the preparation of films using a mixture of NFC suspension and emulsions of blocked isocyanates, one prepared by reacting MDI with phenol (MDI-2Ph) and a commercial one from trimethylol propane and toluene diisocyanate (TDI) blocked with phenol (TMP-TDI-3Ph). MDI-2Ph is bifunctional and TMP-TDI-3Ph is a poliisocyanate with at least three functions. After casting, the films were heated up to 170° C for a sequence of drying followed by deblocking and the formation of high stable urethane linkages within film structure. The materials were characterized by FT-IR, ^{1}H and ^{13}C-NMR, scanning electron microscopy, atomic force microscopy, mechanical tensile test in dry and wet conditions and tear testing. It was observed an increase of wet stiffness and barrier properties to water vapor for films treated with MDI-2Ph and water vapor. Besides, the barrier to oxygen of the films treated with TMP-TDI-3Ph was enhanced significantly.

2. MATERIALS AND METHODS

2.1 Materials

Nanofibrillated cellulose (NFC) from eucalyptus *(Eucalyptus grandis)* with 3.2 % solid content was kindly supplied by Suzano S/A - Brazil. The diameter distribution of the nanofibers was measured using AFM analysis (counting 50 NFC individual fibers) (de Souza et al., 2021) was D_{50}= 23 nm and D_{90}= 73 nm.The size of the eucalyptus NFC obtained through mechanical fibrillation is estimate in 2-3 microns.

Technical grade 4,4-methylenebis(phenyl isocyanate) (MDI), reagent grade phenol, dibutyltin dilaurate (DBTL), reagent grade dimethyl sulfoxide (DMSO) and dodecylbenzenesulfonic acid (DBSA) were supplied by Sigma–Aldrich-USA and used as received. Zinc octanoate was supplied by Iracema Ltda-Brazil. Reagent grade butyl acetate, xylene and methylene chloride were supplied by Sigma–Aldrich - USA and were dried by storing with 4 Å molecular sieves for at least 72 h before use. The commercial blocked isocyanate composed by trimethylol propane, (2,4/ 2,6 – 80/20)-toluene diisocyanate and phenol in the molar proportions of 1:3:3 was supplied by Bayer under the commercial name of Desmodur AP Stabil®. Its reaction path and structure are shown in the supplementary information (Scheme S 1).

2.2 Blocked diisocyanate preparation

A three neck round bottom flask with a constant flow of N_2 was placed into a water bath at 45° C and 5 g (20 mmol) of MDI and 100 ml of anhydrous butyl acetate were added under magnetic stirring. 3.76 g (40 mmol) of phenol and 0.1 ml of DBTL diluted in 30 ml of anhydrous butyl acetate at 45° were then slowly added (15 min dropwise) into the MDI solution under vigorous magnetic stirring. After three hours of reaction, a white precipitate was formed. The completion of reaction was confirmed by titration of free NCO with di-n-butylamine (ASTM D-1638-74). The product was a white powder, isolated by evaporation of the solvent at 30 °C in a rotary evaporator working under reduced pressure. The product was washed twice with 2-propanol and dried at 60° C for 1 hour. Approximately 8 g of the synthesized adduct was obtained at the end of the process, a yield of near 91 %. The depicted structure of the adduct is shown in Scheme S 2.

2.3 Emulsion preparation

The emulsions of blocked isocyanates were produce by adding 350 mg for MDI-2Ph or 310 mg of TMP-TDI-3Ph solubilized in DMSO and 18 mg of zinc octanoate at 50 °C. The mixtures were added directly into 120 g of a NFC suspension (1% wt) and 16 mg of DBSA. Emulsions were homogenized with an Ultra-Turrax IKA model T25 operating at 10,000 rpm for five minutes. Then, It was sonicated using an UP400S Ultrasonic Processor (Hielscher) for five minutes with pulses of 0.5 s and 240 W (60 % power). The amount of blocked isocyanate used was calculated to have 10 times more NCO than the 1 % hydroxyls on the nanofibers surface available for chemical modification(Gironès et al., 2008). The cellulose content of the CNF suspension was adjusted by adding 82.5 ml of distillated water while stirring in a magnetic agitator.

2.4 Films Preparation

To prepare the neat NFC film 90 g of the NFC suspension was degassed in a vacuum desiccator for 10 minutes, poured into glass dish plate mold (15x10 cm) and dried in an air circular oven for 24 h at 60 °C. For each preparation it was used 120 g of previously prepared mixture of NFC/blocked isocyanate emulsion. Cast films were then dried in an oven at 170 °C for ten minutes. This procedure leads to the production of film with a 60 g/m² grammage for the neat NFC film and 80 g/m² for the modified films, dried from emulsions. After demolding, thickness and density were measured as detailed in item 2.5.6.

2.5 Characterization

2.5.1 Fourier Transformed Infrared Spectroscopy - FT-IR

FT-IR spectra were collected with a PerkinElmer Spectrum 100 with an attenuated total diamond covered three reflection (ATR) accessory, in the range from 4000 cm^{-1} to 650 cm^{-1}. Each spectrum was an average of 32 measurements. The spectra were normalized with respect to the absorption of the at 896 cm-1 peak, related to the C-O-C stretching bond.

2.5.2 ^{1}H-Nuclear Magnetic Resonance

^{1}H nuclear magnetic resonance (NMR) analysis was conducted on a Bruker AVANCE 600 NMR. Samples (200 mg) were added to 4 mL of deutered dimethyl sulfoxide and stirred for 5 min in a 10 mL glass NMR tube.

2.5.3 Solid-State ^{13}C-Nuclear Magnetic Resonance

^{13}C nuclear magnetic resonance (NMR) analyses were conducted with a Bruker AVANCE 600 NMR. Films were pulverized using a longitudinal crio-crushing mill device (RETSCH, Germany) working for 10 min at 30Hz.

2.5.4 Scanning Electron Microscopy – SEM

SEM images were acquired in the secondary electrons (SE) mode using an Inspect F-50 (FEI) microscope working with voltage of 2.0 kV and working distances around 8.0 mm. Samples were prepared by bonding films squares onto a double side carbon tape. Stubs were further metalized for 90 s with a platinum target.

2.5.5 Atomic Force Microscopy – AFM

AFM analyses were performed in an AFM model Flex-Axiom (Nanosurf) in the tapping mode with a silicon scanning probe model Tap190Al-G. Film squares of 1 x 1 cm, previously dried at 60 °C for 2 hours, were bonded in a double side tape and pressed in the sample holder. Images were processed with the software Gwyddion®, in which three parameters of roughness set by ASME B46.1-1995 were calculated.

2.5.6 UV-VIS

The in-line light transmittance was measured in the UV-Visible region (200–1000 nm) with a model UVM51 spectrophotometer from BEL photonics. The transmittance spectra were acquired using air as background. Transparency of the films were evaluated by measuring percent light transmittance at 660 nm (T660), in accordance with(Roy & Rhim, 2020). Three measurements were taken per sample and the value presented is the mean value of light transmittance.

193 2.5.7 Gramage, Density and Porosity

194 The gramage, measured as mass per unit area (g/m^2), were obtained by weighing pieces with
195 50 x 50 mm (0.1 mg readability). Sample thicknesses were measured using a digital micrometer
196 (Adamel Lhomargy 120 mm, France). Porosity was calculated using the relation $(1- \rho_m/\rho_t)$ where
197 ρ_m is the measured density and ρ_t the theoretical cellulose density, taken as 1.5 g/cm^3.
198

199 2.5.8 Tensile Test in Dry and Wet Conditions

200 Tensile properties were measured using an Instron 3365 universal testing machine equipped
201 with a load cell of 5 kN and with an extension rate of 0.5 $mm.min^{-1}$ and 25 mm distance between
202 the grips. For each sample, five specimens with a 35 x 5 mm rectangular form were used. Tests
203 were performed in an environment at 23 °C with relative humidity of 48 %. The samples were
204 preconditioned in the same environment for at least 24 h before testing.
205 As a complement to the tensile test, a semi-wet tensile test was performed using the same
206 apparatus. A 10 µl drop of distilled water was placed in the middle length of the specimen and
207 left to rest. After 1 min, the water that did not permeate the specimen was dried with absorbing
208 paper and the sample placed in the testing grips. With the wet tensile the wet/dry ratio was
209 calculated.
210

211 2.5.9 Tear Test

212 Tear resistance of the films was measured using a Noviprofibre tear tester (Elmendorf,
213 France) equipped with a 4000 mN pendulum. The precutting notch was 20 mm in length.
214 Specimens were cut in 50 x 50 mm^2 squares.
215

216 2.5.10 Thermogravimetric Analysis – TGA

217 TGA analyses were performed with a Pyris (Perkin Elmer) thermogravimetric analyser
218 operating under a constant N_2 flow of 20 $mL \cdot min^{-1}$, in the temperature interval from 25 to 700
219 °C, at a heating rate of 10 $°C \cdot min^{-1}$.
220

221 2.4.11 Water contact angle – WCA

222 Static contact angles were measured using a KSV - CAM 101. Five specimens were cut into
223 rectangular shapes with a width of 5 mm and length of 30 mm from different regions of the

films. 40 pictures with 16ms of interval were taken. Five drops with distilled water (droplet with ~5 µl in volume) were performed for each sample. Measurements were performed at 23 °C and 30 % RH.

2.5.12 Water Vapor Absorption Test

The samples were conditioned in desiccator containing a saturated solution of potassium sulphate (K2SO4) at 25 °C which gives a relative humidity of RH= 97.5 %, as stipulated in ASTM E-104 (1985). For each sample, 3 specimens with 2.5 x 2.5 cm was used. The specimens were weighted after 1 h, 3 h, 5 h, 24 h and then at intervals of 24 h in the first week, 48 h in the second and 72 h after the second week until saturation. Before the test samples were dried at 60 °C in a circular oven for 3 days until mass stabilization in the 4th digit scale.

2.5.13 Water Vapor Transmission Rate – WVTR

The WVTR tests were performed using the desiccant method of ASTM E96. Aluminum testing cups with open mount area of 3000 mm² were filled with 15 g of calcium chloride desiccant and sealed at the edges. The assemblies were placed in a 50 % humidity-controlled environment. The increase in mass due to the water vapor absorption by the salt was measured over time. From mass vs time plot WVTR was calculated in $g.m^{-2}.day^{-1}$using equation 1, where (G/t) is the calculated angular coefficient in g/h and A is the cup mouth area in m².

$$WVTR = \left(\frac{G}{t}\right)/A \quad (1)$$

2.5.14 Oxygen Transmission Rate - OTR

OTR measurements were obtained in an 8001 Oxygen Permeation Analyser (Systech Illinois, USA) equipped with a coulometric oxygen sensor according to ASTMF1927-07. Double bonded adhesive aluminum foils, with an open area of 2.54 cm², were used to place film samples in the measurement device.

3. RESULTS AND DISCUSSION

3.1 Blocked isocyanate (MDI-2Ph) preparation and characterization

Figure 1 shows the FTIR spectra of MDI, phenol and the blocked isocyanate prepared from MDI (MDI-2Ph). The isocyanate reaction is confirmed by the disappearance of the NCO vibration at 2262 cm^{-1}, the presence of a narrow sharp vibration at 3323 cm^{-1} due to -NH from urethane and the presence of absorptions at 1720 cm^{-1} and 1590 cm^{-1} related to C=O and H-NCO bond, both groups of phenyl carbamate (Delebecq et al., 2013; Gironès et al., 2008). Urea formation is evidenced by the presence of the characteristic C=O vibration at 1638 cm^{-1}, due to the reaction with residual water. The noticeable increase in the intensity of vibrations at the region of 2920 -2855 cm^{-1} on MDI-2Ph spectrum in relation to those of the precursor reactants can be ascribed to the formation of disubstituted, ureas, allophanates and in less extend, to the presence of residual solvent and catalyst.

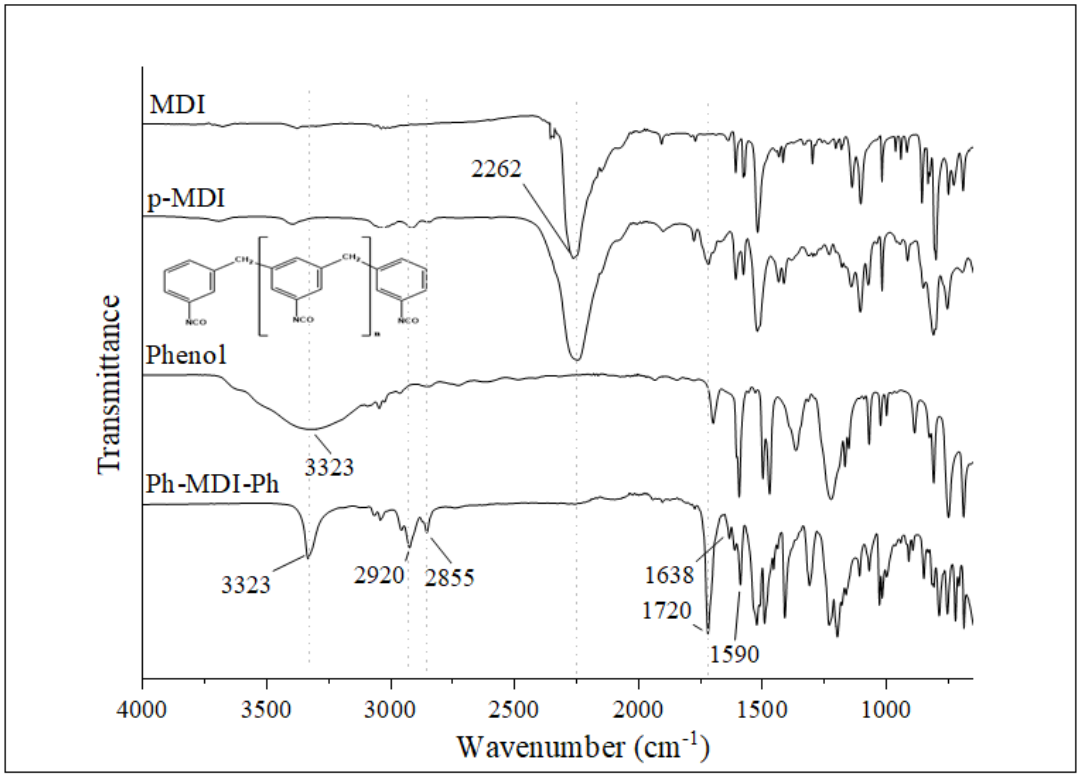

Figure 1FT-IR spectra of the reactants (MDI and phenol) , the polymerized MDI (p-MDI) and the sinthetized adduct (MDI-2Ph).

Figure 2(a) shows the ^{1}H-NMR spectra of MDI-2Ph. N-H characteristic absorption from phenyl carbamates is observed at 9.3 ppm (B) and the C-H shifts from the aromatic rings of phenol and MDI at 7.4-7.3 ppm (D) and 7.1 ppm (E), respectively. Besides, C-H peaks from -CH and -CH_2 of MDI are identified in the region of 4.1-3.9 ppm (G). N-H shifts from primary amines (–NH_2) are observed at 6.9-6.7 ppm (F) and are ascribed to the reaction of MDI with residual water, firstly forming unstable carbamic acids and then decomposing into a primary amine and CO_2 (Delebecq et al., 2013; Wicks & Wicks, 1999). The primary amine formed could further react with another NCO group to form disubstituted ureas, whose N-H resonance is also identified at 8.5 ppm (C). Furthermore, the peak at 10.1 ppm (A) due to the N-H of allophanates is also observed (R. Yang, Wang, & Li, 2014).

Table 1 shows the corresponding areas as being 1.9 for primary amines, 1.0 for disubstituted ureas and 1.2 for allophanates, against 0.6 for the phenyl carbamates. Figure 2 (b) and Figure 2 (c) shows possible paths for disubstituted urea and allophanate formation, illustrating that, although not desired, these products could also lead to the formation of blocked isocyanates.

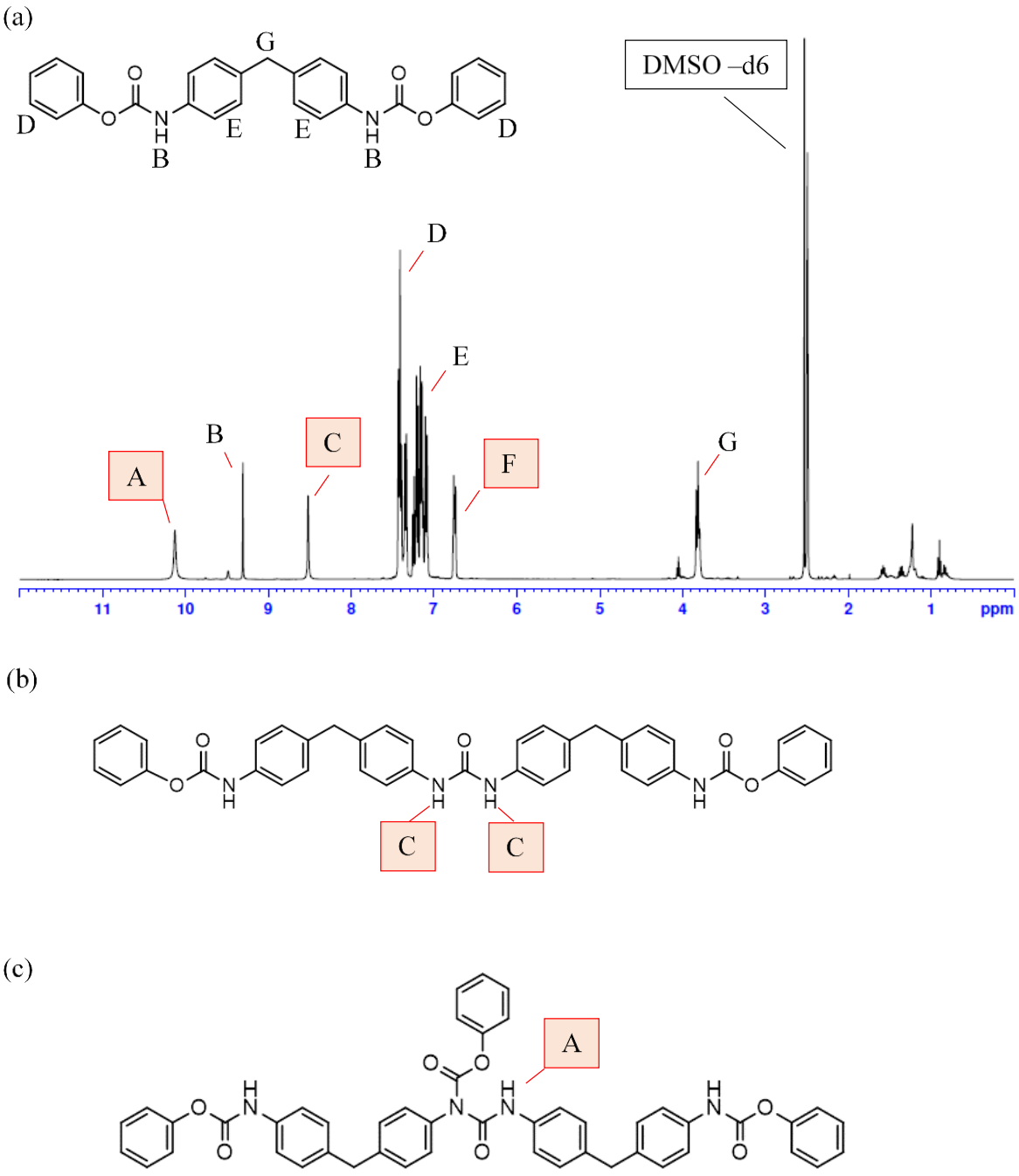

Figure 2.a)[1]H-NMR spectrum of the synthetized Ph-MDI-Ph blocked diisocyanate in DMSO-d6.Possible paths to (b) disubstituted ureas and (c) allophanates formation due the reaction of a partially blocked phenol-MDI with a second MDI molecule

289 Table 1. ^{1}H-NMR peaks identification and their corresponding areas.

Peak	ppm	Identification	Area
A	10.1	Allophanates	1.2
B	9.3	Phenyl carbamate	0.6
C	8.5	Disubstituted urea	1.0
D	7.4-7.3	Aromatic rings (Phenol)	7.5
E	7.1	Aromatic rings (MDI)	10.2
F	6.9-6.7	Primary amine	1.9
G	4.1-3.9	-CH_2- MDI	2.5

290

291 **3.3 Films characterization**

292 Figure 3 (a) shows the FT-IR spectra of the neat NFC, NFC-MDI and NFC-TMP-TDI films.
293 New vibrations related to the formation of urethane bond within the modifies films compounds
294 are observed at 1720 cm^{-1} (C=O stretching from phenyl urethane),at 1630 cm^{-1} (C=O stretching
295 from phenyl urea), at 1600 cm^{-1} (C=C, aromatic stretching), at 1540 cm^{-1} and 1530 cm^{-1} (H-
296 NCO- symmetric stretching), 1235cm^{-1} (C-N stretching) in the spectra of NFC-MDI and NFC-
297 TMP-TDI films.

298 Figure 3(b) gives the solid state ^{13}C-NMR spectra of NFC-MDI and NFC-TMP-TDI films.
299 Peaks ascribed as 1-6 are from the cellulose backbone and are found in both modified films,
300 indicating the maintenance of its primary structures. The presence of resonances at 154.5 ppm
301 (A), related to C=O groups from urethanes, and in the region of 137-130 ppm (B), due to C-C
302 bonds from aromatic rings of TDI and MDI, respectively, are evidences of chemical reaction
303 during the de-blocking step of MDI-2Ph and TMP-TDI-3Ph.

304

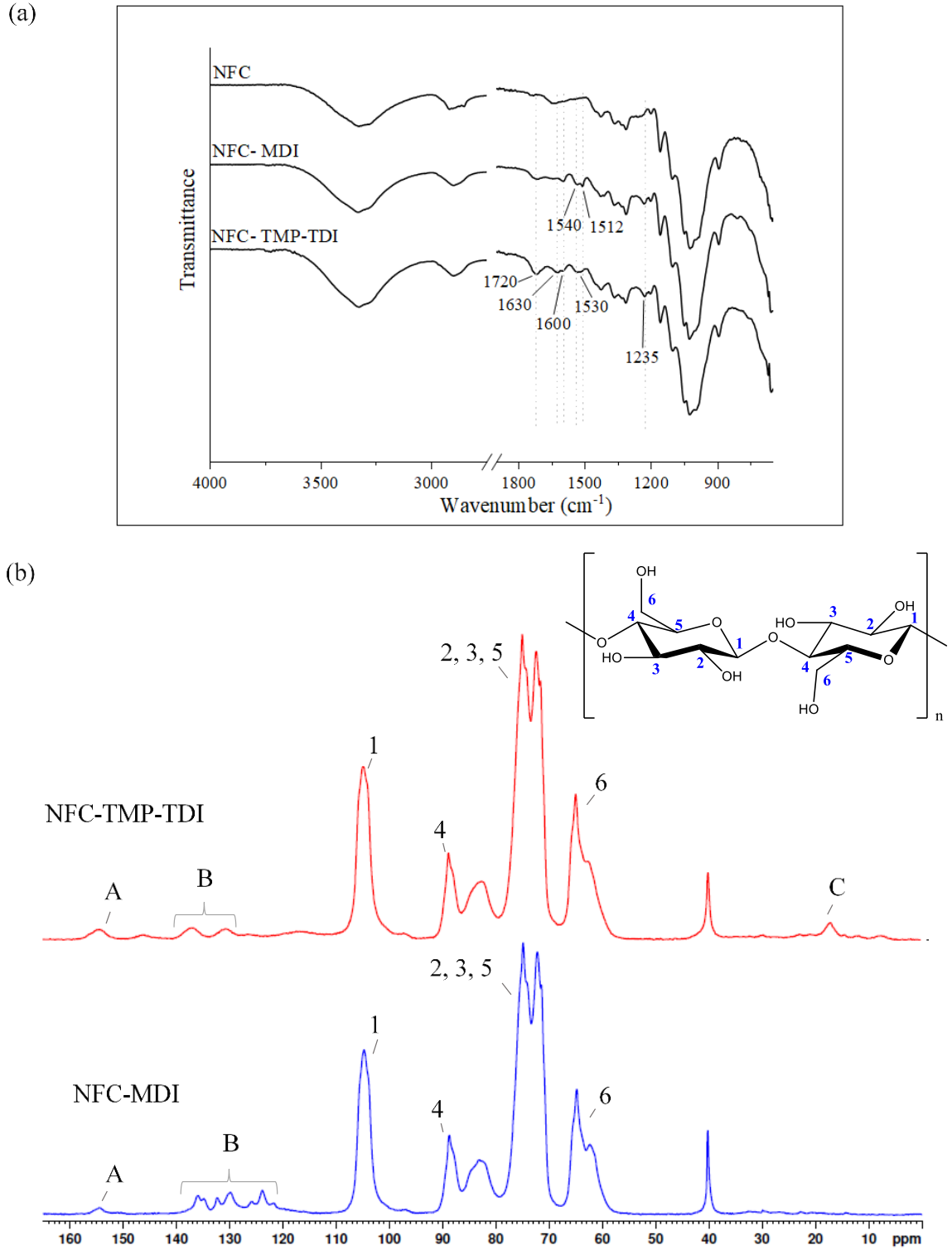

Figure 3. (a) ATR-FTIR spectra and (b) ^{13}C-NMR (solid) spectra of the NFC-TMP TDI and NFC-MDI chemically modified films

Figure 4shows pictures and the isometric AFM images of the pristine (a) and modified films with MDI (b) and TMP-TDI (c), respectively. The pristine film is translucent, while NFC-MDI and NFC-TMP-TDI, are more opaque, with an amber coloration. The values of the light transmission on T660nm are given at the bottom of each image, confirming that modified films provides a lower percentage of light transmittance than the base NFC film. The opaqueness of the film is related to the optical haze effect (Tsalagkas, Zhai, Kim, & Kim, 2017)) On the full UV-VIS spectra presented in Figure S 1 it is observed that NFC-MDI blocks the transmittance of UVB and UVA spectra. NFC-TMP-TDI blocks partially UVB, the entire UVA and a portion of the violet and blue wavelengths whereas non- modified NFC film presents a percentage of light transmittance in UV and entire visible light wavelengths. Similar results were obtained by (Chen et al., 2021) with the incorporation of Cu-Metal organic frameworks in cellulose acetate films. The AFM images show more irregular surfaces for the modified films, suggested by the increase in the maximum height. The three parameters of roughness calculated using the AFM data on the software Gwydion® are given in Table S 1. The values reveal that roughness more than doubled for the modified films in relation to the neat NFC film.

Figure S 2 in supporting information shows SEM surface images of NFC (a), NFC-MDI (b) and NFC-TMP-TDI (c) films, respectively with magnification of 800x. Similar morphologies are observed when comparing the images, indicating that even that the drying processes were different, both conditions provided high entanglement of the NFC though with rougher surface for the modified films. The cross-section SEM image presents a very compacted, layered and homogeneous section for the three compositions. In general, spaced layered section is typical from NFC films and cross linked NFC films (Djafari Petroudy, Rahmani, Rasooly Garmaroody, Rudi, & Ramezani, 2019; Lossada et al., 2019; Sethi, Farooq, Sain, et al., 2018; Sethi et al., 2019; Solala et al., 2018). The films here obtained seem slightly more compacted than the ones observed in literature and one attributed this to our casting protocol. Besides, the homogeneity of the bulk of the modified films indicates that the emulsions remained stable during the entire drying process, as no phase separation from NFC and blocked isocyanates was observed.

Table S 2 provides the data of thickness, gramage, density and porosity of the obtained films. Modified films are thicker and with higher gramage due to the presence of the chemicals. Nonetheless, density and porosity are in the same range of the pristine NFC film, near 1.1 g/cm³ and 25 %, respectively.

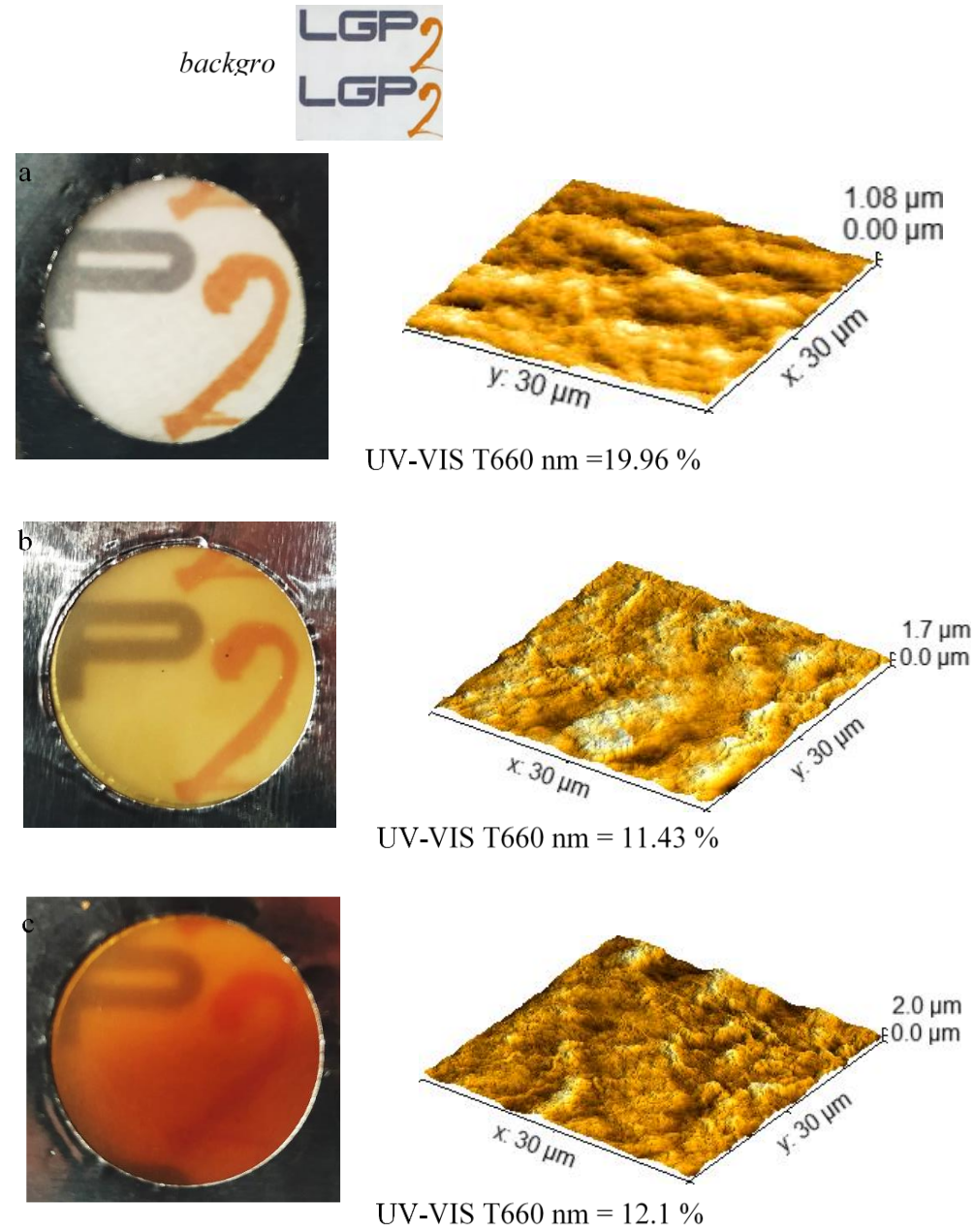

Figure 4. Photographs and surface AFM images of the NFC film (a) and of the modified NFC-MDI (b) and NFC-TMP-TDI (c) counterparts.

Table 2 gives the Young's modulus, the tensile strength (TS), the strain at break and the work of fracture (WOF) of the films. NFC film presents the highest properties among the compositions with modulus of 6.5 GPa, TS of 108 MPa, strain at break of 9 % and work of fracture of 8 MJ/m³. The modified films presents Young's modulus at the range of 5 GPa, well above some

recent reports on polyurethane biobased composites for packaging (Kim et al., 2021; Urbina, Corcuera, Eceiza, & Retegi, 2019). Nonetheless, due to the chemical crosslinks the films are more brittle and with lower WOF in relation to the pristine films. The covalent urethane bonds acted on inhibiting the slippage of the cellulose chains during loading. The strain at break is on the same range as obtained with Clay/NFC composites (Garusinghe, Varanasi, Raghuwanshi, Garnier, & Batchelor, 2018; Liu, Walther, Ikkala, Belova, & Berglund, 2011). In a real application the brittleness could be minimized by making a multilayer biobased film, as suggested by (J. Wang et al., 2018). Table 2 also presents the tear test index, in which is observed that NFC-MDI and NFC-TMP-TDI had its out of plane resistance slightly increased as a function of the chemical modification.

Table 2Mechanical properties obtained from tensile and tear testings

	Young's Modulus (GPa)	Tensile Strength (MPa)	Strain at Break (%)	Work to Fracture (MJ/m^3)	Tear testing index ($mN*m^2/g$)
NFC	6.5 ± 0.7	108 ± 10	9 ± 1	8.0 ± 1.0	0.7 ± 0.1
NFC-MDI	5.2 ± 0.3	62 ± 11	2 ± 1	1.2 ± 0.6	1.3 ± 0.4
NFC-TMP-TDI	5.0 ± 0.1	73 ± 3	3 ± 1	1.4 ± 0.6	1.0 ± 0.2

Figure 5 shows the "wet/dry" ratio of the tensile properties measured at "dry" and "wet" conditions. Values near the unit indicate that the measured property remained unaltered. One can observe that, despite presenting the highest dry tensile properties (as shown in Table 2) NFC film is the most affected by the contact with water, revealing a strong reduction of 90 % in the Young's modulus although the ratio for TS and strain at break remain near 1. Differently from the pristine NFC film, the modified films present Young's modulus wet/dry ratio near 1, with 0.8 for NFC-MDI and 1.0 for NFC-TMP-TDI, revealing that the proposed modifications were successful on reducing or even inhibiting the water plasticizing effect. TS and strain at break have similar values, masked by the error bars.

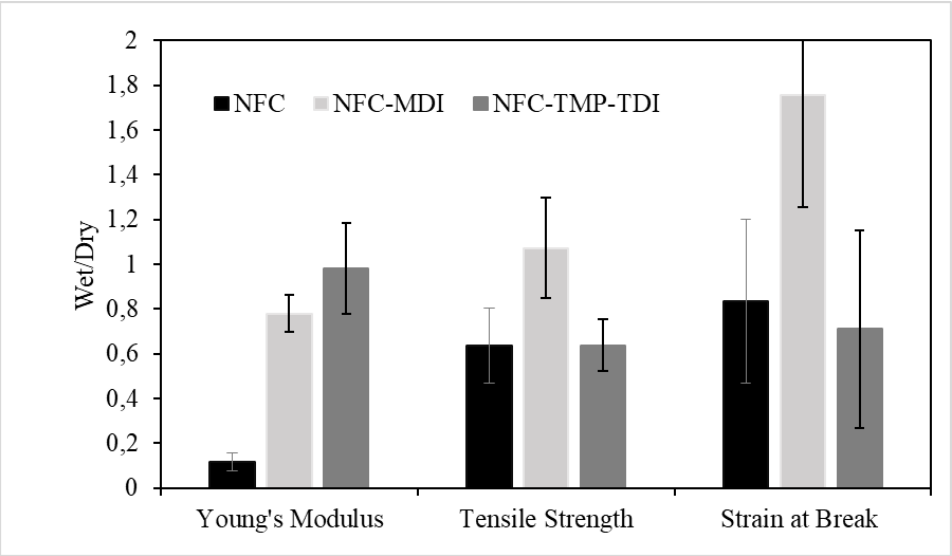

Figure 5.Wet/Dry ratio between the tensile properties of pristine and modified films.

Figure S 3 shows the TG curves for NFC, NFC-MDI and NFC-TMP-TDI films. The three compositions exhibit similar onset of thermal degradation, at around 280 °C, with a large decay of more than 60 % up to 406 °C. NFC film shows another gradual decay starting at 406 °C with total decomposition of the carbon matter until 700 °C while, NFC-MDI and NFC-TMP-TDI, display a modest decomposition above 406 °C, maintaining a residue of 20-30 % at 700 °C due to the chemical modification. NFC-MDI and NFC-TMP-TDI also exhibited values of water vapor uptake between 5 % and 8 % for a period of 500 h (Figure S 4), maintaining a low percentage of water vapor absorption presented by NFC non-modified film.

Figure S 5 provides the water contact angle (WCA). Values of WCA below 90 ° for the modified films indicate that the chemical modification with blocked di- and tri- isocyanates took place mostly within the films structures. NFC-MDI had its WCA increased to 86 ° in relation to the pristine NFC-TMP-TDI film presented 52°, the same value of the non-modified NFC film, implying that there was no surface hydrophobization. Differently from our previous work, in which the NFC film was surface modified with blocked isocyanates, leading to a WCA of 113° (de Souza, Belgacem, Gandini, & Carvalho, 2021), in the present research the films were in bulk modified and this probably led to few urethane functionalized hydroxyl present at the surface. Nonetheless, the wet/dry modulus ratio proves the presence of connecting points in between the nanofibers, which reduced the plasticizing effect and enhancing the water resistance. As

discussed by Hubbe et al., (Hubbe et al., 2015), not always the WCA gives full information about the water resistance feature of a substrate.

3.4 Barrier properties to water vapor and oxygen

Figure 6 shows the mass increase (g) as a function of time (h) obtained in the WVTR test. Raw data of the permeation tests (Fickian diffusion parameters calculated using the data from wet-cup permeance) are shown in the supplementary information in table S3.

Both treatments (NFC-MDI and NFC-TMP-TDI) are equally effective on increasing the barrier to water vapor, with a reduction of WVTR near 74 %. The WVTR values of around 40 $g.m^{-2}.day^{-1}$ of the modified films are well below some recent reports in the literature for biobased packaging, as PVA/lignin nanoparticles (Zhang, Liu, Liu, & Qiu, 2020), alginate/copper sulfide nanoparticle s(Roy & Rhim, 2020), lignocellulose nanopapers (Djafari Petroudy et al., 2019) and NFC/alkaili lignin composite (W. Wang et al., 2021), which at the best reached 60 $g.m^{-2}.day^{-1}$ at the case of NFC/alkyl lignin composites.

Values of the Water Vapor Permeability (WVP), which takes into account not just the water vapor mass transported across the section, but also the humidity gradient and the thickness of the film, are also presented in Table 3. The WVP value of the pristine NFC film categorizes it as a "poor" water vapor barrier material according to the criteria proposed by Wang et al, 2018 (J. Wang et al., 2018). However, the chemical modification with blocked diisocyanates reduced the WVP by almost half, changing the category to a "low" water vapor barrier material, i.e. the same category as PA6 and PLA films.

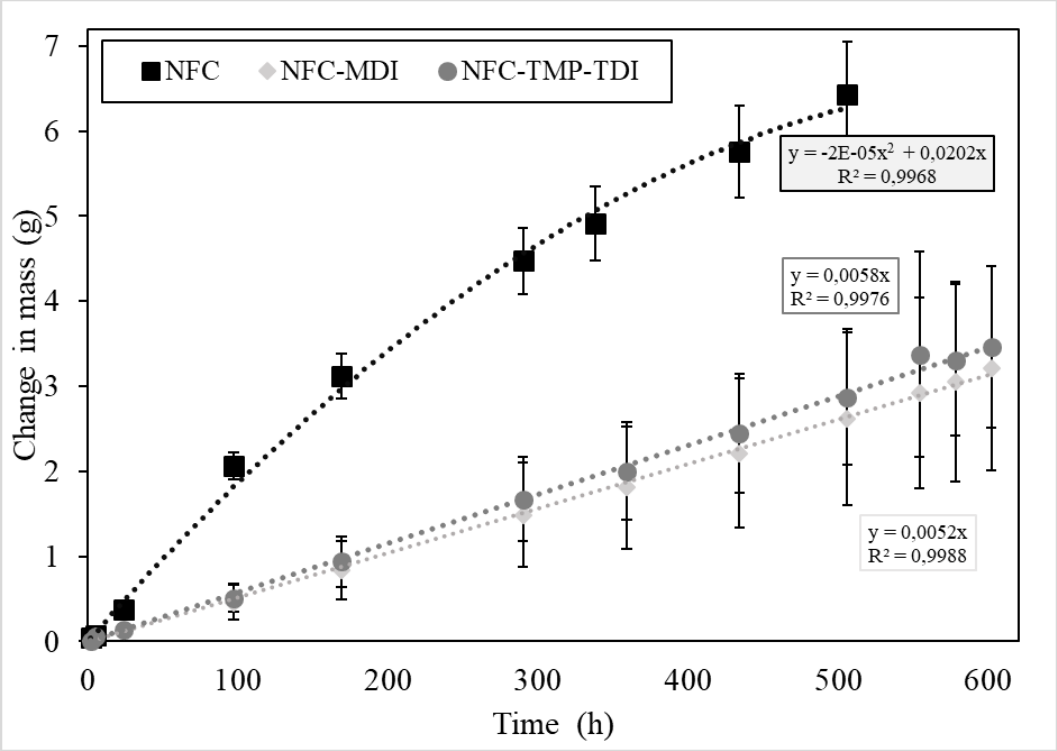

Figure 6. Water mass increase as a function of time for pristine and modified films obtained by the wet cup permeance test

The data of mass increase *vs* time was used to calculate the Fickian flux (J) and the Diffusion coefficient (Deff), shown in Table S 3.The pore space diffusion coefficient (Da), calculated with the set of equations detailed elsewhere (de Souza et al., 2021) is given in Table 3. The order of magnitude (10^{-8} cm/s) for Da is in the range of the values reported in the literature for other compositions of NFC films (Rahmani Seraji, Karimi, & Mahmoudi, 2017). Da was reduced by half due to the chemical modification with the different adducts. The path length were calculated by applying the equation proposed by Hu et al.,(Hu, Acharya, & Abidi, 2019) and are presented in Table 3**.** As the modified films were thicker than the NFC film, the path length was naturally increased, also contributing to the reduction of water vapor permeation.

Using the flux (J) data, and the equations of cylindrical pore model (Hou et al., 2019), values of mean porous radius (Rf) in the range 0.6-0.95 nm are obtained . Table S 4). Rf is more than one order higher than the required mean porous radius of 0.03 nm for Knudsen to be assumed as the main diffusion mechanism, therefore the flux is mainly Fickian.

Table 3 also gives the values of Oxygen Transmission Rate (OTR) in $cm^3/m^2/day$ for the pristine and modified films at 0 % RH. NFC film presents an OTR value of 15 ± 3 $cm^3/m^2/day$,

which is already suitable for application as modified atmosphere packaging films. NFC-MDI, which was modified using bifunctional bridging moieties (MDI-2Ph), exhibits the same OTR as untreated NFC films, and thus the chemical modification apparently had no effect on the oxygen transport inside the film structure. On the other hand, NFC-TMP-TDI, modified with the trifunctional moiety (TMP-TDI-3Ph), displays an OTR of almost zero, i.e, below the detection limits of the equipment. One can assume that the trifunctional structure of TMP-TDI-3Ph promoted more rigid connecting points on the internal structure than MDI-2Ph. Wet tensile test already evidenced more rigid connecting points for NFC-TMP-TDI as the wet/dry ratio for Young's modulus remained at 1.0.

Table 3.physical parameters calculated using the data from the wet-cup permeance, free path length and OTR

	WVTR ($g/(m^2*day)$)	WVP ($g*\mu m/(m^2*day*kPa)$)	Da (cm^2/s)	Path length (μm)	OTR ($cm^3/m^2/day$)
NFC	152.82	5065	6,19E-08	81.66	15±3
NFC-MDI	41.61	2788	2,96E-08	168.31	15±1
NFC-TMP-TDI	46.41	2742	2,83E-08	149.80	0.2±0.2

3.5 Chemical modification with blocked isocyanates: Summary of properties and structure prediction

Based on the results obtained with wet tensile tests, WVTR and OTR, one can estimate that after the thermal treatment that caused the deblock of MDI-2Ph and TMP-TDI-3Ph, the free isocyanate moieties reacted with cellulose hydroxyls, giving rise to water resistant and low permeable films. Figure S 6 and Figure S 7 give insights of possible pathways for these reaction mechanisms with (MDI-2Ph) and the commercial trifunctional blocked isocyanate agent (TMP-TDI-3Ph), respectively.TMP-TDI-3Ph is a polyisocyanate, at least three functional, with an increased molecular mass and, as consequence, its high molar weight in relation to MDI-2Ph leading to a high crosslinked material. Nonetheless, the short chain length of MD-2Ph in relation to the size of the fibers were not as effective as TMP-TDI-3Ph on creating chemical connection among the fibers. Table 4 summarizes the main properties of the films modified with blocked isocyanates and the pristine NFC film, which are ratio of wet/dry Young's modulus, WTR and OTR.

Table 4. Summary of the main properties obtained for NFC, NFC-MDI and NFC-TMP-TDI.

	Ratio of WET/DRY Young's modulus	Water Vapor Transmission Rate ($g/m^{-2}.day^{-1}$)	Oxygen Transmission Rate ($cm^3/m^2/day$)
Pristine NFC film	0.1	153	15
NFC-MDI	0.8	42	15
NFC-TMP-TDI	1.0	46	0.2

4. CONCLUSION

Modified NFC films were obtained by casting a mixture of NFC aqueous suspensions with an emulsion of with bi and trifunctional blocked isocyanates followed by thermal treatment at 170 °C. The coupling urethane- NFC reaction was confirmed by FT-IR and solid ^{13}C-NMR. A semi-wet tensile test showed that the modified films maintained their Young's modulus of 5 GPa almost unchanged when in contact with water, whereas the pristine NFC film display a reduced of 90 % in the Young's modulus. Modified films also had their WVTR reduced by 74 % in relation to their pristine precursor, with values of around 40 g. $m^{-2}.day^{-1}$ Besides, the modification with the trifunctional blocked isocyanate promoted an OTR decrease to 0.2 $cm^3/m^2/day$.

NFC films are good candidates to replace synthetic polymers on packaging films. However, their mechanical and barrier properties are widely affected by the humidity of the environment and means to improve water resistance are necessary to enhance their range of applications. The results show that the strategy proposed here is efficient in maintaining the mechanical and barrier properties of NFC films even in wet environments, an elegant solution for its usage in packaging application. In the future research we should employ a macrodiol blocked isocyanate in the in bulk modifications to enhance the elongation at break of the films, widening the application possibilities.

AUTHOR INFORMATION

Corresponding author

Antonio José Felix Carvalho- Department of Materials Engineering, Sao Carlos School of Engineering (EESC), University of São Paulo (USP), São Paulo, SP, Brazil.

https://orcid.org/0000-0001-8403-1135 E-mail: (toni@sc.usp.br)

Authors

Gustavo de Souza- Department of Materials Engineering, Sao Carlos School of Engineering (EESC), University of São Paulo (USP), São Paulo, SP; Univ. Grenoble Alpes, CNRS, Grenoble INP, LGP2, F-38000, Grenoble, France. https://orcid.org/0000-0002-9056-8550

Mohamed Naceur Belgacem- Univ. Grenoble Alpes, CNRS, Grenoble INP, LGP2, F-38000, Grenoble, France https://orcid.org/0000-0002-3317-7369

Alessandro Gandini- Univ. Grenoble Alpes, CNRS, Grenoble INP, LGP2, F-38000, Grenoble, France

AUTHOR CONTRIBUTIONS

The manuscript was written through contributions of all authors. All authors have given approval to the final version of the manuscript.

ACKNOWLEDGEMENTS

This study was financed in part by the Coordenação de Aperfeiçoamento de Pessoal de Nível Superior - Brazil (CAPES) - Finance Code 001. Also, authors acknowledge CNPq for the doctoral fellowship granted to G.S (CNPq proc. 140249/2017-6). AJFC acknowledge CNPq for research funding project # 03847/2019-0. We also thank to Suzano S/A, Brazil which kindly supplied the NFC from eucalyptus wood pulp.

NOTES

The authors declare no competing financial interest.

5. REFERENCES

Balu, B., Breedveld, V., & Hess, D. W. (2008). Fabrication of “roll-off” and “sticky” superhydrophobic cellulose surfaces-via plasma processing. *Langmuir*, *24*(9), 4785–4790. https://doi.org/10.1021/la703766c

Carvalho, A. J. F., Curvelo, A. A. S., & Gandini, A. (2005). Surface chemical modification of thermoplastic starch: Reactions with isocyanates, epoxy functions and stearoyl chloride. *Industrial Crops and Products*, *21*(3), 331–336. https://doi.org/10.1016/j.indcrop.2004.04.027

Chen, K., Yu, J., Huang, J., Tang, Q., Li, H., & Zou, Z. (2021). Improved mechanical, water vapor barrier and UV-shielding properties of cellulose acetate films with flower-like metal-organic framework nanoparticles. *International Journal of Biological Macromolecules*, *167*, 1–9. https://doi.org/10.1016/j.ijbiomac.2020.11.164

de Souza, G., Belgacem, M. N., Gandini, A., & Carvalho, A. J. F. (2021). Low permeable hydrophobic nanofibrilated cellulose films modified by dipping and heating processing technique. *Cellulose*, *3*. https://doi.org/10.1007/s10570-020-03619-3

Delebecq, E., Pascault, J. P., Boutevin, B., & Ganachaud, F. (2013). On the versatility of urethane/urea bonds: Reversibility, blocked isocyanate, and non-isocyanate polyurethane. *Chemical Reviews*, *113*(1), 80–118. https://doi.org/10.1021/cr300195n

Djafari Petroudy, S. R., Rahmani, N., Rasooly Garmaroody, E., Rudi, H., & Ramezani, O. (2019). Comparative study of cellulose and lignocellulose nanopapers prepared from hard wood pulps: Morphological, structural and barrier properties. *International Journal of Biological Macromolecules*, *135*, 512–520. https://doi.org/10.1016/j.ijbiomac.2019.05.212

Forsman, N., Lozhechnikova, A., Khakalo, A., Johansson, L. S., Vartiainen, J., & Österberg, M. (2017). Layer-by-layer assembled hydrophobic coatings for cellulose nanofibril films and textiles, made of polylysine and natural wax particles. *Carbohydrate Polymers*, *173*, 392–402. https://doi.org/10.1016/j.carbpol.2017.06.007

Gandini, A., & Belgacem, M. N. (2016). The Surface and In-Depth Modification of Cellulose Fibers. In O. J. Rojas (Ed.), *Cellulose Chemistry and Properties: Fibers, Nanocelluloses and Advanced Materials* (pp. 169–206). Cham: Springer International Publishing. https://doi.org/10.1007/12_2015_305

Garusinghe, U. M., Varanasi, S., Raghuwanshi, V. S., Garnier, G., & Batchelor, W. (2018). Nanocellulose-montmorillonite composites of low water vapour permeability. *Colloids and Surfaces A: Physicochemical and Engineering Aspects*, *540*(January), 233–241. https://doi.org/10.1016/j.colsurfa.2018.01.010

Gironès, J., Pimenta, M. T. B., Vilaseca, F., Carvalho, A. J. F., Mutjé, P., & Curvelo, A. A. S. (2008). Blocked diisocyanates as reactive coupling agents: Application to pine fiber-polypropylene composites. *Carbohydrate Polymers*, *74*(1), 106–113. https://doi.org/10.1016/j.carbpol.2008.01.026

Gironès, J., Pimenta, M. T. B., Vilaseca, F., de Carvalho, A. J. F., Mutjé, P., & Curvelo, A. A. S. (2007). Blocked isocyanates as coupling agents for cellulose-based composites. *Carbohydrate Polymers*, *68*(3), 537–543. https://doi.org/10.1016/j.carbpol.2006.10.020

González, I., Alcalà, M., Chinga-Carrasco, G., Vilaseca, F., Boufi, S., & Mutjé, P. (2014). From paper to nanopaper: Evolution of mechanical and physical properties. *Cellulose*, *21*(4), 2599–2609. https://doi.org/10.1007/s10570-014-0341-0

Habibi, Y. (2014). Key advances in the chemical modification of nanocelluloses. *Chemical Society Reviews*, *43*(5), 1519–1542. https://doi.org/10.1039/c3cs60204d

554 Hou, T., Guo, K., Wang, Z., Zhang, X. F., Feng, Y., He, M., & Yao, J. (2019). Glutaraldehyde
555 and polyvinyl alcohol crosslinked cellulose membranes for efficient methyl orange and
556 Congo red removal. *Cellulose*, *26*(8), 5065–5074. https://doi.org/10.1007/s10570-019-
557 02433-w
558 Hu, Y., Acharya, S., & Abidi, N. (2019). Cellulose porosity improves its dissolution by
559 facilitating solvent diffusion. *International Journal of Biological Macromolecules*, *123*,
560 1289–1296. https://doi.org/10.1016/j.ijbiomac.2018.10.062
561 Hubbe, M. A., Gardner, D. J., & Shen, W. (2015). Wettability of cellulosics. *BioResources*,
562 *10*(4), 8657–8749. Retrieved from
563 https://pdfs.semanticscholar.org/5abd/c6f4c89c252cc44f20d584f9db06444c3e52.pdf
564 Indriyati, & Indrarti, L. (2018). Preparation and characterization of bacterial cellulose-beeswax
565 films. *IOP Conference Series: Earth and Environmental Science*, *160*, 012010.
566 https://doi.org/10.1088/1755-1315/160/1/012010
567 Kim, M. S., Ryu, K. M., Lee, S. H., Choi, Y. C., Rho, S., & Jeong, Y. G. (2021). Chitin
568 Nanofiber-Reinforced Waterborne Polyurethane Nanocomposite Films with Enhanced
569 Thermal and Mechanical Performance. *Carbohydrate Polymers*, *258*(January), 117728.
570 https://doi.org/10.1016/j.carbpol.2021.117728
571 Klemm, D., Cranston, E. D., Fischer, D., Gama, M., Kedzior, S. A., Kralisch, D., … Rauchfuß,
572 F. (2018). Nanocellulose as a natural source for groundbreaking applications in materials
573 science: Today's state. *Materials Today*, *21*(7), 720–748.
574 https://doi.org/10.1016/j.mattod.2018.02.001
575 Lindström, T., & Aulin, C. (2014). Market and technical challenges and opportunities in the area
576 of innovative new materials and composites based on nanocellulosics. *Scandinavian*
577 *Journal of Forest Research*, *29*(4), 345–351.
578 https://doi.org/10.1080/02827581.2014.928365
579 Liu, A., Walther, A., Ikkala, O., Belova, L., & Berglund, L. A. (2011). Clay nanopaper with
580 tough cellulose nanofiber matrix for fire retardancy and gas barrier functions.
581 *Biomacromolecules*, *12*(3), 633–641. https://doi.org/10.1021/bm101296z
582 Lossada, F., Guo, J., Jiao, D., Groeer, S., Bourgeat-Lami, E., Montarnal, D., & Walther, A.
583 (2019). Vitrimer Chemistry Meets Cellulose Nanofibrils: Bioinspired Nanopapers with
584 High Water Resistance and Strong Adhesion. *Biomacromolecules*, *20*(2), 1045–1055.
585 research-article. https://doi.org/10.1021/acs.biomac.8b01659
586 Lu, Z., Huang, J., E, S., Li, J., Si, L., Yao, C., … Zhang, M. (2020). All cellulose composites
587 prepared by hydroxyethyl cellulose and cellulose nanocrystals through the crosslink of
588 polyisocyanate. *Carbohydrate Polymers*, *250*(August), 116919.
589 https://doi.org/10.1016/j.carbpol.2020.116919
590 Mahmud, S., Hasan, K. M. F., Jahid, M. A., Mohiuddin, K., Zhang, R., & Zhu, J. (2021).
591 *Comprehensive review on plant fiber-reinforced polymeric biocomposites*. *Journal of*
592 *Materials Science* (Vol. 56). Springer US. https://doi.org/10.1007/s10853-021-05774-9
593 Nechyporchuk, O., Belgacem, M. N., & Bras, J. (2016). Production of cellulose nanofibrils: A
594 review of recent advances. *Industrial Crops and Products*, *93*, 2–25.
595 https://doi.org/10.1016/j.indcrop.2016.02.016
596 Operamolla, A. (2019). Recent advances on renewable and biodegradable cellulose nanopaper
597 substrates for transparent light-harvesting devices: Interaction with humid environment.
598 *International Journal of Photoenergy*, *2019*. https://doi.org/10.1155/2019/3057929
599 Paquet, O., Krouit, M., Bras, J., Thielemans, W., & Belgacem, M. N. (2010). Surface

modification of cellulose by PCL grafts. *Acta Materialia*, *58*(3), 792–801. https://doi.org/10.1016/j.actamat.2009.09.057

Rahmani Seraji, H., Karimi, M., & Mahmoudi, L. (2017). In situ monitoring the change of mechanical response induced by the diffusion of saline water in glassy cellulose acetate. *Desalination*, *420*(July), 191–207. https://doi.org/10.1016/j.desal.2017.07.013

Rol, F., Belgacem, M. N., Gandini, A., & Bras, J. (2019). Recent advances in surface-modified cellulose nanofibrils. *Progress in Polymer Science*, *88*, 241–264. https://doi.org/10.1016/j.progpolymsci.2018.09.002

Roy, S., & Rhim, J. W. (2020). Effect of CuS reinforcement on the mechanical, water vapor barrier, UV-light barrier, and antibacterial properties of alginate-based composite films. *International Journal of Biological Macromolecules*, *164*, 37–44. https://doi.org/10.1016/j.ijbiomac.2020.07.092

Sehaqui, H., Zimmermann, T., & Tingaut, P. (2014). Hydrophobic cellulose nanopaper through a mild esterification procedure. *Cellulose*, *21*(1), 367–382. https://doi.org/10.1007/s10570-013-0110-5

Sethi, J., Farooq, M., Österberg, M., Illikainen, M., & Sirviö, J. A. (2018). Stereoselectively water resistant hybrid nanopapers prepared by cellulose nanofibers and water-based polyurethane. *Carbohydrate Polymers*, *199*(July), 286–293. https://doi.org/10.1016/j.carbpol.2018.07.028

Sethi, J., Farooq, M., Sain, S., Sain, M., Sirviö, J. A., Illikainen, M., & Oksman, K. (2018). Water resistant nanopapers prepared by lactic acid modified cellulose nanofibers. *Cellulose*, *25*(1), 259–268. https://doi.org/10.1007/s10570-017-1540-2

Sethi, J., Visanko, M., Österberg, M., & Sirviö, J. A. (2019). A fast method to prepare mechanically strong and water resistant lignocellulosic nanopapers. *Carbohydrate Polymers*, *203*(September 2018), 148–156. https://doi.org/10.1016/j.carbpol.2018.09.037

Siqueira, G., Bras, J., & Dufresne, A. (2010). Cellulosic bionanocomposites: A review of preparation, properties and applications. *Polymers*, *2*(4), 728–765. https://doi.org/10.3390/polym2040728

Solala, I., Bordes, R., & Larsson, A. (2018). Water vapor mass transport across nanofibrillated cellulose films: effect of surface hydrophobization. *Cellulose*, *25*(1), 347–356. https://doi.org/10.1007/s10570-017-1608-z

Tsalagkas, D., Zhai, L., Kim, H. C., & Kim, J. (2017). Optical and mechanical properties of cellulose nanopaper structures. *Nanosensors, Biosensors, Info-Tech Sensors and 3D Systems 2017*, *10167*(April 2017), 101670E. https://doi.org/10.1117/12.2259839

Urbina, L., Corcuera, M. Á., Eceiza, A., & Retegi, A. (2019). Stiff all-bacterial cellulose nanopaper with enhanced mechanical and barrier properties. *Materials Letters*, *246*, 67–70. https://doi.org/10.1016/j.matlet.2019.03.005

Wang, J., Gardner, D. J., Stark, N. M., Bousfield, D. W., Tajvidi, M., & Cai, Z. (2018). Moisture and Oxygen Barrier Properties of Cellulose Nanomaterial-Based Films. *ACS Sustainable Chemistry & Engineering*, *6*(1), 49–70. https://doi.org/10.1021/acssuschemeng.7b03523

Wang, W., Gu, F., Deng, Z., Zhu, Y., Zhu, J., Guo, T., … Xiao, H. (2021). Multilayer surface construction for enhancing barrier properties of cellulose-based packaging. *Carbohydrate Polymers*, *255*(November 2020), 117431. https://doi.org/10.1016/j.carbpol.2020.117431

Wicks, D. a., & Wicks, Z. W. (1999). Blocked isocyanates III: Part A. Mechanisms and chemistry. *Progress in Organic Coatings*, *36*(3), 148–172. https://doi.org/10.1016/S0300-9440(99)00042-9

Yang, R., Wang, Y., & Li, M. (2014). Homogeneous synthesis of crosslinked cellulose spheres from hemp (Cannabis sativa L.) stem and cotton. *Cellulose Chemistry and Technology*, *48*(5–6), 455–459.

Yang, W., Jiao, L., Min, D., Liu, Z., & Dai, H. (2017). Effects of preparation approaches on optical properties of self-assembled cellulose nanopapers. *RSC Advances*, *7*(17), 10463–10468. https://doi.org/10.1039/C6RA27529J

Zhang, X., Liu, W., Liu, W., & Qiu, X. (2020). High performance PVA/lignin nanocomposite films with excellent water vapor barrier and UV-shielding properties. *International Journal of Biological Macromolecules*, *142*, 551–558. https://doi.org/10.1016/j.ijbiomac.2019.09.129

Zhou, X., Fu, Y., Chen, L., Wang, R., Wang, X., Miao, Y., … Dai, H. (2020). Diisocyanate modifiable commercial filter paper with tunable hydrophobicity, enhanced wet tensile strength and antibacterial activity. *Carbohydrate Polymers*, *248*(July), 116791. https://doi.org/10.1016/j.carbpol.2020.116791

6. . APPENDIX (SUPPLEMENTARY INFORMATION)

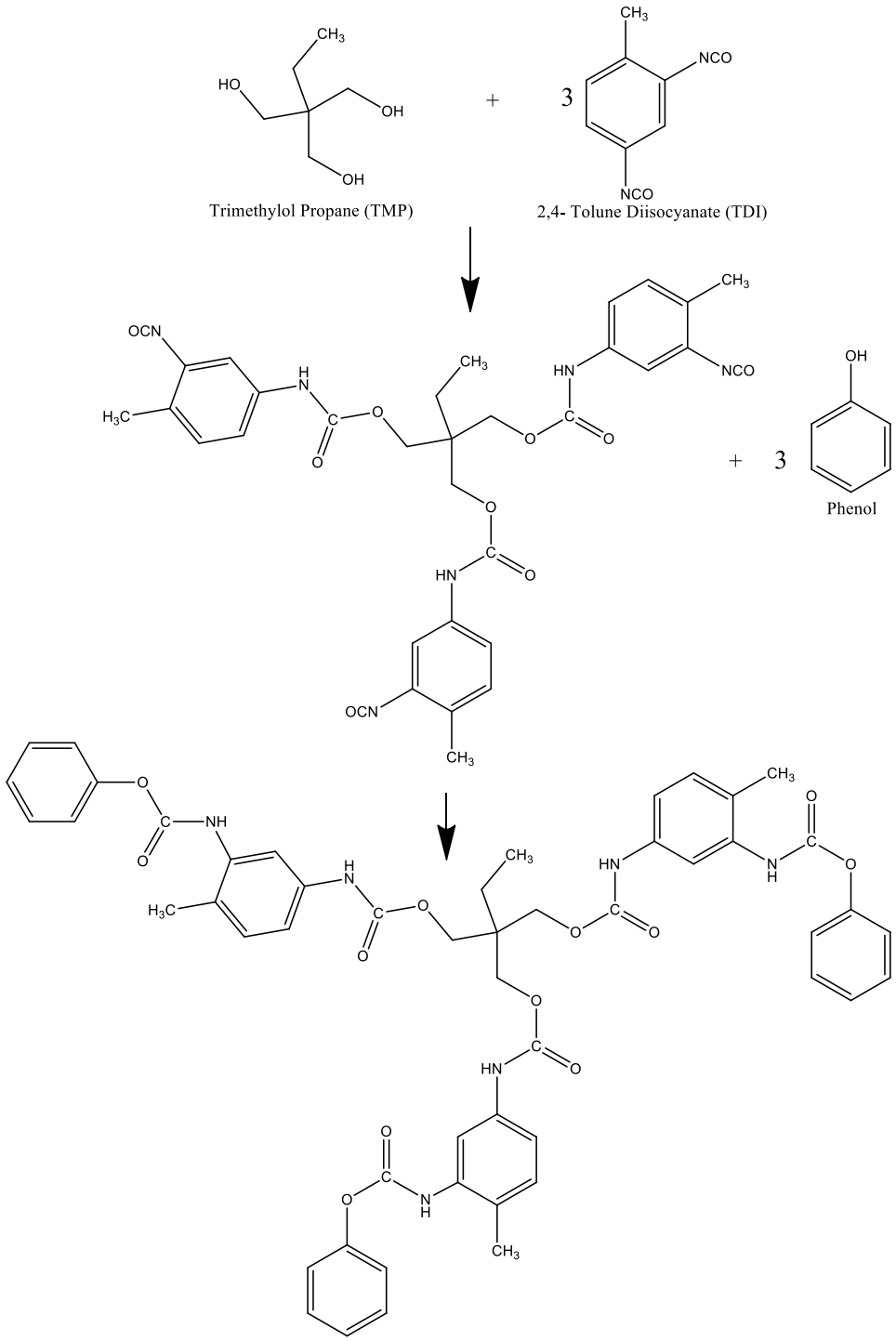

Scheme S 1. Molecular structure of TMP-TDI-Ph.

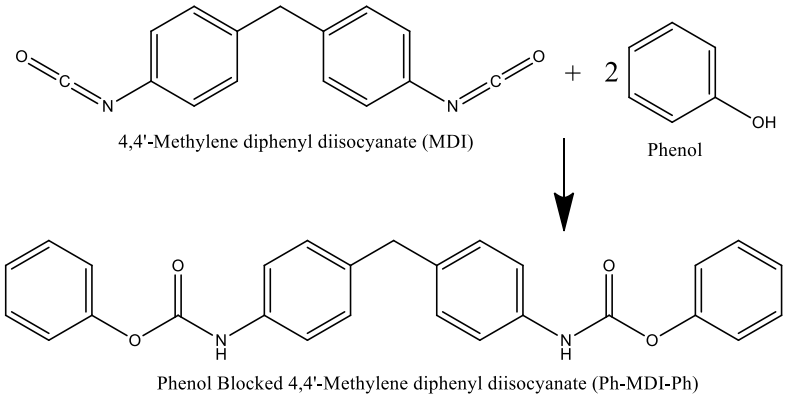

Scheme S 2. Possible path for sinthetis of Ph-MDI-Ph

Table S 1. present parameters of roughness measured for pristine and crosslinked films, with Ra the arithmetic mean of the roughness profile deviations, Rq the mean value of the deviation of heights, and Rt the measure of the absolute value of the largest peak minus the smallest valley of the measurement line

	Ra (nm)	Rq (nm)	Rt (nm)
NFC	19.6 ± 0.8	25 ± 1	165 ± 13
NFC-MDI	44 ± 5	59 ± 1	464 ± 160
NFC-TMP-TDI	53 ± 7	70 ±11	460 ± 85

Table S 2Physical properties of the pristine and crosslinked NFC films

	Thickness (µm)	Grammage (g/m^2)	Density (g/cm^3)	Porosity (%)
NFC	46 ± 2	50 ± 10	1.11 ± 0.07	23 ± 4
NFC-MDI	93 ± 13	102 ± 20	1.10 ± 0.08	27 ± 5
NFC-TMP-TDI	82 ± 14	88 ± 17	1.08 ± 0.04	28 ± 2

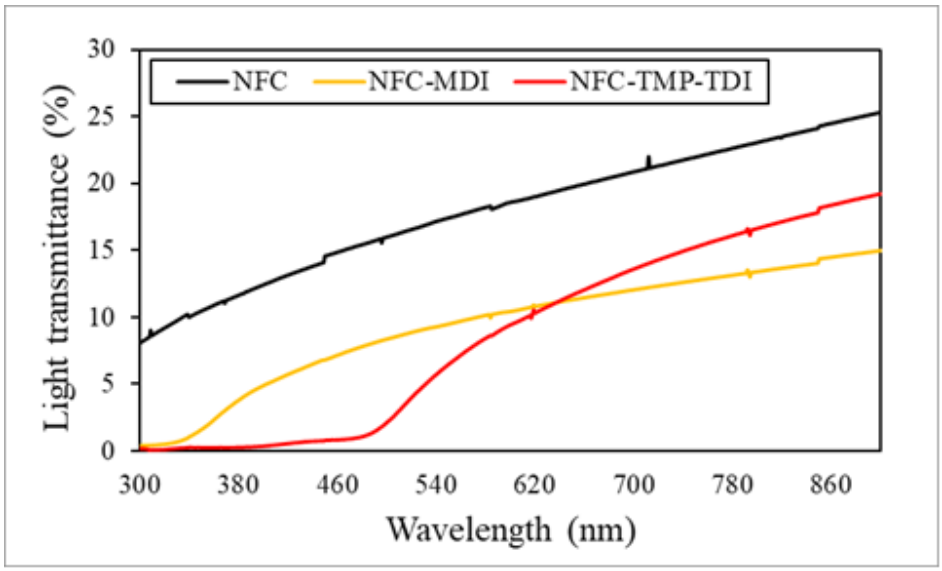

676

677 Figure S 1. UV-Vis light transmittance spectra for NFC, NFC-MDI and NFC-TMP-TDI

678

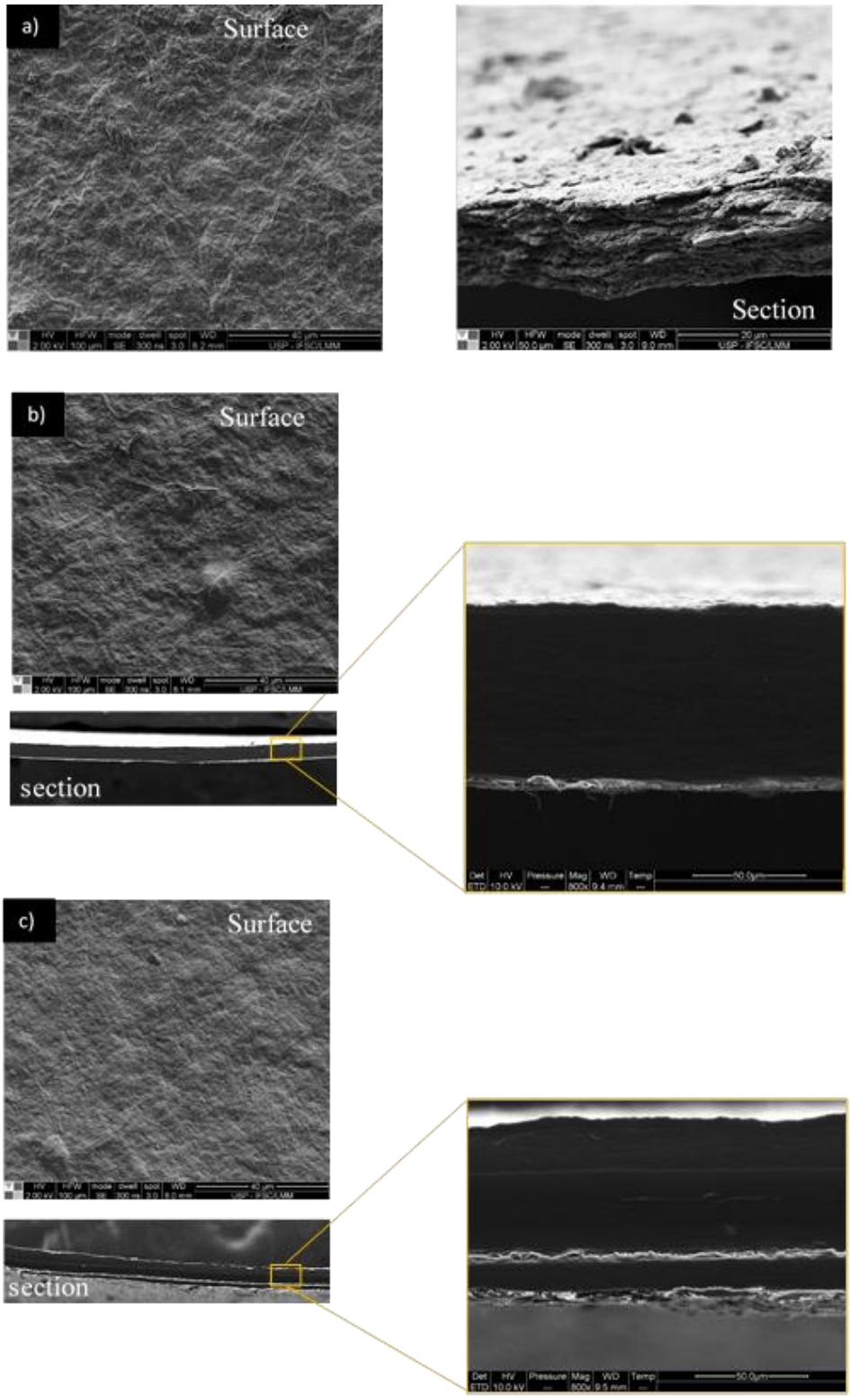

679

680 Figure S 2. Surface and section SEM images NFC (a), NFC-MDI (b) and NFC-TMP-TDI (c). Magnification 800x

681

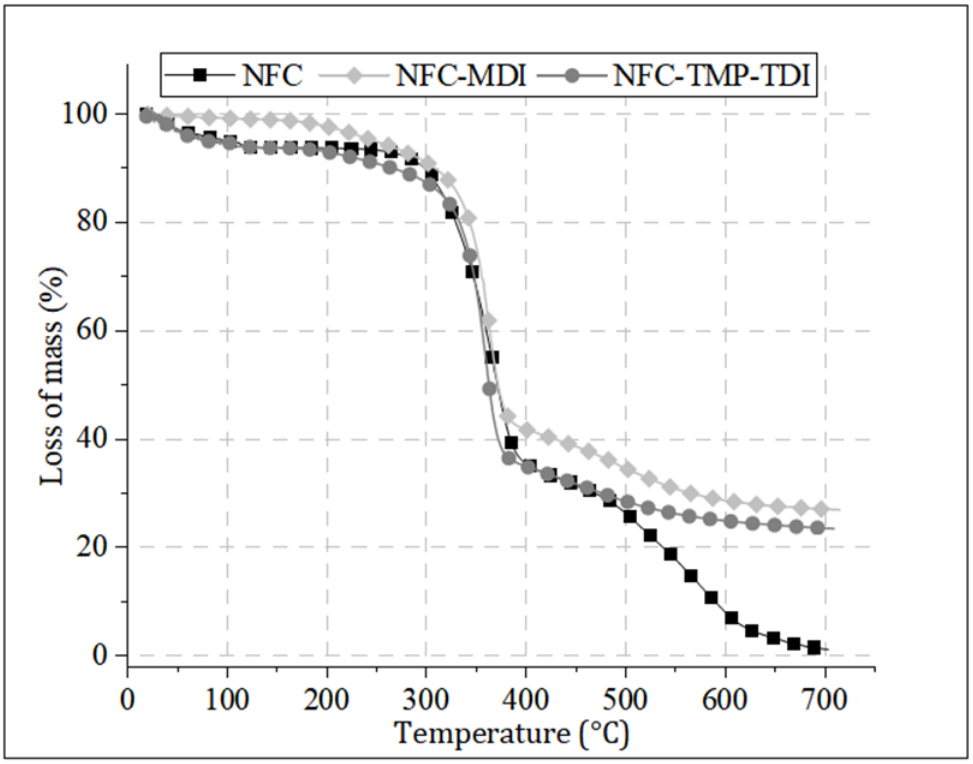

Figure S 3. Loss of mass as function of temperature for neat and modified NFC films.

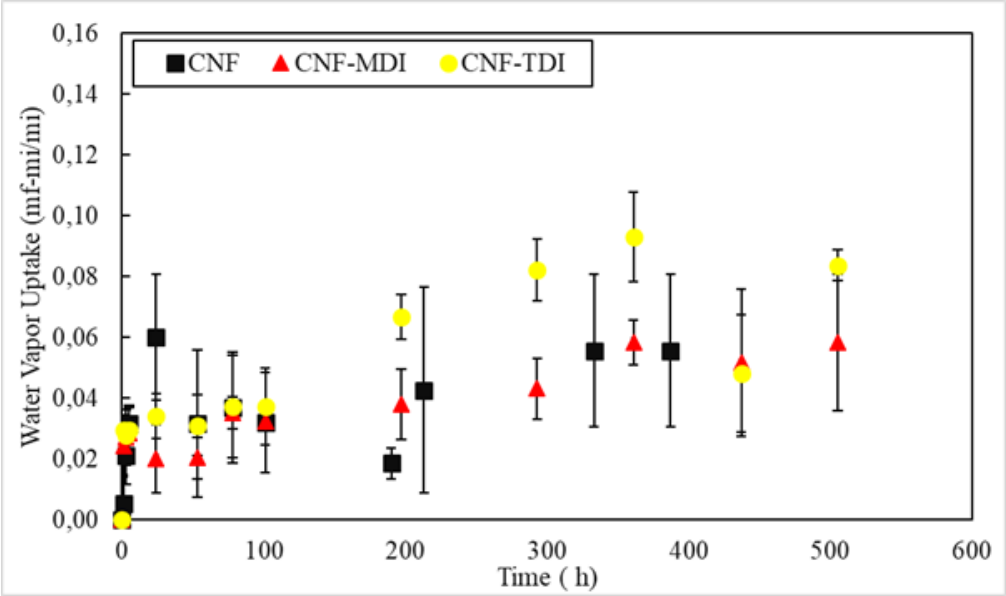

Figure S 4. Water vapor absorption as a function of time for neat and modified NFC films.

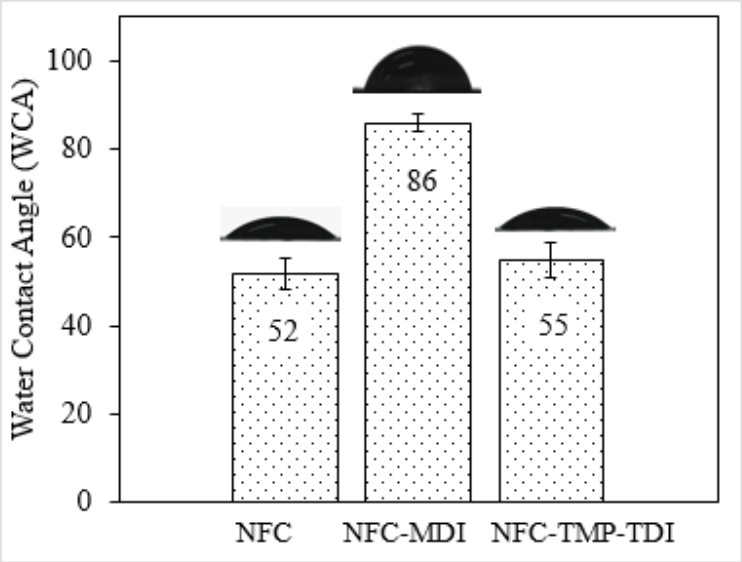

Figure S 5. Water Contact Angle (WCA)for neat and modified NFC films.

Table S 3Fickian diffusion parameters calculated using the data from wet-cup permeance test.

	W (g/h)	w (mol/s)	J (mol/cm²*s)	H (cm)	Deff (cm²/s)
NFC	0.0191	2.95E-07	9.83E-09	0.0046	8.01E-09
NFC-MDI	0.0058	8.02E-08	2.67E-09	0.0093	4.41E-09
NFC-TMP-TDI	0.0052	8.95E-08	2.98E-09	0.0082	4.34E-09

. Table S 4.Knudsen diffusion parameters calculated using the data from wet cup permeance

	Tortuosity τ	Rf (nm)	RKnudsen (nm)
NFC	1.78	0.95	0.032
NFC-MDI	1.81	0.65	0.036
NFC-TMP-TDI	1.83	0.63	0.031

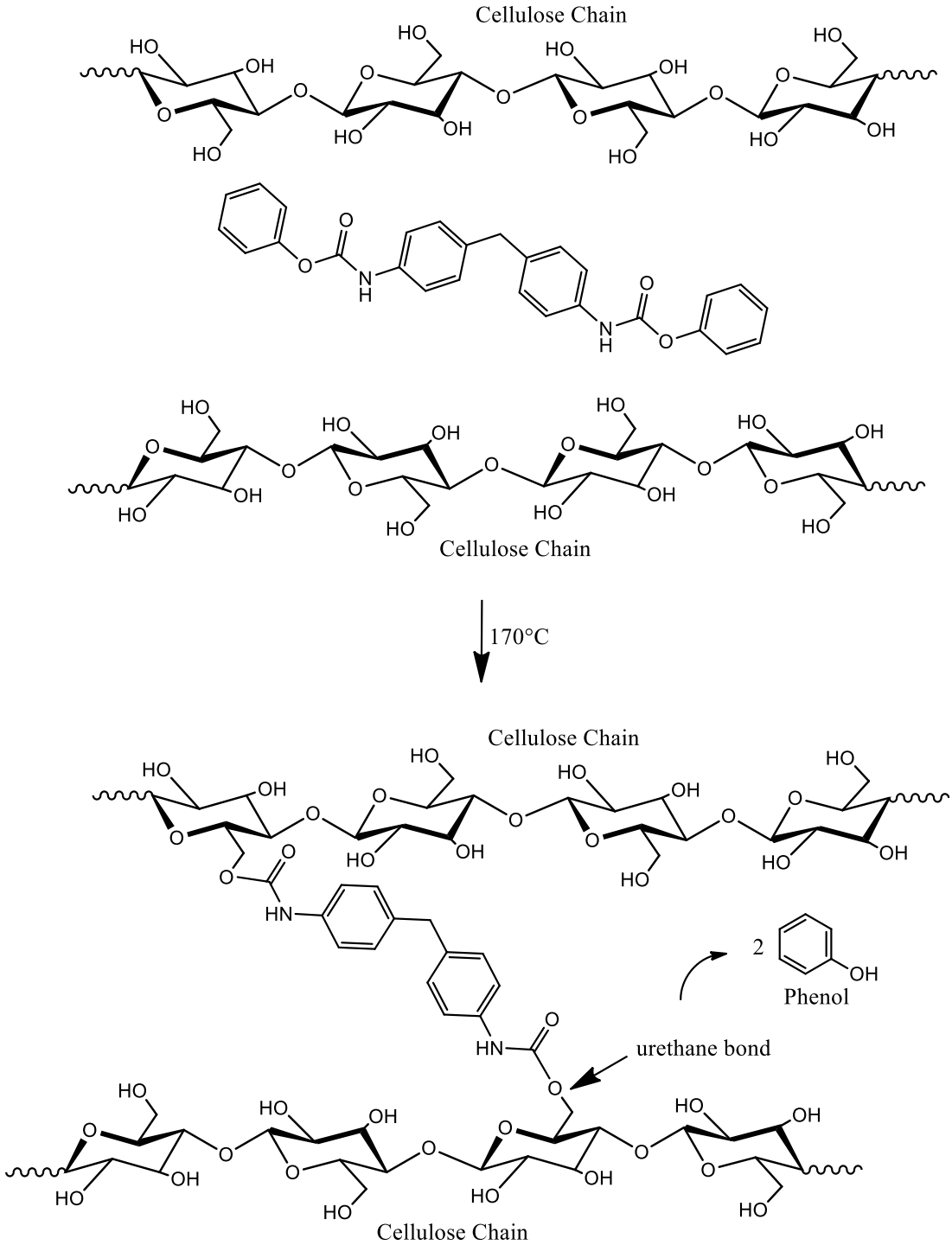

Figure S 6. Possible pathway for NFC films crosslinking after thermal treatment with the bifunctional adduct Ph-MDI-Ph.

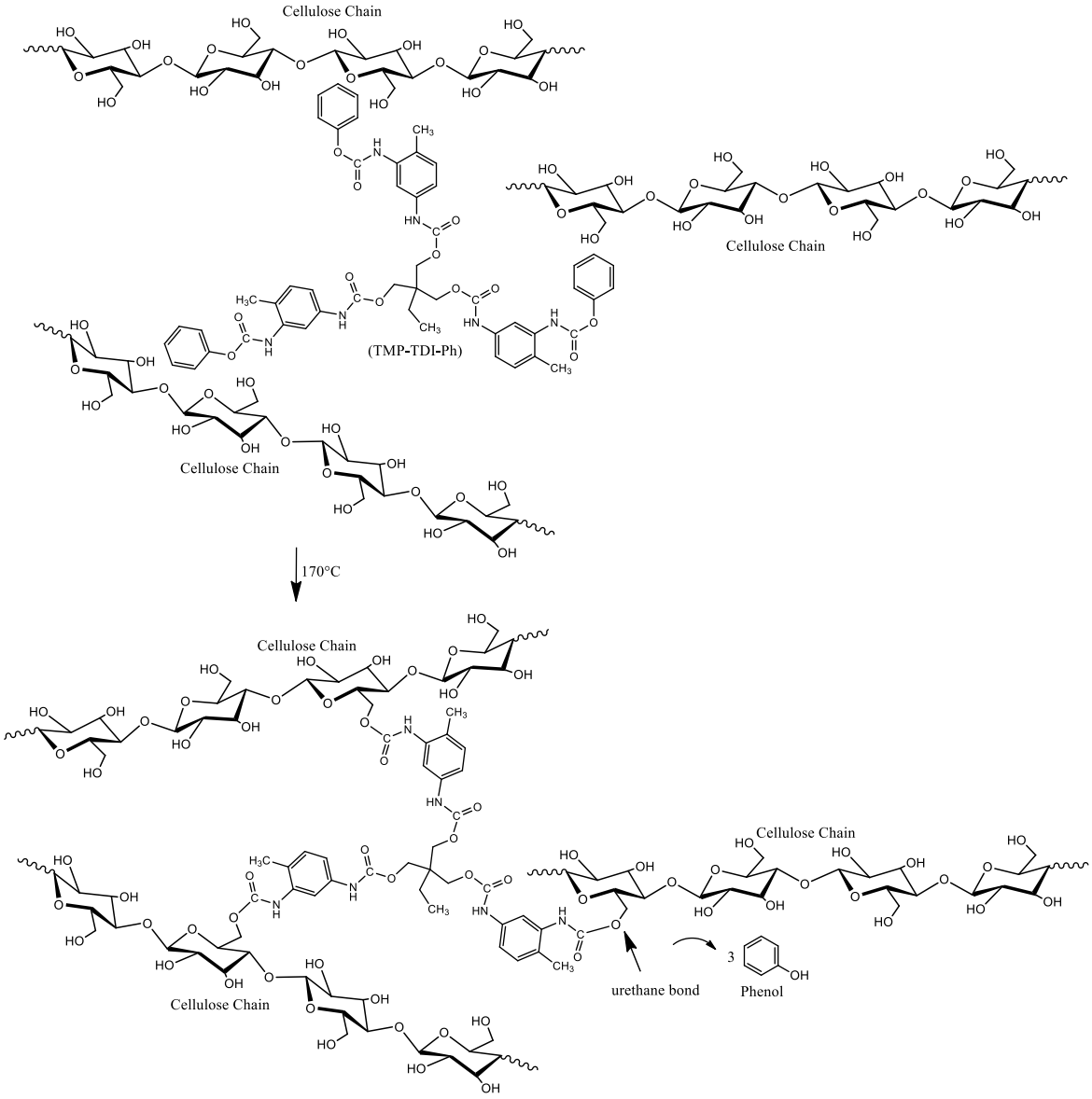

699

700 Figure S 7. Possible pathway for NFC films crosslinking after thermal treatment with the trifunctional adduct TMP-
701 TDI-3Ph.

702

703

PAPER 4

Nanofibrilated cellulose (NFC)/Polyethylene Glycol (PEG) composite films crosslinked with blocked isocyanates: enhanced mechanical properties, thermal stability and barrier to oxygen.

Gustavo de Souza[a,b], Mohamed Naceur Belgacem[b], Alessandro Gandini[a, b], Antonio José Felix Carvalho[a*]

*toni@sc.usp.br

[a]Department of Materials Engineering, Sao Carlos School of Engineering (EESC), University of São Paulo - USP, 13563-120 São Carlos/SP, Brazil

[b]Université Grenoble Alpes, CNRS, Grenoble INP, LGP2, F-38000, Grenoble, France

Abstract

Composites made of nanofibrillated cellulose (NFC) and terminal modified polyethylene glycol (PEG) were prepared and characterized. PEG with terminal blocked isocyanates were prepared by reacting one mole of PEG with two mole of 4,4-methylenebis-(phenyl isocyanate) (MDI) followed with the blocking of both ends with phenol (PEG-MDI-2Ph). An emulsion of this reactant in combination with NFC suspension was casted to give composites with 17, 33 and 50 % of NFC in dry bases. The casting procedure is based in two steps the drying with elimination of water followed a thermal treatment at 170° C for 10 minutes to produce the covalent bond between NFC and PEG-MDI-2Ph. The materials were characterized by FT-IR, ^{1}H-NMR, DSC and SEM. Crosslinked composites exhibited higher thermal stability than non-modified films and a lower hydrophilicity with water contact angle of about 100°. Water uptake was reduced by 45 %, the tear index enhanced by 180 % and the oxygen transmission rate fell from above 1000 cm^3/m^2 /day to near 300 cm^3/m^2 /day. The crosslinked process did not affect the strain at break of

the composites, which was maintained above 10 %. The results indicate the suitability of the process to produce biobased hydrophobic composite with high fraction of NFC.

Keywords: nanofibrilated cellulose (NFC); blocked isocyanates; polyethylene glycol (PEG); crosslinking; barrier properties.

1. INTRODUCTION

Packaging residues are one of the greatest concerns regarding to the pollution caused by polymeric materials [1]. Among the biobased existing solutions for packaging, cellulose derivatives such as cellulose acetate, methylcellulose and carboxymethyl cellulose are applied with limited results in mulch films or secondary packaging materials due to their poor mechanical and barrier properties.[2–7] Nanocelluloses are on the market at a cost of about USS 20 per kg of dry material[1], and can be incorporated in synthetic matrices to increase mechanical properties and reduce the content of petroleum based material [8–13] and also in biobased materials[14–19]. 100 % NFC films, with good mechanical properties, oxygen barrier, and water vapor transmission at the low RH are also promising developments in the field of thin flexible films [20,21].

In general, the hydrophilicity of NFC films is dealt by means of chemical functionalization of the fibers or by chemical and/or physical modification of the entire films[22,23]. However, most of the hydrophobizing processes are in general not suited for large-scale production and are dependable on the use of organic solvents in high quantity, rising environmental and safety concerns. In a recent work we employed blocked isocyanates to address the problem of the high hydrophilicity of NFC [24,25]. Blocked isocyanates are thermally reversible urethanes[26,27]

and are stable below the de-blocking temperature forming stable urethane linkages [26,28–30]. This is an elegant solution to deal with the toxicity and the incompatibility of isocyanates with water[31].

Here, we produce composite material based on NFC and polyethylene glycol modified with blocked isocyanate terminal ends prepared by the reaction of polyethylene glycol (PEG) with 4,4-methylenebis-(phenyl isocyanate) (MDI) and phenol (Ph). Composites were prepared at load of 17, 33 and 50 % of NFC by casting a mixture of blocked isocyanate emulsions and fiber water suspension, using PEG and PEG-MDI-2Ph as matrices.

2. METHODOLOGY

2.1 Materials

Nanofibrilated cellulose (NFC) from eucalyptus was kindly supplied by Suzano S/A., Brazil and received as a 3.2 wt % water suspension. 4,4-Methylenebis (phenyl isocyanate) (MDI), phenol, Polyethylene Glycol (PEG) M_w=1500 g/mol, dibutyltin dilaurate (DBTL) and dimethyl sulfoxide (DMSO) were supplied by Sigma–Aldrich and used as received. Zinc octanoate was supplied by Iracema, Brazil and was used as received. Reagent grade butyl acetate, xylene and methylene chloride were supplied by Sigma–Aldrich and were dried by storing them on activated 4Å molecular sieves for at least 72 h before use.

2.2 PEG-MDI-2Ph synthesis

5 g (20mmol) of MDI and 100ml of anhydrous butyl acetate were introduced into a three neck round bottom flask immersed in a water bath at 45°C. In another flask, 1.88 g (20 mmol) of phenol (blocking agent) and 0.1 ml of DBTL were diluted in 30 ml of anhydrous butyl acetate at 45°C. This mixture was slowly added (15 min) drop-wise into the flask with MDI under vigorous magnetic stirring (step I). After two hours, the initial amount of NCO was reduced to

half as confirmed by titration with di-n-butylamine (ASTM D-1638-74). Then, into a separated flask immersed in a water bath at 60 °C, 30 g of PEG-1500 (20 mmol) were solubilized in 150 ml of anhydrous n-butyl acetate. The solution was then added to MDI-Phenol flask and the agitation was kept for two more hours to ensure full conversion as checked again by titration with di-n-butylamine (step II) [29]. The product, hereafter termed PEG-MDI-2Ph, was recovered by solvent evaporation at room temperature using a rotary evaporator working at reduced pressure and dried at 60 °C for 24 hours. Figure 1 schematically shows the aimed product and the two main reaction steps.

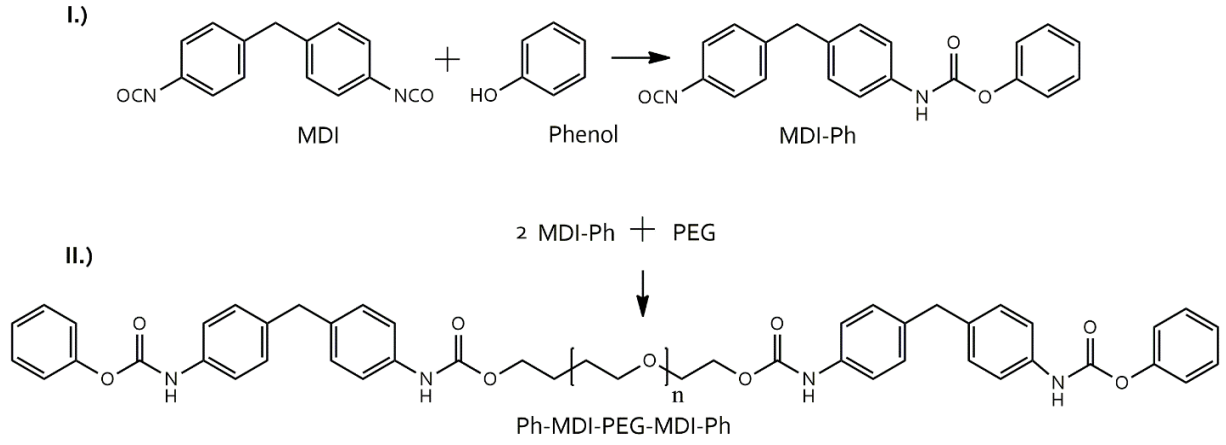

Figure 1. Sinthesis of PEG-MDI-2Ph .i) reaction of MDI with phenol and then ii) reaction of MDI-Ph with PEG.

2.3 NFC-MDI-PEG and NFC/PEG films preparation

PEG-MDI-2Ph (Table 1) dissolved in 100 ml of DMSO with 0.1% in mass of zinc octanoate. Into a separated flask the required amount of distillated water and 16 mg surfactant (DBSA) were mixed under vigorous stirring. After that, NFC 3.2% $_{aq}$ was added to produce 90 g of NFC suspension of 1% wt. Then, the NFC suspension was added dropwise to the PEG-MDI-2Ph solution. The mixtures were further homogenized with an Ultra-Turrax IKA model T25

operating at 10,000 rpm for 5 minutes, to produce the emulsions. After homogenization, films were obtained by casting the emulsions into a glass mold (15x10 cm. The dishes were dried in a circular oven for 24h at 40 °C. After drying, the films were placed in an oven at 170 °C for 10 min, to ensue phenol deblocking, promoting the formation of new urethane bonds.

The unmodified composite films were obtained by direct dissolution of PEG in water followed by the addition of the NFC suspension and dried at 40°C without further thermal treatment. Table 1 gives the label and composition of the prepared films.

Table 1.Label and composition of each mixture prepared to obtain NFC/PEG and NFC-MDI-PEG composite films.

	Label	dry NFC mass (g)	PEG - mass (g)	PEG - MDI-2Ph mass (g)	NFC : PEG ratio	NFC % in the composite
NFC/PEG	E0.2	0.9	4.5	-	1:5 (0.2)	17 %
	E0.5	0.9	1.8	-	1:2 (0.5)	33.3%
	E1.0	0.9	0.9	-	1:1 (1.0)	50 %
NFC-MDI-PEG	E0.2m	0.9	-	5.53	1:5 (0.2)	17 %
	E0.5m	0.9	-	2.21	1:2 (0.5)	33.3%
	E1.0m	0.9	-	1.11	1:1 (1.0)	50 %

2.4 Characterization

Fourier Transformed Infrared (FT-IR) spectra were collected with a Spectrum 100 (PerkinElmer, USA) with an attenuated total reflection (ATR) accessory in the range of 4000 to 650 cm^{-1}.

Liquid Nuclear Magnetic Resonance ^{1}H-NMR analyses were performed with an AVANCE 600 NMR (Bruker, USA). Samples (200 mg) were added to 4 mL of deuterated dimethyl sulfoxide (DMSO-d6). NMR data was analyzed using literature and chemical shifts obtained with model moieties in Chemdraw®.

Thermogravimetric analysis (TG) measurements were conducted with a Pyris analyzer (Perkin Elmer, USA) operating under a constant N_2 flow of 20 mL·min^{-1}, between 25 and 700 °C at a heating rate of 10 °C·min^{-1}.

Differential Scanning Calorimetry (DSC) experiments were carried out in DSC 8000 (Perkin Elmer, USA). Samples of 4 mg sealed in aluminum pans were heated and cooled at rate of 20 ° C. min^{-1} ◦C. min^{-1}, from -10 to 90 °C.

An Inspect F-50 (FEI, USA) microscope working at 2.0 kV and working distances from around 8.0 mm was employed for Scanning Electron Microscopy (SEM) analysis. Images were acquired in the mode of secondary electrons (SE) and samples were metalized for 90s with a platinum target.

Atomic Force Microscopy (AFM) images were obtained using an AFM model Flex-Axiom (Nanosurf, Switzerland) working in tapping air mode. The silicon scanning probe used was a Tap190Al-G with a maximum radius of curvature of 10 nm and 150 kHz as the resonance frequency of the cantilever. Images processing and roughness calculation were performed using the freeware software Gwyddion®.

A universal testing machine model 3365 (Instron, USA) equipped with a load cell of 5 kN was employed to measure tensile properties. The parameters used were extension rate of 0.5 mm min-1 and distance between the grips of 25 mm. For each sample, five rectangular specimens of 35 x 5 mm were tested. The thickness of the specimens was measured using a digital micrometer (Adamel Lhomargy- 120 mm, France). The tests were conducted at 23 °C with a relative humidity of 48%. The samples were preconditioned in the same test conditions at least 24 h before testing.

The out of plane resistance measured as the tear resistance was performed using a Noviprofibre tear tester (Elmendorf, France) equipped with a 4000 mN pendulum. Specimens were cut in squares of 50x50 mm and a notch of 20 mm was automatically made in the midplane of the films. The tear index measured in mN*m²/g was calculated using the grammage values of the dry specimens.

Water contact angle (WCA) were measured using a tensiometer model CAM 101 (KSV Instruments Ltd., Finland). Specimens were cut into rectangular shapes with a width of 5 mm and length of 30 mm from different regions of the films. The values were collected from five measurements with distilled water (droplet of ~5 µl) and the static contact angles were obtained by plotting the contact angle *vs* time, where the equilibrium value (static) was determined. Measurements were performed at 23 °C and 30% RH.

The water vapor absorption test was conducted in accordance with ASTM E-104 1985 using a desiccator with a saturated potassium sulfate (K_2SO_4) in distilled water (RH=97.5%). specimens in dimensions of 2.5x2.5 cm were weighted at regular intervals until complete saturation. The vapor water uptake, and the diffusion coefficient were calculated as reported by Dufresne *et al*. [32], using equation 1, where M_∞ is the mass at saturation point, M_0 the dry mass and M_t the mass at the given time t. 2L is the thickness of the films and D the diffusion coefficient. The Fickian diffusion coefficient was obtained by the plot of $(M_t - M_0)/M_\infty$ as a function of $\sqrt{(t/L^2)}$.

$$\frac{M_t - M_0}{M_\infty} = \frac{2}{L}\sqrt{\left(\frac{D}{\pi}\right) * t} \quad (1)$$

Water vapor transmission rate were measured following the method ASTME96. Samples were attached to aluminum cups filled with 15 g of calcium chloride and open area of 3000 mm^2. The mounted cups were placed in a 50 % humidity environment and the increase in mass was

measured over time. The linear coefficient of the trend line (G/t) was determined in g/h. WVTR values were calculated dividing (G/t) by the open area and is reported in $g.m^{-2}.day^{-1}$. The permeability was calculated by dividing WVTR by the product of vapor pressure difference and the vapor pressure saturation at the test temperature.

A 8001 Oxygen Permeation Analyser (Systech Illinois, USA) equipped with a coulometric oxygen sensor was used to measure the Oxygen Transmission Rate (OTR) of the films in $cm^3/m^2/day$ according to ASTMF1927-07. Samples were double bonded with adhesive aluminum foils with an open area of 2.54 cm^2 were used.

3. RESULTS AND DISCUSSION

3.1 Grafting characterization

Erro! Fonte de referência não encontrada. shows the FT-IR spectra of PEG and PEG-MDI-2Ph, the macrodiol modified with MDI and phenol. PEG-MDI-2Ph displays new bands at 3304 cm^{-1}, related to the N-H bond, at 1728 cm^{-1}, from phenyl carbamates and at 1595 cm^{-1}, due to the presence of C=C from aromatic rings of MDI and phenol. New bands at 1536 cm^{-1} and 1512cm^{-1} related to symmetric stretch of H-NCO are also observed[29,33,34].

Erro! Fonte de referência não encontrada. shows the loss of mass and its derivative obtained as a function of temperature with TG analysis for PEG and PEG-MDI-2Ph. PEG presents only one thermal event starting at 315 °C and ending at 431 °C while the phenol blocked PEG-MDI-2Ph also displays an earlier thermal event starting at 137 °C, responsible for the elimination of 11.3 % of its mass. The higher loss than the theoretical indicates that there was an excess of phenol blocked moieties on the reaction media. **Erro! Fonte de referência não encontrada.** gives the ^{1}H-NMR spectrum of the synthetized adduct and **Erro! Fonte de referência não encontrada.** provides the identification and the area under the peaks for each highlighted

chemical shift. Chemical shifts related to the hydrogen from phenyl carbamates and alkyl carbamates are identified at 9.63 ppm (A) and 9.3 ppm (B), respectively. The area under these peaks are 1.0 and 0.9. The triplet at 7.4-7.2 ppm (D) and the two triplets at 7.2-7.0 (E) are from the aromatic rings of phenol and MDI, respectively. The presence of chemical shifts from PEG are marked as (G), (I) and (J), related to the H-C-O, and -CH_2- in different positions, i.e, near (G) and far (J) from the urethane links. The peak (H) is from the –CH_2- group of MDI. The remaining peaks, (C) at 8.5 ppm and (F) at 6.87-6.7 ppm are product of the reaction of MDI with residual moisture which led to the formation of disubstituted ureas, primary amines and alophanates, as discussed elsewhere [25,29]. The identified bands on FT-IR and the chemical shifts in ^{1}H-NMR spectra along with the phenol release on TG analysis confirmed the occurrence of the blocking and de-blocking reactions of the PEG-MDI-2Ph adduct.

3.2 Composites characterization

Table 2 gives thickness, grammage, density and porosity of the NFC/PEG and NFC-MDI-PEG composites. The thickness of the films increases with PEG content, also resulting in higher grammage. However, there is no significant difference in density as the values around 1.1 g/cm^{3}regardless of the PEG content or chemical modification (presence of MDI). Porosity displays a range from 5 to 35% depending on the composition. In general, the modified films are less porous than the unmodified ones.

Table 2. Physical parameters of NFC/PEG and NFC-MDI-PEG composite films.

	thickness (µm)	grammage (g/m^2)	density (g/cm^3)	porosity (%)
E 0.2	410 ± 36	434 ± 25	1.1 ± 0.1	12 ± 1
E 0.5	152 ± 19	136 ± 8	0.8 ± 0.1	35 ± 4
E 1.0	86 ± 8	99 ± 17	1.2 ± 0.2	13 ± 1
E 0.2m	573 ± 41	546 ± 31	1.0 ± 0.1	20 ± 2
E 0.5m	132 ± 5	158 ± 34	1.2 ± 0.3	5 ± 1
E 1.0m	115 ± 5	130 ± 7	1.1 ± 0.1	15 ± 2

Erro! Fonte de referência não encontrada. gives the FT-IR spectra of PEG, NFC and the modified and non-modified composites loaded with 33 % of NFC (E 0.5 and E0.5m, respectively). One can observe that the modified composite presents new bands at the region of 1730-1500 cm^{-1}, related to amide links.The presence of the band at 1727 cm^{-1} suggests that after phenol deblocking new urethane bonds were formed[26,28], indicating that the free NCO groups underwent reactions with cellulose hydroxyls.

3.2.1 Thermal properties

Figure 2. (a) shows the heat flow as a function of the temperature for PEG and PEG/NFC composites due to the DSC analysis. Melting and crystallization temperatures (T_m and T_c) are given in Table 3 along with the heating of phase changing. PEG has T_m= 52.9 °C and T_c = 19.5 °C. T_m is slightly altered due to the presence of NFC, varying from 50-53 °C whereas T_c is more significantly affected, with composites showing values at least 5 °C above that of PEG, indicating that NFC nucleated the heterogeneous crystallization of the macrodiol. The heating of phase changing for the non-modified composites shows a peak of 200 J/g for the composition E0.5.

Figure 2. (b) presents the heat flow as a function of temperature for NFC-MDI-PEG composites. E0.2m exhibits small melting and crystallization peaks, at 33.6° C and 1.4 °C, respectively, with a reduced heat of phase change of around 30 J/g also shown in Table 3. The compositions with high percentages of NFC, E0.5m and E1.0m, did not show any thermal transition on the temperature span. The suppression of the first order thermal transitions are good evidence of self-crosslinking (PEG-MDI-PEG) and of new urethane bonds formation with the NFC hydroxyls (NFC-MDI-PEG).

Erro! Fonte de referência não encontrada. (a) shows the loss of mass as a function of temperature for PEG, NFC and for modified and non-modified PEG/NFC composites. **Erro! Fonte de referência não encontrada.** (b) presents the derivative of the decomposition curves, from which the thermal events were obtained (showed in **Erro! Fonte de referência não encontrada.**). Only one thermal event starting at 377 °C is observed for PEG while NFC exhibits two, one starting at 267 °C and the other at 407 °C. The modified and non-modified composites also display two thermal events with temperatures of onset of degradation in between the isolated phases.

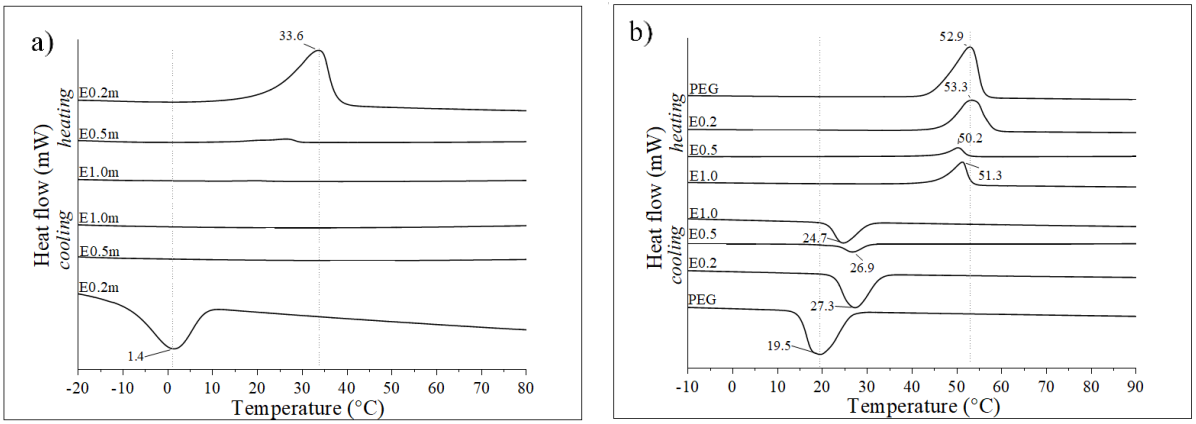

Figure 2.Heating and cooling thermograms of (a) PEG, NFC/PEG and (b) NFC-MDI-PEG composites.

Regarding the thermal stability, it is observed that E0.5, E1.0 and E1.0m maintained the same onset of degradation as NFC, whereas E 0.2 presents its onset of loss of mass 17 °C above the NFC, attributed to the presence of higher fraction of PEG. E0.2m and E0.5m, prepared with PEG-MDI-2Ph exhibited onset of degradation at 294 °C and 285 °C, 27 °C and 18 °C higher than NFC, respectively. Therefore, the crosslinking process enhanced the thermal stability of the

modified PEG-MDI-NFC films above the range achieved by the composites prepared only by dissolution of PEG and mixture with the NFC suspension.

3.2.2 Morphology

Erro! Fonte de referência não encontrada. presents images of the NFC/PEG and NFC-MDI-PEG composites. The non-modified films are slightly white transparent, while the modified ones exhibit a transparent amber coloration. Figure 3 shows the surface SEM images of (a) E0.2 and (b) E0.2m, the compositions with higher PEG content. Both films are compact and with no apparent defects. E0.2 shows a rougher surface, ascribed to the presence of PEG crystals, better observed on the detailed image. On the other hand, due to the crosslinking process, PEG crystals are scarcely observed on the E0.2m surface. The section SEM images on Figure 3 (c) and (d) indicate that the difference in morphology between the compositions did not remain just at the surface, but extended through the bulk. A wrinkled section arising from PEG crystals is observed for E0.2 in Figure 3 (c) without presence of NFC fibers, whereas E0.2m (d) displays a compact and smooth section, in which PEG crystals are not present.

Table 3. Transition temperatures (T_m and T_c) and heating of phase change for PEG, NFC/PEG and NFC-MDI-PEG

	Heating		Cooling	
	T_m (°C)	Δ (J/g)	T_c (°C)	Δ(J/g)
PEG	52.92	150.6	19.43	146.7
E0.2	53.33	113.3	27.26	113.0
E0.5	50.23	203.0	26.71	191.0
E1.0	51.25	81.2	24.64	81.2
E0.2m	33.7	32.17	1.4	27.4
E0.5m	-	-	-	-
E1.0m	-	-	-	-

Erro! Fonte de referência não encontrada. gives the surface and section images of E1.0 and E1.0m, the modified and non-modified PEG/NFC composites with a higher NFC fraction. In

contrast with what was observed in Figure 3, E0.1 and E1.0m exhibit similar morphologies, with a dense entanglement of fibers (a, b) and no clear observation of PEG crystals. Nonetheless, in the section images (c, d) it is observed that E0.1 film shows a cross section covered by PEG crystals, while E1.0m shows a layered and compact section, similar to those displayed by 100% NFC films [25]. **Erro! Fonte de referência não encontrada.** shows the AFM topology and isometric views for (a) E0.5 and (b) E0.5m. The unmodified composition presented a maximum height of 7.15 µm due to the presence of the PEG crystals, against 3.85 µm for the modified E0.5m. **Erro! Fonte de referência não encontrada.** gives three parameters of roughness calculated with the AFM data. Despite the differences observed on the morphology, no clear tendency is noticed, as all compositions remained within the nanometric roughness scale.

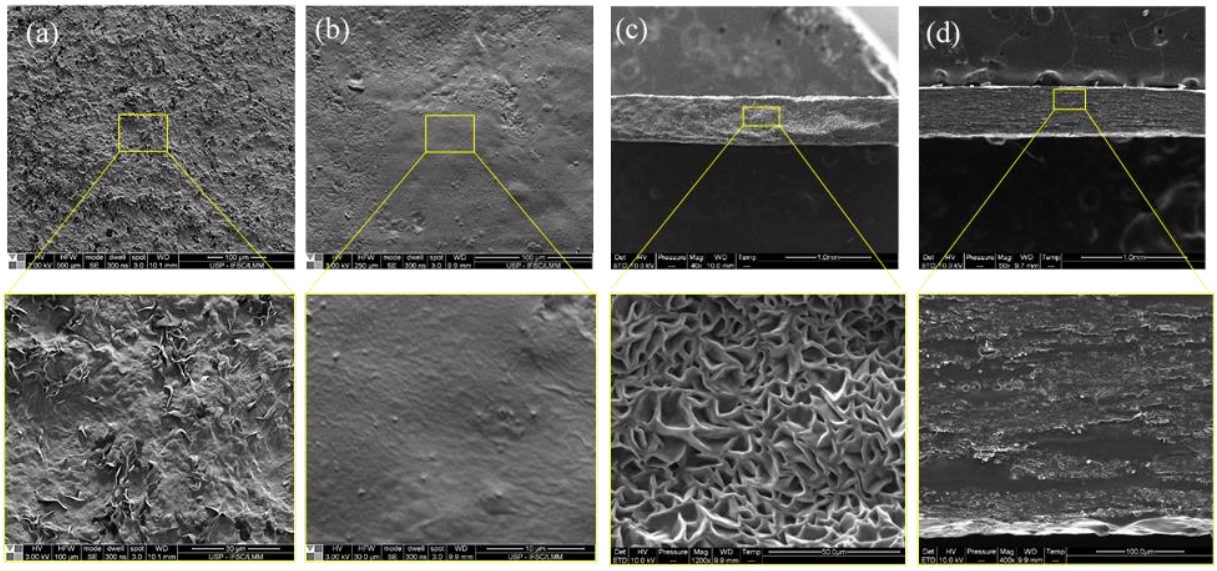

Figure 3.SEM images of the surface of (a) E0.2 and (b) E0.2m and of the section of (c) E0.2 and (d) E0.2m PEG/NFC composites

3.2.3 Mechanical properties

Table 4 gives the tensile properties of NFC/PEG and NFC-MDI-PEG. Unmodified composites exhibit higher Young's modulus for all compositions, indicating that the hydrogen bonds between PEG crystals and NFC provided a higher stiffness to the composite structures than the

crosslinking process. Values of tensile strength and strain at break remained in the same range of 20 MPa and 12 %, respectively for E0.5, E0.5m, E1.0 and E1.0m. On the other hand, a remarkable change is noticed on the strain at break for the low NFC fraction compositions. E0.2 presents a brittle behavior, deforming only by 1.1 %, whereas E0.2m sees this value rising up to 14 %, enhancing considerably its elongation. Maintain the elongation at break despite the crosslinking process is a good feature of the NFC-MDI-PEG films.

Table 4 also gives the tear resistance of the films. E0.2 and E0.2m were not tested due to its increased thickness that impeded proper gripping in the testing apparatus. Comparing E0.5/E0.5m and E1.0/E1.0m one can infer that the crosslinking process enhanced the out-of-plane resistance of the films by almost three times, with values increasing from 0.6 to 1.7 $mN*m^2/g$.

Table 4. Mechanical properties, water uptake and barrier properties to water vapor (WVTR) and oxygen (OTR) of NFC/PEG and NFC-MDI-PEG composite films

	Young's Modulus (GPa)	Tensile Strength (MPa)	Strain at Break (%)	Tear testing index ($mN*m^2/g$)	Value at saturation point	WVTR (g/m^2*day)	OTR ($cm^3/m^2/day$)
E0.2	0.4 ± 0.1	4 ± 2	1.1 ± 0.2	-	1.03 ± 0.01	-	26 ± 2
E0.5	1.2 ± 0.2	23 ± 8	15 ± 3	0.6 ± 0.1	0.63 ± 0.08	86	>1000
E1.0	1.6 ± 0.3	23 ± 3	11 ± 3	0.73 ± 0.03	0.57 ± 0.13	162	>1000
E0.2m	0.10 ± 0.01	3 ± 0.2	14 ± 2	-	0.46 ± 0.01	-	101 ± 2
E0.5m	0.5± 0.1	17 ± 2	13 ± 2	1.7 ± 0.2	0.37 ± 0.01	141	297 ± 32
E1.0m	1.2± 0.1	24 ± 3	10 ± 2	1.7 ± 0.2	0.33 ± 0.01	131	103 ± 14

3.2.4 Water repellency and barrier properties.

Figure 4 a) gives the water contact angle (WCA) as a function of PEG content for PEG/NFC and PEG-MDI-NFC composites. Unmodified composites (E0.2, E0.5 and E1.0) possess WCA between 18° and 40, whereas the values of WCA are around 100° for all modified compositions (E0.2m, E0.5m and E1.0m), an increase of at least 60°. Figure 4 b) presents the water uptake as a

function of time for modified and unmodified composites and Table 4 gives the values of water vapor uptake at the saturation point. All compositions of modified composites display a considerable reduction in water vapor absorption as values at the saturation point were reduced by nearly 45 %. Modified composites present remarkable enhancement of hydrophobicity in relation to the neat composites and the hydrophobic character of the modified composites were also reflected in their water absorption.

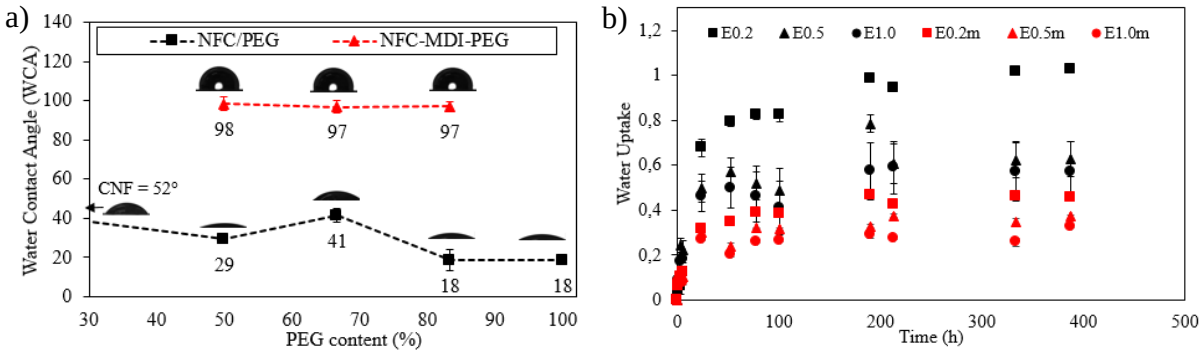

Figure 4. (a) Water contact angle (WCA) for NFC, NFC/PEG and NFC-MDI-PEG composite films and (b) Water uptake evolution as a function of time for NFC/PEG and NFC-MDI-PEG composite films.

Table 4 provides the Water Vapor Transmission Rate (WVTR) and the Oxygen Transmission Rate (OTR) of the composite films. Due to their major thickness, E 0.2 and E 0.2m could not be placed in the test cup, thus their WVTR values were not measured. There is no clear evidence that the crosslinking affected the WVTR, since the values are close to those displayed by the neat NFC film, of around 150 $g.m^{-2}.day^{-1}$[25]. Nonetheless, making composite films of NFC with the PEG macrodiol modified with MDI provides an advantage in that the hydrophobicity and water resistance of the films are increased without hampering the barrier to water vapor exhibited by the compact NFC film. Regarding to the OTR values, when the NFC fraction is increased, the effect of the chemical modification becomes evident. E0.5 and E1.0 show OTR values higher than 1000 $cm^3/m^2/day$, while E0.5m and E1.0m give 297 $cm^3/m^2/day$ and 103 $cm^3/m^2/day$,

307 respectively, evidencing that the crosslinking was capable of reducing considerably the passage
308 of O_2 for composites with high load of NFC.

309 3.2.5Structure prediction

310 The higher thermal stability and water resistance displayed by the PEG-MDI-NFC composites
311 (E0.2m, E0.5m and E1.0m), along with the suppression of the melting and crystallization peaks
312 of PEG on DSC analysis, indicate that after the deblocking reaction at 170 °C, new urethane
313 bonds were formed between the free isocyanates groups (self-reaction) and between the free
314 isocyanates groups and the hydroxyls at the NFC surface, thus promoting crosslinking reactions.
315 Figure 5 gives the most relevant path for the crosslinking reaction at the outmost layer of the
316 NFC fibers.

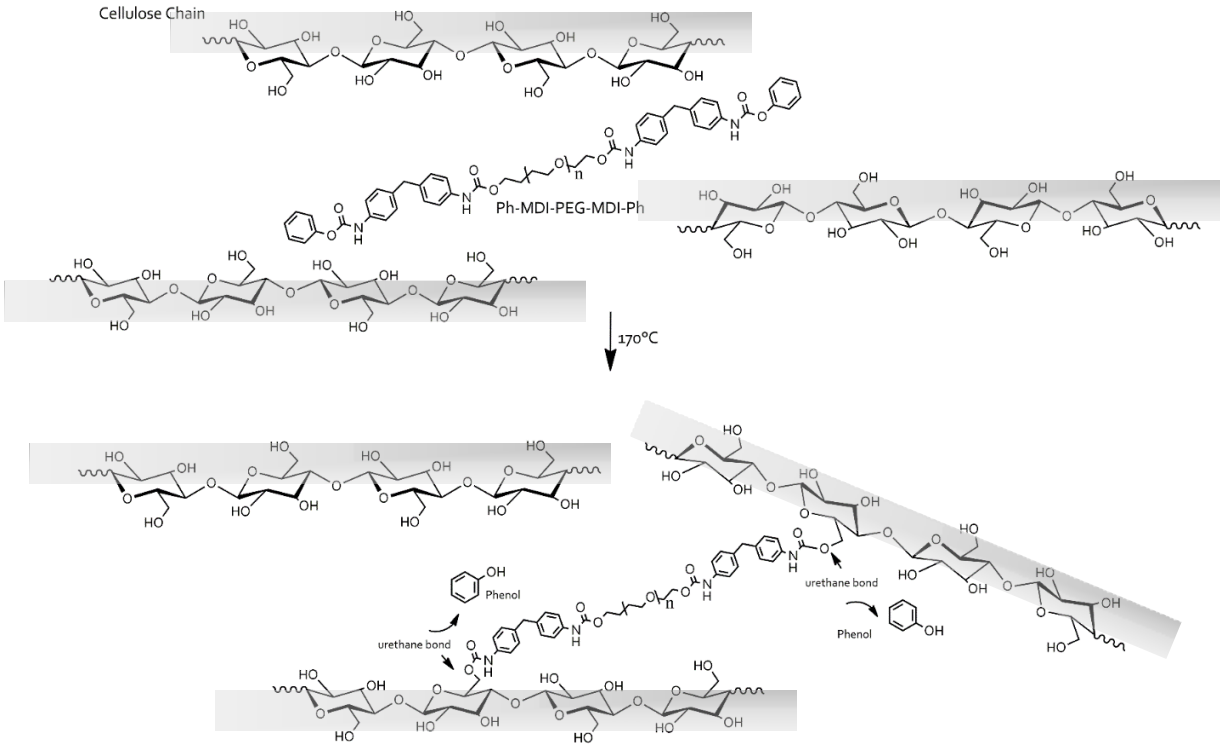

317

318 Figure 5. Structure prediction at the outmost layer of NFC fibers due to the PEG-MDI urethane reaction, leading to crosslinking
319 NFC-MDI-PEG composite films.
320

4. CONCLUSIONS

A blocked macrodiol was prepared by the reaction of PEG with MDI and phenol and was used to prepare modified composites films reinforced with cellulose nanofibers (NFC) at the load of 17, 33 and 50 %. After drying the films were heated to 170 °C in order to deblock de PEG-based adduct, ensuing crosslinking between PEG-MDI and NFC. The reaction was confirmed by FT-IR and ^{1}H-NRM analysis. The crosslinking process enhanced the thermal stability of the composites in the range of 18 – 27 °C, and the tear resistance of the films in three times along with keeping their strain at break in traction above 10 %. Modified composites turned into hydrophobic materials with an increase in water contact angle from 40° to near 100° and a reduction in 45 % on the water vapor uptake. The oxygen transmission rate was reduced from more than 1000 $cm^{-3}.m^{-2}.day^{-1}$ to values below 260 $cm^{-3}.m^{-2}.day^{-1}$ and the Water Vapor Transmission rate (WVTR) remained in the range of 150 $g.m^{-2}.day^{-1}$. The strategy proposed here reduced the hydrophilicity of PEG/NFC composites, thus providing an interesting alternative for the production of water resistant and low permeable biobased packaging with high elongation at break.

AUTHOR INFORMATION

Corresponding author

Antonio José Felix Carvalho- Department of Materials Engineering, Sao Carlos School of Engineering (EESC), University of São Paulo (USP), São Paulo, SP, Brazil.

https://orcid.org/0000-0001-8403-1135 E-mail: (toni@sc.usp.br)

Authors

342 Gustavo de Souza- Department of Materials Engineering, Sao Carlos School of Engineering
343 (EESC), University of São Paulo (USP), São Paulo, SP; Univ. Grenoble Alpes, CNRS, Grenoble
344 INP, LGP2, F-38000, Grenoble, France. https://orcid.org/0000-0002-9056-8550

345 Mohamed Naceur Belgacem- Univ. Grenoble Alpes, CNRS, Grenoble INP, LGP2, F-38000,
346 Grenoble, France https://orcid.org/0000-0002-3317-7369

347 Alessandro Gandini- Univ. Grenoble Alpes, CNRS, Grenoble INP, LGP2, F-38000, Grenoble,
348 France

349 AUTHOR CONTRIBUTIONS

350 The manuscript was written through contributions of all authors. All authors have given
351 approval to the final version of the manuscript.

352 ACKNOWLEDGEMENTS

353 This study was financed in part by the Coordenação de Aperfeiçoamento de Pessoal de Nível
354 Superior - Brazil (CAPES) - Finance Code 001. Also, authors acknowledge CNPq for the
355 doctoral fellowship granted to G.S (CNPq proc. 140249/2017-6). AJFC acknowledge CNPq for
356 research funding project # 03847/2019-0. We also thank to Suzano S/A, Brazil which kindly
357 supplied the NFC from eucalyptus wood pulp.

358 NOTES

359 The authors declare no competing financial interest.

360 **REFERENCES**

361 [1] T. Li, C. Chen, A.H. Brozena, J.Y. Zhu, L. Xu, C. Driemeier, J. Dai, O.J. Rojas, A. Isogai,
362 L. Wågberg, L. Hu, Developing fibrillated cellulose as a sustainable technological

material, Nature. 590 (2021) 47–56. doi:10.1038/s41586-020-03167-7.

[2] H.L. Tan, D. Kai, P. Pasbakhsh, S.Y. Teow, Y.Y. Lim, J. Pushpamalar, Electrospun cellulose acetate butyrate/polyethylene glycol (CAB/PEG) composite nanofibers: A potential scaffold for tissue engineering, Colloids Surfaces B Biointerfaces. 188 (2020) 110713. doi:10.1016/j.colsurfb.2019.110713.

[3] P.R. Chinnam, R. Mantravadi, J.C. Jimenez, D.A. Dikin, S.L. Wunder, Lamellar, micro-phase separated blends of methyl cellulose and dendritic polyethylene glycol, POSS-PEG, Carbohydr. Polym. 136 (2016) 19–29. doi:10.1016/j.carbpol.2015.08.087.

[4] A. Idris, L.K. Yet, The effect of different molecular weight PEG additives on cellulose acetate asymmetric dialysis membrane performance, J. Memb. Sci. 280 (2006) 920–927. doi:10.1016/j.memsci.2006.03.010.

[5] D. Li, Y. Ye, D. Li, X. Li, C. Mu, Biological properties of dialdehyde carboxymethyl cellulose crosslinked gelatin-PEG composite hydrogel fibers for wound dressings, Carbohydr. Polym. 137 (2016) 508–514. doi:10.1016/j.carbpol.2015.11.024.

[6] M. Foroughi-Dahr, R. Sotudeh-Gharebagh, N. Mostoufi, Effect of operation conditions on coating of pharmaceutical pellets with a film of HPMC/PEG in a Wurster coater, Powder Technol. 354 (2019) 804–814. doi:10.1016/j.powtec.2019.06.027.

[7] K. Huntrakul, N. Harnkarnsujarit, Effects of plasticizers on water sorption and aging stability of whey protein/carboxy methyl cellulose films, J. Food Eng. 272 (2020) 109809. doi:10.1016/j.jfoodeng.2019.109809.

[8] R. Ghafari, R. Scaffaro, A. Maio, E.F. Gulino, G. Lo Re, M. Jonoobi, Processing-structure-property relationships of electrospun PLA-PEO membranes reinforced with enzymatic cellulose nanofibers, Polym. Test. 81 (2020) 106182.

386 doi:10.1016/j.polymertesting.2019.106182.
387 [9] W. Wang, Z. Yu, F.K. Alsammarraie, F. Kong, M. Lin, A. Mustapha, Properties and
388 antimicrobial activity of polyvinyl alcohol-modified bacterial nanocellulose packaging
389 films incorporated with silver nanoparticles, Food Hydrocoll. 100 (2020) 105411.
390 doi:10.1016/j.foodhyd.2019.105411.
391 [10] J. Cailloux, J.M. Raquez, G. Lo Re, O. Santana, L. Bonnaud, P. Dubois, M.L. Maspoch,
392 Melt-processing of cellulose nanofibril/polylactide bionanocomposites via a sustainable
393 polyethylene glycol-based carrier system, Carbohydr. Polym. 224 (2019) 115188.
394 doi:10.1016/j.carbpol.2019.115188.
395 [11] D. Mishra, P. Khare, D.K. Singh, S. Luqman, P. V. Ajaya Kumar, A. Yadav, T. Das, B.K.
396 Saikia, Retention of antibacterial and antioxidant properties of lemongrass oil loaded on
397 cellulose nanofibre-poly ethylene glycol composite, Ind. Crops Prod. 114 (2018) 68–80.
398 doi:10.1016/j.indcrop.2018.01.077.
399 [12] P. Cazón, M. Vázquez, G. Velazquez, Cellulose-glycerol-polyvinyl alcohol composite
400 films for food packaging: Evaluation of water adsorption, mechanical properties, light-
401 barrier properties and transparency, Carbohydr. Polym. 195 (2018) 432–443.
402 doi:10.1016/j.carbpol.2018.04.120.
403 [13] N.R. Saha, I. Roy, G. Sarkar, A. Bhattacharyya, R. Das, D. Rana, R. Banerjee, A.K. Paul,
404 R. Mishra, D. Chattopadhyay, Development of active packaging material based on
405 cellulose acetate butyrate/polyethylene glycol/aryl ammonium cation modified clay,
406 Carbohydr. Polym. 187 (2018) 8–18. doi:10.1016/j.carbpol.2018.01.065.
407 [14] R.N. Wijesena, N.D. Tissera, V.W.S.G. Rathnayaka, H.D. Rajapakse, R.M. de Silva,
408 K.M.N. de Silva, Shape-stabilization of polyethylene glycol phase change materials with

chitin nanofibers for applications in “smart” windows, Carbohydr. Polym. 237 (2020) 116132. doi:10.1016/j.carbpol.2020.116132.

[15] C. López de Dicastillo, F. Bustos, A. Guarda, M.J. Galotto, Cross-linked methyl cellulose films with murta fruit extract for antioxidant and antimicrobial active food packaging, Food Hydrocoll. 60 (2016) 335–344. doi:10.1016/j.foodhyd.2016.03.020.

[16] S. Gopi, A. Amalraj, N. Kalarikkal, J. Zhang, S. Thomas, Q. Guo, Preparation and characterization of nanocomposite films based on gum arabic, maltodextrin and polyethylene glycol reinforced with turmeric nanofiber isolated from turmeric spent, Mater. Sci. Eng. C. 97 (2019) 723–729. doi:10.1016/j.msec.2018.12.089.

[17] S. Mahmud, K.M.F. Hasan, M.A. Jahid, K. Mohiuddin, R. Zhang, J. Zhu, Comprehensive review on plant fiber-reinforced polymeric biocomposites, Springer US, 2021. doi:10.1007/s10853-021-05774-9.

[18] P.A. Vinodhini, K. Sangeetha, G. Thandapani, P.N. Sudha, V. Jayachandran, A. Sukumaran, FTIR, XRD and DSC studies of nanochitosan, cellulose acetate and polyethylene glycol blend ultrafiltration membranes, Int. J. Biol. Macromol. 104 (2017) 1721–1729. doi:10.1016/j.ijbiomac.2017.03.122.

[19] R.F. Faradilla, G. Lee, P. Sivakumar, M. Stenzel, J. Arcot, Effect of polyethylene glycol (PEG) molecular weight and nanofillers on the properties of banana pseudostem nanocellulose films, Carbohydr. Polym. 205 (2019) 330–339. doi:10.1016/j.carbpol.2018.10.049.

[20] J. Wang, D.J. Gardner, N.M. Stark, D.W. Bousfield, M. Tajvidi, Z. Cai, Moisture and Oxygen Barrier Properties of Cellulose Nanomaterial-Based Films, ACS Sustain. Chem. Eng. 6 (2018) 49–70. doi:10.1021/acssuschemeng.7b03523.

[21] J.B. Nathalie Lavoine, Isabelle Desloges, Alain Dufresne, Microfibrillated cellulose – Its barrier properties and applications in cellulosic materials: A review, Carbohydr. Polym. 90 (2012) 735–764. doi:http://dx.doi.org/10.1016/j.carbpol.2012.05.026.

[22] F. Rol, M.N. Belgacem, A. Gandini, J. Bras, Recent advances in surface-modified cellulose nanofibrils, Prog. Polym. Sci. 88 (2019) 241–264. doi:10.1016/j.progpolymsci.2018.09.002.

[23] A. Gandini, M.N. Belgacem, The Surface and In-Depth Modification of Cellulose Fibers, in: O.J. Rojas (Ed.), Cellul. Chem. Prop. Fibers, Nanocelluloses Adv. Mater., Springer International Publishing, Cham, 2016: pp. 169–206. doi:10.1007/12_2015_305.

[24] A.J.F. Carvalho, A.A.S. Curvelo, A. Gandini, Surface chemical modification of thermoplastic starch: Reactions with isocyanates, epoxy functions and stearoyl chloride, Ind. Crops Prod. 21 (2005) 331–336. doi:10.1016/j.indcrop.2004.04.027.

[25] G. de Souza, M.N. Belgacem, A. Gandini, A.J.F. Carvalho, Low permeable hydrophobic nanofibrilated cellulose films modified by dipping and heating processing technique, Cellulose. 3 (2021). doi:10.1007/s10570-020-03619-3.

[26] E. Delebecq, J.P. Pascault, B. Boutevin, F. Ganachaud, On the versatility of urethane/urea bonds: Reversibility, blocked isocyanate, and non-isocyanate polyurethane, Chem. Rev. 113 (2013) 80–118. doi:10.1021/cr300195n.

[27] X. Zhou, Y. Fu, L. Chen, R. Wang, X. Wang, Y. Miao, X. Ji, H. Bian, H. Dai, Diisocyanate modifiable commercial filter paper with tunable hydrophobicity, enhanced wet tensile strength and antibacterial activity, Carbohydr. Polym. 248 (2020) 116791. doi:10.1016/j.carbpol.2020.116791.

[28] D. a. Wicks, Z.W. Wicks, Blocked isocyanates III: Part A. Mechanisms and chemistry,

Prog. Org. Coatings. 36 (1999) 148–172. doi:10.1016/S0300-9440(99)00042-9.

[29] J. Gironès, M.T.B. Pimenta, F. Vilaseca, A.J.F. de Carvalho, P. Mutjé, A.A.S. Curvelo, Blocked isocyanates as coupling agents for cellulose-based composites, Carbohydr. Polym. 68 (2007) 537–543. doi:10.1016/j.carbpol.2006.10.020.

[30] J. Gironès, M.T.B. Pimenta, F. Vilaseca, A.J.F. Carvalho, P. Mutjé, A.A.S. Curvelo, Blocked diisocyanates as reactive coupling agents: Application to pine fiber-polypropylene composites, Carbohydr. Polym. 74 (2008) 106–113. doi:10.1016/j.carbpol.2008.01.026.

[31] G. min Wu, G. feng Liu, J. Chen, Z. wu Kong, Preparation and properties of thermoset composite films from two-component waterborne polyurethane with low loading level nanofibrillated cellulose, Prog. Org. Coatings. 106 (2017) 170–176. doi:10.1016/j.porgcoat.2016.10.031.

[32] A. Dufresne, D. Dupeyre, M.R. Vignon, Cellulose microfibrils from potato tuber cells: Processing and characterization of starch-cellulose microfibril composites, J. Appl. Polym. Sci. 76 (2000) 2080–2092. doi:10.1002/(SICI)1097-4628(20000628)76:14<2080::AID-APP12>3.0.CO;2-U.

[33] F.E. Tabaght, A. El Idrissi, R. Bellaouchi, A. Asehraou, M. Aqil, S. El Barkany, A. Benarbia, N. Achalhi, A. Tahani, Cellulose grafted aliphatic polyesters: Synthesis, characterization and biodegradation under controlled conditions in a laboratory test system, J. Mol. Struct. 1205 (2020). doi:10.1016/j.molstruc.2019.127582.

[34] X. Shi, S. Bai, Y. Li, X. Yu, K. Naito, Q. Zhang, Effect of polyethylene glycol surface modified nanodiamond on properties of polylactic acid nanocomposite films, Diam. Relat. Mater. 109 (2020) 108092. doi:10.1016/j.diamond.2020.108092.

PAPER 5

Nanofibrilated Cellulose/Beeswax Films: Barrier Properties and Perspective Application in Packaging

Gustavo de Souza[a,b], Ricardo Klaus Kramer [a,b], Mohamed Naceur Belgacem[b], Alessandro Gandini[b], Antonio José Felix Carvalho[a]*

gustavo2.souza@usp.br

kramer.iqsc@gmail.com

naceur.belgacem@pagora.grenoble-inp.fr

agandini@iqsc.usp.br

*toni@sc.usp.br

[a] Department of Materials Engineering, Sao Carlos School of Engineering (EESC), University of São Paulo (USP), São Paulo, SP, Brazil

[b] University of Grenoble Alpes, CNRS, Grenoble INP, LGP2, F-38000, Grenoble, France

Highlights

- Nanocellulose/beeswax films were obtained from emulsions with 10, 25 and 50 $\%_{wt}$ of beeswax.
- Composites were almost 40 % less dense and slightly more transparent.
- Water Contact Angle (WCA) increased and water absorption significantly reduced.
- Water Vapor Transmission Rate (WVTR) reduced from 153 to 9.6 $g.m^{-2}.day^{-1}$ for NFC-E50.
- Nanocellulose/beeswax films with high mechanical properties were obtained.

26 **Table of Content (TOC)**

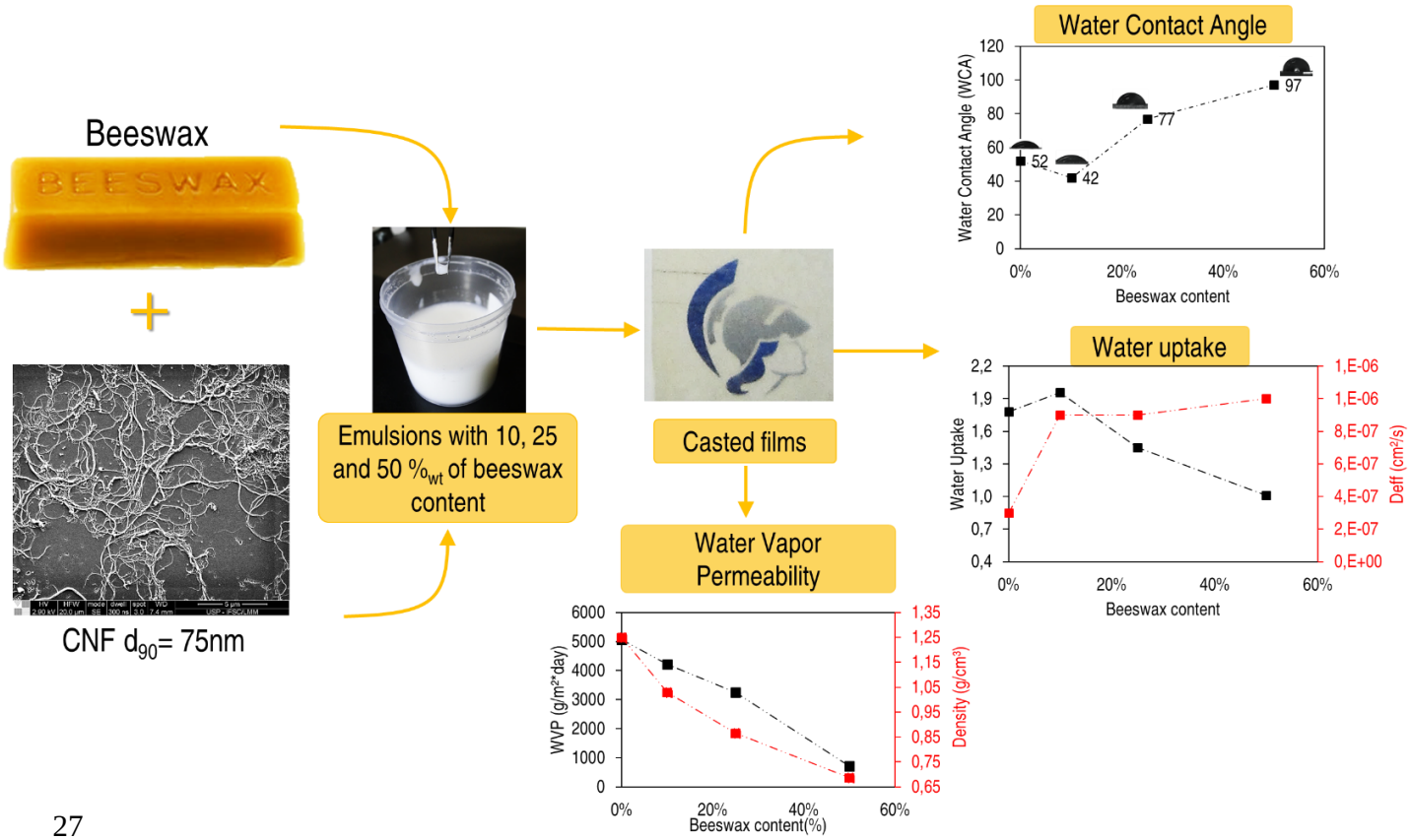

27

28

Abstract

Single-used plastics used for packages and biomedical materials account for most of the polymeric waste stream worldwide. Cellulose is a high available material possessing tunable properties that make them good candidates to replace polymers in some applications. Thus, alternatives to tune cellulose properties and in special increase its hydrophobic character are of great interest. Here, we described biobased composite films obtained by casting a composition of a nanofibrilated cellulose (NFC) suspension and beeswax (BW) emulsion to give a final composition with 10, 25 and 50 $\%_{wt}$ of BW. NFC/BW biocomposites were 40 % less dense, more transparent and displayed a hydrophobic character with water contact angle close to 100°. Besides, NFC/BW composite films presented water vapor transmission rate (WVTR) of about 9.6 $g.m^{-2}.day^{-1}$, which is of the same order of synthetic polymeric films such as LDPE, representing a reduction of almost 95 % with respect to NFC film. This is one of the lowest value reported until now for biobased films. In spite of the high load of BW, these biocomposites presented good mechanical properties with minimal Young's modulus of 3 GPa and tensile strength of 36 MPa. These results indicate that NFC/BW films are suited green alternatives for packaging applications.

Key-words: Nanofibrilated cellulose (NFC); beeswax (BW); biobased films; barrier properties; packaging;

1. Introduction

There is no doubt that the use of petroleum based polymeric materials have helped to evolve our society to better living conditions. However, the rate of its unbalanced consumption cannot longer be sustained without severe and irreversible impact on nature. In 2014, some 26 million tons of the plastic produced in the EU were converted into plastic waste, being short-lived packaging accounting for 63 % of this waste stream.

It is estimated that 32 % of the global waste have ended up in the environment and studies predict a twofold increase on the number of plastic debris by 2030 (Wagner & Schlummer, 2020). Nonetheless, this value can be dramatically increased due to the pandemic situation caused by the COVID-19 virus due to the increase in disposable materials such as gloves, face shields, masks, dish plates, etc. Therefore, there is an increasing interest in the development of biodegradable alternatives to replace petroleum-based polymers, particularly in food packaging and health applications.

One relevant characteristic for packaging is barrier properties such as water vapor transmission rate (WVRT) that must be in the range of 10-20 $g.m^{-2}.day^{-1}$ for most applications, which is met by polymers such as low density polyethylene (LDPE) (Han, Salmieri, Le Tien, & Lacroix, 2010; Lavoine, Desloges, Dufresne, & Bras, 2012). Alternatives such as cellulose acetate (CA) and oleic acid produced by Tedeschi et al (2018) (Tedeschi, Guzman-Puyol, et al., 2018) presented remarkable reduction of WVTR when compared with that of the pure CA film, a decrease from 6000 $g.m^{-2}.day^{-1}$ to 670 $g.m^{-2}.day^{-1}$, but still far from LDPE. The gluten/PCL composite film developed by Gutiérrez et al (2020) (Gutiérrez et al., 2020), though completely biodegradable after 90 days, exhibited an elastic modulus that was lower than 100 MPa (Gutiérrez et al., 2020).Therefore, biobased materials with higher properties must be sought (Cazón, Velazquez, Ramírez, & Vázquez, 2017).

Biocomposites of nanofibrillated cellulose (NFC) containing considerable amounts of NFC are serious candidates to produce films for packaging. Cellulose is the most widely available biobased material on earth and NFC is of special interest for food packaging as the strength and toughness of NFC films increase simultaneously as the diameter of the fibers is reduced. Additionally, the hydrogen bonds formed in the amorphous region of cellulose (hornification), aid to promote a dense and compact entanglement of nanofibers, giving rise to mechanically

strong and low permeable films. These films enhance the possibilities of reaching stiffness and barrier requirements(Klemm et al., 2018; Lavoine et al., 2012).

The market of nanoceluloses is going to reach US$ 700 millions by 2023 (Vartiainen & Malm, 2016) and cellulose is part of the 2015 global sustainability development goals (SDGs) (Lindström & Aulin, 2014; Näyhä, 2019; Pätäri, Tuppura, Toppinen, & Korhonen, 2016; Vartiainen & Malm, 2016). However, the major problem faced by NFC-based films is its high hydrophilicity. In high humidity or wet environments, the mechanical and barrier properties of NFC films decrease considerably due to the water plasticizing effect. Bedane et al (2015)(Bedane et al., 2015) measured a WVTR of 29 $g.m^{-2}.day^{-1}$ for NFC films at a RH 10 % and observed that the values sharply rose to 650 $g.m^{-2}.day^{-1}$ at RH 90 %.

Natural waxes like carnauba and beeswax (BW) appear as suitable alternatives to promote hydrophobization of biobased films (Morrissette et al., 2018; Tedeschi, Benitez, et al., 2018; Vimala Bharathi, Murugesan, Moses, & Anandharamakrishnan, 2020). BW is a natural material of complex structure and has been considered as a barrier layer for paper packaging since the 1990s by Fennema and co-workers (Donhowe & Fennema, 1993; Fennema, Donhowe, & Kester, 1994; GONTARD, DUCHEZ, CUQ, & GUILBERT, 1994; KESTER & FENNEMA, 1989). From there, many authors have reported the used of BW for coating paper and NFC films towards improving water resistance of cellulose-based films (Forsman et al., 2017; Lu, Xiao, Zhang, & Gong, 2014; Pan, Xiao, Li, & Xu, 2015; Sethi, Visanko, Österberg, & Sirviö, 2019b; Sethi et al., 2019a; Yang & Paulson, 2000; D. Zhang & Xiao, 2013; W. Zhang, Xiao, & Qian, 2014). In addition, some studies have pointed out that the presence of BW can accelerate the biodegradation of cellulose, which is not desired for paper conservation, but very attractive for short lived biobased packaging(Choi, Kang, & Cho, 2016; Jeong et al., 2014). Nonetheless, new strategies are needed to incorporate BW in NFC films to give rise to hydrophobic and low permeable biobased films but also maintaining its mechanical strength and storage stability as BW coating can be broken and BW load may reduce the H-bond ability of NFC.

Here, we describe the preparation of NFC/BW composite films by casting emulsions of NFC and BW, with an increasing load of BW, with 10, 25 and 50 $\%_{wt}$ in relation to the cellulose dry matter. The emulsions were characterized by Zeta potential and DLS. The effect of different amounts of BW on the obtained composites were characterized by spectroscopy, morphology, mechanical and thermal analyses. Also, special attention was dedicated to its water repellent

properties and barrier towards water vapor and O_2. Finally, we show that the addition of BW at high load decreases the WVTR of NFC/BW composite films to below the value of LDPE, reaching the lowest values reported in the literature for biobased films in the last 10 years, as shown by a discussion of the literature reports.

2. MATERIALS AND METHODS

2.1 Materials

Nanofibrilated cellulose from eucalyptus in aqueous suspension (3.2 $\%_{wt}$) were kindly supplied by Suzano S/A., Brazil. Beeswax was supplied by C.H.O Indústria e Comércio LTDA®, Brazil. Surfactant dodecyl benzene sulfonic acid (DBSA) was from Sigma Aldrich® - USA and was used as received.

2.2 Emulsion and films preparation

80 g of 1 $\%_{aq}$ NFC suspension was poured into a beaker with ~16 mg of DBSA and allowed to homogenize for five minutes in a magnetic stirrer. The necessary amount of beeswax for each mixture (Table 1) was heated at 200 °C and added dropwise into the NFC suspension under vigorous stirring. Further homogenization was conducted with an Ultra-Turrax IKA model T25 operating at 10,000 rpm for 5 minutes. The emulsion was then sonicated using an UP400S Ultrasonic Processor (Hielscher) for five minutes with pulses of 50 % of time and 60 % power (240 W). The emulsions were then deaerated by applying vacuum for 10 minutes. NFC/beeswax composites films were obtained by casting the emulsions into rectangular glass dishes (15x10 cm). The dishes were dried in a circular oven for 24 h at 60 °C.

Table 1. Label and composition of each mixture prepared to obtain NFC and NFC/BW composite films.

	NFC (1%aq)	Beeswax	DBSA	% of beeswax in relation to dry NFC content
NFC	80 g	-	-	0
NFC - E10	80 g	0,08 g	~16 mg	10 %
NFC - E25	80 g	0,2 g	~16 mg	25 %
NFC - E50	80 g	0,8 g	~16 mg	50 %

2.3 Characterization

2.3.1 Scanning Electron Microscopy - SEM

SEM images were acquired in the mode of secondary electrons (SE) using an Inspect F-50 (FEI) microscope working with voltage in the range of 2.0 – 3.0 kV and working distances of 7.0-8.0 mm.. Stubs were metalized for 90 s with a platinum target.

2.3.2 Atomic Force Microscopy - AFM

The average length of NFC and the films roughness were measured using an Atomic Force Microscope Flex-Axiom (Nanosurf) working in tapping air mode with a tip model Tap190Al-G with a radius of curvature of 10 nm. After acquisition, images were processed with the software Gwyddion®, in which five horizontal parallel lines of 30 µm in length were drawn spaced by 5 µm each. In each line, three roughness parameters, being the average roughness (Ra), the mean square root roughness (Rq), and the maximum profile height (Rt), were calculated. For each sample, the average value of the five lines was taken as the average Ra, Rt and Rq values.

2.3.3 Liquid ^{13}C-Nuclear Magnetic Resonance -NMR

^{13}C NMR analysis of the beeswax was conducted on a Bruker AVANCE 600 NMR. 200 mg of beeswax was added to 4 mL of deutered chloroform and stirred for 5 min to get a homogeneous solution and then the solution was poured into a 10 mL glass NMR tube.

2.3.4 Zeta potential and Dynamic Light Scaterring - DLS

Zeta potential and DLS were performed in a particle analyzer model Litesizer 500, Anton Paar®. For both analyses, emulsions were diluted with deionized water to a 0.1 % of the initial concentration before being poured into the cuvettes. Data was acquired at 25 °C.

159 2.3.5 Optical Microscopy

160 The images were acquired using a DM2700M, LEICA® microscope with coupled cam model
161 DMC2900. The acquisition was in the mode of transmitted light with a 90° polarizer.
162

163 2.3.6 UV-VIS

164 The in-line light transmittance was measured in the UV-Visible region (200–800 nm) with a
165 model UVM51 spectrophotometer from BEL photonics. The transmittance spectra were acquired
166 using air as background.
167

168 2.3.7 Fourier Transformed Infrared – FT-IR

169 FITR Spectra were acquired using a PerkinElmer Spectrum 100 Fourier transform infrared
170 spectrometer equipped with an attenuated total reflection (ATR) accessory. Measurements were
171 performed in the range of mid infrared from 4000 cm^{-1} to 650cm^{-1}, and each spectrum was an
172 average of 32 measurements.
173

174 2.3.8 Grammage, density and porosity

175 The grammage, measured as mass per unit area (g/m^2), were obtained by weighing pieces with
176 50 x 50 mm (0.1 mg readability). Samples thickness were measured using a digital micrometer
177 (Adamel Lhomargy 120 mm, France) and the density values were calculated in g/cm^3. Porosity
178 was calculated using the relation $(1- \rho_m/\rho_t)$ where ρ_m is the measured density and ρ_t the
179 theoretical cellulose density, used as 1.5 g/cm^3.
180

181 2.3.9 Tensile test and Semi Wet Tensile Test

182 Tests were performed in an universal test machine Instron 3365 with a load cell of 5kN using
183 miniaturized rectangular testing specimens (35x5 mm) with extension rate of 0.5 mm min^{-1} and
184 25 mm of distance between the grips (Hervy, Santmarti, Lahtinen, Tammelin, & Lee, 2017).
185 Temperature and relative humidity were controlled at 23 °C and 48 %RH, respectively, during
186 all tests. The specimens were conditioned in the test room for at least 24 h before loading. For

the semi wet tensile tests, a 10 μL drop of distilled water was placed in the middle length of the specimen and allowed to rest. After 1 min, the water excess was carefully dried with absorbing paper and the test was performed using the same apparatus of the dry test. With the wet tensile proprieties, the wet/dry ratio was calculated.

2.3.10 Tear Testing

The tear resistance was measured using a Noviprofibre tear tester (Elmendorf, France) equipped with a 4000 mN pendulum. Specimens were cut in square shape of 50 x 50 mm and the tear index was calculated using gramage values of the dry specimens.

2.3.11 Thermogravimetric analysis - TG

TG analysis was performed in a thermogravimetric Pyris (Perkin Elmer) analyzer operating under a constant N_2 flow of 20 mL·min^{-1}, in the temperature interval of 25 to 700 °C, at a heating rate of 10 °C·++min^{-1}.

2.3.12 Differential Scanning Calorimetry - DSC

DSC experiments were carried out with DSC 8000 (Perkin Elmer) analyzer. The heating and cooling rate for the scans was 20 ° C min^{-1}, from 0 to 100 ° C with samples of about 4 mg kept in hermetic aluminum pans.

2.3.13 Water Contact Angle (WCA)

WCA measurements were taken with a KSV - CAM 101 equipment. The films were first cut into rectangular specimens of 30 x 5 mm. Five droplets of distilled water of ~5 μL were dropped on each specimen. 40 pictures at 16 ms of interval were taken and the static contact angles were obtained by plotting the contact angle vs time, where the equilibrium value (static) was determined. All the measurements were performed at 23°C and 30 %RH.

214 2.3.14 Water Absorption Test

215 3 specimens of each composition, in dimensions of 2.5x2.5 cm were placed in a dish with
216 distilled water and weighted at 1 h,3 h, 5 h, 24 h and then at intervals of 24 h in the first week, 48
217 h in the second and 72 h after the second week until complete saturation. Before the test,
218 specimens were conditioned at 60 °C for 3 days in a circular oven for mass stabilization. The
219 water uptake and the diffusion coefficient were calculated as reported by Dufresne et al, 2000
220 (Dufresne, Dupeyre, & Vignon, 2000)
221

222 2.3.15 Water Vapor Transmission Rate (WVTR)

223 Permeance test was performed in accordance with ASTME96, using the desiccant. 15g of
224 calcium chloride was placed in the bottom of the sealed cup with mount area of 3000 mm². The
225 test was conducted in a 50 % humidity chamber and WVTR values were determined by the
226 linear coefficient of mass increase (g) over time (h). Permeability was calculated dividing
227 WVTR by the product of vapor pressure difference and the vapor pressure saturation at the test
228 temperature. With WVTR data, the interpore diffusion coefficient D_a was calculated (Hu,
229 Acharya, & Abidi, 2019). Also, the Knudsen number N_{Kn} and Knudsen diffusivity D_{KA} were
230 calculated as reported elsewhere (Spence et al., 2011). Details about the test are given as
231 supplementary information (Appendice A.1-Figure S 1)
232

233 2.3.17 Oxygen Transmission rate - OTR

234 OTR given in cm³/m²/day (ASTMF1927-07) was determined with an 8001 Oxygen Permeation
235 Analyzer (Systech Illinois, USA) equipped with a coulometric oxygen sensor. Films were placed
236 in between adhesive aluminum foils, with an open area of 2.54 cm².
237

238 **3. RESULTS AND DISCUSSION**

239 **3.1 NFC, BW and emulsion Characterization**

240 Figure S 2 (a) and (b) present the SEM and AFM images of the dried NFC suspension
241 after being diluted to 0.01%. 50 nanofilaments were measured to calculate the diameter

distribution of the as-received NFC suspension. Measurements showed a D_{50} of 23 nm and D_{90} of 75 nm. The ^{13}C NMR spectra showed in Figure S 3 illustrates the chemical shifts of BW and Table S 1 gives the identification and the area under the peaks of the signals. Signals A, B and C are related to carbonyl functions presented in monoesters, diesters and free acids. Signal D is from carbon linked to hydroxyl groups also from free acids, hydroxy esters and in less-extended alcohols. Signals at E region are due to chemical shifts from carbon adjacent to esters functions. Signals F, G and I are related to methylene groups and are responsible for the major intensities of the spectra as it is estimated that beeswax is composed mainly by C_{40} –C_{50} components. Signals H and J are related to methyl groups from hydroxy mono and polyesters and hydrocarbons, respectively (Basson & Reynhardt, 1988; Hossain, Ketata, Mann, & Islam, 2009; Kameda, 2004; Tulloch, 1980).

Figure S 4(a) shows a photograph of the emulsion after the preparation process and 4(b) shows the drop diameter distribution of each emulsion composition measured by DLS analyzer and the table in 4(c) shows the mean ζ potential. The average diameter of beeswax drops in the emulsion ranged from 100 to 400 nm with a mean value of 200 nm, regardless of the amount of beeswax. The stability of the emulsions increased as the content of beeswax was enhanced, as verified by the increasing of ζ potential from -30 mV to -46 mV.

3.2 NFC/BW Composite Films Characterization

3.2.1 Morphology

Figure 1(a) shows photographs of pristine NFC and NFC/BW composite films. The films are homogeneous, smooth and free of wrinkles on the edges. The transparency of the films is slightly enhanced as the BW content is increased, as shown by the values of the light transmission on minimum (violet - 380 nm) and maximum (red - 750 nm) wavelengths at the bottom of the image. The full UV-VIS spectra are presented in the supplementary information (Figure S 5). The polarized light microscopy images on Figure 1(b) show a homogeneous composition for the pristine film, suggesting an internal structure compacted and free of defects (voids). Composite films on the other hand, display a rougher structure, with the appearance of cavities and small black dots on the images, which could be attributed to interfiber spaces, indicating less compaction. Also, there is an increasing area of brown clusters of BW distributed over the images.

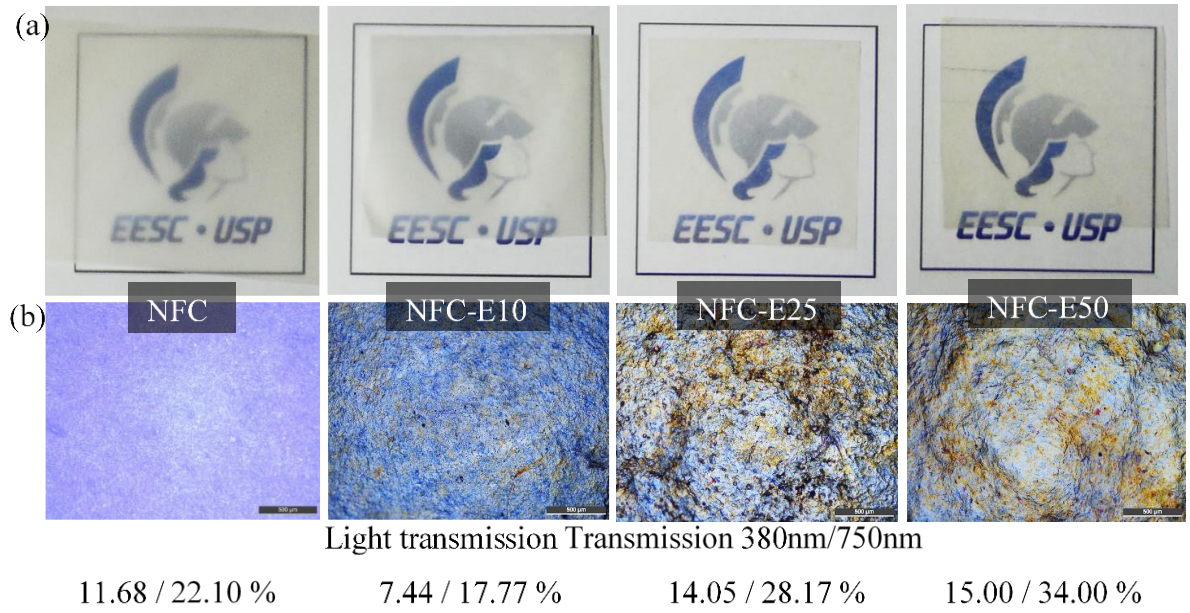

Figure 1. (a) Photographs and (b) cross-polarized microscopy images of NFC and NFC/BW composites with the percentage of light transmission a380nm/ 750 nm.

AFM data is given in Table S 2. The maximum height and roughness of NFC-E25 and NFC-E50 are lower than NFC and NFC-E10. By increasing the BW content, a layer of wax was formed on the surface, reducing the roughness, as already observed in other studies(KESTER & FENNEMA, 1989). A smooth surface is a desired feature not only for packaging films, but also for printed circuits, that require roughness in the range of 30-50 nm (Willberg-Keyriläinen, Vartiainen, Pelto, & Ropponen, 2017)

Figure S 6 gives the SEM images of cryogenic fracture section of the films. One can observe that NFC film maintained a compacted structure through the thickness, with little space between the nanofibers. The composite films present a lamellar structure, with less compaction between the filaments than that observed for the NFC film. As BW content increased, a thin lamellar section becomes more evident, with NFC-E25 and NFC-E50 presenting also some fiber pull-out as fracture mechanisms, indicating loosening of H-bond interaction among the nanofibers, due to the presence of BW. The more porous structures of NFC-E25 and NFC-E50 confirmed the observed features in the optical microscopy images (Figure 1.). The homogenous section, with no BW agglomeration, evidences that the emulsions remained stable until complete drying.

3.2.2 Spectroscopy

Figure 2 shows the FT-IR spectra of the obtained films and of pure BW. BW is composed in its majority by long aliphatic mono and polyesters, hydrocarbons and free acids, which are identified by signals related to ester at 1735 cm^{-1} (C=O stretching vibrations), asymmetric and symmetric stretching of $–CH_2$ groups at 2917 cm^{-1} and 2850 cm^{-1} and asymmetric and symmetric stretching of hydrocarbons at 1473 cm^{-1} and 1464 cm^{-1}. These vibrations are easily identified in the composite films but are not present on the spectrum of the NFC film.

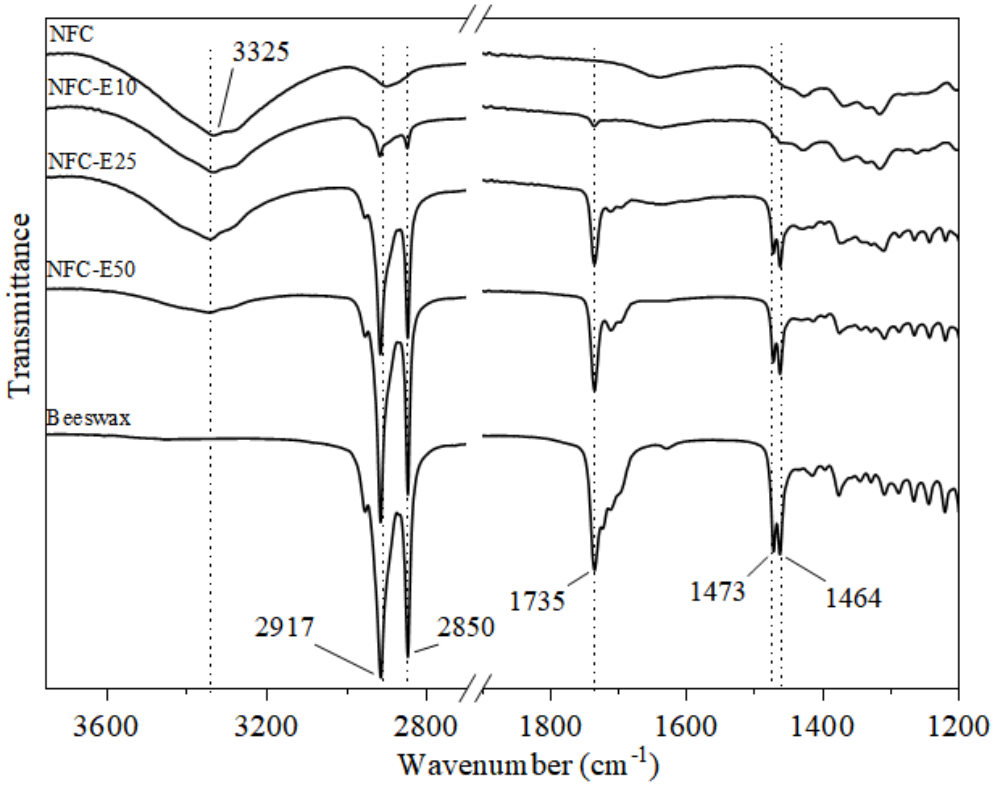

Figure 2. FT-IR spectra of NFC, BW and NFC/BW composite films.

3.2.3 Physical and Mechanical Properties

Table 2 gives the thickness, grammage, density and porosity of the films. Thickness is progressively increasing as the beeswax fraction increases, whereas the grammage is maintained in the same range, with the average values of beeswax/NFC composites slightly higher. A noticeable decrease in the density of the films is observed with the addition of beeswax, with a reduction of almost 40 % for NFC-E50 in relation to NFC film. Thicker and low density films

resulted in a porosity of almost 50 % for the composites, a value substantially above that of the NFC film, in accordance with the observed on SEM images.

Table 2. Physical parameters of NFC and NFC/BW composite films.

	Thickness (μm)	Grammage (g/m^2)	Density (g/cm^3)	Porosity (%)
NFC	46 ± 2	50 ± 10	1.11 ± 0.07	23 ± 4
NFC - E10	69 ± 8	71 ± 10	1.0 ± 0.1	31 ± 8
NFC - E25	74 ± 5	64 ± 13	0.87 ± 0.06	41 ± 4
NFC - E50	104 ± 7	72 ± 14	0.69 ± 0.05	49 ± 4

Table 3 gives the Young's modulus, tensile strength, strain at break and work of fracture obtained from the tensile tests. The loss of compaction resulted in a continuum decay of tensile properties with the addition of beeswax in the composite films, reaching considerable reductions at 50 $\%_{wt.}$ (NFC-E50). The reductions were as high as 50 % on the Young's modulus, 70 % on the tensile strength and 70 % strain at break, impacting up to 90 % of reduction on the work to fracture. The tear index is also given in Table 3 and little difference is observed among the compositions up to 25 $\%_{wt.}$ of beeswax, whereas NFC-E50 exhibits an important reduction of more than 50 % in the tear resistance, in comparison with the other compositions, an indication of loss of out-of-plane resistance. The decrease in mechanical properties is related to the higher level of porosity and also to the fact that the apolar beeswax is attenuating the hydrogen bond density among NFCs, reducing the inter fiber adhesion energy (W. Zhang et al., 2014). Nonetheless, the stiffness and strength presented by NFC-E50 are suited for applications in food packaging, with values comparable to those displayed by the most frequently used packaging polymers (Vimala Bharathi et al., 2020) and well above those of green composite films, such as starch (Sethi et al., 2019a), chitosan (Soni, Hassan, Schilling, & Mahmoud, 2016) and PCL (Gutiérrez et al., 2020).

Table 3. Mechanical properties and Parameters calculated using the data from the wet cup WVTR test of the NFC and NFC/BW composite films.

	Young's Modulus	Tensile Strength	Strain at Break	Work of Fracture	Tear index ($mN*m^2/g$)	*w* (g/h)	WVTR ($g/(m^2*day)$)	WVP (g*μm/

	(GPa)	(MPa)	(%)	(MJ/m³)				(m²*day*kPa)
NFC	6.5 ± 0.7	108 ± 10	10 ± 1	8 ± 1	0.7 ± 0.1	0.0191	152.82	5065
NFC - E10	3.3 ± 0.5	59 ± 5	4.4 ± 0.6	2.4 ± 0.6	0.7 ± 0.1	0.0106	84.81	4216
NFC - E25	4.4 ± 0.3	54 ± 9	3.4 ± 0.6	1.3 ± 0.5	0.9 ± 0.1	0.0076	60.81	3242
NFC - E50	3.1 ± 0.2	36 ± 3	3.0 ± 0.8	0.8 ± 0.2	0.3 ± 0.1	0.0012	9.60	719

3.2.4 Thermal Properties

Figure S 7 shows the mass loss (%) as a function of temperature in the TG tests of the films and beeswax. Beeswax showed its onset of thermal degradation at around 230 °C while NFC begins to significantly loose mass at 260°C. As both components have close thermal events, there is an overlap on the decay of degradation of the NFC/beeswax composites. NFC has two slopes characteristic pattern of cellulose degradation whereas the composite film tracings are more similar to that of beeswax, with only one decay between 300-400 °C. The lower adhesion between the NFC fibers in the composite films did not affect the thermal stability of the films that kept around 300 °C.

Figure 3 presents the heat flow as a function of temperature during the heating and cooling steps given by the DSC analysis of BW and NFC/BW composite films. During the melting, BW present two characteristic elbows at 49 °C and at 54 °C and on the cooling, the crystallization peaks are pronounced at 68 °C and 54 °C. With the addition of NFC, one can observe that the shape of the melting and crystallization peaks change from large to steep single peaks, an indication of transcrystallization, in which the NFC network acted as nucleating agents for interfacial crystallization. Moreover, in the cooling step it is observed that the crystallization is delayed until 22 °C for the composites, implying that NFC network confined the BW particles, hindering diffusion, and consequently inducing the formation and compaction of wax crystals.

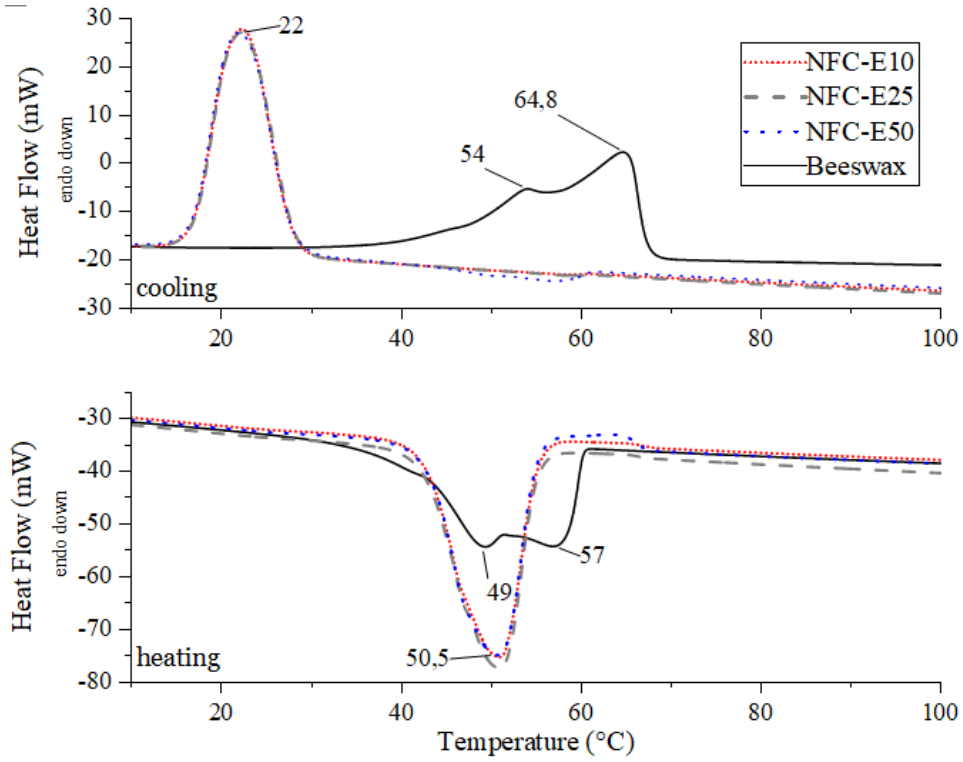

Figure 3. Heating and cooling thermograms of BW and NFC/BW composites.

3.2.5 Water Repellency

Figure 4 gives the water contact angle (WCA) for NFC and NFC/BW films. NFC-E25 and NFC-E50 composites show improved hydrophobicity with WCA of 77 and 97 °, respectively, i.e. values of 25 and 45 ° above that of NFC film. On the other hand, NFC-E10 had a reduction on its WCA in 10 °, i.e, an enhanced hydrophilicity.

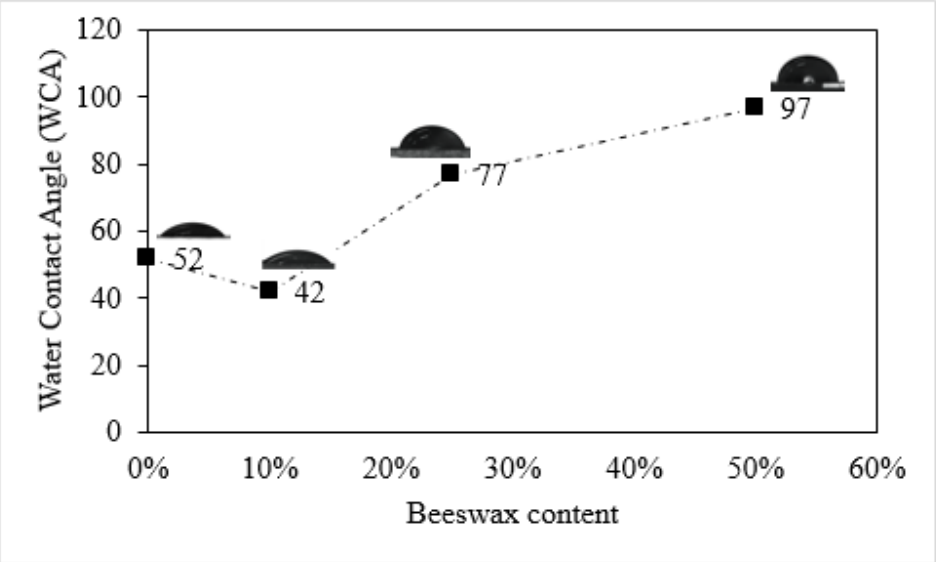

Figure 4. Water contact angle (WCA) for NFC and NFC/BW composite films.

Through the water uptake plot (Figure S 8) it was possible to measure the water absorption saturation point, given in Figure 5.a. The water uptake is constantly reduced as a function of beeswax, reaching a decrease 75 % in absorption of NFC-E50 in comparison with NFC film. NFC-E10 followed the same behavior as measured for WCA, with its more hydrophilic structure absorbing almost twice its weight and taking 300 h to complete saturation. Figure 5.a) also presents the Fickian diffusion coefficient *(D*), calculated from water absorption data. Composite films displayed enhanced diffusivity by almost 10 times, increasing as the BW content increased, in a linear correlation with the porosity of the films.

The "wet/dry" ratio of tensile properties obtained through the semi-wet tensile test (section 2.4.13), is given in Figure S 9. Young's modulus of pristine NFC film is deeply affected by water plasticization, with a ratio near 0.1, i.e. a reduction of 90 %. NFC-E25 and NFC-E50 exhibited an average wet/dry ratio of around 0.4, with more stability of the stiffness in the wet state. Interestingly, despite presenting a lower WCA and a higher water uptake absorption, NFC-E10 gave a wet/dry ratio for Young's modulus of almost 0.8. Tensile strength and strain at break remain within the same range for all compositions.

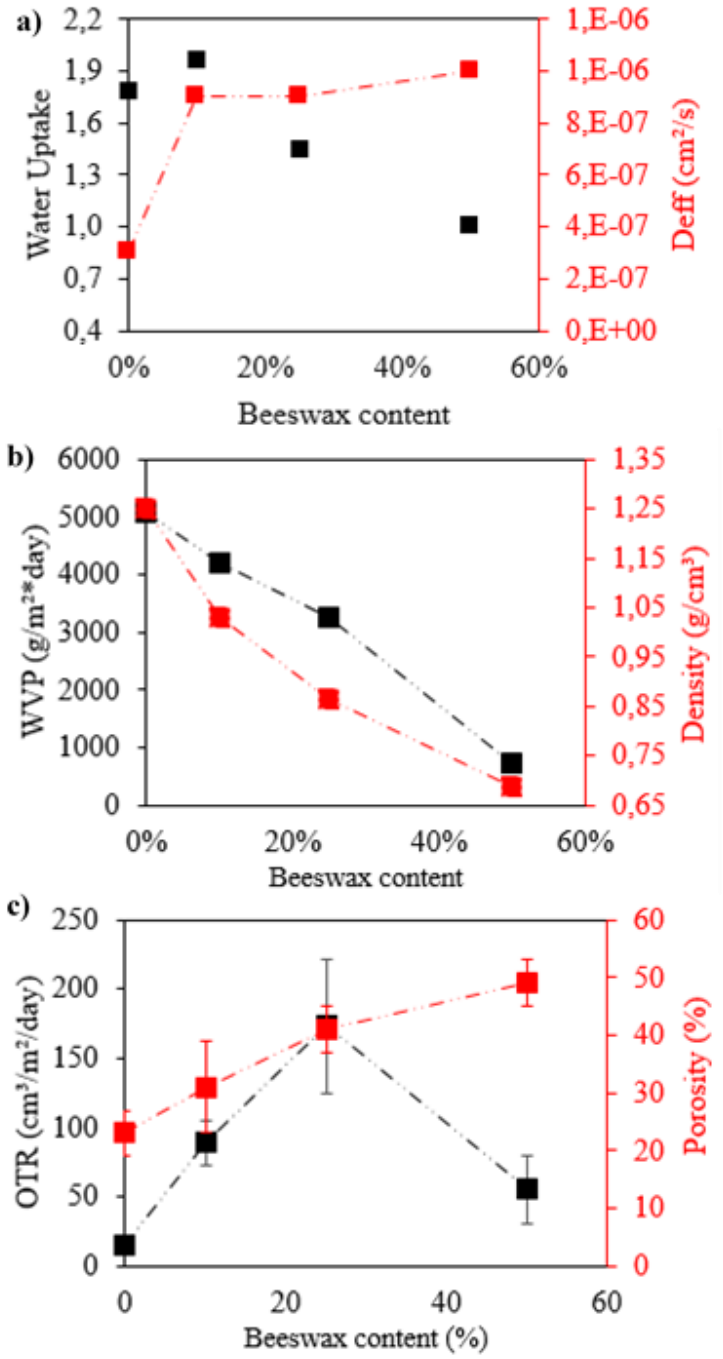

382

383 Figure 5. a) Water uptake and Fickian Diffusion coefficient as a function of BW content. b) Water Vapor Permeability (WVP)
384 and density as a function of BW content c) OTR and porosity of NFC and NFC/BW films as a function of the BW content.
385

3.2.6 Barrier to water vapor and oxygen properties

With the plot of mass increasing as a function of time (Figure S 10), nine data points were collected over almost 1300 h of Water Vapor Transmission Rate (WVTR) tests. The plot shows that transport of water vapor through the thickness is considerably reduced as BW content in composites film increases, given the presence of a thin hydrophobic layer responsible for avoiding adsorption and hindering the interfiber and interpore diffusion. Table 3 shows that WVTR decreased from 152.82 $g.m^{-2}day^{-1}$ for pristine NFC film to only 9.60 $g.m^{-2}day^{-1}$ for NFC-E50, namely a reduction of 93.7 %. Figure 5 b) presents the WVP and the density as a function of BW for the obtained films. According to the rank proposed by Wang et al, 2018 (Wang et al., 2018), NFC film is categorized as a poor barrier, whereas NFC-E50, that exhibits a WVP 85.8% lower, is categorized as a medium barrier film, the same rank as PS, PHA and PLA (Wang et al., 2018). Remarkably, NFC-E50 had 50 % of porosity and yet was still exhibiting an outstanding improvement on the water vapor barrier due to its compact, smooth and hydrophobic surface.

Figure 6a) gives the plot of the last ten years data of WVTR of biobased films designed for packaging applications from literature with the composition summarized in Figure 6b). It is observed that, despite the very low WVTR values obtained in recent work, there is not a trend of significant improvement on water barrier for biobased films in the last 10 years. We believe that this target should be pursued by the community in order to enable biobased films reaching the market with significant competitiveness against petroleum based packaging polymeric materials. The value obtained here for NFC-E50 is the lowest measured for biobased composites, even below the value presented by LDPE.

Erro! Fonte de referência não encontrada. gives the flux, the diffusion coefficient (D) and the interpore diffusion coefficient (Da) calculated with WVTR data using the set of equations described elsewhere (de Souza, Belgacem, Gandini, & Carvalho, 2021). Unlike the water absorption coefficient (*Deff* - calculated in section 3.3.2), which was higher for the composites than for the NFC film, the water vapor diffusion coefficient is progressively reduced as the BW fraction increases in the films. NFC-E50 exhibits D and Da values almost ten times lower than that of the NFC film. This performance is ascribed to the presence of the hydrophobic wax covering the surface and homogeneously dispersed within the structure, which was responsible for hampering the adsorption of the water molecules. The results suggest that in the case of water

absorption, since there is direct contact between liquid water and the films, the adsorption was less important because water was permeating by capillarity. In that case, the porosity was more critical in determining the diffusivity.

a)

b)

Year	Film characteristic and composition	WVTR (g/m²*day)	Ref.
2010	poly vinyl butyral (PVB) +Zein/BW	24	(Han et al., 2010)
2013	Coating of BW onto copy paper	236.4	(D. Zhang & Xiao, 2013)
2014	Coating of BW + chitosan onto paper	350	(W. Zhang et al., 2014)
2014	Coating of BW+ latex onto soybean epoxidized treated NFC film	188	(Lu, Xiao, Zhang, & Gong, 2014b)
2015	BW emulsified latex	460	(Pan et al., 2015)
2016	Coating of BW+ silver particles onto paper	53.1	(Liu et al., 2016)
2017	Coating of cellulose esters onto NFC films	350	(Willberg-Keyriläinen et al., 2017)
2019	Coating of BW onto NFC films	40	(Sethi et al., 2019a)
2021	Composites of NFC/Beeswax	9.6	This work

Figure 6. a) plot and b) list of Water Vapor Transmission Rate (WVRT) of biobased films as a function of the year of publication.

Table S 3gives the flux, the diffusion coefficient (D) and the interpore diffusion coefficient (Da) calculated with WVTR data using the set of equations described elsewhere (de Souza et al., 2021). Unlike the water absorption coefficient (*Deff* - calculated in section 3.3.2), the water vapor diffusion coefficient is progressively reduced as the BW fraction increases in the films. NFC-E50 exhibits D and Da values almost ten times lower than that of the NFC film. Table S 4

gives the tortuosity, the path length and the mean pore radius calculated with the WVTR data using the set of equations described elsewhere (de Souza et al., 2021). It is observed that tortuosity is decreasing as the BW load increases but, since composite films are thicker, the path length increases substantially, also contributing to the lower values of D and Da exhibited by the composites. Furthermore, the mean pore radius (Rf) was calculated based on flux (J) along with the Knudsen pore radii using D values. Porosity radii is one order of magnitude higher than the need for our system to display Knudsen as the main diffusion mechanism, thus indicating that the diffusion is predominantly Fickian.

The plot in Figure 5 c) shows the OTR and the porosity as a function of BW load. One can observe that up to 25 % of BW (NFC-E25) the OTR increases linearly with the porosity level, as the more opened structure of the composites offers less resistance to the passage of the gas, hence reducing its barrier to O_2. Nonetheless at the load of 50 % of beeswax (NFC-E50) the behavior changes. NFC-E50 displays the highest porosity percentage and yet its OTR is the second lowest, which can be attributed to the presence of a beeswax layer uniformly covering the surface, hindering the oxygen diffusion.

4. CONCLUSION

NFC/beeswax composite films with 10, 25 and 50 % in weight of beeswax were obtained by casting of emulsions. Composite films were in general almost 40 % less dense, slightly more transparent and with reduced roughness, as confirmed through a series of morphological analyses. NFC-E25 and NFC-E50 presented a layer of beeswax homogeneously covering its surface, leading to excellent water repellent properties. Contact angle with water was increased from 52° to 97°, water absorption was reduced by half and water vapor transmission was reduced from 153 to 9.6 $g/m^{-2}day^{-1}$ (almost 95 %), i.e. in the same range as synthetic polymeric films like LDPE and BOPP. NFC/beeswax composites still exhibited good mechanical properties, with Young's modulus of 3 GPa and tensile strength of 36 MPa in the worst case (NFC-E50). The hydrophobicity, barrier properties towards H_2O vapor and reduction on mechanical properties were expected from the hypotheses of the research. However, films with high porosity and even more, the porosity not affecting negatively on the barrier properties, mainly because of the presence of a beeswax layer on the surface, were unexpected good results.

Green alternatives with competitive properties are being sought in order to reduce the dependency of petroleum based polymers in packaging applications. Here, we propose a high performance renewable and biodegradable option based on NFC and beeswax with competitive barrier and mechanical properties which enhance its suitability towards the replacement of fossil-based polymers.

AUTHOR INFORMATION

Corresponding author

Antonio José Felix Carvalho- Department of Materials Engineering, Sao Carlos School of Engineering (EESC), University of São Paulo (USP), São Paulo, SP, Brazil.

https://orcid.org/0000-0001-8403-1135 E-mail: (toni@sc.usp.br)

Authors

Gustavo de Souza- Department of Materials Engineering, Sao Carlos School of Engineering (EESC), University of São Paulo (USP), São Paulo, SP; Univ. Grenoble Alpes, CNRS, Grenoble INP, LGP2, F-38000, Grenoble, France. https://orcid.org/0000-0002-9056-8550

Ricardo Klaus Kramer- Department of Materials Engineering, Sao Carlos School of Engineering (EESC), University of São Paulo (USP), São Paulo, SP; Univ. Grenoble Alpes, CNRS, Grenoble INP, LGP2, F-38000, Grenoble, France https://orcid.org/0000-0001-7860-6895

Mohamed Naceur Belgacem- Univ. Grenoble Alpes, CNRS, Grenoble INP, LGP2, F-38000, Grenoble, France https://orcid.org/0000-0002-3317-7369

Alessandro Gandini- Univ. Grenoble Alpes, CNRS, Grenoble INP, LGP2, F-38000, Grenoble, France

AUTHOR CONTRIBUTIONS

The manuscript was written through contributions of all authors. All authors have given approval to the final version of the manuscript.

ACKNOWLEDGEMENTS

This study was financed in part by the Coordenação de Aperfeiçoamento de Pessoal de Nível Superior - Brazil (CAPES) - Finance Code 001. Also, authors acknowledge CNPq for the doctoral fellowship granted to G.S (CNPq proc. 140249/2017-6). AJFC acknowledge CNPq for research funding project # 03847/2019-0. We also thank to Suzano S/A, Brazil which kindly sypplied the NFC from eucalyptus wood pulp.

NOTES

The authors declare no competing financial interest.

5. REFERENCES

Basson, I., & Reynhardt, E. C. (1988). An investigation of the structures and molecular dynamics of natural waxes. I. Beeswax. *Journal of Physics D: Applied Physics*, *21*(9), 1421–1428. https://doi.org/10.1088/0022-3727/21/9/016

Baswal, A. K., Dhaliwal, H. S., Singh, Z., Mahajan, B. V. C., Kalia, A., & S Gill, K. (2020). Influence of carboxy methylcellulose, chitosan and beeswax coatings on cold storage life and quality of Kinnow mandarin fruit. *Scientia Horticulturae*, *260*(July 2019), 108887. https://doi.org/10.1016/j.scienta.2019.108887

Bedane, A. H., Eić, M., Farmahini-Farahani, M., & Xiao, H. (2015). Water vapor transport properties of regenerated cellulose and nanofibrillated cellulose films. *Journal of Membrane Science*, *493*, 46–57. https://doi.org/10.1016/j.memsci.2015.06.009

Cazón, P., Velazquez, G., Ramírez, J. A., & Vázquez, M. (2017). Polysaccharide-based films and coatings for food packaging: A review. *Food Hydrocolloids*, *68*, 136–148.

https://doi.org/10.1016/j.foodhyd.2016.09.009

Cerempei, A., Guguianu, E., Muresan, E. I., Horhogea, C., Rîmbu, C., & Borhan, O. (2015). Antimicrobial controlled release systems for the knitted cotton fabrics based on natural substances. *Fibers and Polymers*, *16*(8), 1688–1695. https://doi.org/10.1007/s12221-015-4551-3

Chitprasert, P., & Sutaphanit, P. (2014). Holy basil (ocimum sanctum linn.) Essential oil delivery to swine gastrointestinal tract using gelatin microcapsules coated with aluminum carboxymethyl cellulose and beeswax. *Journal of Agricultural and Food Chemistry*, *62*(52), 12641–12648. https://doi.org/10.1021/jf5019438

Choi, K. H., Kang, Y. S., & Cho, B. U. (2016). Comparison of aging characteristics of the duplicated beeswax-treated and non-treated paper books during artificial thermal aging. *Journal of Industrial and Engineering Chemistry*, *41*, 68–74. https://doi.org/10.1016/j.jiec.2016.07.009

de Souza, G., Belgacem, M. N., Gandini, A., & Carvalho, A. J. F. (2021). Low permeable hydrophobic nanofibrilated cellulose films modified by dipping and heating processing technique. *Cellulose*, *3*. https://doi.org/10.1007/s10570-020-03619-3

Donhowe, G., & Fennema, O. (1993). Water vapor and oxygen permeability of wax films. *Journal of the American Oil Chemists' Society*, *70*(9), 867–873. https://doi.org/10.1007/BF02545345

Dufresne, A., Dupeyre, D., & Vignon, M. R. (2000). Cellulose microfibrils from potato tuber cells: Processing and characterization of starch-cellulose microfibril composites. *Journal of Applied Polymer Science*, *76*(14), 2080–2092. https://doi.org/10.1002/(SICI)1097-4628(20000628)76:14<2080::AID-APP12>3.0.CO;2-U

Eshetu, A., Ibrahim, A. M., Forsido, S. F., & Kuyu, C. G. (2019). Effect of beeswax and chitosan treatments on quality and shelf life of selected mango (Mangifera indica L.) cultivars. *Heliyon*, *5*(1), e01116. https://doi.org/10.1016/j.heliyon.2018.e01116

Fennema, O., Donhowe, I. G., & Kester, J. J. (1994). Lipid type and location of the relative humidity gradient influence on the barrier properties of lipids to water vapor. *Journal of Food Engineering*, *22*(1–4), 225–239. https://doi.org/10.1016/0260-8774(94)90032-9

Forsman, N., Lozhechnikova, A., Khakalo, A., Johansson, L. S., Vartiainen, J., & Österberg, M. (2017). Layer-by-layer assembled hydrophobic coatings for cellulose nanofibril films and

textiles, made of polylysine and natural wax particles. *Carbohydrate Polymers*, *173*, 392–402. https://doi.org/10.1016/j.carbpol.2017.06.007

Geueke, B., Groh, K., & Muncke, J. (2018). Food packaging in the circular economy: Overview of chemical safety aspects for commonly used materials. *Journal of Cleaner Production*, *193*, 491–505. https://doi.org/10.1016/j.jclepro.2018.05.005

Gómez-Estaca, J., Pintado, T., Jiménez-Colmenero, F., & Cofrades, S. (2019). Assessment of a healthy oil combination structured in ethyl cellulose and beeswax oleogels as animal fat replacers in low-fat, PUFA-enriched pork burgers. *Food and Bioprocess Technology*, *12*(6), 1068–1081. https://doi.org/10.1007/s11947-019-02281-3

GONTARD, N., DUCHEZ, C., CUQ, J. -L, & GUILBERT, S. (1994). Edible composite films of wheat gluten and lipids: water vapour permeability and other physical properties. *International Journal of Food Science & Technology*, *29*(1), 39–50. https://doi.org/10.1111/j.1365-2621.1994.tb02045.x

Gutiérrez, T. J., Mendieta, J. R., & Ortega-Toro, R. (2020). In-depth study from gluten/PCL-based food packaging films obtained under reactive extrusion conditions using chrome octanoate as a potential food grade catalyst. *Food Hydrocolloids*, *111*(August 2020), 106255. https://doi.org/10.1016/j.foodhyd.2020.106255

Han, J., Salmieri, S., Le Tien, C., & Lacroix, M. (2010). Improvement of water barrier property of paperboard by coating application with biodegradable polymers. *Journal of Agricultural and Food Chemistry*, *58*(5), 3125–3131. https://doi.org/10.1021/jf904443n

Hervy, M., Santmarti, A., Lahtinen, P., Tammelin, T., & Lee, K. Y. (2017). Sample geometry dependency on the measured tensile properties of cellulose nanopapers. *Materials and Design*, *121*, 421–429. https://doi.org/10.1016/j.matdes.2017.02.081

Hossain, M. E., Ketata, C., Mann, H., & Islam, M. R. (2009). a Nalysis of P Araffin W Ax and B Eeswax for P Etroleum a Pplications, *1*(1), 21–38.

Hu, Y., Acharya, S., & Abidi, N. (2019). Cellulose porosity improves its dissolution by facilitating solvent diffusion. *International Journal of Biological Macromolecules*, *123*, 1289–1296. https://doi.org/10.1016/j.ijbiomac.2018.10.062

Indriyati, & Indrarti, L. (2018). Preparation and characterization of bacterial cellulose-beeswax films. *IOP Conference Series: Earth and Environmental Science*, *160*(1). https://doi.org/10.1088/1755-1315/160/1/012010

Jeong, M. J., Bogolitsyna, A., Jo, B. M., Kang, K. Y., Rosenau, T., & Potthast, A. (2014). Deterioration of ancient Korean paper (Hanji), treated with beeswax: A mechanistic study. *Carbohydrate Polymers*, *101*(1), 1249–1254. https://doi.org/10.1016/j.carbpol.2013.10.033

Kameda, T. (2004). Molecular structure of crude beeswax studied by solid-state 13C NMR. *Journal of Insect Science*, *4*(1). https://doi.org/10.1093/jis/4.1.29

KESTER, J. J., & FENNEMA, O. (1989). An Edible Film of Lipids and Cellulose Ethers: Barrier Properties to Moisture Vapor Transmission and Structural Evaluation. *Journal of Food Science*, *54*(6), 1383–1389. https://doi.org/10.1111/j.1365-2621.1989.tb05118.x

Klemm, D., Cranston, E. D., Fischer, D., Gama, M., Kedzior, S. A., Kralisch, D., … Rauchfuß, F. (2018). Nanocellulose as a natural source for groundbreaking applications in materials science: Today's state. *Materials Today*, *21*(7), 720–748. https://doi.org/10.1016/j.mattod.2018.02.001

Lavoine, N., Desloges, I., Dufresne, A., & Bras, J. (2012). Microfibrillated cellulose – Its barrier properties and applications in cellulosic materials: A review. *Carbohydrate Polymers*, *90*(2), 735–764. https://doi.org/10.1016/j.carbpol.2012.05.026

Lindström, T., & Aulin, C. (2014). Market and technical challenges and opportunities in the area of innovative new materials and composites based on nanocellulosics. *Scandinavian Journal of Forest Research*, *29*(4), 345–351. https://doi.org/10.1080/02827581.2014.928365

Lu, P., Xiao, H., Zhang, W., & Gong, G. (2014). Reactive coating of soybean oil-based polymer on nanofibrillated cellulose film for water vapor barrier packaging. *Carbohydrate Polymers*, *111*, 524–529. https://doi.org/10.1016/j.carbpol.2014.04.071

Morrissette, J. M., Carroll, P. J., Bayer, I. S., Qin, J., Waldroup, D., & Megaridis, C. M. (2018). A methodology to produce eco-friendly superhydrophobic coatings produced from all-water-processed plant-based filler materials. *Green Chemistry*, *20*(22), 5169–5178. https://doi.org/10.1039/c8gc02439a

Näyhä, A. (2019). Transition in the Finnish forest-based sector: Company perspectives on the bioeconomy, circular economy and sustainability. *Journal of Cleaner Production*, *209*, 1294–1306. https://doi.org/10.1016/j.jclepro.2018.10.260

Ngamekaue, N., & Chitprasert, P. (2019). Effects of beeswax-carboxymethyl cellulose composite coating on shelf-life stability and intestinal delivery of holy basil essential oil-

loaded gelatin microcapsules. *International Journal of Biological Macromolecules*, *135*, 1088–1097. https://doi.org/10.1016/j.ijbiomac.2019.06.002

O'Connor, L. J., Favreau-Farhadi, N., & Barrett, A. H. (2018). Use of edible barriers in intermediate moisture food systems to inhibit moisture migration. *Journal of Food Processing and Preservation*, *42*(2), 1–6. https://doi.org/10.1111/jfpp.13512

Pan, Y., Xiao, H., Li, K., & Xu, J. (2015). Cationic Starch Emulsified Beeswax for Enhancing Moisture Barrier of Paper as Packaging Materials (pp. 1126–1129).

Pätäri, S., Tuppura, A., Toppinen, A., & Korhonen, J. (2016). Global sustainability megaforces in shaping the future of the European pulp and paper industry towards a bioeconomy. *Forest Policy and Economics*, *66*, 38–46. https://doi.org/10.1016/j.forpol.2015.10.009

Patrício Silva, A. L., Prata, J. C., Walker, T. R., Duarte, A. C., Ouyang, W., Barcelò, D., & Rocha-Santos, T. (2021). Increased plastic pollution due to COVID-19 pandemic: Challenges and recommendations. *Chemical Engineering Journal*, *405*(August 2020), 126683. https://doi.org/10.1016/j.cej.2020.126683

Payne, J., McKeown, P., & Jones, M. D. (2019). A circular economy approach to plastic waste. *Polymer Degradation and Stability*, *165*, 170–181. https://doi.org/10.1016/j.polymdegradstab.2019.05.014

Sethi, J., Visanko, M., Österberg, M., & Sirviö, J. A. (2019a). A fast method to prepare mechanically strong and water resistant lignocellulosic nanopapers. *Carbohydrate Polymers*, *203*(August 2018), 148–156. https://doi.org/10.1016/j.carbpol.2018.09.037

Sethi, J., Visanko, M., Österberg, M., & Sirviö, J. A. (2019b). A fast method to prepare mechanically strong and water resistant lignocellulosic nanopapers. *Carbohydrate Polymers*, *203*(September 2018), 148–156. https://doi.org/10.1016/j.carbpol.2018.09.037

Soni, B., Hassan, E. B., Schilling, M. W., & Mahmoud, B. (2016). Transparent bionanocomposite films based on chitosan and TEMPO-oxidized cellulose nanofibers with enhanced mechanical and barrier properties. *Carbohydrate Polymers*, *151*, 779–789. https://doi.org/10.1016/j.carbpol.2016.06.022

Spence, K. L., Venditti, R. A., Rojas, O. J., Pawlak, J. J., & Hubbe, M. A. (2011). Water vapor barrier properties of coated and filled microfibrillated cellulose composite films. *BioResources*, *6*(4), 4370–4388.

Tedeschi, G., Benitez, J. J., Ceseracciu, L., Dastmalchi, K., Itin, B., Stark, R. E., … Heredia-

Guerrero, J. A. (2018). Sustainable Fabrication of Plant Cuticle-Like Packaging Films from Tomato Pomace Agro-Waste, Beeswax, and Alginate. *ACS Sustainable Chemistry and Engineering*, *6*(11), 14955–14966. https://doi.org/10.1021/acssuschemeng.8b03450

Tedeschi, G., Guzman-Puyol, S., Paul, U. C., Barthel, M. J., Goldoni, L., Caputo, G., … Heredia-Guerrero, J. A. (2018). Thermoplastic cellulose acetate oleate films with high barrier properties and ductile behaviour. *Chemical Engineering Journal*, *348*(January), 840–849. https://doi.org/10.1016/j.cej.2018.05.031

Toğrul, H., & Arslan, N. (2004). Carboxymethyl cellulose from sugar beet pulp cellulose as a hydrophilic polymer in coating of mandarin. *Journal of Food Engineering*, *62*(3), 271–279. https://doi.org/10.1016/S0260-8774(03)00240-1

Tulloch, A. P. (1980). Beeswax—Composition and Analysis. *Bee World*, *61*(2), 47–62. https://doi.org/10.1080/0005772X.1980.11097776

Vartiainen, J., & Malm, T. (2016). Surface hydrophobization of CNF films by roll-to-roll HMDSO plasma deposition. *Journal of Coatings Technology and Research*, *13*(6), 1145–1149. https://doi.org/10.1007/s11998-016-9833-1

Vimala Bharathi, S. K., Murugesan, P., Moses, J. A., & Anandharamakrishnan, C. (2020). *Recent Trends in Nanocomposite Packaging Materials*. *Reference Module in Food Science* (Vol. 3). Elsevier. https://doi.org/10.1016/b978-0-08-100596-5.23027-8

Wagner, S., & Schlummer, M. (2020). Legacy additives in a circular economy of plastics: Current dilemma, policy analysis, and emerging countermeasures. *Resources, Conservation and Recycling*, *158*(May 2019), 104800. https://doi.org/10.1016/j.resconrec.2020.104800

Wang, J., Gardner, D. J., Stark, N. M., Bousfield, D. W., Tajvidi, M., & Cai, Z. (2018). Moisture and Oxygen Barrier Properties of Cellulose Nanomaterial-Based Films. *ACS Sustainable Chemistry & Engineering*, *6*(1), 49–70. https://doi.org/10.1021/acssuschemeng.7b03523

Wardhono, E. Y., Pinem, M. P., Kustiningsih, I., Agustina, S., Oudet, F., Lefebvre, C., … Guénin, E. (2019). Cellulose nanocrystals to improve stability and functional properties of emulsified film based on chitosan nanoparticles and beeswax. *Nanomaterials*, *9*(12), 1–17. https://doi.org/10.3390/nano9121707

Willberg-Keyriläinen, P., Vartiainen, J., Pelto, J., & Ropponen, J. (2017). Hydrophobization and smoothing of cellulose nanofibril films by cellulose ester coatings. *Carbohydrate Polymers*, *170*, 160–165. https://doi.org/10.1016/j.carbpol.2017.04.082

Yang, L., & Paulson, A. T. (2000). Effects of lipids on mechanical and moisture barrier properties of edible gellan film. *Food Research International*, *33*(7), 571–578. https://doi.org/10.1016/S0963-9969(00)00093-4

Zhang, D., & Xiao, H. (2013). Dual-functional beeswaxes on enhancing antimicrobial activity and water vapor barrier property of paper. *ACS Applied Materials and Interfaces*, *5*(8), 3464–3468. https://doi.org/10.1021/am400585m

Zhang, W., Xiao, H., & Qian, L. (2014). Beeswax-chitosan emulsion coated paper with enhanced water vapor barrier efficiency. *Applied Surface Science*, *300*, 80–85. https://doi.org/10.1016/j.apsusc.2014.02.005

6. APPENDICES

A.1 Water vapor transmission rate test.

The dissecting method the test consists of coupling the film to an open mouth device container with a minimum area of 3000 mm², previously filled with 15 g (6 cm from the bottom) of calcium chloride dissecting salt. The device is then sealed at the edges with a sealing ring, sealed with a hollow lid and placed in a 50 % humidity controlled environment. The moisture gradient is the driving force for the permeation of water vapor from the environment into the container, which diffuses through the film. The standard recommends between 6-10 spaced measurements over the test period to construct the mass change curve as a function of time. From time-varying mass plot with the minimum necessary measurements, the linear trend line is estimated and its angular coefficient is the transmission rate. The Water Vapor Transmission (WVT) can be calculated from equation 1 below, where (G / t) is the calculated angular coefficient in g / h and A is the cup mouth area in m². WVT is frequently reported in the literature in g / m² / day (Lavoine et al., 2012; Spence et al., 2011).Figure S 1 summarizes the method and the testing apparatus.

$$WVT = \left(\frac{G}{t}\right)/A \quad (1)$$

The permeation can then be calculated by the equation 2 where ΔP is the pressure vapor difference in mmHg (1,333 x 10² Pa), S is the vapor pressure saturation at the test temperature, R1 and R2 = relative humidity (%) of the environment, and inside the glass, respectively.

$$Permeação = \frac{WVT}{\Delta P} = \frac{WVT}{S(R1 - R2)} \quad (2)$$

S can be obtained by equation 3, where T is the room temperature in Kelvin. According to ASTME96 permeation is reported in ng·m^{-2}·s^{-1}·Pa^{-1} or in Perms, where 1 Perm = 240 ng·m^{-2}·s^{-1}·Pa$^{-1.}$

$$S = e^{(77{,}3450 + 0{,}0057 * T - \frac{7235}{T})}/T^{8,2} \quad (3)$$

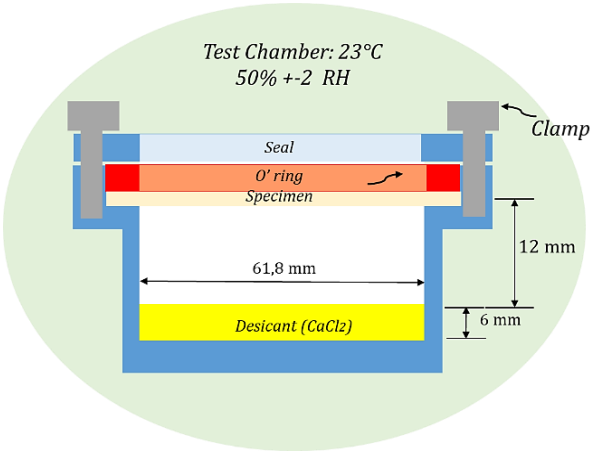

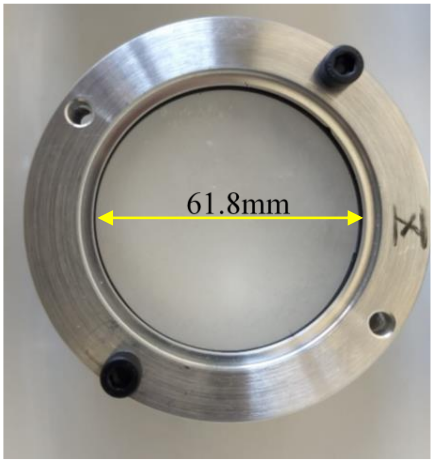

Figure S 1. Dispositive designed for the water vapor transmission rate test.

A.2 SUPPLEMENTARY INFORMATION

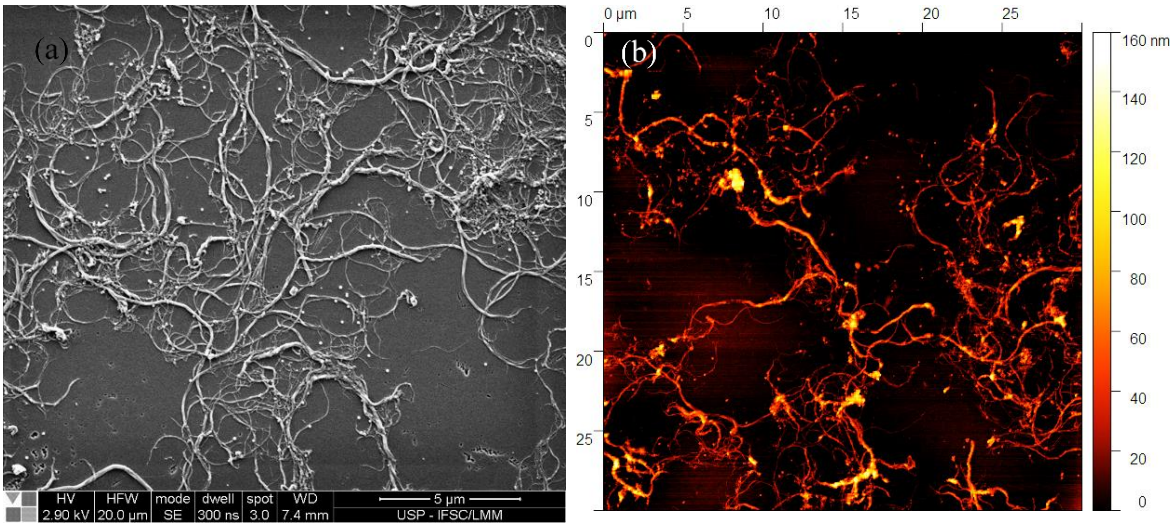

Figure S 2. (a) SEM and (b) AFM images of a homogeneized NFC suspension after drying.

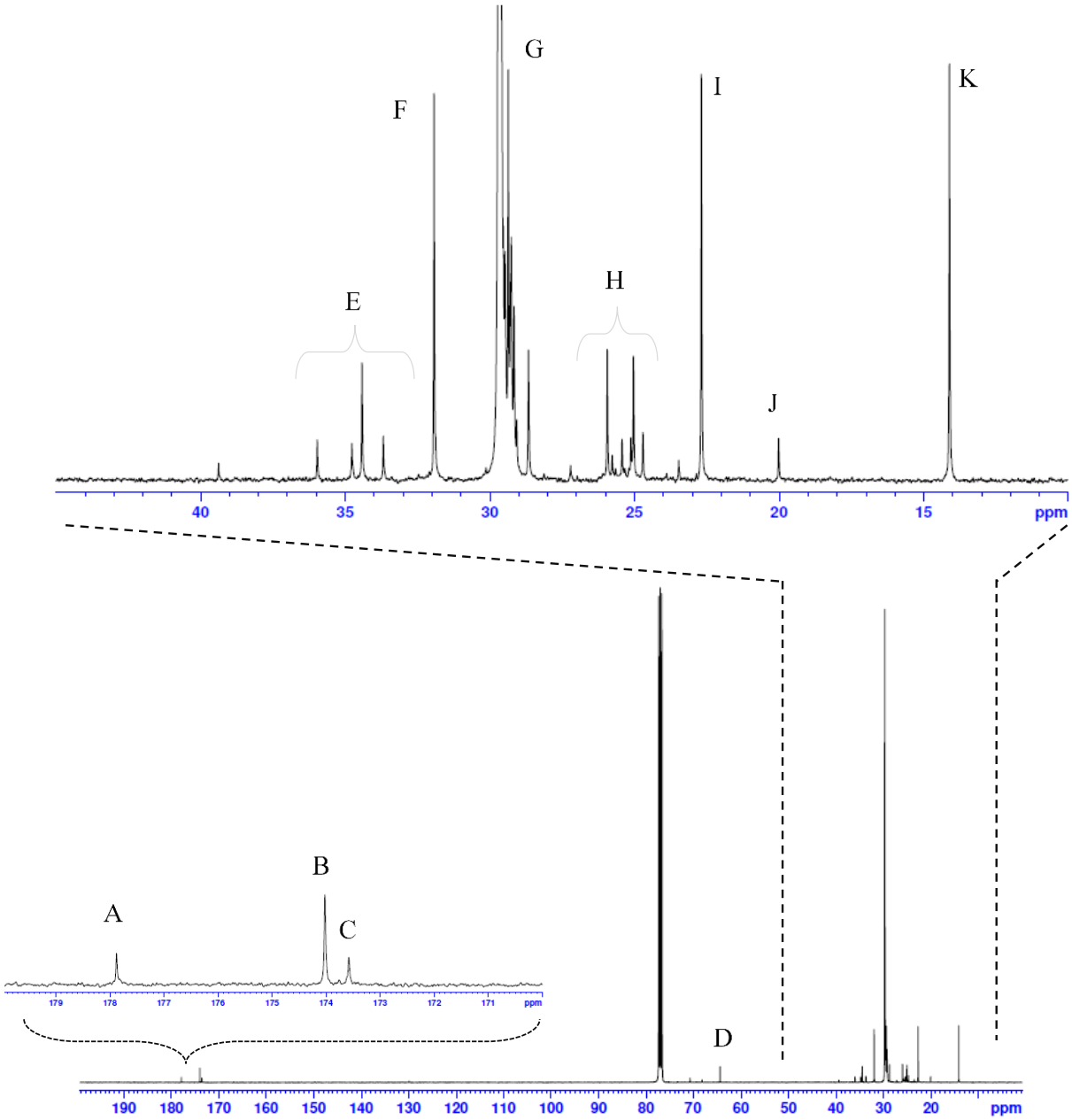

Figure S 3. ^{13}C NMR spectra of beeswax.

Table S 1. Identification of the chemical shifts of the ^{13}C NMR spectra of beeswax.

Peak	ppm	Identification	Area
A	177.88	Free acids -(C=O)-	1
B	174.02	Mono/diesters -(C=O)-	2.8
C	173.58	Mono/diesters -(C=O)-	1
D	70.72	free acids, hydroxy esters, alcohols -(C-OH)-	1.6
E	35.97 -33.69	Carbon adjacent to esters	8.5
F	31.93	(-CH_2)- hydrocarbons	10.8
G	29.7 – 28.66	(-CH_2)-	184.9
H	25.94 – 24.71	(-CH_3) from hydroxy mono and polyesters	14.9
I	22.69	(-αCH_2)-	10.6
J	14.11	(-CH_3) from Hydrocarbons	10.8

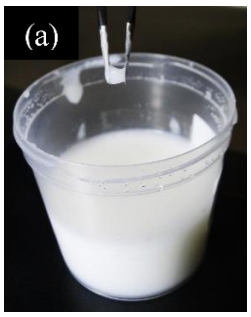

(c)	Potencial ζ (mV)
E10	-30±1
E25	-40±1
E50	-46±1

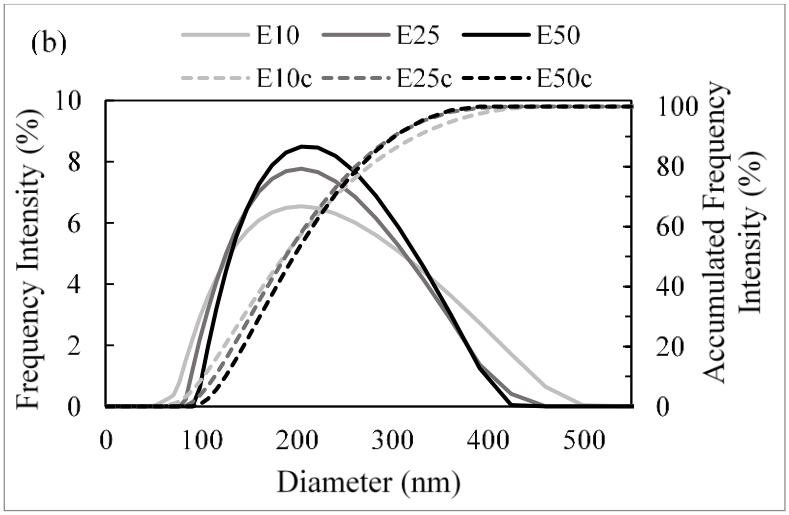

Figure S 4. (a) photo of a NFC/BW emulsion after prepared. (b) diameter distribuition of the BW drops in the emulsion. (c) Zeta potential of each emulsion composition.

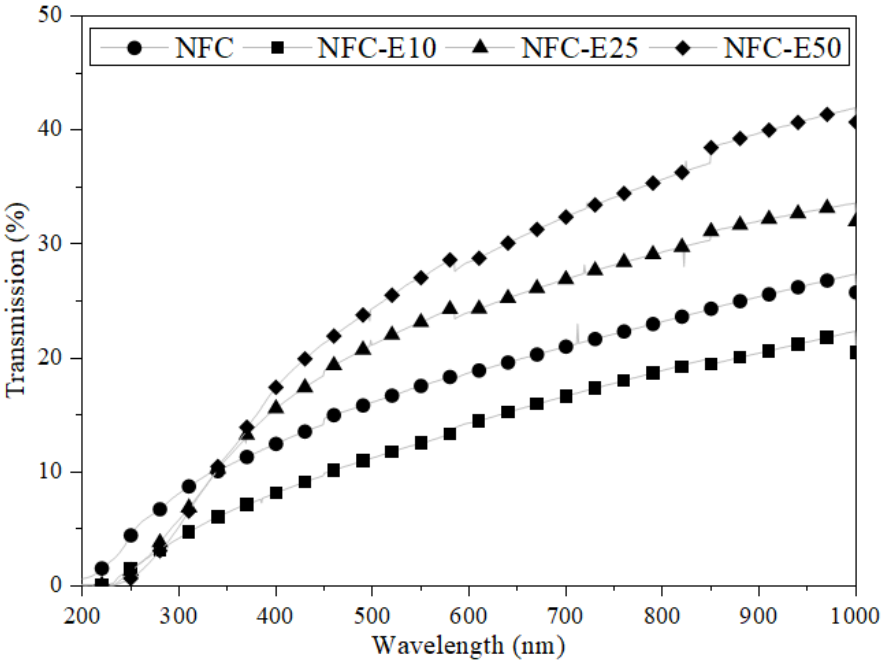

Figure S 5. UV-Vis spectra of the NFC and NFC/BW composite films.

Table S 2. Three parameters of roughness calculated with the AFM data for and NFC/BW composites.

	Ra (nm)	Rq (nm)	Rt(nm)
NFC	20 ± 1	25 ± 1	165 ± 13
NFC - E10	43 ± 2	55 ± 3	373 ± 73
NFC - E25	18 ± 2	25 ± 4	139 ± 11
NFC - E50	16 ± 4	21 ± 5	157 ± 41

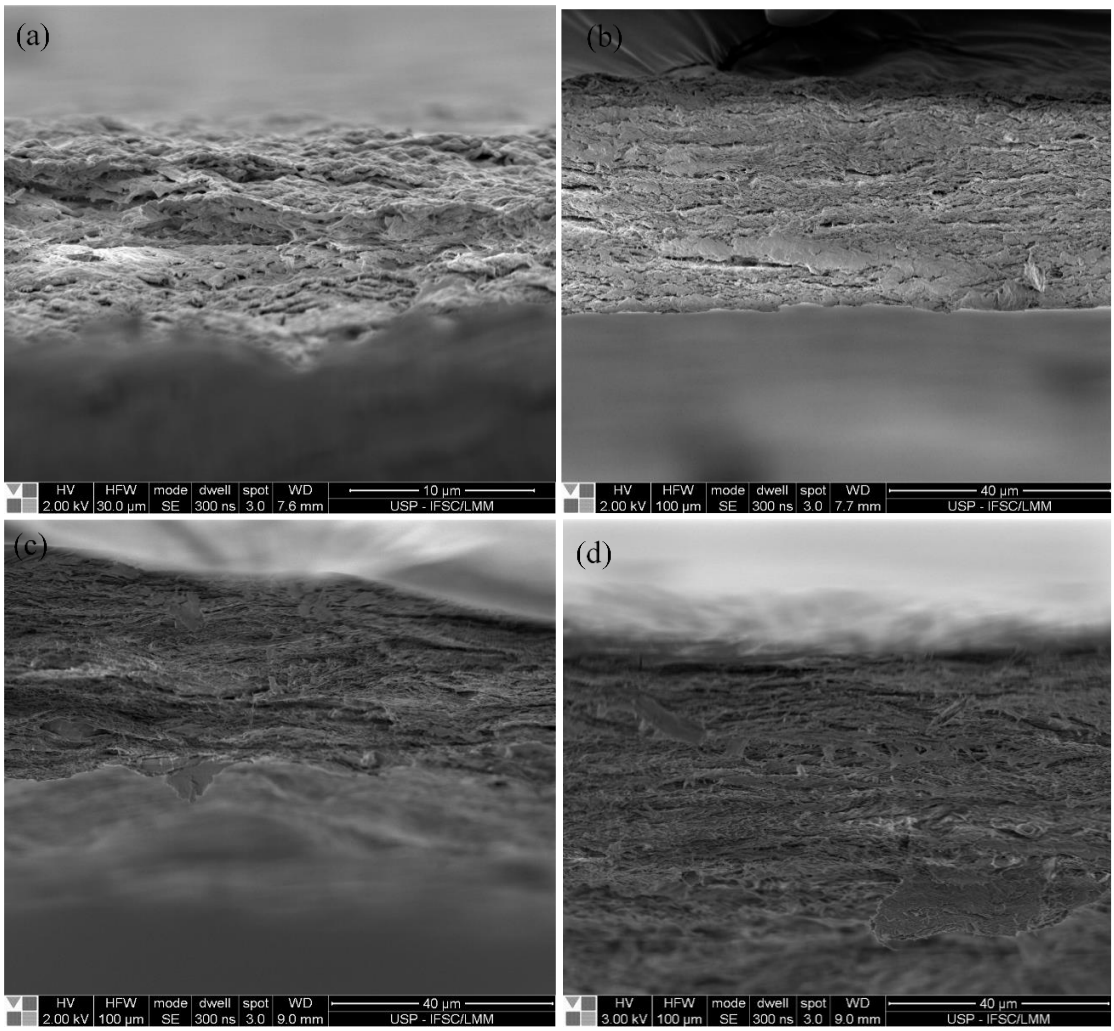

729
730 Figure S 6. Section SEM images of (a) NFC, (b) NFC-E10, (c) NFC-E25 and (d) NFC-E50
731

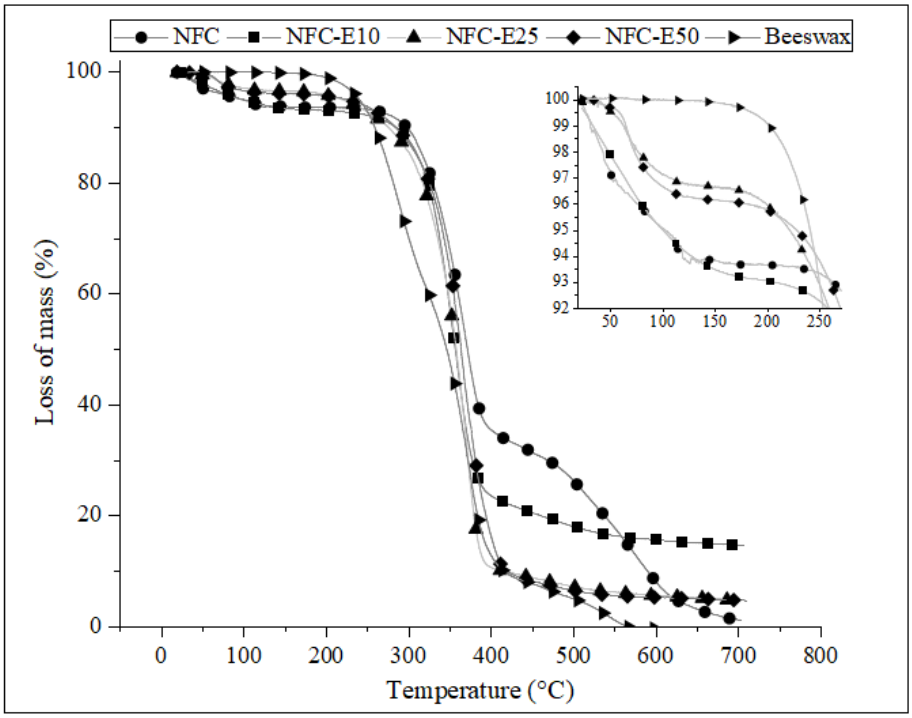

Figure S 7. Loss of mass as a function of temperature for NFC, BW and NFC/BW composite films.

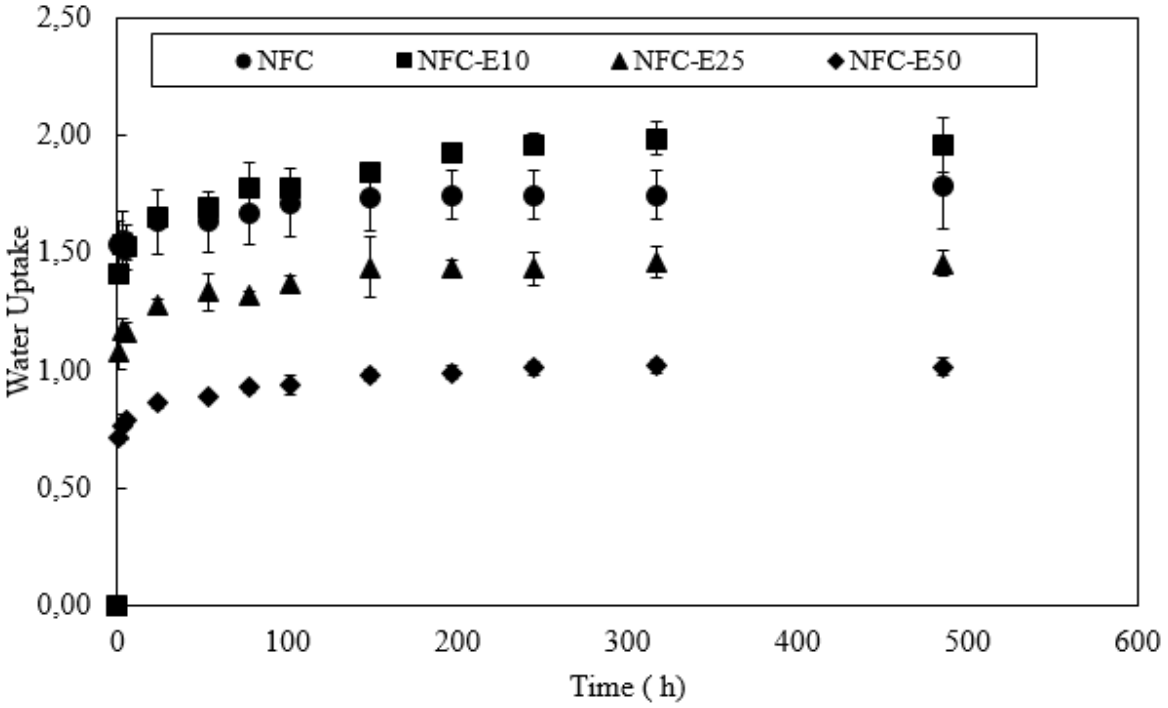

Figure S 8. Water vapor uptake as a function of time (h) for NFC and NFC/BW films.

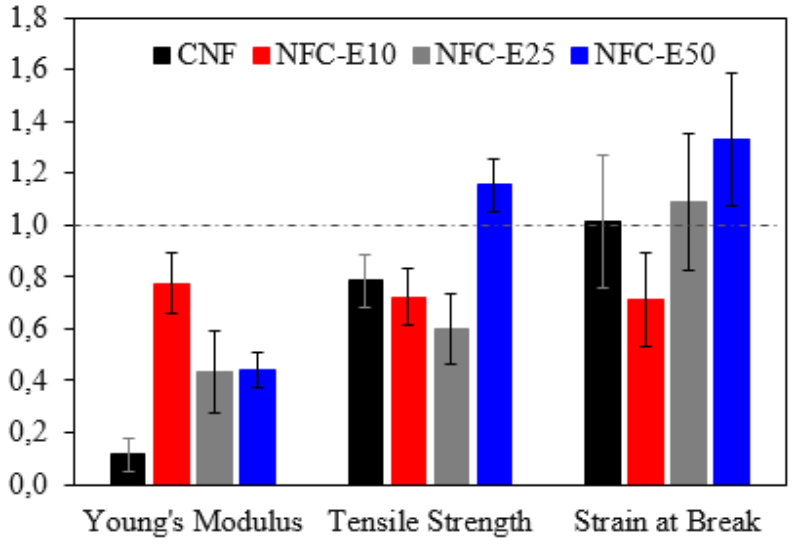

Figure S 9.Wet/dry" ratio for tensile properties measured for NFC and NFC/BW composite films.

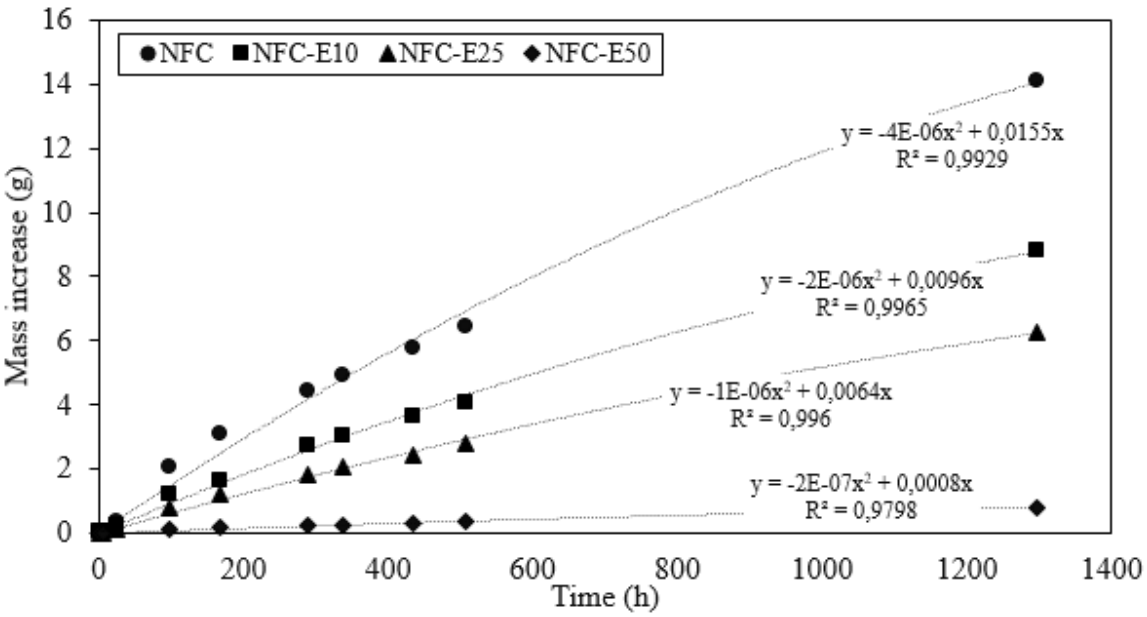

Figure S 10. Mass increase as a function of time for NFC and NFC/BW films obtained by the wet cup permeance test.

749 Table S 3. Fickian diffusion parameters calculated using the data from the wet cup permeance tests.

	w (mol/s)	J (mol/cm²*s)	H (cm)	D (cm²/s)	Da (cm²/s)
NFC	2.95E-07	9.83E-09	0.0046	8.01E-09	5.11E-08
NFC - E10	1.51E-07	5.04E-09	0.0069	6.15E-09	3.85E-08
NFC - E25	1.03E-07	3.45E-09	0.0074	4.50E-09	1.78E-08
NFC - E50	1.54E-08	1.15E-10	0.0104	9.52E-10	3.19E-09

750

751 Table S 4. Knudsen diffusion parameters calculated using the data from the wet cup WVTR tests.
752

	Porosity	Tortuosity τ	Path length (µm)	Rf (nm)	RKnudsen (nm)
NFC	0.29	1.85	85.13	0.85	0.032
NFC - E10	0.31	1.94	113.14	0.72	0.036
NFC - E25	0.41	1.62	119.33	0.54	0.029
NFC - E50	0.49	1.52	159.02	0.07	0.009

753

5 DISCUSSION

The main objective of the thesis was to produce NFC films by different routes of chemical and physical modification in order to provide to them hydrophobic character and better barrier properties to oxygen and water vapor. Four strategies were used and the results of each one were presented in five papers in the previous section. Strategy 1 corresponds to surface modification by dipping the NFC film in a blocked isocyanate solution. In strategy 2, an emulsion was made with NFC suspension and blocked isocyanate solution. In strategy 3, a blocked isocyanate was synthesized using PEG, in which the modified macrodiol was used to make cross-linked composites with NFC. After drying, the films obtained by strategies 1, 2 and 3 went through a step of thermal treatment to deblock the isocyanate, ensuing chemical modification by the formation of urethane bonds. In strategy 4, an emulsion of suspension of NFC and liquid beeswax was prepared and after drying, composite films were obtained. The strategies used are summarized schematically in Figure 21. In this chapter, we will discuss the results already presented individually in the papers in an integrated way, comparing the benefits and limitation of each strategy among themselves. This discussion may in the future lead to the publication of a paper where the data from the previous ones are used together, adding to new results or with results not yet published. The discussion below compares the different films obtained in relation to their physical, mechanical and water resistance properties. In the case of NFC-MDI-PEG and NFC/BW composites, only the properties of the composition with the highest NFC incorporation value (50%) are presented, with the other compositions previously presented and discussed on the papers.

Figure 21 – Strategies for chemical and physical modification of NFC based films.

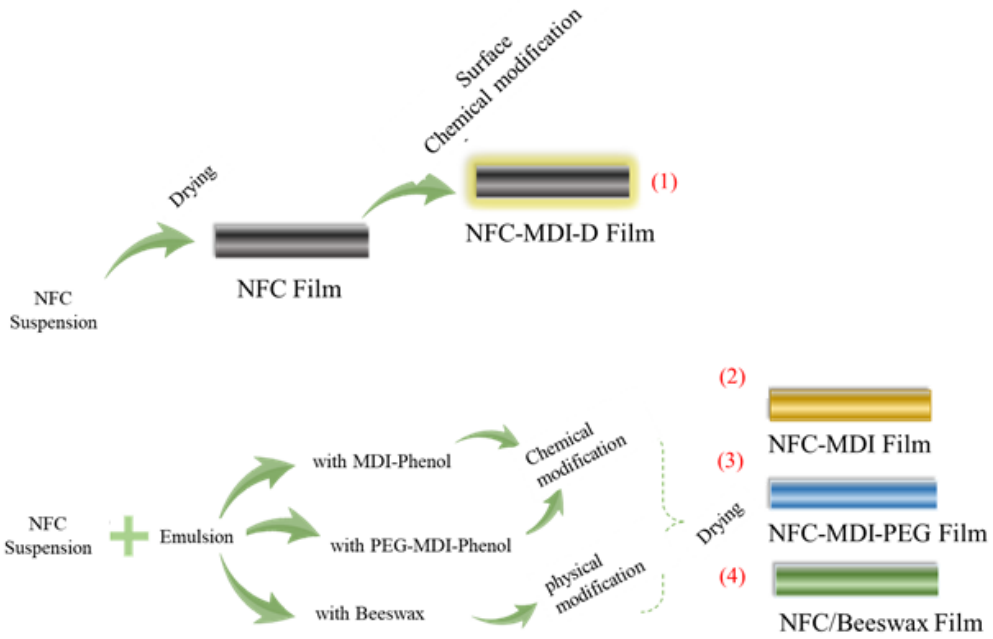

Source: Author.

5.1 Physical Properties

Figure 22 presents the data of (a) thickness, (b) density, (c) porosity and (d) grammage, determined for the NFC films (1) and the films obtained by the different modification strategies. Thickness and grammage are extensive properties (dependent on the mass of the material) and density and porosity are intensive properties (not dependent on the mass).

Data presentation follows the order (1) NFC base film, obtained by drying the suspension without chemical or physical modification, (2) film obtained by the surface modification strategy (NFC-MDI-D), (3) film obtained by drying of suspension emulsion of NFC and blocked isocyanate (NFC-MDI), (4) composite film, obtained by modification of macrodiol PEG with MDI and phenol (NFC-MDI-PEG), and (5) composite film of NFC and beeswax (NFC/BW). The legend is also displayed alongside the graphics.

The NFC film and the surface treated film (NFC-MDI-D), with the exception of its hydrophobic nature, had very similar physical characteristics and properties, such as thickness, density, porosity and grammage. These results shows that the hydrophobization process performed on NFC-MDI-D did not affect the physical properties of the neat NFC film when modified by dipping. On the other hand, the film obtained from the drying of the mixture of emulsion of MDI-2Ph and aqueous suspension of NFC, (NFC-MDI) had twice the thickness (> 100 µm), resulting in a higher grammage. Density and porosity remained

similar to those observed in NFC films, showing that although drying was done from an emulsion, there was adequate packaging of the nanofibers during the drying process, limiting the void content, which remained around 27%.

Strategies involving the preparation of composite films of NFC with PEG modified with MDI and with beeswax in fractions of 50% m/m obtained from drying emulsions (compositions 4 and 5, respectively) also resulted in films with thickness above 100 µm. However, it is observed that the density, porosity and grammage of these films varied according to the chemical nature of the material used. The NFC-MDI-PEG composite maintained its density close to that presented by the NFC base film (1.13 g/cm^2), but with a significantly lower porosity of 15%. Therefore, it can be said that, due to greater chemical affinity (polar-polar interaction), the modified PEG partially filled the porosity of the matrix formed by the NFC entanglement due to the formation of new urethane bonds between PEG-MDI and cellulose and/or self-crosslinking between the PEG-MDI chains. On the other hand, the density of the NFC/BW composite showed a remarkable reduction of 37% compared to the base NFC film (0.69 g/cm^2), resulting in a porosity of 49%. This behavior is attributed to low adhesion between phases due to the non-polar nature of beeswax. The presence of beeswax droplets in the emulsion reduced the number of hydrogen bonds between the nanofibers, affecting the packing during film formation. Naturally, porosity affected the film grammage, compact and thicker NFC-MDI-PEG films had the highest grammage value of 130 g/m^2 while thicker but more porous NFC/BW films had an intermediate grammage value of 72 g/m^2.

Table 5 presents data of thickness, density, porosity and grammage, separated by quartiles of shades of blue. The separation was done for a better visual comparison between the different compositions. In the context of packaging, films that are thinner, with lower density, lower porosity and great grammage are the most interesting from the point of view of material economy. Therefore, this was the criterion used to separate the different films obtained. The quartiles were then separated according to which film had the best performance in each property, being assigned a value of 100% in such case. For example, NFC was the thinnest film (i.e. 100%), so the thickness of the other films was normalized according to NFC value for the quartile separation. Thus, from the relationship with the other compositions, the quartiles were formed and distributed in an increasing scale of shades of blue according to the range of percentage values of the quartile; that is, variations 0 a 25%, 25 a 50%, 50 a 75% e 75 a 100%, as illustrated on the drawing next to Table 5.

Figure 22 – Physical properties of NFC-based films obtained by different manufacturing strategies. 1 refers to the unmodified film, 2 to the superficially modified film, 3 to the emulsion-modified film, 4 to the emulsion-modified film with blocked macrodiol, and 5 to the composite film of NFC and beeswax, indicated by their nomenclatures on the right side of the graph.

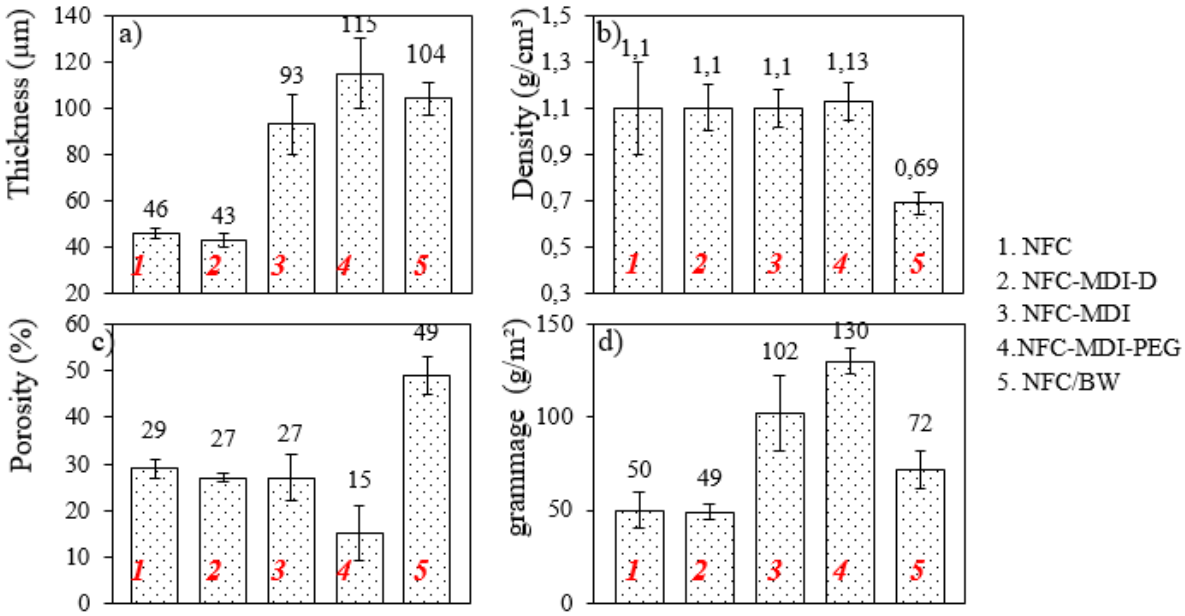

Source: Author.

Table 5 – Graphic physical properties of the films obtained by the four different modification strategies separated into quartiles of blue tones. Each shade of blue represents a quartile, with the darkest blue referring to 100% of the property, followed by 50-75% of the value, 25 -50% and the lightest 0-25%.

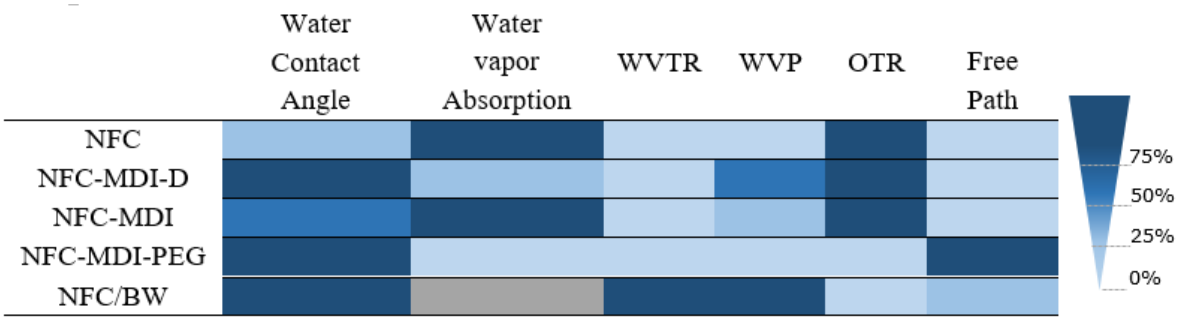

Source: Author.

5.2 Mechanical Properties

Figure 23shows data for Young's modulus, tensile strength, elongation at break and tear strength index obtained in the tensile and tear tests. The NFC film has the highest values of Young's modulus, tensile strength and strain at break (6.5 GPa, 110 MPa and 9%, respectively). In the same figure it is observed that the NFC-MDI-D film, surface treated

by dipping in a blocked isocyanate solution, maintained the tensile properties of the base film, therefore without significant changes due to chemical modification. On the other hand, the NFC-MDI film, obtained through the drying of a mixture of NFC suspension and blocked isocyanate emulsion, had elastic modulus and tensile strength reduced by 20 and 40%, respectively, while the elongation at break presented a sudden drop of 80%. As the density and porosity of the NFC-MDI film remained close to the values presented by the base NFC film, the reduction in mechanical properties in tensile cannot, in principle, be attributed to defects arising from drying. As the physical properties remained similar, it is possible to state that the presence of MDI molecules between the nanofibers were responsible for reducing the amount of hydrogen bonds, due to the formation of urethane bonds. Thus, in this composition, NFCs lost the ability to slide in relation to each other by breaking and forming new hydrogen bonds and the film became more brittle.

Regarding the composite films with 50% dispersed phase (NFC-MDI-PEG and NFC/BW) it is observed that the Young's modulus and tensile strength are considerably lower in relation to both the NFC base film and in relation to the NFC films chemically modified by dipping and in emulsion. Such a reduction was expected, since the two added phases (PEG and beeswax) have mechanical properties remarkably lower than those of NFC. However, thanks to the formation of the three-dimensional NFC reinforcement network, the resulting films still have competitive tensile properties when compared to synthetic polymers and, mainly, to biopolymers available on the market. The addition of the PEG-MDI- phase, with formation of urethane bonds between PEG-MDI and between PEG-MDI and NFC, provided greater elongation to the film, overcoming a brittleness limitation found in the preparation of NFC-MDI film.

The NFC/BW film also showed a considerable drop on the elongation at break due to the presence of beeswax between the nanofibers. By preventing the direct interaction of the fibers, a decrease in the tear strength of the NFC/BW films was also observed, with a reduction of 60% in relation to the mean values observed in the NFC films.

Also with regard to tear resistance, Figure 23d shows that films that underwent the process of formation of urethane bonds in their internal structures, such as NFC-MDI and NFC-MDI-PEG, had their tear resistance significantly increased in 185% and 243%. . Table 6 shows the separation into quartiles for mechanical properties, with the division made in shades of blue. As in Table 5, lighter colors indicate lower properties while dark colors indicate higher properties.

Figure 23 – Mechanical properties of NFC-based films obtained by different preparation strategies. 1 refers to the unmodified film, 2 to the superficially modified film, 3 to the emulsion-modified film, 4 to the emulsion-modified film with blocked macrodiol and 5 to the composite film of NFC and beeswax, indicated by their nomenclatures on the right side of the graph.

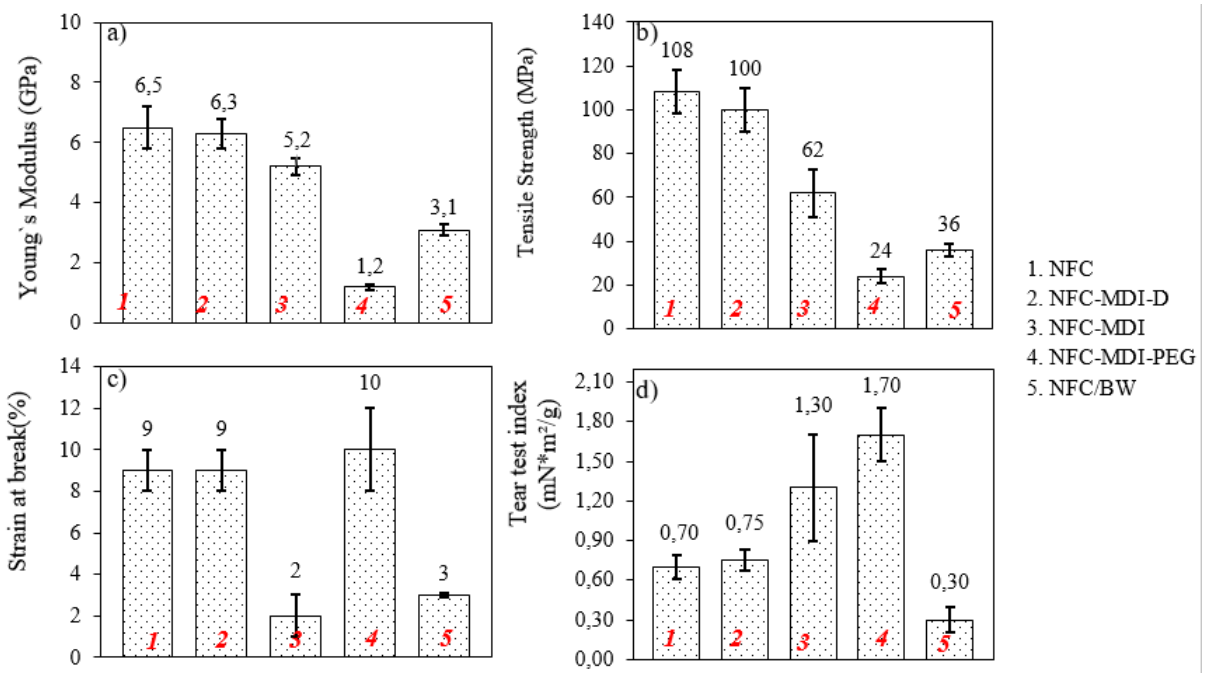

Source: Author.

Table 6 – Color graph of the mechanical properties of the films obtained by the different strategies. Each shade of blue represents a quartile, with the darkest blue referring to 100% of the property, followed by 50-75% of the value, 25-50% and the lightest 0-25%.

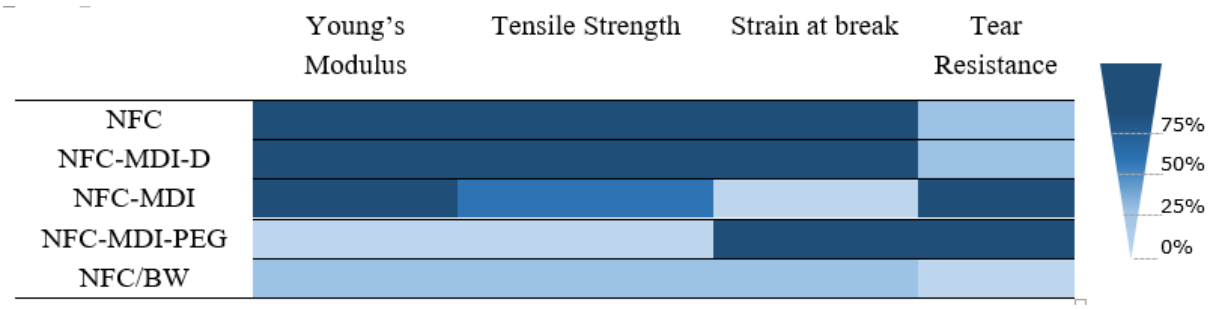

Source: Author.

5.3 Water resistance and barrier properties

Figure 24 shows the average water contact angle (WCA) values between the material substrates and water for the different films. It is possible to observe that, in general, the contact angles of the modified films are greater than the average contact angle measured

for NFC films, which was 52°. Among the modified compositions, the highest WCA value was observed for the surface treatment by dipping in blocked isocyanate solution (2-NFC-MDI-D), with 113°. The composites of NFC-MDI-PEG and NFC/BW (films 4 and 5, respectively) also presented a WCA close to 100°, due to the crosslinking process through the formation of urethane bonds in the case of film 4 and due to the presence of the hydrophobic beeswax phase covering the fibers in the case of film 5. The film obtained from the drying of the mixture of isocyanate emulsion and NFC suspension (3-NFC-MDI) presented a contact angle of 75° and, although 20° above the base film, the treatment was not sufficient to change the hydrophilic nature of the surface. Unlike the NFC-MDI-D film which had the modifying agents concentrated on its surface, in the NFC-MDI film the blocked isocyanate molecules were dispersed among the nanofiber entanglement. Thus, even though increasing the water resistance of the film in relation to the base film and reducing the plasticizing effect of water (paper 3), the surface had a lower concentration of hydrophobic molecules, and, therefore, a lower WCA.

Figure 25 shows the surface roughness values obtained through the analysis of AFM images. It is observed that treatments 2, 3 and 4 changed the surface roughness in relation to the base film. According to equation 4, a rougher surface amplifies the hydrophilic or hydrophobic nature of the surface in relation to a smooth surface of the same chemical composition. Therefore, the increased contact angle for these compositions was due to a combination of chemical treatment and morphology change. In the case of the 5-NFC/BW film, there was no significant change in roughness, since, as discussed in paper 5, a smooth, hydrophobic layer was formed on the film surface with 50% beeswax, responsible for the water-repellent effect. The graph 26 illustrates the WCA and roughness for each composition where the influence of roughness on WCA values is better observed. For films chemically modified with isocyanate, the greater the roughness, the greater the contact angle. However, in the case of the NFC/BW film, there was an increase in the contact angle, but not accompanied by an increase in surface roughness.

Figure 24 – WCA for films obtained by different modification strategies. 1 refers to unmodified film, 2 to surface-modified film, 3 to emulsion-modified film, 4 to emulsion-modified film with blocked macrodiol, and 5 to NFC-beeswax composite film.

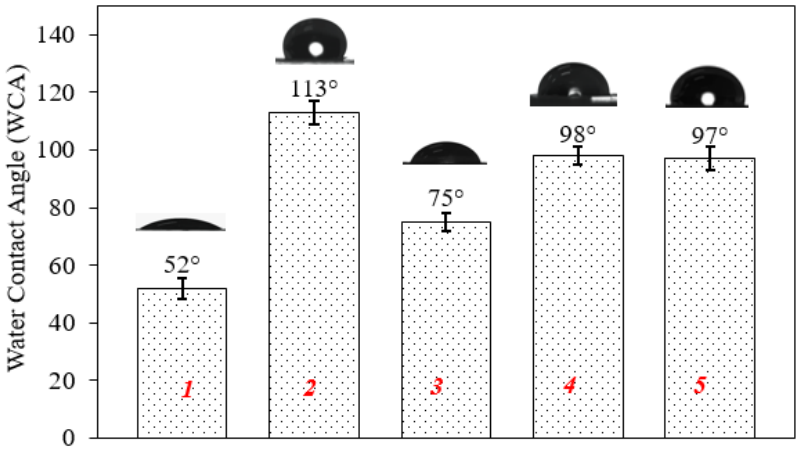

Source: Author.

Figure 25 – Roughness of films obtained by different modification strategies.

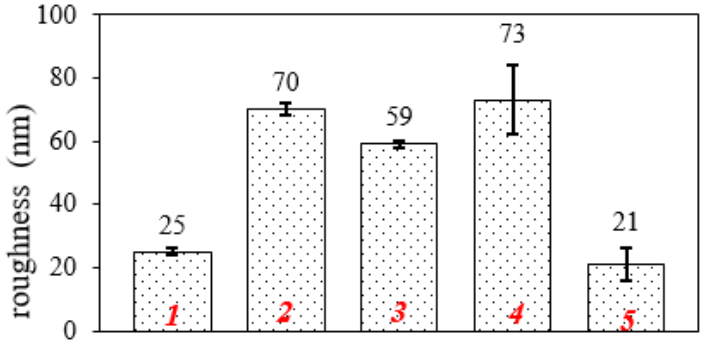

Source: Author.

Figure 26 – Water contact angle and roughness depending on the composition of each film.

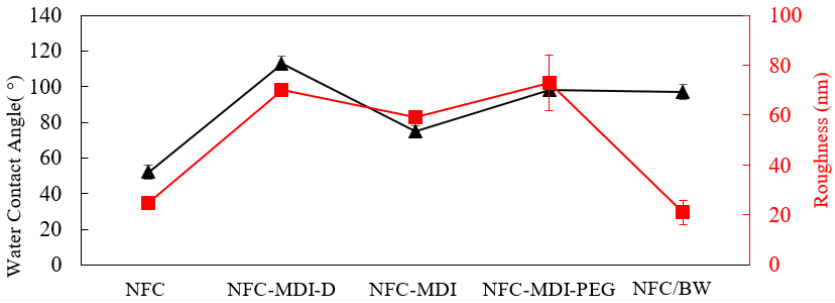

Source: Author.

Figure 27a) shows the water vapor absorption calculated through the mass gain for the different compositions at RH of 97.5%. Surprisingly, the NFC hydrophilic film had the lowest absorption value, reaching the saturation point with a mass gain of only 6%. The NFC-MDI film, modified in emulsion with isocyanate, also showed saturation with 6%. On the other hand, the hydrophobic films NFC-MDI-D and NFC-MDI-PEG showed saturation at 18% and 33%, respectively. Factors such as the greater roughness of the modified films may have influenced the water vapor absorption process. For the NFC-MDI-PEG film, in addition to the greater roughness in relation to the base film, it is estimated that the determining factor in the greater absorption of water vapor was the amorphous structure of the modified polymer. Although the porosity of this composition was the lowest, confirming that the modified PEG-MDI polymer filled the voids between the packed nanofibers, the absence of a crystalline structure, may have contributed to greater free volume, resulting in greater absorption. However, it is noteworthy that all films had a low saturation point of water vapor, when compared to films obtained from biomass found in the literature, as pointed out on the written papers.

The graph in Figure 27b compares the WVTR values between the films obtained by the different strategies. The NFC base film presented a WVTR of 153 g/m².day, a value compatible with the values found in the literature for eucalyptus NFC films, measured under the relative humidity difference condition of 0/50 % (NATHALIE LAVOINE, ISABELLE DESLOGES, ALAIN DUFRESNE, 2012). The result close to the literature shows that the method used to measure WVTR of films is reliable. Modifications with isocyanate on the film surface (NFC-MDI-D) and on the internal structure (NFC-MDI) resulted in a significant reduction in the passage of water vapor, reducing the WVTR to the order of 40 g/m^2.day for the two compositions. The NFC-MDI-PEG film had the highest WVTR value among the modified compositions of 130 g/m^2.day, with a barrier just a little higher than that presented by the base film. Thus, the greater absorption of water vapor from this composition was also reflected in poor barrier properties. On the other hand, the NFC/BW film presented the lowest WVTR value, reaching 10 g/m^2.day, a reduction of more than 90% compared to the NFC base film. As discussed in paper 5, the beeswax layer formed on the surface of the film contributed to this expressive increase on the barrier to water vapor, with values close to those measured for synthetic films such as low-density polyethylene.

The graph in Figure 27c compares the WVP values, a more complete permeation calculation that takes into account the film thickness in addition to the WVTR. According to the classification proposed by Wang et al, 2018 (WANG et al., 2018) othe films prepared here fit into the following categories with regard to their water vapor barrier properties: 5 medium (400-1000 g $\cdot$ m/m^2 $\cdot$ day $\cdot$ kPa), 2 e 3 low (1000-3000 g $\cdot$ m/m^2 $\cdot$ day $\cdot$ kPa), 1 e 4 poor (>3000 g $\cdot$ m/m^2 $\cdot$ day $\cdot$ kPa). Therefore, treatments with isocyanate, both in surface modification and in the modification within the internal structure, resulted in an increase

of one category in relation to the base film, while the composite made with beeswax, showed even greater improvement, increasing two categories, with similar values to the ones presented by PS 66, PHA 824 and PLA 898. The greater thickness of film 4, with WVTR values close to the NFC base film, resulted in WVP above 15000 $g \cdot m/m^2 \cdot day \cdot kPa$.

The graph in Figure 27d shows the OTR values (in $cm^3/m^2/day$) of the studied compositions. Hydroxylated polymers, synthetic or natural, in general have excellent O2 barrier properties, confirmed here by the lower OTR value presented by the NFC base film, of 15 $cm^3/m^2/day$. The internal modification with isocyanate (NFC-MDI) did not change the O2 barrier property in relation to the unmodified film. On the other hand, the surface modification (NFC-MDI-D) reduced the OTR to values below the detection limit of the equipment (below $0.1cm^3/m^2/day$). Since the porosity of the isocyanate-modified films remained in the same order of 27%, it is possible to say that the higher density of urethanes on the surface together with the steric hindrance caused by the presence of pending dodecanol molecules contributed to increase the difficulty of passage of O2 of composition 2. The NFC-MDI-PEG film followed the trend observed for WVP, with lower O2 barrier property than other compositions. The NFC/BW film presented OTR values considerably above the base composition and chemically modified films, probably due to lower adhesion between the polar-apolar phases, which resulted in a porosity of almost 50%. As the hydrophobic beeswax surface is not as effective against the passage of O_2 as it is against the passage of H_2O, once diffused into the film, the oxygen molecules had an easier path, due to the greater amount of internal voids. Still, the measured values are suitable for application in food packaging, as will be discussed in detail below.

Figure 27 – Barrier properties of NFC-based films obtained by different preparation strategies. 1 refers to the unmodified film, 2 to the superficially modified film, 3 to the emulsion-modified film, 4 to the emulsion-modified film with blocked macrodiol and 5 to the composite film of NFC and beeswax, indicated by their nomenclatures on the right side of the graph.

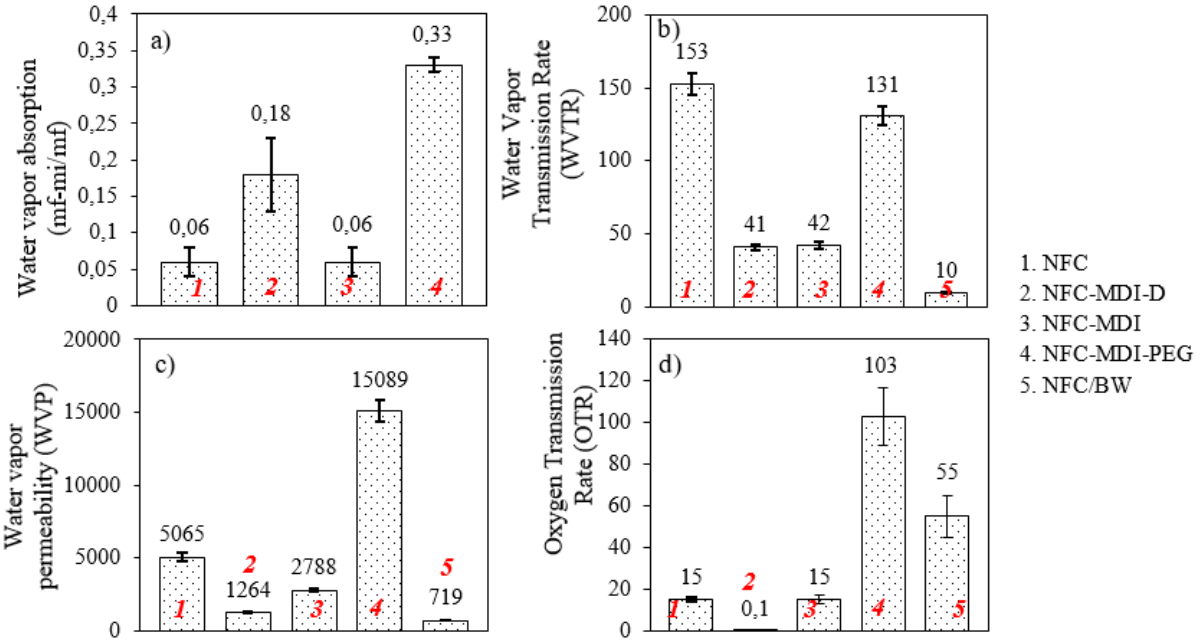

Source: Author.

The graphs in Figure 28 and Figure 29 relate WVTR and OTR with the porosity of each film and, despite expectations, it is observed that there is no apparent relationship between high barrier and porosity, ie, less porous films are not necessarily the films that presented the lowest permeation values of water vapor or O_2. On the contrary, in some cases the behavior was the opposite, for example, in the case of the NFC/BW, film that presented the lowest WVTR value and at the same time exhibited the highest porosity, of almost 50%. From the standpoint of application in packaging, the combination of high barrier to H2O together with low density (high porosity) obtained for the NFC/BW film is very interesting, since low weight packaging with the same performance reduces the costs of transport and storage volume. Another example is the NFC-MDI-PEG film, which had the lowest void content of 15%, but presented the highest measured OTR in relation to the other compositions.

As discussed above, other factors such as chemical composition, NFC fiber packing, and crystalline or amorphous structure played a more crucial role in determining the barrier properties of the films. It is estimated that specifically for O_2 permeation, the dominant factor in the good performance was the packaging and hornification of the nanofibers. The films that presented the lowest OTR were those that did not use the composites preparation strategy, that is, films where the fiber-fiber contact was higher, as is the case

of unmodified or only superficially modified compositions (NFC-MDI-D), which presented O_2 passage below the detection limit of the equipment. Since hydroxylated polymers, synthetic or natural, in general have low O_2 permeation when the relative humidity of the environment is low, the surface hydrophobization strategy seems to be the most suitable for this purpose as it keeps the compact structure intact and hydrophobizes the surface, allowing the use of the film also in environments with higher humidity.

Figure 28 – WVTR (water vapor transmission rate) data measured according to ASTM E96 and porosity, measured by the difference between the ideal density and real density as a function of the composition of the studied films.

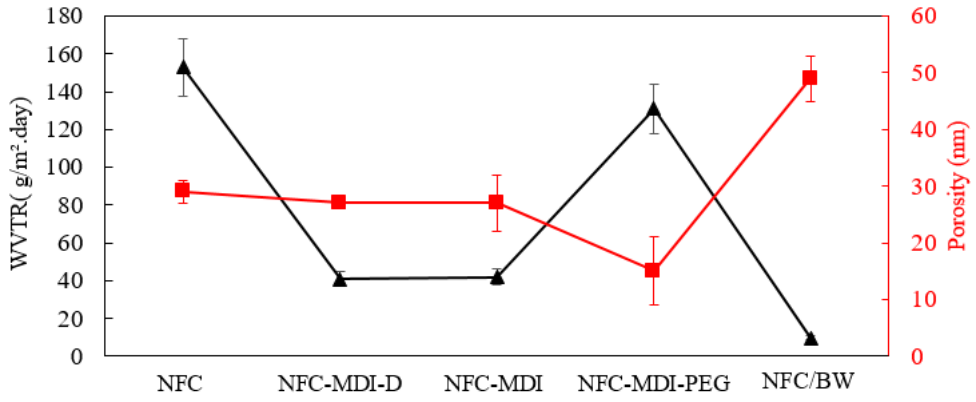

Source: Author.

Figure 29 – OTR (Oxygen Transmission Rate) data, measured according to ASTMF1927 and porosity measured by the difference between the ideal density and the real density as a function of the composition of the studied films.

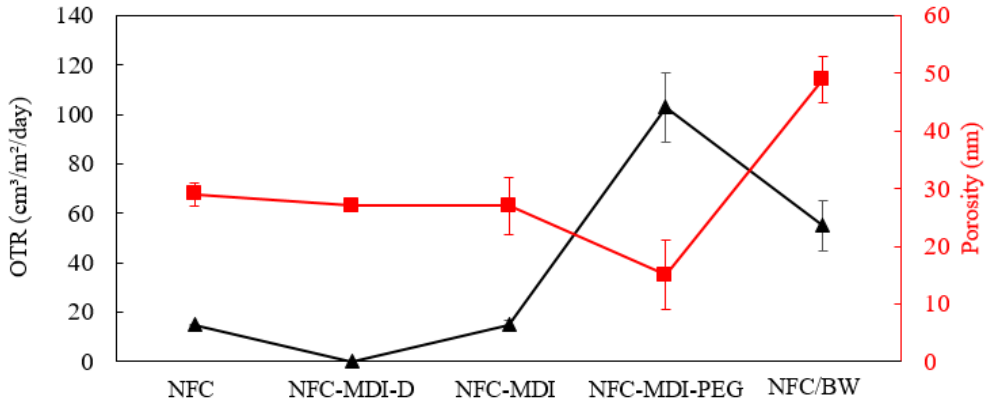

Source: Author.

The graph in Figure 30presents the thickness and OTR values of the films. Although a greater thickness also contributes to a higher mean free path value (Figure 31), nnot

necessarily, a thicker film had a lower OTR. On the contrary, the lower OTR values were obtained for thinner films. As the amount of NFC was fixed at 1.2 g for each prepared film regardless of the applied treatment (chemical modification or composites), the composite films became thicker due to the presence of the other phase but not necessarily its barrier to O_2 increased. Thus, as already mentioned above, the fiber-fiber interaction due to hornification was the main responsible for low OTR values. Table 7 ranks the discussed properties into quartiles, in shades of blue.

Figure 32 shows the minimum storage requirements in terms of water vapor transmission rate and oxygen transmission rate for various foods types. In green were placed the results obtained here for the films prepared by the different strategies. Generally speaking, these films would be suitable for preserving fruits, vegetables, salads, bakery products and cheese. The NFC-MDI film could also be used to preserve some types of meat in modified atmosphere packages due to its combination of moderate OTR and WVTR. The NFC-MDI-D and NFC/BW films, although presenting the lowest individual values of OTR and WVTR, respectively, do not have the adequate combination of these properties to preserve foods that need greater barriers to the passage of these gases, such as coffee, peanuts and fresh meat. As can be seen, even the unmodified NFC base film would be suitable for preserving these foods if they were kept in dry environments. The modified films were mostly hydrophobic and resistant to contact with water, which would allow their application in environments with higher relative humidity. Of course, the barrier properties to water vapor and O_2 are just two of the many requirements for a film to be used as food packaging. To proceed with the use, it would be necessary to evaluate the migration of elements and especially the toxicity of isocyanates present in the packaging. In addition, it would be necessary to develop industrial production routes for films to reach the market at a competitive price. Nonetheless, a general picture can be drawn with the properties obtained.

Figure 30 – Thickness data measured using automatic micrometer and OTR (oxygen transmission rate), measured according to ASTMF1927 as a function of the composition of the studied films.

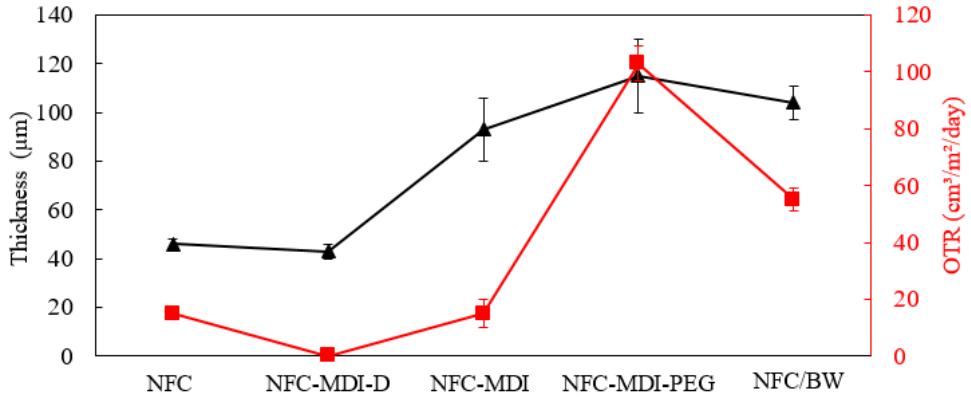

Source: Author.

Figure 31 – Average free path for each studied film composition.

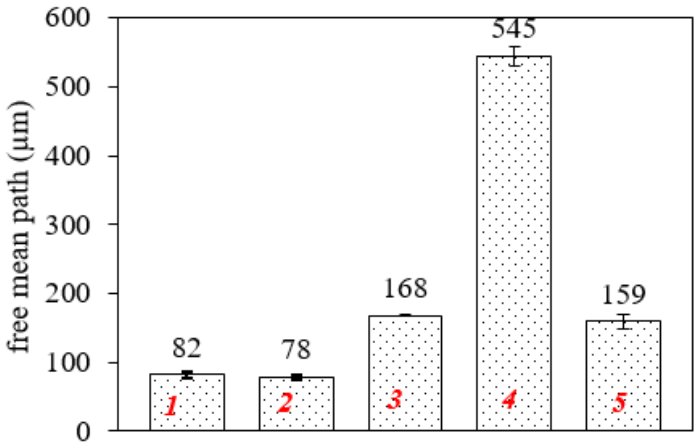

Source: Author.

Table 7 – Color graph of barrier properties of films obtained by different strategies. Each shade of blue represents a quartile, with the darkest blue referring to 100% of the property, followed by 50-75% of the value, 25-50% and the lightest 0-25%.

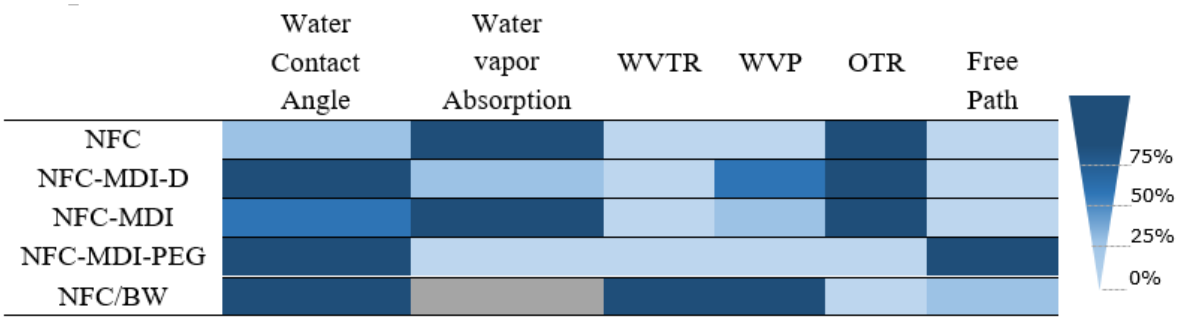

Source: Author.

Figure 32 – Barrier property values obtained by different strategies with OTR and WVTR required for conservation of various foods. In green the corresponding properties of the prepared materials.

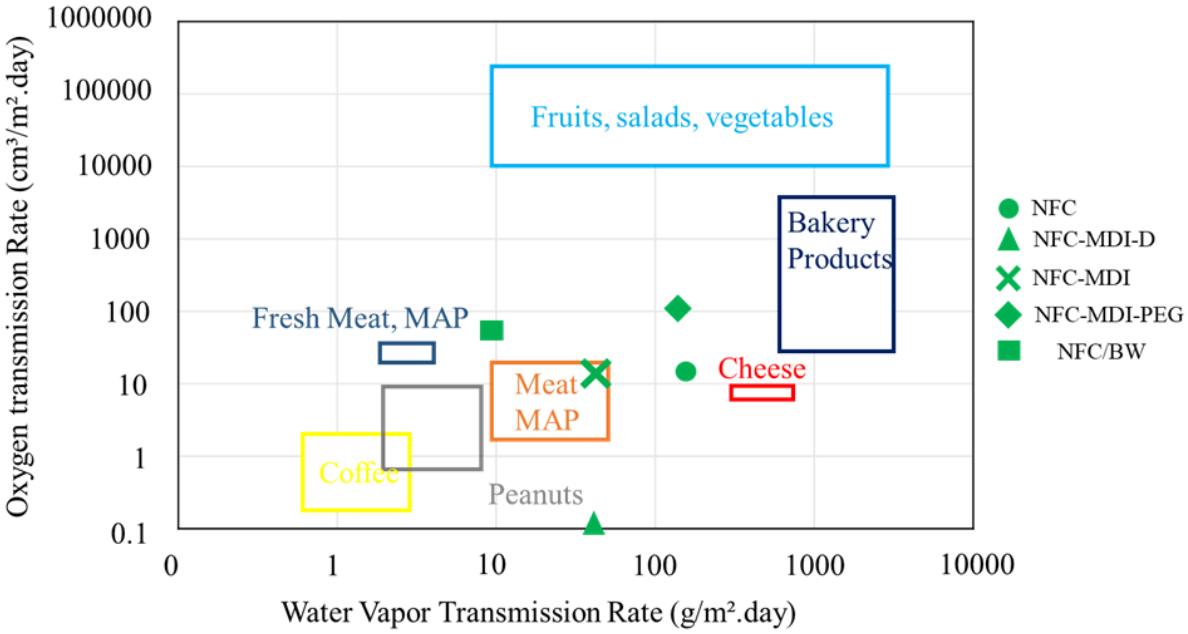

Source: Author.

6 CONCLUSION

Nanofibrillated cellulose (NFC) films and composite films containing up to 50% $_{w/w}$ NFC were produced via solvent evaporation, using different chemical and physical modification protocols to increase, mainly, the hydrophobicity and barrier properties to water vapor and oxygen.

It was demonstrated that it is possible to use blocked isocyanates as a chemical modifying agent for the purpose proposed here, which was obtaining hydrophobic NFC films, resistant to contact with water and with low permeation to gases. The strategies used allowed i) surface modification of NFC films, ii) modification via mixing and drying of blocked isocyanate emulsion and NFC suspension and iii) modification, also by drying emulsions, via blocked isocyanate synthesis using a macrodiol (PEG) as a chain-extending agent to produce hydrophobic composite films. Chemically modified films had different physical, mechanical and water resistance and barrier properties depending on the strategy used. The advantage of using blocked isocyanates lies in the benefit of obtaining hydrophobic films in a practical modification process, without the need for large amounts of modifying agents and organic solvents. Furthermore, there is no need for modification in anhydrous medium, since the blocked isocyanates proved to be chemically inert at room temperature and in aqueous medium, which enables the industrial application of the developed protocols.

With regard to the physical modification proposed by the use of beeswax as a hydrophobizing agent, it allowed to obtain composite films with up to 50% of NFC via drying of emulsions. These films were smooth, hydrophobic and low permeable to water vapor and oxygen. This strategy, in addition to presenting the highest gas barrier values, with vapor transmission values compared to high-density polyethylene, presented the advantage of using an entirely green route of production.

Barrier properties to water vapor and O_2 are decisive on the selection of films for packaging. Currently, biodegradable polymers or polymers from a renewable source do not have the same barrier properties as non-biodegradable polymers, especially in environments of high humidity, and this makes it difficult for them to be used in this type of application. The present work shows that it is possible to obtain nanocellulose films, hydrophobized by different strategies and with barrier properties compared to the ones presented by synthetic polymers.

7 SUGGESTIONS FOR FUTURE WORKS

Overall, each hydrophobization strategy resulted in a film with one main feature. For example, the NFC-MDI-PEG films, although with a low gas barrier property compared to other compositions, showed the highest elongation at break. The NFC/BW film had the lowest vapor transmission value, but its oxygen transmission was above the base NFC film. The NFC-MDI-D film, superficially modified with the use of blocked isocyanate, presented almost zero oxygen permeation. Thus, an interesting study would be to produce multilayer films, where each layer would be modified due to a different treatment proposed here. Multilayer films from renewable sources would possibly have a more competitive set of properties compared to synthetic polymers. Furthermore, choosing adhesives and studying the application of adhesives from these layers would be a first step in the study of multilayer films.

BIBLIOGRAPHY

ASTM. Disponível em: <https://doi.org/10.1023

AHMADZADEH, S.; KHANEGHAH, A. M. Role of green polymers in food packaging. In: **Encyclopedia of Renewable and Sustainable Materials**. Elsevier, 2020. p. 305–319. Disponível em: <https://doi.org/10.1016%2Fb978-0-12-803581-8.10576-4>.

ANAGNOSTI, L. et al. Worldwide actions against plastic pollution from microbeads and microplastics in cosmetics focusing on european policies. has the issue been handled effectively? **Marine Pollution Bulletin**, Elsevier BV, v. 162, p. 111883, 2021. Disponível em: <https://doi.org/10.1016%2Fj.marpolbul.2020.111883>.

ARBATAN, T. et al. Cellulose nanofibers as binder for fabrication of superhydrophobic paper. **Chemical Engineering Journal**, Elsevier BV, v. 210, p. 74–79, 2012. Disponível em: <https://doi.org/10.1016%2Fj.cej.2012.08.074>.

ASTM. **Test Methods for Water Vapor Transmission of Materials**. ASTM International, 2002. Disponível em: <https://doi.org/10.1520%2Fe0096_e0096m-16>.

BARLOW, C.; MORGAN, D. Polymer film packaging for food: An environmental assessment. **Resources, Conservation and Recycling**, Elsevier BV, v. 78, p. 74–80, 2013. Disponível em: <https://doi.org/10.1016%2Fj.resconrec.2013.07.003>.

BHARATHI, S. K. V.; MOSES, J. A.; ANANDHARAMAKRISHNAN, C. Interaction phenomena between packaging and product. In: **Bio-based Materials for Food Packaging**. Springer Singapore, 2018. p. 33–56. Disponível em: <https://doi.org/10.1007%2F978-981-13-1909-9_2>.

BHARATHI, S. V. et al. Recent trends in nanocomposite packaging materials. In: **Innovative Food Processing Technologies**. Elsevier, 2021. p. 731–755. Disponível em: <https://doi.org/10.1016%2Fb978-0-08-100596-5.23027-8>.

BORÉM, F. M. et al. Sensory analysis and fatty acid profile of specialty coffees stored in different packages. **Journal of Food Science and Technology**, Springer Science and Business Media LLC, v. 56, n. 9, p. 4101–4109, 2019. Disponível em: <https://doi.org/10.1007%2Fs13197-019-03879-3>.

BRIASSOULIS, D.; GIANNOULIS, A. Evaluation of the functionality of bio-based food packaging films. **Polymer Testing**, Elsevier BV, v. 69, p. 39–51, 2018. Disponível em: <https://doi.org/10.1016%2Fj.polymertesting.2018.05.003>.

CAO, N. et al. Facile synthesis of fluorinated polydopamine/chitosan/reduced graphene oxide composite aerogel for efficient oil/water separation. **Chemical Engineering Journal**, Elsevier BV, v. 326, p. 17–28, 2017. Disponível em: <https://doi.org/10.1016%2Fj.cej.2017.05.117>.

CARVALHO, A.; CURVELO, A.; GANDINI, A. Surface chemical modification of thermoplastic starch: reactions with isocyanates, epoxy functions and stearoyl chloride. **Industrial Crops and Products**, Elsevier BV, v. 21, n. 3, p. 331–336, 2005. Disponível em: <https://doi.org/10.1016%2Fj.indcrop.2004.04.027>.

CARVALHO, A. J. F.; TROVATTI, E.; CASALE, C. A. Polystyrene/cellulose nanofibril composites: Fiber dispersion driven by nanoemulsion flocculation. **Journal of Molecular Liquids**, Elsevier BV, v. 272, p. 387–394, 2018. Disponível em: <https://doi.org/10.1016%2Fj.molliq.2018.09.089>.

CEREMPEI, A. et al. Antimicrobial controlled release systems for the knitted cotton fabrics based on natural substances. **Fibers and Polymers**, Springer Science and Business Media LLC, v. 16, n. 8, p. 1688–1695, 2015. Disponível em: <https://doi.org/10.1007%2Fs12221-015-4551-3>.

CHIROMITO, E. M. S.; TROVATTI, E.; CARVALHO, A. J. F. Water-based processing of fiberboard of acrylic resin composites reinforced with cellulose wood pulp and cellulose nanofibrils. **Journal of Renewable Materials**, Computers, Materials and Continua (Tech Science Press), v. 7, n. 5, p. 403–413, 2019. Disponível em: <https://doi.org/10.32604%2Fjrm.2019.01846>.

CHITPRASERT, P.; SUTAPHANIT, P. Holy basil (ocimum sanctum linn.) essential oil delivery to swine gastrointestinal tract using gelatin microcapsules coated with aluminum carboxymethyl cellulose and beeswax. **Journal of Agricultural and Food Chemistry**, American Chemical Society (ACS), v. 62, n. 52, p. 12641–12648, 2014. Disponível em: <https://doi.org/10.1021%2Fjf5019438>.

CHOI, K.-H.; KANG, Y. S.; CHO, B.-U. Comparison of aging characteristics of the duplicated beeswax-treated and non-treated paper books during artificial thermal aging. **Journal of Industrial and Engineering Chemistry**, Elsevier BV, v. 41, p. 68–74, sep 2016. Disponível em: <https://doi.org/10.1016%2Fj.jiec.2016.07.009>.

DELEBECQ, E. et al. On the versatility of urethane/urea bonds: Reversibility, blocked isocyanate, and non-isocyanate polyurethane. **Chemical Reviews**, American Chemical Society (ACS), v. 113, n. 1, p. 80–118, 2012. Disponível em: <https://doi.org/10.1021%2Fcr300195n>.

DU, X. et al. Switchable and simultaneous oil/water separation induced by prewetting with a superamphiphilic self-cleaning mesh. **Chemical Engineering Journal**, Elsevier BV, v. 313, p. 398–403, 2017. Disponível em: <https://doi.org/10.1016%2Fj.cej.2016.12.092>.

DUFRESNE, A. Nanocellulose: a new ageless bionanomaterial. **Materials Today**, Elsevier BV, v. 16, n. 6, p. 220–227, 2013. Disponível em: <https://doi.org/10.1016%2Fj.mattod.2013.06.004>.

DUFRESNE, A. **Handbook of Nanocellulose and Cellulose Nanocomposites**. Wiley-VCH Verlag GmbH & Co. KGaA, 2017. Disponível em: <https://doi.org/10.1002%2F9783527689972>.

DUFRESNE, A.; DUPEYRE, D.; VIGNON, M. R. Cellulose microfibrils from potato tuber cells: Processing and characterization of starch-cellulose microfibril composites. **Journal of Applied Polymer Science**, Wiley, v. 76, n. 14, p. 2080–2092, 2000. Disponível em: <https://doi.org/10.1002%2F%28sici%291097-4628%2820000628%2976%3A14%3C2080%3A%3Aaid-app12%3E3.0.co%3B2-u>.

EBNESAJJAD, S. **Plastic films in food packaging : materials, technology and applications**. Amsterdam: Elsevier, William Andrew, 2013. ISBN 978-1455731121.

EUROMONITOR INTERNATIONAL. **Tendências do mercado de cafés em 2017**. ABIC Associação Brasileira da Indústria do Café, 2017. 1–43 p. Disponível em: <http://abic.com.br/estatisticas/pesquisas/pesquisa-tendencias-de-consumo>.

FARUK, O. et al. Biocomposites reinforced with natural fibers: 2000–2010. **Progress in Polymer Science**, Elsevier BV, v. 37, n. 11, p. 1552–1596, 2012. Disponível em: <https://doi.org/10.1016%2Fj.progpolymsci.2012.04.003>.

FERRER, A.; PAL, L.; HUBBE, M. Nanocellulose in packaging: Advances in barrier layer technologies. **Industrial Crops and Products**, Elsevier BV, v. 95, p. 574–582, 2017. Disponível em: <https://doi.org/10.1016%2Fj.indcrop.2016.11.012>.

FORSMAN, N. et al. Layer-by-layer assembled hydrophobic coatings for cellulose nanofibril films and textiles, made of polylysine and natural wax particles. **Carbohydrate Polymers**, Elsevier BV, v. 173, p. 392–402, 2017. Disponível em: <https://doi.org/10.1016%2Fj.carbpol.2017.06.007>.

FRENCH, A. D. Glucose, not cellobiose, is the repeating unit of cellulose and why that is important. **Cellulose**, Springer Science and Business Media LLC, v. 24, n. 11, p. 4605–4609, ago. 2017. Disponível em: <https://doi.org/10.1007/s10570-017-1450-3>.

GANDINI, A. The irruption of polymers from renewable resources on the scene of macromolecular science and technology. **Green Chemistry**, Royal Society of Chemistry (RSC), v. 13, n. 5, p. 1061, 2011. Disponível em: <https://doi.org/10.1039%2Fc0gc00789g>.

GANDINI, A.; BELGACEM, M. N. The surface and in-depth modification of cellulose fibers. In: **Advances in Polymer Science**. Springer International Publishing, 2015. p. 169–206. Disponível em: <https://doi.org/10.1007%2F12_2015_305>.

GEUEKE, B.; GROH, K.; MUNCKE, J. Food packaging in the circular economy: Overview of chemical safety aspects for commonly used materials. **Journal of Cleaner Production**, Elsevier BV, v. 193, p. 491–505, 2018. Disponível em: <https://doi.org/10.1016%2Fj.jclepro.2018.05.005>.

GIRONÈS, J. et al. Blocked isocyanates as coupling agents for cellulose-based composites. **Carbohydrate Polymers**, Elsevier BV, v. 68, n. 3, p. 537–543, 2007. Disponível em: <https://doi.org/10.1016%2Fj.carbpol.2006.10.020>.

GIRONÈS, J. et al. Blocked diisocyanates as reactive coupling agents: Application to pine fiber–polypropylene composites. **Carbohydrate Polymers**, Elsevier BV, v. 74, n. 1, p. 106–113, 2008. Disponível em: <https://doi.org/10.1016%2Fj.carbpol.2008.01.026>.

GUTIÉRREZ, T. J.; MENDIETA, J. R.; ORTEGA-TORO, R. In-depth study from gluten/PCL-based food packaging films obtained under reactive extrusion conditions using chrome octanoate as a potential food grade catalyst. **Food Hydrocolloids**, Elsevier BV, v. 111, p. 106255, 2021. Disponível em: <https://doi.org/10.1016%2Fj.foodhyd.2020.106255>.

HUBBE, M. A.; GARDNER, D. J.; SHEN, W. Contact angles and wettability of cellulosic surfaces: A review of proposed mechanisms and test strategies. **BioResources**, BioResources, v. 10, n. 4, 2015. Disponível em: <https://doi.org/10.15376%2Fbiores.10.4.hubbe_gardner_shen>.

HUBBE, M. A. et al. Cellulosic nanocomposites. a review. **BioResources**, BioResources, v. 3, n. 3, p. 929–980, 2008. Disponível em: <https://doi.org/10.15376%2Fbiores.3.3.929-980>.

INDRIYATI; INDRARTI, L. Preparation and characterization of bacterial cellulose-beeswax films. **IOP Conference Series: Earth and Environmental Science**, IOP Publishing, v. 160, p. 012010, 2018. Disponível em: <https://doi.org/10.1088%2F1755-1315%2F160%2F1%2F012010>.

JEONG, M.-J. et al. Deterioration of ancient korean paper (hanji), treated with beeswax: A mechanistic study. **Carbohydrate Polymers**, Elsevier BV, v. 101, p. 1249–1254, 2014. Disponível em: <https://doi.org/10.1016%2Fj.carbpol.2013.10.033>.

KLEMM, D. et al. Nanocellulose as a natural source for groundbreaking applications in materials science: Today's state. **Materials Today**, Elsevier BV, v. 21, n. 7, p. 720–748, 2018. Disponível em: <https://doi.org/10.1016%2Fj.mattod.2018.02.001>.

KLEMM, D. et al. Cellulose: Fascinating biopolymer and sustainable raw material. **Angewandte Chemie International Edition**, Wiley, v. 44, n. 22, p. 3358–3393, 2005. Disponível em: <https://doi.org/10.1002%2Fanie.200460587>.

KRAMER, R. K. **Estudo da interação da água com a celulose e o amido por meio da técnica de termogravimetria**. Dissertação (Mestrado) — Universidade de São Paulo, 2014. Disponível em: <https://doi.org/10.11606%2Fd.18.2015.tde-16032015-154829>.

LAVOINE, N. et al. Microfibrillated cellulose – its barrier properties and applications in cellulosic materials: A review. **Carbohydrate Polymers**, Elsevier BV, v. 90, n. 2, p. 735–764, 2012. Disponível em: <https://doi.org/10.1016%2Fj.carbpol.2012.05.026>.

LI, T. et al. Developing fibrillated cellulose as a sustainable technological material. **Nature**, Springer Science and Business Media LLC, v. 590, n. 7844, p. 47–56, 2021. Disponível em: <https://doi.org/10.1038%2Fs41586-020-03167-7>.

LU, P. et al. Reactive coating of soybean oil-based polymer on nanofibrillated cellulose film for water vapor barrier packaging. **Carbohydrate Polymers**, Elsevier BV, v. 111, p. 524–529, 2014. Disponível em: <https://doi.org/10.1016%2Fj.carbpol.2014.04.071>.

LU, Z. et al. All cellulose composites prepared by hydroxyethyl cellulose and cellulose nanocrystals through the crosslink of polyisocyanate. **Carbohydrate Polymers**, Elsevier BV, v. 250, p. 116919, 2020. Disponível em: <https://doi.org/10.1016%2Fj.carbpol.2020.116919>.

MEYER-STORK, L. S.; HöCKER, H.; BERNDT, H. Syntheses and reactions of urethanes of cellobiose and cellulose-containing uretdione groups. **Journal of Applied Polymer Science**, Wiley, v. 44, n. 6, p. 1043–1049, 1992. Disponível em: <https://doi.org/10.1002%2Fapp.1992.070440613>.

MORRISSETTE, J. M. et al. A methodology to produce eco-friendly superhydrophobic coatings produced from all-water-processed plant-based filler materials. **Green Chemistry**, Royal Society of Chemistry (RSC), v. 20, n. 22, p. 5169–5178, 2018. Disponível em: <https://doi.org/10.1039%2Fc8gc02439a>.

NGAMEKAUE, N.; CHITPRASERT, P. Effects of beeswax-carboxymethyl cellulose composite coating on shelf-life stability and intestinal delivery of holy basil essential oil-loaded gelatin microcapsules. **International Journal of Biological Macromolecules**, Elsevier BV, v. 135, p. 1088–1097, 2019. Disponível em: <https://doi.org/10.1016%2Fj.ijbiomac.2019.06.002>.

PAN, Y. et al. Cationic starch emulsified beeswax for enhancing moisture barrier of paper as packaging materials. In: **Proceedings of the 2015 6th International Conference on Manufacturing Science and Engineering**. Atlantis Press, 2015. Disponível em: <https://doi.org/10.2991%2Ficmse-15.2015.204>.

PAYNE, J.; MCKEOWN, P.; JONES, M. D. A circular economy approach to plastic waste. **Polymer Degradation and Stability**, Elsevier BV, v. 165, p. 170–181, 2019. Disponível em: <https://doi.org/10.1016%2Fj.polymdegradstab.2019.05.014>.

RAS, R. H. A.; TIAN, X.; BAYER, I. S. Superhydrophobic and superoleophobic nanostructured cellulose and cellulose composites. In: **Handbook of Nanocellulose and Cellulose Nanocomposites**. Wiley-VCH Verlag GmbH & Co. KGaA, 2017. p. 731–760. Disponível em: <https://doi.org/10.1002%2F9783527689972.ch22>.

REVERDY, C. et al. One-step superhydrophobic coating using hydrophobized cellulose nanofibrils. **Colloids and Surfaces A: Physicochemical and Engineering Aspects**, Elsevier BV, v. 544, p. 152–158, 2018. Disponível em: <https://doi.org/10.1016%2Fj.colsurfa.2017.12.059>.

RODRÍGUEZ-ROJAS, A. et al. ¿what is the new about food packaging material? a bibliometric review during 1996–2016. **Trends in Food Science & Technology**, Elsevier BV, v. 85, p. 252–261, 2019. Disponível em: <https://doi.org/10.1016%2Fj.tifs.2019.01.016>.

ROL, F. et al. Recent advances in surface-modified cellulose nanofibrils. **Progress in Polymer Science**, Elsevier BV, v. 88, p. 241–264, 2019. Disponível em: <https://doi.org/10.1016%2Fj.progpolymsci.2018.09.002>.

SAUNDERS, J. H.; SLOCOMBE, R. J. The chemistry of the organic isocyanates. **Chemical Reviews**, American Chemical Society (ACS), v. 43, n. 2, p. 203–218, 1948. Disponível em: <https://doi.org/10.1021%2Fcr60135a001>.

SEHAQUI, H.; ZIMMERMANN, T.; TINGAUT, P. Hydrophobic cellulose nanopaper through a mild esterification procedure. **Cellulose**, Springer Science and Business Media LLC, v. 21, n. 1, p. 367–382, 2013. Disponível em: <https://doi.org/10.1007%2Fs10570-013-0110-5>.

SETHI, J. et al. A fast method to prepare mechanically strong and water resistant lignocellulosic nanopapers. **Carbohydrate Polymers**, Elsevier BV, v. 203, p. 148–156, 2019. Disponível em: <https://doi.org/10.1016%2Fj.carbpol.2018.09.037>.

SILVA, A. L. P. et al. Increased plastic pollution due to COVID-19 pandemic: Challenges and recommendations. **Chemical Engineering Journal**, Elsevier BV, v. 405, p. 126683, 2021. Disponível em: <https://doi.org/10.1016%2Fj.cej.2020.126683>.

SIQUEIRA, G.; BRAS, J.; DUFRESNE, A. Cellulosic bionanocomposites: A review of preparation, properties and applications. **Polymers**, MDPI AG, v. 2, n. 4, p. 728–765, 2010. Disponível em: <https://doi.org/10.3390%2Fpolym2040728>.

SONG, J.; ROJAS, O. J. PAPER CHEMISTRY. approaching super-hydrophobicity from cellulosic materials: A review. **Nordic Pulp & Paper Research Journal**, Walter de Gruyter GmbH, v. 28, n. 2, p. 216–238, 2013. Disponível em: <https://doi.org/10.3183%2Fnpprj-2013-28-02-p216-238>.

SPENCE, K. et al. Water vapor barrier properties of coated and filled microfibrillated cellulose composite films. **BioResources**, BioResources, v. 6, n. 4, p. 4370–4388, 2011. Disponível em: <https://doi.org/10.15376%2Fbiores.6.4.4370-4388>.

TAN, H.; ZHANG, Y.; WENG, X. Preparation of the plywood using starch-based adhesives modified with blocked isocyanates. **Procedia Engineering**, Elsevier BV, v. 15, p. 1171–1175, 2011. Disponível em: <https://doi.org/10.1016%2Fj.proeng.2011.08.216>.

TEDESCHI, G. et al. Sustainable fabrication of plant cuticle-like packaging films from tomato pomace agro-waste, beeswax, and alginate. **ACS Sustainable Chemistry & Engineering**, American Chemical Society (ACS), v. 6, n. 11, p. 14955–14966, 2018. Disponível em: <https://doi.org/10.1021%2Facssuschemeng.8b03450>.

TULLOCH, A. P. Beeswax—composition and analysis. **Bee World**, Informa UK Limited, v. 61, n. 2, p. 47–62, 1980. Disponível em: <https://doi.org/10.1080%2F0005772x.1980.11097776>.

VARTIAINEN, J.; MALM, T. Surface hydrophobization of CNF films by roll-to-roll HMDSO plasma deposition. **Journal of Coatings Technology and Research**, Springer Science and Business Media LLC, v. 13, n. 6, p. 1145–1149, 2016. Disponível em: <https://doi.org/10.1007%2Fs11998-016-9833-1>.

VILARINHO, F. et al. Nanocellulose in green food packaging. **Critical Reviews in Food Science and Nutrition**, Informa UK Limited, v. 58, n. 9, p. 1526–1537, 2017. Disponível em: <https://doi.org/10.1080%2F10408398.2016.1270254>.

WAGNER, S.; SCHLUMMER, M. Legacy additives in a circular economy of plastics: Current dilemma, policy analysis, and emerging countermeasures. **Resources, Conservation and Recycling**, Elsevier BV, v. 158, p. 104800, 2020. Disponível em: <https://doi.org/10.1016%2Fj.resconrec.2020.104800>.

WANG, J. et al. Moisture and oxygen barrier properties of cellulose nanomaterial-based films. **ACS Sustainable Chemistry & Engineering**, American Chemical Society (ACS), v. 6, n. 1, p. 49–70, 2017. Disponível em: <https://doi.org/10.1021%2Facssuschemeng.7b03523>.

WICKS, D. A.; WICKS, Z. W. Blocked isocyanates III: Part a. mechanisms and chemistry. **Progress in Organic Coatings**, Elsevier BV, v. 36, n. 3, p. 148–172, 1999. Disponível em: <https://doi.org/10.1016%2Fs0300-9440%2899%2900042-9>.

WICKS, D. A.; WICKS, Z. W. Blocked isocyanates III. **Progress in Organic Coatings**, Elsevier BV, v. 41, n. 1-3, p. 1–83, 2001. Disponível em: <https://doi.org/10.1016%2Fs0300-9440%2800%2900164-8>.

YANG, L. et al. Nanocrystalline cellulose-dispersed AKD emulsion for enhancing the mechanical and multiple barrier properties of surface-sized paper. **Carbohydrate Polymers**, Elsevier BV, v. 136, p. 1035–1040, 2016. Disponível em: <https://doi.org/10.1016%2Fj.carbpol.2015.10.011>.

YANG, L.; PAULSON, A. Effects of lipids on mechanical and moisture barrier properties of edible gellan film. **Food Research International**, Elsevier BV, v. 33, n. 7, p. 571–578, 2000. Disponível em: <https://doi.org/10.1016%2Fs0963-9969%2800%2900093-4>.

ZHANG, D.; XIAO, H. Dual-functional beeswaxes on enhancing antimicrobial activity and water vapor barrier property of paper. **ACS Applied Materials & Interfaces**, American Chemical Society (ACS), v. 5, n. 8, p. 3464–3468, 2013. Disponível em: <https://doi.org/10.1021%2Fam400585m>.

ZHANG, W.; XIAO, H.; QIAN, L. Beeswax–chitosan emulsion coated paper with enhanced water vapor barrier efficiency. **Applied Surface Science**, Elsevier BV, v. 300, p. 80–85, 2014. Disponível em: <https://doi.org/10.1016%2Fj.apsusc.2014.02.005>.

ZHOU, X. et al. Diisocyanate modifiable commercial filter paper with tunable hydrophobicity, enhanced wet tensile strength and antibacterial activity. **Carbohydrate Polymers**, Elsevier BV, v. 248, p. 116791, 2020. Disponível em: <https://doi.org/10.1016%2Fj.carbpol.2020.116791>.